Inaugural dissertation

for

obtaining the doctoral degree

of the

Combined Faculty of Mathematics, Engineering and Natural Sciences

of the

Ruprecht - Karls - University

Heidelberg

Presented by

Stefan Oliver Bassler, M.Sc.

born in: Weinheim, Germany

Oral examination: 9th July 2024

Genomic landscape of resistance evolution

Referees: Prof. Dr. Lars Steinmetz

Prof. Dr. Stefan Wölfl

Summary

Antimicrobial resistance (AMR) presents a major public health challenge threatening the foundations of modern medicine, with gaps in our understanding of the evolutionary pathways leading to AMR. Through genetic interactions with resistance genes, the genetic background offers a way to understand and modulate AMR evolution. To systematically assess how the genetic background affects the evolution of AMR, I established a high-throughput (HT) experimental evolution protocol that allowed me to grow and track thousands of lineages over time. I used this protocol to profile a genome-wide single-gene knockout (KO) collection of *Escherichia coli* K12 during treatment with the commonly used cephalosporin cefotaxime.

By quantifying the contribution of every non-essential gene to AMR evolvability, I uncovered several genes that delayed or promoted cefotaxime resistance evolution. While several mutants with decreased evolvability (evolvability genes) were involved in peptidoglycan (PG) remodeling and metabolism, mutants with increased evolvability were enriched for phospholipid transport and enterobacterial common antigen biosynthetic process. I uncovered two evolvability genes, *dpaA*, which cleaves linkages between PG and outer membrane (OM), and *ivy*, which folds periplasmic proteins and is required for DpaA protein presence. The absence of these evolvability genes blocks evolutionary trajectories towards cefotaxime AMR *via* epistatic genetic interactions with the known cefotaxime resistance genes *marR* and *ompR*. Using HT microscopy, proteomics, and quantitative genetics, I uncovered that LPS biosynthesis and transport are deregulated in *marR*-resistant mutants, and these phenotypes are exacerbated in the absence of the evolvability gene *dpaA*. This negative genetic interaction is likely caused by the increased abundance of crosslinks between PG and OM in *dpaA* KO mutants, which could prevent the compensatory shedding of LPS *via* OM vesicles and blebs in *marR* mutants. This epistatic interaction can be relieved in mutants with reduced LPS biosynthesis or decreased abundance of PG-OM crosslinks.

Uncovering deregulated LPS biosynthesis and transport in *marR* mutants leading to a compromised OM barrier function allowed me to identify several drugs that inhibit AMR evolution against cefotaxime, potentially by selectively preventing the evolution of *marR* mutations. Furthermore, to assess the specificity of evolvability genes, I evolved nine evolvability gene mutants against 12 other antibiotics. I found that all of them delayed antibiotic resistance evolution of multiple antibiotics in a drug-, target- or resistance-dependent manner.

Furthermore, I developed a complementary approach using Clustered Regularly Interspaced Short Palindromic Repeats interference (CRISPRi) to measure the global epistasis of antibiotic targets or resistance genes with the KO collection in the absence or presence of an antibiotic. This approach is more scalable and can support the insights gained from the experimental evolution of a genome-wide KO library. I applied this method to probe genome-wide genetic interactions of the antibiotic target and resistance gene DNA topoisomerase IV (*parC*) and discovered that gene KOs with negative epistasis were enriched for binding DNA. The identified evolvability genes represent potential targets for AMR-inhibiting drugs against multiple antibiotics. They can guide combinatorial strategies with existing drugs to delay resistance evolution, resensitize resistant populations, and improve antimicrobial therapies.

Zusammenfassung

Antimikrobielle Resistenz (AMR) stellt ein großes Gesundheitsproblem dar, insbesondere da die genetischen Abhängigkeiten des Evolutionsprozesses unbekannt sind. Durch genetische Interaktionen mit Resistenzgenen bietet der genetische Hintergrund eine Möglichkeit, evolutionäre Pfade, die zu AMR führen, zu verstehen und zu modulieren. Um einen systematischen Überblick zu erlangen, wie der genetische Hintergrund die Evolution von AMR beeinflusst, habe ich in diesem Projekt mittels experimenteller Evolution AMR in einer Genom-weiten Knock-Out (KO) Kollektion von *Escherichia coli* Stämmen gegen das häufig verwendete Cephalosporin Cefotaxim evolviert. Somit lässt sich der Einfluss von jedem Gen auf die Evolution von AMR quantifizieren.

Mehrere Gene, deren Abwesenheit die Resistenzevolution verlangsamten (Evolutionsgene), waren an Stoffwechsel und Instandhaltung der Peptidoglykan-Zellwand (PG) beteiligt. Gene, deren Abwesenheit die Resistenzevolution beschleunigten, waren hingegen überrepräsentiert in den Funktionen Phospholipid Transport und Biosynthese des enterobakteriellen gemeinsamen Antigens. Ich identifizierte zwei Evolutionsgene, *dpaA*, das Verbindungen zwischen PG und äußerer Membran (OM) schneidet, und *ivy*, das Proteine im Periplasma faltet und für die Präsenz des DpaA Proteins erforderlich ist. Die Abwesenheit dieser Evolutionsgene blockierte evolutionäre Pfade, die zu Cefotaxim Resistenz führen, durch genetische Interaktionen mit zwei bekannten Cefotaxim Resistanzgenen *marR* und *ompR*.

Mittels Hochdurchsatz Mikroskopie, Proteomik und quantitativer Genetik entdeckte ich, dass sich resistente *marR* Stämme durch die Deregulierung von Lipopolysaccharid (LPS) Biosynthese und Transport auszeichnen, welche durch die Abwesenheit des Evolutionsgens *dpaA* potenziert wird. Diese negative genetische Interaktion beruht vermutlich auf dem kompensatorischen Absondern von überschüssigem LPS mittels Vesikeln der äußeren Membran (OM) in *marR* resistenten Stämmen, welches durch die erhöhte Anzahl an Verbindungen zwischen PG und OM in *dpaA* KO Stämmen verhindert wird. Diese negative genetische Interaktion konnte in Stämmen mit reduzierter LPS Synthese oder weniger PG-OM Verbindungen verhindert werden.

Das Aufdecken von deregulierter LPS Biosynthese und Transport in *marR* resistenten Stämmen und die infolgedessen verringerte Barrierefunktion der OM ermöglichte mir das Identifizieren mehrerer Wirkstoffe, welche die Evolution von AMR gegen Cefotaxim verlangsamten, möglicherweise mittels selektiver Inhibierung der Evolution *marR* resistenter Stämme. Desweiteren habe ich die Spezifizität der identifizierten Evolutionsgene mittels

experimenteller Evolution gegen 12 weitere Antibiotika ermittelt. So zeigte ich, dass Evolutionsgene die Resistenzevolution mehrerer Antibiotika, basierend auf deren Wirk- oder Resistenzmechanismen, verlangsamten.

Zusätzlich entwickelte ich eine komplementäre, CRISPRi (Clustered Regularly Interspaced Short Palindromic Repeats interference) basierte Methode zur Quantifizierung der globalen Epistase von Antibiotika Ziel- oder Resistenzgenen mit der KO Kollektion in Ab- und Anwesenheit von Antibiotika. Diese Methode ist skalierbarer und kann die durch experimentelle Evolution einer Genom-weiten KO Kollektion gewonnenen Erkenntnisse komplementieren. Ich wand diese Methode an, um die Genom-weiten genetischen Interaktionen des Antibiotika-Resistenzgens und -Ziels DNA topoisomerase IV (*parC*) zu ermitteln, und fand, dass Gen KOs mit negativer Epistase überrepresentiert DNA binden. Identifizierte Evolutionsgene repräsentieren Wirkstoffziele, die inhibiert werden können, um die Resistenzevolution verschiedener Antibiotika zu verlangsamen, resistente Bakterien spezifisch zu behandeln und antimikrobielle Therapien langfristig beständiger einzusetzen.

Acknowledgements

The work of this thesis was only possible with the support of many people whom I want to name and thank here. First of all, I would like to thank Dr. Nassos Typas for the opportunity to join his research group, repeatedly, and who had to go to great lengths to make it possible. Thank you for your trust, inspiring mentorship, stimulating discussions, a highly creative, open-minded research environment, and constructive guidance throughout my project. You always encouraged personal development and gave me much freedom to develop my ideas. I want to thank my Thesis Advisory Committee, Prof. Dr. Lars Steinmetz, Prof. Dr. Stefan Wölfl, Dr. Justin Crocker, and the additional member, Prof. Dr. Urs Jenal, for their constructive feedback, valuable advice, and scientific discussions during and outside the TAC meetings. Furthermore, I want to thank the EMBL International PhD Programme for the fantastic opportunity to join the Predoc course, great teambuilding, and excellent training, the European Research Council for providing the funding for my position, and the Joachim Herz Foundation for awarding me with the Add-on Fellowship for Interdisciplinary Life Science. This fellowship gave me the financial freedom to join Prof. Dr. Kerwyn Casey Huang's research group at Stanford University for three months to learn high-throughput microscopy. Thank you for hosting and supervising me and for countless discussions and valuable advice. My gratitude also goes to my mentors, Prof. Dr. Sebastian Maerkl, Prof. Dr. Maha Farhat, Prof Dr. Médéric Diard, and Prof. Dr. Michael Wink, who shaped my scientific thinking and personal development by allowing me to join their research groups.

I want to thank the entire Typas Lab for being such a wonderful environment in which to work. Special thanks go to Prof. Dr. Ana-Rita Brochado for introducing me to the captivating world of systems biology and high-throughput screening. I thank Dr. Michael Knopp for excellent guidance, support, discussions, and feedback throughout my project. Thanks to Dr. Carlos Voogdt for your continuous mentorship and friendship at EMBL and Stanford. I thank Dr. Vallo Varik for countless thoughtful discussions and for reminding me daily that we are living the dream as scientists. Furthermore, I thank Vallo, Michael, and Carlos for spending their time and providing me with valuable feedback on this thesis.

My gratitude goes to the philosophy group Florian, Donnacha, Luoyan, Luca, and Guido, the board game group Carlos, Diënty, Nic, and Alessio, as well as the Rangers in their entirety. Finally, I want to express my deepest gratitude to my parents, Ursula and Peter, my brother Florian and his wife Miri, Alessa and her family, and my friends for their never-ending support and love.

Table of Contents

Summary ..... ***i***
Zusammenfassung ..... ***iii***
Acknowledgements ..... ***v***
List of Figures ..... ***ix***
List of Tables ..... ***xi***
List of Abbreviation ..... ***xi***
Chapter I: Introduction ***1***
1. Principles of evolutionary systems **2**
2. Antibiotics target different cellular processes **2**
3. Antimicrobial resistance **4**
4. Bacterial cell envelope **7**
5. Antibiotic resistance evolution **12**
6. Experimental evolution to assess AMR **13**
7. Epistasis shapes resistance evolution **16**
8. Resistance evolution can rewire essentiality **16**
9. Quantifying epistatic interactions using CRISPR interference **17**
10. Shortcomings and unknowns of current approaches **17**
Chapter II: Establishing a method for high-throughput experimental evolution ***19***
1. Summary **20**
2. Contributions **21**
3. Using genome-wide experimental evolution to uncover epistatic interactions **21**
3.1. Preliminary testing identified the optimal evolution conditions and antibiotic **22**
3.2. Evolving cefotaxime resistance in the genome-wide KO library **27**
3.3. Analyzing the dataset to identify gene deletions affecting only evolvability **29**
4. Validating hits in larger population sizes confirms conserved epistasis **31**
5. Identifying required cellular functions during resistance evolution **34**
6. Uncovering detrimental cellular functions during resistance evolution **38**
6.1. Investigating detrimental cellular functions at low antibiotic concentrations **38**
6.2. Identifying detrimental cellular functions at high antibiotic concentrations **41**
7. Conclusions **44**
Chapter III: Dissecting epistatic interactions delaying resistance evolution ***47***
1. Summary **48**
2. Contributions **48**
3. Mutations impacting drug uptake and influx arise during cefotaxime resistance evolution **49**
4. CRISPRi can be used to quantify gene-gene and gene-gene-drug interactions **52**

4.1. Constructing a CRISPRi plasmid to modulate gene expression levels....52
4.2. Quantifying gene-gene and gene-gene-drug interaction using CRISPRi....53
5. Using high-throughput microscopy to dissect epistatic interactions....57
5.1. Live imaging reveals morphological aberrations by gene-gene interactions....57
5.2. Live imaging reveals resistance levels affected by gene-gene-drug interactions....65
6. Using proteomics to uncover the molecular signature of epistasis....72
6.1. Proteomics analysis reveals vulnerabilities in single KO mutants....72
6.2. Proteomics analysis of double mutants uncovers activated stress response....80
7. Breaking epistatic interactions that delay resistance evolution....82
8. Using identified genetic vulnerabilities to delay resistance evolution with drugs....89
9. Evolvability genes delay the evolution of resistance to other antibiotics....93
10. Conclusions....96
Chapter IV: Global epistasis of antibiotic targets and resistance genes....110
1. Summary....111
2. Contributions....111
3. Measuring global epistasis of antibiotic targets and resistance genes....111
3.1. Preliminary testing identified the optimal conditions to quantify epistasis....112
3.2. Quantifying global epistasis of the DNA topoisomerase IV....115
3.2. Next steps to systematically test antibiotic targets and resistance genes....117
4. Conclusions....119
Chapter V: Discussion and outlook....122
1. Genome-wide experimental evolution....123
1.1. Brief recap of results....123
1.1. Measuring genome-wide evolvability reveals global epistasis....124
1.2. Genomic landscape of cefotaxime resistance evolution....125
1.3. Shortcomings and potential pitfalls....128
1.4. Conclusion and outlook....130
2. Epistatic interactions delaying resistance evolution....131
2.1. Brief recap of results....131
2.2. Mechanistic insights into epistatic gene-gene and gene-gene-drug interactions....134
2.3. Shortcomings and potential pitfalls....142
2.4. Conclusion and outlook....145
3. Global epistasis of antibiotic targets and resistance elements....146
3.1. Brief recap of results....146
3.2. A novel method to measure global epistasis of essential genes....147
3.3. Shortcomings and potential pitfalls....151
3.4. Conclusion and outlook....152

4. Final remarks **152**
Chapter VI: Experimental procedures ***155***
1. List of primers and plasmids **156**
2. List of strains used in this work **158**
3. Bacterial growth conditions **162**
4. Electroporation **162**
5. Transforming non-competent cells using Transformation and Storage Solution (TSS) **163**
6. P1 phage transduction **163**
6.1. Preparation of the P1 lysate **163**
6.2. P1 transduction **164**
7. Flip out the Kanamycin resistance cassette using pCP20 ..... **164**
8. High-throughput experimental evolution 384-well plates **165**
8.1. Pilot experiments **165**
8.2. Main screen **165**
8.3. Data analysis **166**
9. High-throughput experimental evolution 96-well plates **167**
9.1. Validation **167**
9.2. Delay resistance evolution with drugs **167**
9.3. Multi-drug resistance evolution of evolvability genes **168**
10. Whole genome sequencing of bacterial mutants **168**
11. Epistatic interaction measurement using CRISPRi **169**
11.1. Plasmid construction **169**
11.2. Adding new guide RNAs using Golden Gate **170**
11.3. Quantifying gene-gene and gene-gene-drug interactions **170**
11.4. Quantifying gene-gene-gene interactions **171**
12. High-throughput microscopy using SLIP **172**
12.1. Sample preparation and imaging **172**
13. Mass-spectrometry based proteomics **173**
14. High-throughput epistatic interaction measurement using CRISPRi **173**
14.1. High-throughput conjugation **173**
14.2. Data processing **174**
15. Supplementary data **175**
Bibliography ***180***

List of Figures

Figure 1: Overview of antibiotic resistance mechanisms. 6
Figure 2: Biosynthesis and transport of lipopolysaccharides. 9

Figure 3: Synthesis, cleavage, and modification of peptidoglycan in Gram-negative bacteria. 11
Figure 4: Identifying gene-gene and gene-gene-drug interactions delaying resistance evolution. 21
Figure 5: Evolving antibiotic resistance against multiple antibiotics. 23
Figure 6: Evolving antibiotic resistance against cefotaxime and ciprofloxacin under multiple conditions. 26
Figure 7: A method for genome-wide experimental evolution. 28
Figure 8: Identifying gene deletions with decreased cefotaxime evolvability. 30
Figure 9: Validation of gene deletions with decreased evolvability in large volumes. 32
Figure 10: Cefotaxime sensitivity and MICs of evolvability gene KOs relative to the wildtype. 34
Figure 11: Hits with decreased evolvability at 1.5x MIC cefotaxime. 35
Figure 12: Identifying gene deletions with increased cefotaxime evolvability at 1.5x MIC. 39
Figure 13: Hits with increased evolvability at 1.5x MIC. 40
Figure 14: Hits with increased evolvability at 13.5x MIC. 43
Figure 15: Cefotaxime resistance mutations identified by whole-genome sequencing. 50
Figure 16: Epistasis of resistance elements blocks evolutionary trajectories. 53
Figure 17: Quantifying gene-drug and gene-gene interactions. 54
Figure 18: Quantifying gene-gene-drug interactions. 55
Figure 19: Live microscopy reveals single gene deletion phenotypes. 59
Figure 20: Dissecting the gene-gene interactions between marR and evolvability genes using live microscopy. 61
Figure 21: Dissecting the gene-gene interactions between ompR and evolvability genes using live microscopy. 63
Figure 22: Live microscopy of single gene deletion mutants in the presence of cefotaxime. 67
Figure 23: Dissecting gene-gene-drug interactions of marR in the presence of cefotaxime by live microscopy. 67
Figure 24: Dissecting gene-gene-drug interactions of ompR in the presence of cefotaxime by live microscopy. 69
Figure 25: Mass spectrometry-based proteomics reveals protein abundance changes in marR (a) and ompR (b) deletion mutants. 73
Figure 26: Chemical genetics data reveals drug sensitivities of the marR KO mutant (data from (Nichols et al. 2011)). 74
Figure 27: Proteomics reveals protein abundance changes in dpaA (a) and ivy (b) deletion mutants. 78
Figure 28: Using proteomics to identify the proteomic signature of gene-gene interactions in double mutants. 81
Figure 29: Measuring gene-gene interactions in an evolved cefotaxime-resistant mutant. 83
Figure 30: Measuring gene-gene-gene interactions reverting epistasis between dpaA and marR. 86
Figure 31: Delay cefotaxime resistance evolution with small molecules. 90
Figure 32: Resistance evolution of cefotaxime evolvability genes against multiple antibiotics. 94
Figure 33: Quantifying epistatic interactions. 112
Figure 34: CRISPRi-mediated KDs specifically reduce CFUs, protein abundance, and colony size. 114

Figure 35: Global epistasis of antibiotic target and resistance gene parC with >80 % of non-essential gene KOs. 116
Figure 36: Global epistasis method recapitulates known interaction partners of parC. 117

List of Tables

Table 1: All plasmids used in the study. 156
Table 2: All oligos and primers used in the study. 157
Table 3: All bacterial strains used in this work. 159

List of Abbreviation

Amp	Ampicillin
AMR	Antimicrobial resistance
aTc	Anhydrotetracycline
AUC	Area Under the Curve
CFU	Colony-forming unit
CPases	Carboxypeptidases
CRISPR	Clustered Regularly Interspaced Short Palindromic Repeats
CRISPRi	CRISPR interference
CV	Coefficient of variation
E. coli	*Escherichia coli*
D-ala	D-alanine
ECA	Enterobacterial common antigen
EPases	Endopeptidases
GlcNAc	N-acetylglucosamine
gRNA	guide RNA
GTases	Glycosyltransferases
IM	Inner membrane
Kan	Kanamycin
KD	Knockdown
KO	Knockout
L2FC	Log_2(fold-change)
LDT	LD-transpeptidase
LOF	Loss-of-function
Lpp	Braun's lipoprotein

LPS	Lipopolysaccharide
Lpt	Lipopolysaccharide transport
LT	Lytic transglycosylase
LTEE	Long-term evolution experiment
Mar	Multiple antibiotic resistance
MS	Mass spectrometry
m-DAP	meso- diaminopimelic acid
MIC	Minimum inhibitory concentration
Mla	Maintenance of lipid asymmetry
Mlt	lytic murein transglycosylase
MurNAc	N-acetylmuramic acid
Nucleotide	nt
OD	Optical density
OM	Outer membrane
OMP	Outer membrane protein
OMV	Outer membrane vesicle
PEP	Phosphoenolpyruvate
PBP	Penicillin-binding protein
PG	Peptidoglycan
PL	Phospholipid
SL	Synthetic lethality
SNP	Single nucleotide polymorphism
Spec	Spectinomycin
SV	Structural variant
THF	Tetrahydrofolate
TPases	Transpeptidases
Und-PP	Undecaprenyl pyrophosphate
WGS	Whole-genome sequencing

Chapter I: Introduction

Chapter I: Introduction

1. Principles of evolutionary systems

Evolution is based on replication, mutation, and selection. Evolution acts upon cells or organisms that reproduce, replicate their genetic material, and inherit it to their progeny. Replication is imperfect and causes mutations that create biological novelty and result in diversity. This diversity is filtered by the environment that selects for the fittest cells or organisms outcompeting others, which is selection. Selection rewards some innovations and penalizes others (Nowak 2006).

"Yet of those which do survive, the best adapted individuals, supposing that there is any variability in a favourable direction, will tend to propagate their kind in larger numbers than the less well adapted." (Darwin 1859). As Charles Darwin described, natural selection acts as the primary source of directionality across biology by filtering organisms with natural variation, produced by mutation through replication and recombination *via* sexual or asexual reproduction, for their ability to survive and reproduce in a particular environment. As the environment changes, so does the objective function of adaptation. The global spread of antimicrobial resistance directly results from microbial evolution and natural selection in environments with abundant antibiotics, such as wastewater, agriculture, and hospitals (Larsson & Flach 2022), representing a major challenge for humanity.

2. Antibiotics target different cellular processes

Several antibiotics target processes involved in building, maintaining, and remodeling cell envelope components. Polymyxins are one class of drugs targeting the bacterial cell envelope, of which polymyxin B and E (colistin) are the most prominent examples. Polymyxins perturb membrane integrity *via* a proposed two-step mechanism. With their cationic peptide region, polymyxins bind the negatively charged LPS in the OM, and with their hydrophobic fatty acid chain, the lipid A of the LPS chain. Binding LPS in the OM displaces membrane-stabilizing cations such as Ca^{2+} and Mg^{2+}, facilitates the uptake of polymyxins, and leads to overall increased permeability and breakage of the OM (Mohapatra et al. 2021; Trimble et al. 2016). Then, polymyxins can also interfere with the IM by binding to lipid or LPS components (Sabnis et al. 2021). One way to directly inhibit LPS biosynthesis are compounds such as CHIR-090 or the recently discovered LPC-233. Both target LpxC, an essential component of LPS biosynthesis catalyzing the second reaction and first committed step of lipid A biosynthesis

(Zhao et al. 2023; Barb, McClerren, et al. 2007; Barb, Jiang, et al. 2007). A recently discovered antibiotic with a novel target is darobactin, targeting BamA, an essential part of the BAM complex that folds and inserts proteins into the OM (Kaur et al. 2021; Imai et al. 2019).

The glycopeptide vancomycin inhibits peptidoglycan (PG), also called cell wall, assembly by forming hydrogen bonds with the D-alanine-D-alanine peptide motif of PG precursor lipid II and inhibits polymerization and transglycosylation of the PG as a result (Mühlberg et al. 2019; Murray 1997; Pootoolal et al. 2002; Barna & Williams 1984). Gram-negative bacteria have orders-of-magnitude higher minimum inhibitory concentrations (MICs) to vancomycin than Gram-positive bacteria due to their distinct cell envelope with an OM serving as a hydrophobic barrier (Johnson et al. 1990). One way vancomycin resistance emerges is by replacing the terminal D-alanine vancomycin binding site with D-lactate (Boneca & Chiosis 2003).

Fosfomycin inhibits PG biosynthesis by covalently binding and inhibiting MurA, which is an essential enzyme of PG biosynthesis, by catalyzing the first committed step from UDP-N-acetylglucosamine (UDP-GlcNAc) and phosphoenolpyruvate (PEP) to UDP-GlcNAc-enoyl pyruvate and inorganic phosphate. Fosfomycin is actively imported into the cell by sugar transporters: either GlpT, responsible for the uptake of α-glycerophosphate, or UhpT, responsible for hexose-phosphate uptake (Silver 2017).

The primary class of antibiotics targeting the cell envelope and, more specifically, PG biosynthesis are β-lactams. They can be divided into penicillins, cephalosporins, monobactams, carbapenems, and cephamycins. Generally speaking, β-lactams target PG crosslinking by inhibiting Penicillin-binding protein (PBPs) and, therefore, crosslinking of peptide chains in the PG (Lima et al. 2020), ultimately resulting in cell lysis (Baquero & Levin 2021). Due to their essentiality for growth and division, class A and B PBP's represent potent targets for β-lactam antibiotics. While elongasome inhibiting β-lactams target PBP2 and cause cell elongation defects and rounding of cells, divisome inhibiting β-lactams target PBP3 and cause chain formation and cell division defects (Spratt 1975).

Multiple antibiotics such as cefotaxime, cefuroxime, ceftriaxone, and piperacillin selectively target PBP3. This thesis focuses on understanding cefotaxime resistance evolution because of its clinical use against Gram-positive, Gram-negative, and anaerobic organisms for various

disease indications (Carmine et al. 1983). Resistance mutations during cefotaxime resistance evolution have been systematically mapped under different population sizes (Schenk et al. 2022). Finally, the specificity of cefotaxime for PBP3, targeted by multiple antibiotics, allowed me to assess similarities and differences during their resistance evolution and identify ways to delay resistance evolution against multiple antibiotics as part of this thesis.

Other β-lactams show specificity for different subsets of PBPs, such as ampicillin and penicillin V and G (PBP4, PBP7, and PBP8), amoxicillin (PBP4), mecillinam/amdinocillin (PBP2), meropenem (PBP2 and PBP4) and cefsulodin (PBP1a and PBP1b). This diversity of functionally related targets and structures makes β-lactams an interesting drug class for studying the impact of structure-target relationships on resistance evolution. Both structural features and the subclass of β-lactam determine their specificity (Ozden & Carlson 2015).

Other essential processes antibiotics target are replication, transcription, translation, and folate biosynthesis. Multiple antibiotic classes target translation through inhibition of the 30S and 50S ribosome subunit (Paternoga et al. 2023), such as aminoglycosides (Roopal & Scott 2002; Fourmy et al. 1996), tetracyclines (Chopra & Roberts 2001), macrolides (Vázquez-Laslop & Mankin 2018), and chloramphenicol (Pongs et al. 1973). Rifampicin targets transcription through RNA polymerase inhibition (Jin & Gross 1988; Campbell et al. 2001). DNA replication can be targeted through gyrase and DNA topoisomerase IV inhibition by (fluoro)-quinolones (Hooper 2000) and aminocoumarins (Alt et al. 2011). Folate biosynthesis is inhibited by trimethoprim (Roth et al. 1962) and sulfonamides (Wise & Abou Donia 1975). The heavy usage of antibiotics targeting multiple essential components has revealed many single- and multi-drug resistance mechanisms, which will be discussed next. Understanding genetic interactions of drug resistance mechanisms is paramount to delaying or reverting AMR and represents the primary focus of this thesis.

3. Antimicrobial resistance

Infections caused by drug-resistant pathogens are threatening the foundations of modern medicine and global health and resulted in 4.95 million deaths associated with and 1.27 million deaths attributable to drug-resistant bacterial infections in 2019 (Murray et al. 2022). Reasons for this development are the mis- and overuse of antibiotics in healthcare and agriculture in combination with the stop of antibiotic drug development efforts by most major pharmaceutical

companies due to low profitability (Kwon & Powderly 2021; WHO 2016). Upon chemical stress on essential cellular processes, bacteria undergo a selective pressure to alleviate the stress mainly *via* four resistance mechanisms: (1) drug exclusion, (2) drug inactivation, (3) target protection/modification, or (4) rewiring of essentiality (Figure 1) (Darby et al. 2023). Given that this thesis focuses on resistance evolution in *Escherichia coli* (*E. coli*), examples of these four resistance mechanisms will be discussed with a focus on *E. coli*.

Drug exclusion works by decreasing the intracellular and, therefore, effective drug concentration either by downregulating porins to decrease drug influx (*e.g.* OmpC and OmpF porins downregulated *via* mutation of the *ompR* regulator that is part of the EnvZ-OmpR two-component system (Masi et al. 2022; Yoshida et al. 2006)) or by upregulating efflux pumps to increase active drug efflux (*e.g.* AcrAB-TolC efflux pump upregulated *via* mutation of the *marR* regulator (Nicoloff & Andersson 2013; Sharma et al. 2017; Hao et al. 2014)).

Drug inactivation includes resistance either by degrading or modifying the antibiotic. Examples of the degradation of antibiotics are β-lactamases that hydrolyze the β-lactam ring of β-lactam antibiotics (Tooke et al. 2019) or the inactivation of tetracyclines by the binding through tetracycline hydroxylases (Markley & Wencewicz 2018). Drug modification includes enzymes such as acetyltransferases, phosphotransferases, or nucleotidyltransferases, which can inactivate aminoglycoside antibiotics such as gentamicin, streptomycin, and kanamycin by reducing their affinity to the target (Ramirez & Tolmasky 2010).

Target modification can also result in resistance by decreasing the binding affinity between the target and antibiotic, for example, by altering, protecting, or obscuring the target. Examples are mutations in the topoisomerase that reduce quinolone binding (Bush et al. 2020) or mutations in PBP3 that reduce the binding of aztreonam and avibactam (Periasamy et al. 2020). An example of obscuring (transiently modifying) the target is the methylation of the 16S rRNA by ribosomal methyltransferases, providing resistance against macrolides (Bhujbalrao & Anand 2019) and aminoglycosides (Doi et al. 2016). One example of target protection is TetR, which represses the expression of the tetracycline efflux pump TetA (Ramos et al. 2005). If present, tetracycline binds TetR, which releases the repression of TetA and triggers tetracycline efflux (Ramos et al. 2005).

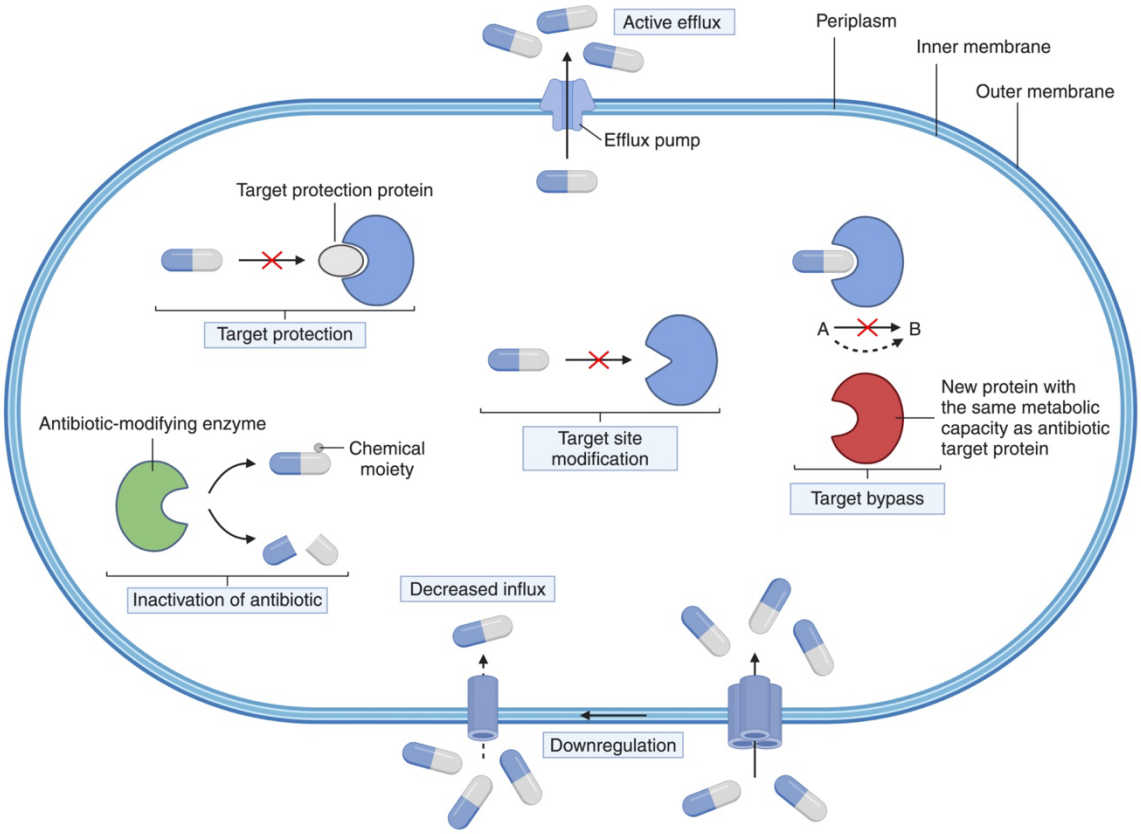

Figure 1: Overview of antibiotic resistance mechanisms. *Mechanisms of antibiotic resistance are shown for a Gram-negative bacterium and can be classified into four classes: a) drug exclusion mediating antibiotic resistance by active efflux and decreased influx, b) drug inactivation is achieved by the inactivation of the antibiotic using different antibiotic-modifying enzymes, c) target modification relies on target protection or target site modification and d) rewiring essentiality, where the target is bypassed using an alternative protein that shares the metabolic function with the target protein. Figure adapted from* (Darby et al. 2023).

Rewiring essentiality or bypassing the target can provide resistance in multiple different ways. The original target can be rendered redundant by acquiring an alternative gene, or essentiality can be rewired so that the essential drug target becomes non-essential by utilizing different pathways in the genetic network. One example of a homologous gene replacing the drug target is *mecA*, an exogenous methicillin-resistance gene expressed from the staphylococcal cassette chromosome mec (SCCmec). It serves *Staphylococcus aureus* as a PBP2a homolog with lower binding affinity by β-lactam antibiotics and confers methicillin resistance by continuing PBP2a transpeptidation activity in the presence of methicillin (Stapleton & Taylor 2002). One example of rewired essentiality in *E. coli* includes alternative crosslinking, where the L,D-transpeptidase LdtD circumvents the D,D-transpeptidase activity of PBPs and results in β-lactam resistance (Caveney et al. 2019). However, a high-level synthesis of (p)ppGpp, the D,D-carboxypeptidase DacA, and the glycosyltransferase PBP1b, which are typically not essential, become essential for this activity (Hugonnet et al. 2016; Egan et al. 2020). Therefore, it provides an example of

a novel vulnerability that arises from the rewiring of essentiality during resistance evolution. I want to identify such vulnerabilities for cefotaxime resistance evolution as part of this thesis.

For cefotaxime, the focus of this thesis, but similarly for other cephalosporins, resistance primarily evolves through mutation in *marR* increasing efflux *via* upregulation of the AcrAB-TolC efflux pump (Sulavik et al. 1995; Sharma et al. 2017), *ompR* decreasing influx by decreased expression of the porins OmpF and OmpC (Norioka et al. 1986; Yoshida et al. 2006b; Masi et al. 2022), and at large population sizes also in the target PBP3 (Schenk et al. 2022). Furthermore, (extended-spectrum) β-lactamases such as TEM-1 can provide resistance but must be acquired through horizontal gene transfer, *e.g.*, through a conjugative plasmid (Schenk et al. 2022). Both the cefotaxime target and the resistance mechanisms are located in the bacterial cell envelope, which makes it the focal point of this thesis.

4. Bacterial cell envelope

The bacterial cell envelope is one of the most critical cellular structures antibiotics can target, providing sensitivity to and resistance against antibiotics by hosting multiple essential cellular functions. This section discusses the different components of the cell envelope and their function with a focus on *E. coli*. The cell envelope provides stability and shape, allows nutrient uptake and waste disposal, determines division and growth, mediates cellular interactions, resists turgor pressure, and serves as a barrier to block toxic molecule entry (Silhavy et al. 2010). The Gram-negative bacterial cell envelope is comprised of an inner membrane (IM) and outer membrane (OM), which are separated by the aqueous periplasm (Bos & Tommassen 2004; Typas et al. 2012; Egan et al. 2020). Within the periplasm is the cell wall or peptidoglycan (PG), a mesh-like polymer of glycan strands crosslinked by short peptides that contribute to shape and stability against mechanical stresses such as turgor pressure (Vollmer, Blanot, et al. 2008; Egan et al. 2020; Typas et al. 2012).

The asymmetric OM is a bilayer consisting of phospholipids (PL) in the inner and lipopolysaccharide (LPS) in the outer leaflet (Hiroshi 2003) and embeds many outer-membrane proteins (OMPs) and lipoproteins. The PG and OM contribute to stiffness and strength in resisting the mechanical loads from the turgor pressure (Rojas et al. 2018). The OMP network spans the bacterial surface and is only interrupted by OMP-depleted patches enriched in LPS (Benn et al. 2021).

LPS molecules have a lipid A component composed of four to seven saturated acyl chains, an inner and outer oligosaccharide core, and the O antigen composed of a long polysaccharide chain. LPS displays essential biophysical properties in providing stiffness, strength, and a hydrophobic barrier against antibiotics, detergents, and bile salts (Hiroshi 2003) while being permeable to small water-soluble molecules *via* porins. These biophysical properties are achieved by the tight packing of LPS and strong lateral interactions, where divalent cations bridge the accessible negative charges from phosphate and acid groups located on inner core sugars and lipid A (Hiroshi 2003; Guest et al. 2021). When LPS biosynthesis or transport are impaired, PLs replace the decreased number of LPS molecules in the outer leaflet by flipping from the inner to the outer leaflet (Nikaido 2005). These PLs form rafts that allow hydrophobic molecules to enter. The cell has several mechanisms to remove or destroy PL from the outer leaflet to prevent damage (Ruiz et al. 2006; Benn et al. 2021).

The OM-located palmitoyltransferase PagP can remove palmitate from PL exposed to the surface and transfer the removed palmitate to lipid A or phosphatidylglycerol (Bishop 2008; Dalebroux et al. 2014). The phospholipase PldA can remove palmitate from both PLs and PLs after the removal of a fatty acid (lyso-PLs) (Dekker 2000). The maintenance of lipid asymmetry (Mla) system can transport PLs from the OM back to the IM (Malinverni & Silhavy 2009). The Mla system requires the lipoprotein MlaA to form a complex with OmpC to remove PLs first from the outer leaflet of the OM (Yeow et al. 2018; Chong et al. 2015). The removed PLs are shuttled to periplasm-located MlaC and delivered to MlaFEDB to be integrated into the IM (Malinverni & Silhavy 2009). LPS levels (Sutterlin et al. 2016), as well as the (multiple antibiotic resistance Activator) MarA (Sharma et al. 2017), regulate the Mla system. Cells lacking the *mla* operon have defective barrier function and increased surface hydrophobicity, which leads to sensitivity to hydrophobic antibiotics such as doxycycline and minocycline (Sharma et al. 2017). Balanced transport and synthesis of LPS and PLs are vital to ensure the mechanical integrity of the cell envelope and the OM barrier function (Raetz & Whitfield 2002).

LPS biosynthesis and transport are summarized in Figure 2. LPS synthesis is initiated in the cytoplasm by a series of steps where LpxC acts as a rate-limiting step and regulatory focal point (Emiola et al. 2013; Emiola et al. 2015). LpxC is also a drug target bound and inhibited by CHIR-090 (Barb, Jiang, et al. 2007; Barb, McClerren, et al. 2007). After biosynthesis of the lipid A disaccharide, Kdo2-lipid A is formed, followed by the addition of inner and outer core

oligosaccharides to finalize the lipid A core (Emiola et al. 2016; Emiola et al. 2015). MsbA transports the lipid A core to the periplasmic leaflet of the IM, where undecaprenyl phosphate oligosaccharide units are appended to attach the different antigens, including O antigen.

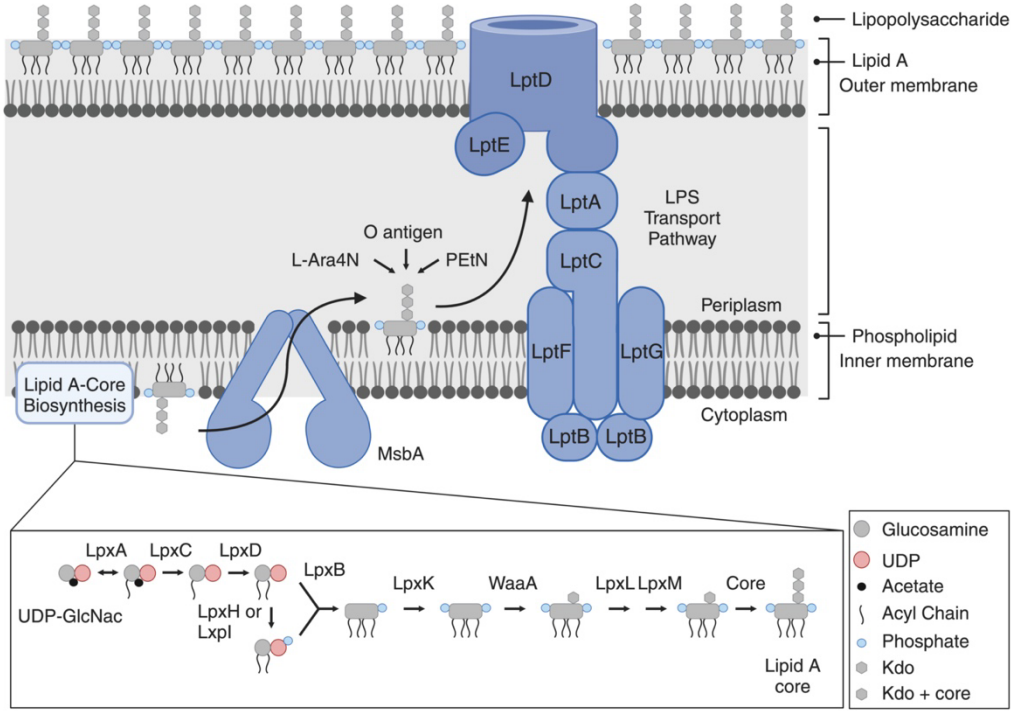

Figure 2: Biosynthesis and transport of lipopolysaccharides. *The synthesis of the core oligosaccharide and lipid A occurs in the cytoplasm and at the cytoplasmic leaflet of the inner membrane. The lipid A-core is flipped across the inner membrane, and the O antigen is attached. Following the addition of several modifications, the LPS transport machinery (Lpt) extracts LPS from the inner membrane, transports it across the periplasm, and inserts it into the outer membrane. Figure adapted from* (Guest et al. 2021).

The *E. coli* wildtype K-12 strain synthesizes the complete core oligosaccharide structures (rough LPS). However, it lacks K and O antigens due to *rfb* mutations potentially selected for by the growth of the ancestor in bile salt-containing MacConkey media (Qin et al. 2023). After synthesis, the essential LPS transport system (Lpt) takes LPS out of the IM (LptB), shuttles it through the periplasm (LptC and LptA) and places it in the outer leaflet of the OM (LptD and LptE) (Okuda et al. 2012; Owens et al. 2019; Sherman et al. 2014; Malojčić et al. 2014; Guest et al. 2021; Sperandeo et al. 2011). LptC levels are controlled by FtsH-mediated degradation. Upon LPS buildup in the IM, LPS binds to LapC, thereby outcompeting LapB. The adaptor LapB is released and binds to FtsH to form the complex that degrades LpxC *via* proteolysis. Therefore, a *lapC* mutant has the LapB-FtsH pathway constantly active, degrades LpxC, and

lacks LPS, while a lethal *lapB* mutant degrades not enough LpxC and has too much LPS whose accumulation in the IM is toxic (Shu & Mi 2022; Guest et al. 2020). It has been shown that overexpression of MarA can suppress the toxicity of *lapC* mutants in a *mla* pathway-dependent way (Maniyeri et al. 2023).

While the mechanical load is balanced by both PG and OM individually, they are also connected by proteins such as the lipoprotein Lpp or Braun's lipoprotein, which has more than 1 million copies per cell and is the most abundant protein in *E. coli* (Braun & Rehn 1969; Li et al. 2014). Lpp forms a covalent bridge between the OM and PG, which determines their distance (Mathelié-Guinlet et al. 2020; Asmar et al. 2017; Cohen et al. 2017) and is important for flagellum assembly (Cohen et al. 2017), stress signal transmission from outer to IM (Asmar et al. 2017) as well as PG function, envelope stiffness and vancomycin sensitivity (Mathelié-Guinlet et al. 2020). In contrast to the covalent PG-Lpp crosslinks, other envelope proteins such as the β-barrel OmpA and the lipoprotein Pal as part of the Tol-Pal complex are involved in noncovalent OM-PG crosslinks (Rojas et al. 2018; Samsudin et al. 2016; Eric et al. 2002).

The PG 'sacculus' assembles in a spatiotemporally controlled multi-step process (Figure 3). The two nucleotide precursors UDP-N-acetylmuramyl pentapeptide and UDP-N-acetylglucosamine are synthesized in the cytoplasm (Barreteau et al. 2008), assembled with undecaprenyl phosphate into lipid II (lipid-anchored disaccharide-pentapeptide monomer subunit) and transferred across the IM (Barreteau et al. 2008; Mohammadi et al. 2011). Undecaprenyl pyrophosphate (Und-PP) is released during polymerization, and glycan chains are inserted into the sacculus. PG glycosyltransferases (GTases) polymerize the glycan chains while transpeptidases (TPases) attach the nascent PG chains to the sacculus, to other chains, or the OM-anchored lipoprotein Lpp by creating peptide crosslinks (Egan et al. 2020; Typas et al. 2012). PG needs to be constantly synthesized and cleaved. This turnover is necessary for cell shape maintenance during growth, division, and bacterial interactions. Cleavage is mainly performed by hydrolases such as DD-, LD- or DL-carboxypeptidases (CPases) that trim peptides, DD- or LD-endopeptidases (EPases) that remove crosslinks, amidases that remove peptides from glycan chains and N-acetylglucosaminidases and N-acetylmuramidases including lysozymes and lytic transglycosylases (LT) that cleave glycan chains (Figure 3) (Vollmer, Joris, et al. 2008; Egan et al. 2020).

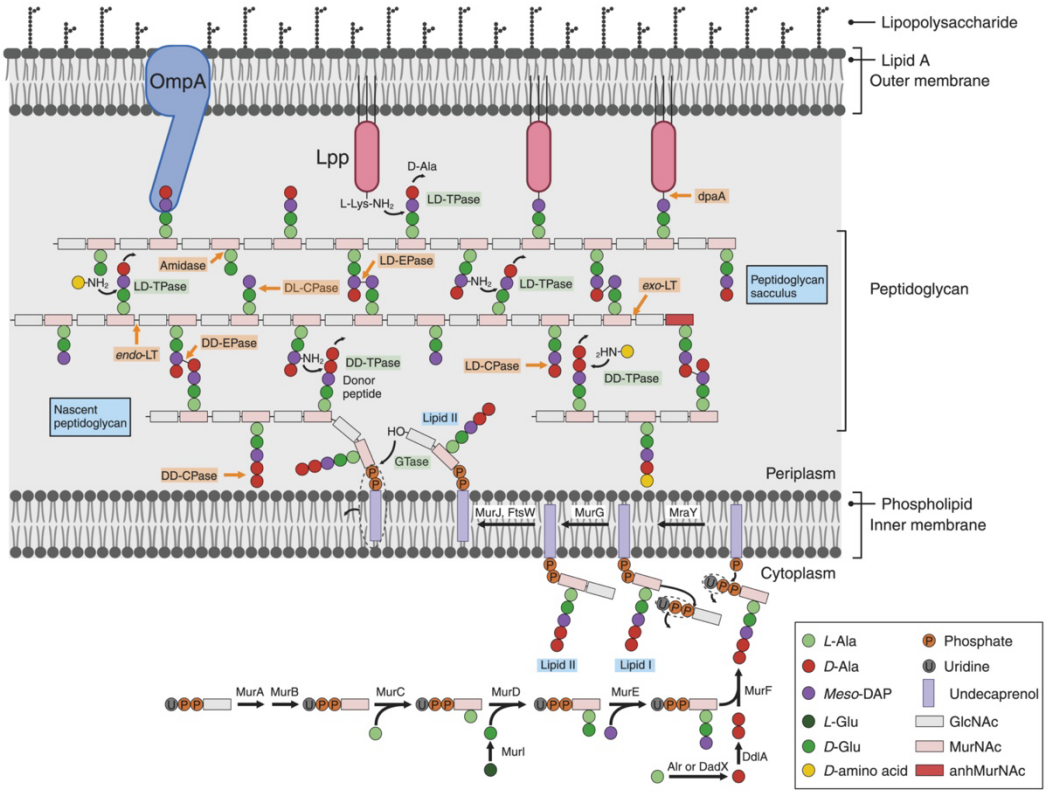

Figure 3: Synthesis, cleavage, and modification of peptidoglycan in Gram-negative bacteria. *Several cytosolic and inner membrane-associated steps are needed to synthesize lipids I and II. Lipid II is flipped across the inner membrane. The nascent peptidoglycan chain is polymerized by glycosyltransferases and attached to other chains or the sacculus by DD-transpeptidases. Carboxypeptidases trim the peptides, lytic transglycosylases cleave the glycan chains, and endopeptidases cleave crosslinks, while amidases remove the peptide from glycan chains. LD-transpeptidases produce crosslinks between peptides or between a peptide and Brain's lipoprotein anchored in the outer membrane. Figure adapted from* (Egan et al. 2020).

In rod-shaped bacteria, at least two multi-protein complexes are required to balance PG biosynthesis during cell division and elongation. The elongasome or Rod complex inserts new material during lateral growth and is guided by the actin homolog MreB. The divisome controls PG biosynthesis during cell division and is guided by the tubulin homolog FtsZ. Penicillin-binding proteins (PBPs) contribute to PG biosynthesis and can be separated into class A (PBP1a, 1b and 1c), B (PBP2 and 3), and C (PBP4(b), 5, 6(b), 7 and AmpH) PBPs (Pratt 2008; Hugonnet et al. 2016). While class A or aPBPs carry both GTase or TPase functions, while monofunctional class B PBPs (bPBPs) are only TPases.

During growth, class A PBP1A forms the elongasome for cell wall elongation by localization to the cell periphery and interaction with the essential class B PBP2 and the essential GTase RodA (Banzhaf et al. 2012; Den Blaauwen et al. 2008). The class A PBP1B interacts with essential cell division proteins such as FtsBLNQW and class B PBP3 to form the septum by

assembling the divisome complex (Bertsche et al. 2006; Den Blaauwen et al. 2008). The OM-anchored Lpo lipoproteins LpoA and LpoB activate the IM-anchored class a PBPs PBP1a and PBP1b (Typas et al. 2010; Paradis-Bleau et al. 2010), respectively, to coordinate PG synthesis between the IM and OM (Typas et al. 2012). While the majority of peptide crosslinks are produced from pentapeptides by PBPs, LD-transpeptidases (LDTs) can attach the OM-anchored Lpp to PG to stabilize the cell envelope (LdtA, LdtB and LdtC) (Magnet et al. 2007) or form LD-crosslinks between two stem peptides in PG (LdtD and LdtE) (Morè et al. 2019; Sophie et al. 2008). LdtF was recently renamed to DpaA (meso-diaminopimelic acid protein amidase A) because of its ability to hydrolyze the Lpp-PG linkage and thereby detach Lpp from PG (Bahadur et al. 2021; Matthias et al. 2021).

This complex interplay of multiple essential components underlines the high interconnectedness of the bacterial cell envelope. It stresses the importance of studying its plasticity to respond to environmental perturbations such as antibiotics. In order to prevent AMR, we need to understand the underlying mechanisms by which resistances evolve and how the genetic background modulates them, as I investigated systematically in this project.

5. Antibiotic resistance evolution

Antimicrobial resistance can be acquired either by *de novo* chromosomal mutations (intrinsic) or by horizontal gene transfer (acquired), where antibiotic resistance elements are received by DNA uptake, phage transduction, or conjugative transfer of plasmids (Sommer et al. 2017). Experimental evolution, as used in this work, explores only intrinsic mutations. Evolution through chromosomal alteration is determined by the probability of a given resistance mutation to occur and the probability of survival in a population before, during, and after antibiotic exposure (Levin-Reisman et al. 2017), which depend on the population size. For example, during cefotaxime resistance evolution, mutants isolated from small populations often had fewer SNPs but instead more SVs than mutants isolated from large populations, showcasing that the type of resistance variants evolved depends on the population size (Schenk et al. 2022).

The population size can be controlled by the volume determining the carrying capacity, *i.e.*, the maximum population size that can be sustained in a given environment. The transfer volume controls the bottleneck and determines the number of cells and low-frequency mutations being transferred. The selective pressure applied by antibiotic exposure influences the type and rate

of mutations that are positively selected during evolution. While antibiotic concentrations above the minimum inhibitory concentration (MIC) select for single genetic events causing high levels of resistance, concentrations below the MIC allow for the accumulation of mutations with small effects, causing a cumulative increase in resistance (Andersson & Hughes 2014; Schenk et al. 2022). Antibiotic resistance evolution is also affected by the number of mutations acquired, which is influenced by the number of generations and the mutation supply rate (the product of effective population size and mutation rate). The number of evolved lineages sets the solution space that can be probed.

Besides positive or negative fitness effects of mutations, antibiotic tolerance, *i.e.*, increased minimum duration to kill without a change in MIC, can facilitate antibiotic resistance evolution (Levin-Reisman et al. 2017), most likely by increasing the fraction of surviving bacteria and thereby the effective population size able to undergo spontaneous mutations. Moreover, although spontaneous mutation rates are approximately 10^{-10} per nucleotide per generation for prokaryotes (Lynch 2010), these rates can be modulated by the genetic background (Ragheb et al. 2019) and external factors like DNA damaging agents (Long et al. 2016; Pribis et al. 2019).

In this thesis, I used experimental evolution to quantitatively investigate the evolution of AMR reproducibly by controlling multiple parameters that influence evolution, which I will discuss next.

6. Experimental evolution to assess AMR

Various studies have characterized the evolutionary capacity of microorganisms to evolve to many distinct conditions. Batch experimental evolution setups grow microorganisms in a fixed volume until the carrying capacity is reached, dilute the culture with a fixed rate into fresh nutrients, and optionally, an additional selective pressure. This process can be repeated to select genotypes well adapted to the conditions by competition of replicating and mutating individuals.

The advantages of batch experimental evolution are the scalability to multiple conditions in parallel and the possibility to start, end, or sample the experiment at any moment. Therefore, batch experimental evolution can be continued indefinitely, as was shown for the Lenski long-term evolution experiment (LTEE), where 12 *Escherichia coli* (*E. coli*) populations have been

evolving for approximately 60.000 generations across 35 years (Lenski & Travisano 1994; Good et al. 2017). These cultures are transferred daily to fresh media and sampled/cryo-preserved every 500 generations (~75 days). Mutants from different time points of the LTEE have been investigated using a variety of different approaches to tracking their evolutionary trajectories, as well as to characterize the accompanying changes in fitness, evolvability, and gene essentiality (Ascensao et al. 2023; Good et al. 2017; Consuegra et al. 2021; Deatherage & Barrick 2014; Deatherage & Barrick 2021).

By tracking the evolutionary trajectories, eco-evolutionary feedback (populations alter the environment, and the environment influences evolution), clonal interference (beneficial mutations in different strains outcompeting each other), and genetic hitchhiking (mutations increasing in frequency due to a different mutation) were observed. The continuous high molecular evolution rate after thousands of generations suggests that adapting genetic backgrounds and emergent ecological interactions change the targets of selection over time, thereby creating novel opportunities for adaptation (Good et al. 2017). Investigating the distribution of fitness effects and gene essentiality of two divergent lineages, one optimized for fast growth on glucose during exponential phase and the other one for stationary phase survival and utilizing acetate, found global diminishing returns epistasis, *i.e.*, a decreasing fitness effects over time, as it has been reported before (Good & Desai 2015; Wiser et al. 2013). They also found a negative frequency-fitness correlation (fitness increases when relative abundance decreases) when competing the lineages across different conditions. In addition, the distribution of fitness effects shows large fitness effects for both detrimental and beneficial rare ecotypes in a frequency-dependent manner (Ascensao et al. 2023).

Methods such as high-resolution lineage tracking by barcode sequencing can be used to create genotype-phenotype-fitness maps. Relevant fitness effects are probable enough to occur repeatedly and fit enough to reach high cell counts. Even though mutant-caused changes in the ecology of the environment can drive frequency-dependent selection, beneficial mutants show mostly frequency-independent fitness effects. Therefore, adaptation in asexually evolving populations is mainly driven by competition of subpopulations arising from many independent beneficial mutations. Even though each mutation is rare, collectively, they can make population dynamics predictable. Although rare, some mutations drive population dynamics more than others, causing a balance between stochastic and deterministic effects (Levy et al. 2015; Venkataram et al. 2016).

Adaptive mutants are locally modular by only modulating a small number of phenotypes, such as the genes and pathways most relevant to the condition-dependent fitness during evolution. In conditions similar to the evolution condition, the genotype-phenotype-fitness map masks the resulting phenotypic complexity of adaptive mutants from natural selection. This phenotypic complexity can be revealed once the fitness effects of adaptive mutants are probed across diverse environments, making them globally pleiotropic despite being locally modular (fitness-relevant modularity) (Kinsler et al. 2020).

Even though small and large populations adapt through similar mechanisms, mutation supply rate differences can result in distinct frequencies and types of mutations evolved. The trade-off between mutation rate and fitness effect of major mutation classes reinforces clonal interference between large-benefit and high-rate mutations, resulting in divergent evolutionary trajectories for populations of different sizes. During cefotaxime resistance evolution, single nucleotide polymorphisms (SNPs) show a lower rate, larger benefits, and a greater adaptive potential than structural variants (SVs), which display a higher rate but whose fitness benefits are limited by their pleiotropic and detrimental off-target effects (fitness-relevant modularity) (Schenk et al. 2022). Also, the genomic context can influence the trade-off between fitness effect and mutation rate. Flanking repeat sequences can facilitate the amplification or deletion of antibiotic-resistance genes through SVs, promoting antibiotic resistance evolution (Sandegren & Andersson 2009). The mutation rate favoring the occurrence of SNPs over SVs can be affected by DNA-repair deficient mutator strains (Gifford et al. 2023; Cox 1976) and in regions where replication and transcription conflict (Million-Weaver et al. 2015).

During continuous experimental evolution, the culture is constantly diluted to control the growth rate and selective pressure, such as antibiotic concentration. This can be achieved either using a morbidostat with continuous control but low throughput (Toprak et al. 2012; Toprak et al. 2013) or robotic automation systems with periodically diluted cultures (every 3-5 h) and medium throughput (Lukačišinová et al. 2020). Quantifying evolvability for ~ 100 KO mutants in *E. coli* identified decreased effects of resistance mutations in backgrounds with higher resistance levels, also called diminishing-returns epistasis, as well as genetic interactions between KO mutants and resistance mutations (Lukačišinová et al. 2020). Systematically uncovering such epistatic interactions between the genetic background and resistance mutations as part of this thesis allowed me to reveal vulnerabilities during the resistance evolution of cefotaxime that can be exploited to delay AMR evolution.

7. Epistasis shapes resistance evolution

The order and type of resistance mutations, the resistance level they provide, and the fitness effects they cause depend on the genetic background defined as the sum of all epistatic interactions (Knopp & Andersson 2018; Trindade et al. 2009; Weinreich et al. 2005; Weinreich et al. 2006). Positive epistatic interactions, *i.e.*, higher fitness than expected by multiplying the fitness effects of two genetic events, can alleviate fitness defects caused by resistance mutations *via* compensatory mutations (Sommer et al. 2017). Negative epistatic interactions, *i.e.*, lower fitness than expected by multiplying the fitness effects of two genetic events, can aggravate such fitness defects and render mutations intolerable. In the most extreme case, the epistatic interactions between two non-essential genes can cause lethal effects, a phenomenon called synthetic lethality (SL) (Dobzhansky 1946; Rancati et al. 2018). SL pairs represent an avenue to exploit genomic weaknesses in bacteria. In addition, as the genetic network affects evolutionary trajectories, evolution can result in an altered wiring of the genetic network in response to a chemical or genetic perturbation (Rancati et al. 2018). Essentiality is an evolvable quantitative property (Liu et al. 2015) that depends on the environment (Nichols et al. 2011) and the genetic background (Rousset et al. 2021). As a dynamic and evolvable property, essentiality likely changes during resistance evolution. I used this concept to systematically identify processes that become essential during cefotaxime resistance evolution in this thesis.

8. Resistance evolution can rewire essentiality

Previous studies on bacterial responses to environmental or genetic perturbations have focussed on characterizing gene-gene and gene-drug interactions. While gene-drug interactions have been mapped systematically (Nichols et al. 2011), systematic studies characterizing the majority of gene-gene interactions, as has been done in yeast (Costanzo et al. 2016), are missing for bacteria even though tools for high-throughput quantification of gene-gene interactions are available (Typas et al. 2008; Gagarinova et al. 2016; Kumar et al. 2016; Babu et al. 2014; Babu et al. 2011). Existing studies have shown that mutants with decreased fitness and increased drug sensitivity have a lower capacity to evolve antibiotic resistance, most likely by reduced growth, thereby reducing effective population size and mutation supply rate, or by gene-drug interactions (Schenk et al. 2022; Nichols et al. 2011; Lukačišinová et al. 2020). A previous study that measured the evolvability of ~100 KO mutants in *E. coli* found that mutants of efflux pumps like *tolC* with increased drug sensitivity and chaperones like *dnaK* with decreased fitness decrease the evolvability of tetracycline resistance. Delayed resistance evolution in

several gene deletion strains was shown to be caused by epistatic interactions with resistance elements (Lukačišinová et al. 2020). One way to quantitatively measure genetic interactions is using CRISPR interference, which I harnessed to measure gene-gene and gene-gene-drug interactions as part of this project.

9. Quantifying epistatic interactions using CRISPR interference

Until recently, the quantification of epistatic interactions was limited to measuring the growth of double deletion mutants of two non-essential genes to infer the strength of epistatic interactions (Typas et al. 2008). The use of knockouts (KO) restricts the quantification of epistatic interaction to non-essential genes, as essential genes cannot be deleted. In addition, epistasis with KOs can only be studied after each gene has been knocked out and the cell has reached a new steady state, without the possibility to study the impact of gene expression levels by titration. Titrating a genetic perturbation allows for studying the dynamics of the cell after depleting one gene. It also allows for adjusting the dynamic range for double genetic interactions even if the double KO is synthetic lethal and entirely prevents growth, which is necessary when the effect of drugs on gene-gene interactions is of interest.

Both challenges can be solved by the discovery of CRISPR (Clustered Regularly Interspaced Short Palindromic Repeats)/Cas9 (CRISPR-associated protein 9) systems. CRISPR interference (CRISPRi) employs a catalytically inactive endonuclease Cas9 from *Streptococcus pyogenes* and a guide RNA (gRRNA) scaffold for sequence-specific transcriptional repression of the expression of a target gene (Qi et al. 2013). CRISPRi has already been used to investigate gene essentiality across diverse *E. coli* species (Rousset et al. 2021) and other species (Liu et al. 2023), as well as to study genetic interactions of essential genes with non-essential genes in KO or transposon libraries (Rachwalski et al. 2024; Jana et al. 2023).

10. Shortcomings and unknowns of current approaches

Even though the effects of non-essential genes on antibiotic resistance have been mapped systematically (Nichols et al. 2011), resistance alone only provides a snapshot. It does not predict antibiotic treatment success well since it neglects the evolutionary time component. In order to accurately portray the plasticity of the genome to overcome environmental perturbations and systematically identify genes contributing to the evolutionary capacity, we

need to probe a genome-wide KO library during antibiotic resistance evolution. Pre-selecting genes for such assays provides a good starting point to probe the accuracy of our current understanding (Lukačišinová et al. 2020). However, such assays must be performed unbiasedly to find the most critical evolvability genes conditional-essential during antibiotic resistance evolution. A genome-wide KO library would allow for this, as has been done before for other complex phenotypes (Cacace et al. 2017; Nichols et al. 2011), but it poses technical challenges. To overcome this challenge, I developed a method for the experimental evolution of a genome-wide *E. coli* KO library against the cell wall targeting antibiotic cefotaxime and identified several gene KO mutants that delayed or accelerated resistance evolution in Chapter II. In Chapter III, I discovered two evolvability gene KO mutants with delayed resistance evolution that interact with cefotaxime resistance mutations *via* epistatic gene-gene and gene-gene-drug interactions. Also, in Chapter III, I investigated the molecular mechanism underlying these interactions using quantitative genetics, proteomics, high-throughput imaging, and evolution against multiple antibiotics. I discovered that the identified evolvability genes are required for the resistance evolution of multiple antibiotics and used the uncovered vulnerabilities in resistant mutants to delay resistance evolution with drugs.

Furthermore, we need more methods to quantitatively measure genetic interactions in the presence or absence of antibiotics across multiple genetic backgrounds. Even though double deletion mutants can be used to measure interactions of two non-essential genes in high-throughput (Typas et al. 2008), existing methods are a) limited to non-essential genes, b) cannot be titrated but require two deletions, so they decrease the dynamic range to study the interaction, *e.g.*, in the presence of a chemical perturbation, and c) require specific genetic setups of the crossing strains. Developing such a tool would allow us to quantitatively dissect interactions between evolvability genes and resistance elements and map genome-wide epistasis of essential antibiotic targets and resistance genes with all non-essential genes, which I did in Chapter IV. Using high-density colony arrays, I developed an approach based on CRISPRi to measure the global epistasis of an antibiotic target and resistance element with all non-essential genes. I discovered negatively interacting genes that represent vulnerabilities in the genetic network and can be used to prevent resistance evolution or increase antibiotic effectiveness. Combining genome-wide experimental evolution developed in Chapter II with genome-wide epistasis developed in Chapter IV allowed me to systematically map the genomic landscape of resistance evolution at unprecedented resolution. Applying multiple follow-up methods in Chapter III revealed potential molecular mechanisms underlining such interactions.

Chapter II: Establishing a method for high-throughput experimental evolution

Chapter II: Establishing a method for high-throughput experimental evolution

1. Summary

Antimicrobial resistance is a major challenge for humanity, and our understanding of the genetic dependencies accompanying resistance evolution is limited. The genetic background can promote the evolution of AMR, *e.g.*, through increased mutagenesis (Ragheb et al. 2019) or delay it through negative epistasis with resistance genes (Lukačišinová et al. 2020). However, the number of genetic backgrounds that can be tested for such effects is limited due to the low throughput of existing experimental evolution methods. Reverse-genetics approaches have been powerful in assigning novel gene functions and annotating genetic modules for complex phenotypes by testing KO or overexpression libraries under diverse conditions. This chapter describes my effort to perform experimental evolution with the genome-wide KO library of *E. coli* against the commonly used antibiotic cefotaxime. Through epistatic interactions, such gene KO mutants can either interact with a resistance gene and modulate its fitness levels (gene-gene interaction) or interact with a resistance gene in the presence of cefotaxime and modulate its resistance levels (gene-gene-drug interactions) (Figure 4a). The goal is to identify non-essential gene KOs that modulate resistance evolution through epistatic interactions using AMR evolvability as a readout (Figure 4b). As a well-studied model organism, I choose *E. coli* since extensive tools of genetic manipulation (Typas et al. 2008), detailed knowledge about the genomic organization, gene annotations, as well as genome-wide chemical genetics (Nichols et al. 2011), and metabolomics (Fuhrer et al. 2017) datasets were available, allowing the systematic analysis of potential findings. Chemical genetics has been used to assess antibiotic resistance and sensitivity across non-essential KO mutants (Nichols et al. 2011), which can be compared to their evolvability. Furthermore, *E. coli* caused more global deaths associated with and attributable to AMR than any other bacterial pathogen in 2019. Hence, understanding resistance evolution in *E. coli* is paramount (Murray et al. 2022).

To establish a method for genome-wide experimental evolution, I first performed extensive preliminary testing to identify the optimal experimental evolution conditions and antibiotic to be tested. Once I identified these conditions, I evolved cefotaxime resistance in the ~ 4,000 mutants of the genome-wide *E. coli* KO (Yamamoto et al. 2009; Baba et al. 2006), including all non-essential genes. This chapter describes the experimental and computational details of the optimization process, screen design, analysis workflow, validation of identified hits, and

the results which gene KOs displayed an increased or decreased evolvability of antibiotic resistance (Figure 4).

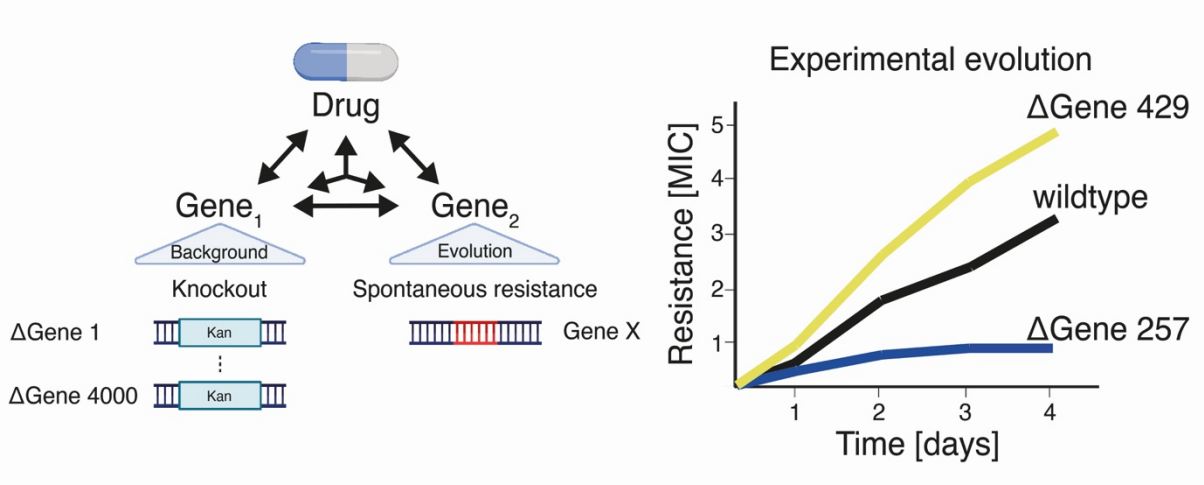

Figure 4: Identifying gene-gene and gene-gene-drug interactions delaying resistance evolution. *Gene-gene and gene-gene-drug interactions between evolved resistance elements and the genetic background modulate the evolvability of antibiotic resistance. Such genetic interactions can delay resistance evolution by negative epistasis with resistance elements or accelerate resistance evolution by positive epistasis with resistance elements.*

2. Contributions

Dr. Michael Knopp (EMBL) contributed to the planning, designing, and interpreting of the evolution experiments. I conducted all other experimental and computational work presented in this chapter. Dr. Michael Knopp (EMBL), Dr. Athanasios Typas, and I conceived the experimental design and method for preliminary testing, the genome-wide screen, and the validation experiments. Dr. Athanasios Typas and myself discussed the pipeline for data analysis and visualization.

3. Using genome-wide experimental evolution to uncover epistatic interactions

To measure the global epistasis of resistance elements with every non-essential gene, I wanted to systematically determine the impact of each non-essential gene KO on resistance evolution rates in *E. coli*. I used a reverse genetics approach with antibiotic resistance evolvability as a readout (Cacace et al. 2017). First, I needed to develop an assay capable of high-throughput experimental evolution of the gene knockout library 'KEIO collection' (~4,000 in-frame single-gene knockouts) (Baba et al. 2006; Yamamoto et al. 2009). To reach the throughput of ~24,000 evolution experiments (6 replicates of ~4,000 KO mutants) spanning several days, I assessed resistance evolvability by a short-term evolution experiment with daily passages under increasing antibiotic concentrations.

3.1. Preliminary testing identified the optimal evolution conditions and antibiotic

To assess the role of ~4,000 gene KO mutants on the ability of *E. coli* to evolve antibiotic resistance, I needed an adjustable high-throughput experimental evolution setup. Factors that influence the outcome of experimental evolution are (i) the number of cells (population size), which are limited by the carrying capacity and the total volume of media, (ii) the population bottleneck, defined by the inoculum and volume used, (iii) the selective pressure, defined by the steps in the gradual increase in antibiotic concentration and (iv) the mutation supply rate, which in addition to population size and bottleneck, it is also affected by the mutation rate and the number of possible solutions (*i.e.* mutations that provide resistance). Furthermore, experimental evolution is influenced by (v) the media (in our case, Mueller Hinton Broth (MHB), which is used for clinical antibiotic susceptibility testing), (vi) the number of generations, defined by the bottleneck and the periodic transfer (in our case daily) and (vii) the number of replicates that sets the number of possible solutions tested.

I performed several pilot experiments to determine the optimal high-throughput conditions to identify gene KO mutants with accelerated or delayed AMR evolvability. Therefore, I tested different antibiotics, plate types, population sizes limited by the total volume, increases in selective pressure set by the antibiotic concentrations, and population bottlenecks determined by the dilution. Primary constraints were the number of plates and experiments needed to test ~4,000 KO mutants in 6 replicates across several days and the maximum volume per plate limiting the population size. Since I had to perform the evolution experiment with 12 384-well plates in 6 replicates (72 plates), I prioritized a short experimental evolution workflow of a maximum of 6 days.

To decrease bottleneck effects and increase population size and mutation supply rate, I determined the maximum volume for each plate, 1 ml in a 96-deep well plate and 150 µl for a 384-deep well plate, and the necessary centrifugation steps to reduce cross-contamination before and after every liquid transfer and exchange of the breathable membrane. In a second step, I tested how the wildtype and a *dnaK* KO, reported to show a decreased ability to evolve resistance against tetracycline (Lukačišinová et al. 2020), evolved resistance against various antibiotics. I used two a selective pressure of 2- or 3-fold daily increase in antibiotic concentration in 384-deep well plates, 150 µl volume, and a 1:25 dilution (Figure 5). The 1:25 dilution limits the experimental evolution to 4-5 generations at each concentration. Even

though 4-5 generations is less than used in traditional experimental evolution in flasks and limits the number of evolved mutations, I chose this dilution to ensure that the robot can reproducibly transfer the volume and that enough cells, including low-frequency mutations, are transferred.

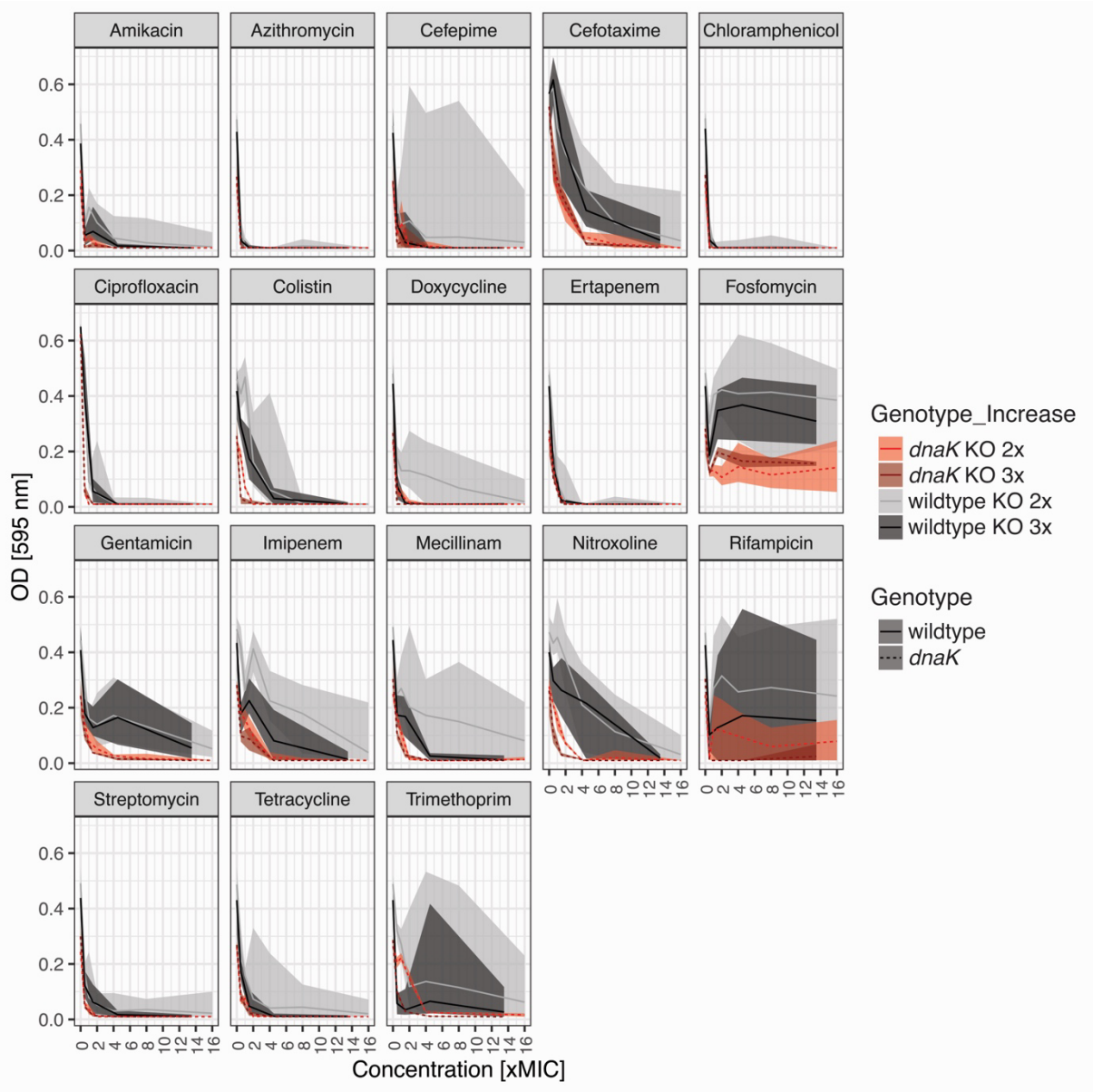

Figure 5: Evolving antibiotic resistance against multiple antibiotics. *Antibiotic resistance was evolved in several wildtype and dnaK KO mutant replicates against 18 different antibiotics in 384-well plates using 150 µl volume per well and a 1:25 dilution every 24 h. $OD_{595\ nm}$ is shown, and large differences can be observed across antibiotics. Both wildtype and the dnaK KO mutant failed to evolve resistance against azithromycin and chloramphenicol but evolved rapidly full resistance against fosfomycin and rifampicin. Gentamicin, imipenem, nitroxoline, and cefotaxime showed intermediate resistance levels, which were optimal for the high-throughput experimental evolution screen. The dnaK KO mutants grew to a lower yield ($OD_{595\ nm}$) and exhibited a lower capacity to evolve resistance.*

My first objective was to see detectable growth up to 2-6x minimum inhibitory concentration (MIC) in the wildtype to identify KO mutants with delayed evolution that grow to significantly lower yields than the wildtype at these concentrations. My second objective was to see the extinction of most populations at 10-12x MIC to identify KO mutants with accelerated evolution that grow to significantly higher yields than the wildtype at these concentrations. Meeting both objectives would allow me to identify both KO mutants with decreased and increased capacities to evolve resistance, the former characterized by low growth at 2-6x MIC and the latter by better growth than wildtype at 10-12x MIC within the same experimental workflow. Different antibiotics showed different evolutionary trajectories, which I will discuss hereafter.

For rifampicin and fosfomycin (plus the addition of glucose-6-phosphate to allow import), there were easily accessible evolutionary trajectories available providing high levels of resistance, target *rpoB* mutations for rifampicin (Jin & Gross 1988), and *glpT*/*uhpT* mutations in the transporters or *murA* mutations in the target of fosfomycin (Castañeda-García et al. 2013). Using antibiotics with easily accessible high-resistance trajectories prohibited identifying better evolving KO mutants since only a few of the lineages stopped growing at concentrations above 10x MIC, which is why those drugs were not further considered for the main screen of this thesis. As the mutational supply is high and concentrated mainly on the target, these drugs are well suited to study epistatic interactions of KO mutants with the antibiotic target since epistatic interactions may be more concentrated.

For other antibiotics, such as azithromycin, doxycycline, chloramphenicol, and ertapenem, resistance could not evolve under the chosen conditions, which excluded them as candidates for the screen. Possible explanations are the low population size and low number of generations that limit the number of low-frequency mutations. Given my two objectives (high yield at 2-6x MIC and no growth at 10-12x MIC for the wildtype), optimal candidates for resistance evolution under the conditions used were cefotaxime, nitroxoline, gentamicin, imipenem, mecillinam, and colistin, with the first three showing the largest difference between the wildtype and the *dnaK* KO at 3x antibiotic increase (Figure 5).

This difference in OD between a mutant known to evolve resistance slower and the wildtype defines the assay's dynamic range to quantify evolvability and identify other gene KO mutants in the library that do so. My primary decision criteria for selecting an antibiotic were (i) the

dynamic range between wildtype-like and worse evolving KO mutants and (ii) the extinction of most populations at 6-10x MIC to identify better evolving KO mutants within a feasible number of transfers. Other decision criteria included (iii) clinical relevance, (iv) widespread use of the antibiotic, (v) multiple available resistance mechanisms, and (vi) a diverse antibiotic class, ideally with multiple sub-classes to determine the specificity of evolvability genes required during antibiotic resistance evolution. To probe the dynamic range more concretely across different mutants, I decided to use cefotaxime, which matches those criteria best, as well as ciprofloxacin, which matches all categories except the large dynamic range, for a comparison of different volumes, selective pressures, bottlenecks, and genetic backgrounds (Figure 6). In this second pilot experiment, I tested eight single-gene KO mutants in 7 biological replicates and the wildtype strain in 21 replicates for up to 9 days (Figure 6). All cultures started with 24 h growth without the drug (day 0), followed by 0.5x wildtype MIC of cefotaxime or ciprofloxacin (day 1) and the respective antibiotic increase strategy (2x/3x). I selected the KO mutants to include controls reported to delay resistance evolution of tetracycline (*dnaK* and *tatC*) (Lukačišinová et al. 2020), accelerate resistance evolution to all antibiotics (*mutL*) (Cox, 1976), involved in the general stress response, antibiotic tolerance and stationary phase survival (*rpoS*) (Lucinda et al. 2002; Gutierrez et al. 2013; Deter et al. 2021), and provide resistance to both antibiotics (*ompR*) (Yoshida et al. 2006).

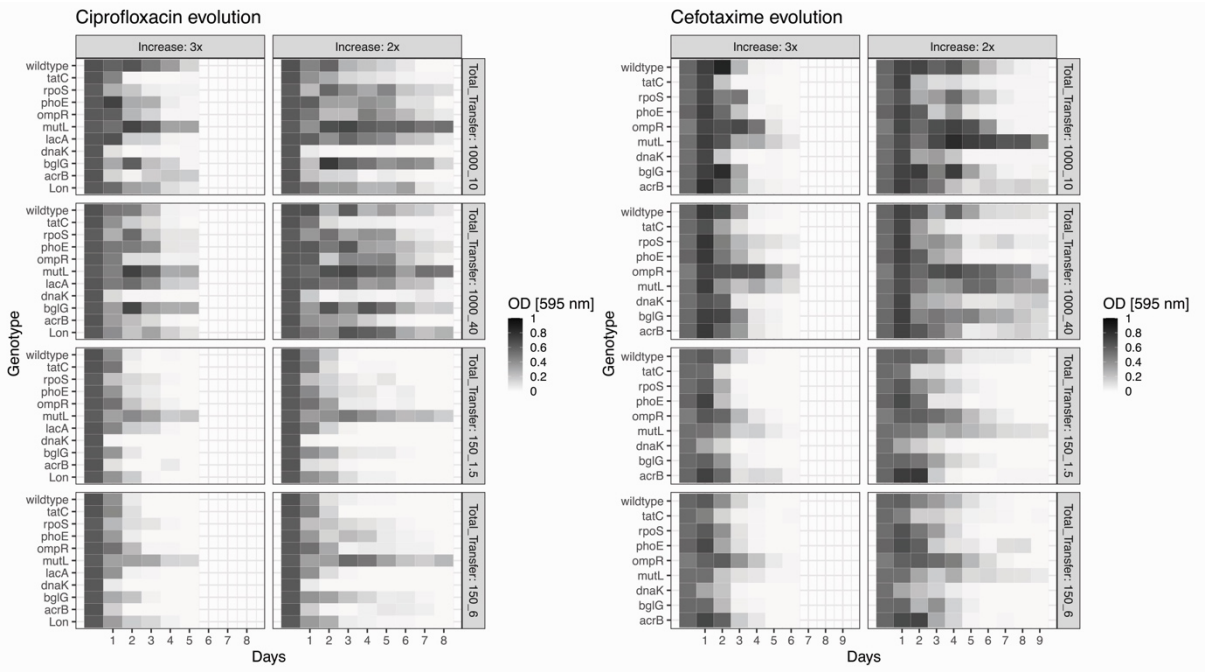

Figure 6: Evolving antibiotic resistance against cefotaxime and ciprofloxacin under multiple conditions. *Antibiotic resistance was evolved in several replicates of a wildtype and several KO mutants against cefotaxime and ciprofloxacin. Different total volumes 1000 µl (96-well plate) and 150 µl (384-well plate), transfer volumes 40 µl and 10 µl for 1000 µl (96-well plate), and 6 µl and 1.5 µl for 150 µl (384-well plate) corresponding to a 1:25 and 1:100 dilution, as well as 2x and 3x antibiotic increases per day were compared to identify the optimal conditions for the high-throughput experimental evolution screen. Evolving resistance against cefotaxime using 1:25 dilution and a 3x antibiotic increase in 384-well plates represents the optimal trade-off between the dynamic range to identify changes in evolvability and throughput.*

In summary, experimental evolution against cefotaxime led to better resistance evolution (higher antibiotic concentrations) than against ciprofloxacin (Figure 6), which is in line with the resistance evolution experiment against multiple antibiotics (Figure 5). Increasing the selective pressure from 2x to 3x increase in drug concentration per day prevented the growth of most mutants at days 4-5 instead of 6-8, shortening the experiment from 9 to 6 days (Figure 6). Interestingly, mutants reached similar resistance levels in both the 3x increase (5-6 days) and the 2x increase (8-9 days), which suggests that the step increase poses no bottleneck and that single mutations are likely leading to final resistance without time or room to evolve higher resistance. That supported using a 3x increase in antibiotic increase pressure to gain equivalent information with a shorter experimental duration. I probed 1:100 and 1:25 as bottlenecks to quantify the trade-off between transferring more cells, including rare mutations, and allowing more generations, resulting in more mutations. The larger 1:25 bottleneck increased evolutionary capacity, visible by growth at the next higher antibiotic concentrations for many evolved mutants with otherwise identical conditions. The transfer of more cells likely resulted in a more diverse population, including rare mutations, being transferred, and thereby allowed the populations to grow at higher antibiotic concentrations. These findings suggest that the

population bottleneck is more important than the capacity to build new mutations in the small volumes I used.

The larger volume of 1000 µl in 96-deep square well plates allowed more mutants to evolve higher antibiotic resistance levels and grow at higher antibiotic concentrations than those in 150 µl in 384-deep well plates (Figure 6). The population size and the bottleneck are larger in larger volumes despite using the same dilution, increasing the mutation supply rate.

Although the results in 384-well plates provide less resolution, differences in evolvability of the mutant controls are almost as discernible as for 96-well plates, *i.e.*, tatC and *dnaK* KO mutants stopping growth reproducibly and significantly earlier than wildtype (Figure 6) (adjusted p-value = $7.3e^{-6}$ with BH-adjusted Wilcoxon signed-rank test for 1:25 bottleneck and 3x increase for both 96-well and 384-well plates). The key differences were the higher ODs and resistance levels reached during cefotaxime than during ciprofloxacin resistance evolution, which determined the dynamic range of the final screen. Based on the discussed parameters, I selected 384-deep well plates with 150 µl volume, 1:25 bottleneck, 3x increases of the selective pressure, and cefotaxime as the antibiotic since these conditions allowed me to identify mutants significantly delaying and accelerating resistance evolution compared to wildtype while maximizing feasibility in a high-throughput setup. Given these conditions, I could finally perform the evolution experiment for six replicates of 800 mutants in 6 days and the whole library in 30 days. Given that resistance evolution is a stochastic process, *i.e.*, different lineages acquire different resistance mutations, the use of multiple replicates (minimum of four and optimum of six as determined by power analysis) is necessary to identify KO mutants with delayed and accelerated resistance evolution across multiple lineages carrying different resistance mutations that provide different resistance levels.

3.2. Evolving cefotaxime resistance in the genome-wide KO library

After determining the optimal protocol to quantify evolvability, I screened the complete KEIO library. I first pinned the KEIO library on agar plates for overnight growth before I grew six replicates of 800 mutants in 12 384-deep well plates sealed with a breathable membrane for two daily passages in MHB to determine growth defects already present in the absence of antibiotics. This was followed by daily passages at 3-fold increasing antibiotic concentrations starting at 0.5x MIC with shaking at 600 rpm and 37 °C (Figure 7a). After every 24 hours of

growth, I diluted the culture 1:25 dilution into a new plate with a higher antibiotic concentration, which I repeated daily. I measured growth by $OD_{595\ nm}$ in every well daily before the transfer to determine if resistance could evolve for each KO mutant. To systematically identify single-gene (non-essential) KOs delaying resistance evolution, I performed the proposed experimental workflow for ~4,000 gene KO mutants in 4-8 replicates for six days. Full details on the methodology can be found in Chapter VI.

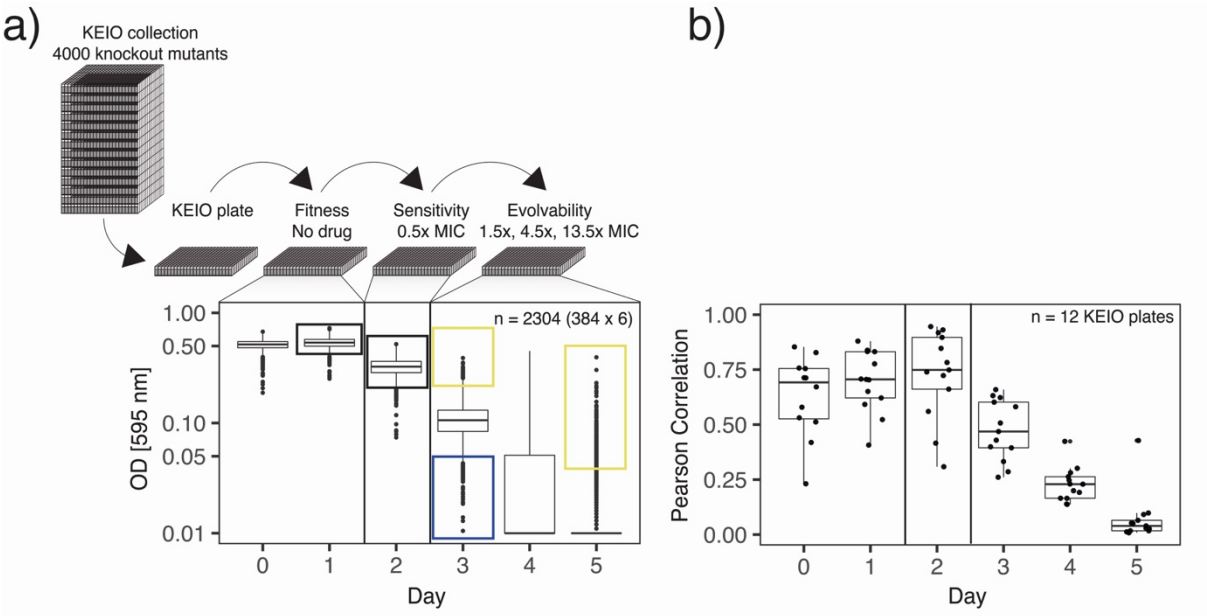

Figure 7: A method for genome-wide experimental evolution. *a) The resistance evolvability of every non-essential KO mutant against cefotaxime was quantified using high-throughput experimental evolution. Scheme to visualize the experimental workflow, including days used for the calculation of fitness and sensitivity for each mutant, as well as the identification of lower (blue) and higher (yellow) evolvability quantified by log_2(fold-change). $OD_{595\ nm}$ is shown. n_{plate} = 384 wells * 6 replicates. Each dot represents one mutant strain lacking a single gene. b) The replicate correlation per day across all 12 tested KEIO library plates is shown and was calculated for each mutant per plate by Pearson correlation of each replicate with all other replicates. The replicate correlation drops for later days since only a subset of the 6 lineages can grow.*

Generally, strains grew to their highest $OD_{595\ nm}$ on the second day without the drug (day 1) and showed a slight decrease in $OD_{595\ nm}$ with 0.5x MIC of cefotaxime on day 2 (Figure 7a). At 1.5x MIC, most mutants could still grow, while some only reached a significantly lower $OD_{595\ nm}$. Other mutants grew better than the average mutant. This dynamic range allowed me to identify genes whose KOs hinder or promote resistance evolution. The first step of the evolution experiment represents a selection for existing resistance mutations rather than the evolution of new mutations. This explains why population size and bottleneck affected resistance evolution more than the number of generations in the pilot experiments. Due to the stochastic nature of the experiment with different lineages evolving different resistance mutations that provide different resistance levels, about half of the replicates of most mutants

stopped growing at 4.5x MIC (day 4), and nearly all replicates of all mutants at 13.5x MIC (day 5), which made it possible to identify the best evolving KO mutants by their higher $OD_{595\ nm}$ at 13.5x MIC (Figure 7a). In order to identify better and worse evolving KO mutants, I devised a data analysis strategy taking the fitness and sensitivity of every mutant into account.

3.3. Analyzing the dataset to identify gene deletions affecting only evolvability

The fitness and drug sensitivity of KO mutants can be confounding factors for resistance evolution experiments. Not accounting for those factors results in identifying mutants that affect these processes and, hence, the evolution trajectories (Figure 8). To focus on evolvability specifically, I calculated fitness and sensitivity using background-subtracted yield measured by $OD_{595\ nm}$ for each KO mutant relative to their respective plate. I estimated fitness from the yield in drug-free MHB (day 1) relative to all other mutants of their respective plate. Drug sensitivity I calculated from the yield in 0.5x MIC (day 2) of cefotaxime relative to the fitness (yield in MHB at day 1), also relative to all other mutants of their respective plate (Figure 7a). I multiplicatively adjusted medians in media, 0.5x MIC, and 1.5x MIC across plates.

Mutants with worse capabilities for resistance evolution I identified by comparing $OD_{595\ nm}$ at 1.5x MIC (day 3) with all other mutants of their plate, and mutants with better capabilities for resistance evolution by comparing growth at 1.5x MIC (day 3) or 13.5x MIC (day 5) with all other mutants of their plate. I calculated the effect size of evolvability using the $\log_2$(fold-change) (L2FC) and the significance based on $OD_{595\ nm}$ of all replicates for each mutant relative to its respective plate using a BH-adjusted non-parametric Wilcoxon signed-rank test due to the non-normality of the individual plate's OD distribution. Also, independently evolved lineages carrying different resistance elements required us to use a non-parametric test due to non-normality and varying variance. I multiplicatively scaled the L2FC across all plates for day 2 to have the same standard deviation to compare the effect size across different KEIO plates probed in different experiment runs using different media batches. Replicate correlation per day across all tested KEIO plates, calculated by the Pearson correlation of each replicate with all other replicates per mutant, was on average 0.7 in media and 0.5x MIC and dropped at higher antibiotic concentrations as expected for a stochastic process such as resistance evolution (Figure 7b). This drop can be explained by independent lineages evolving different resistance mutations that provide different resistance levels.

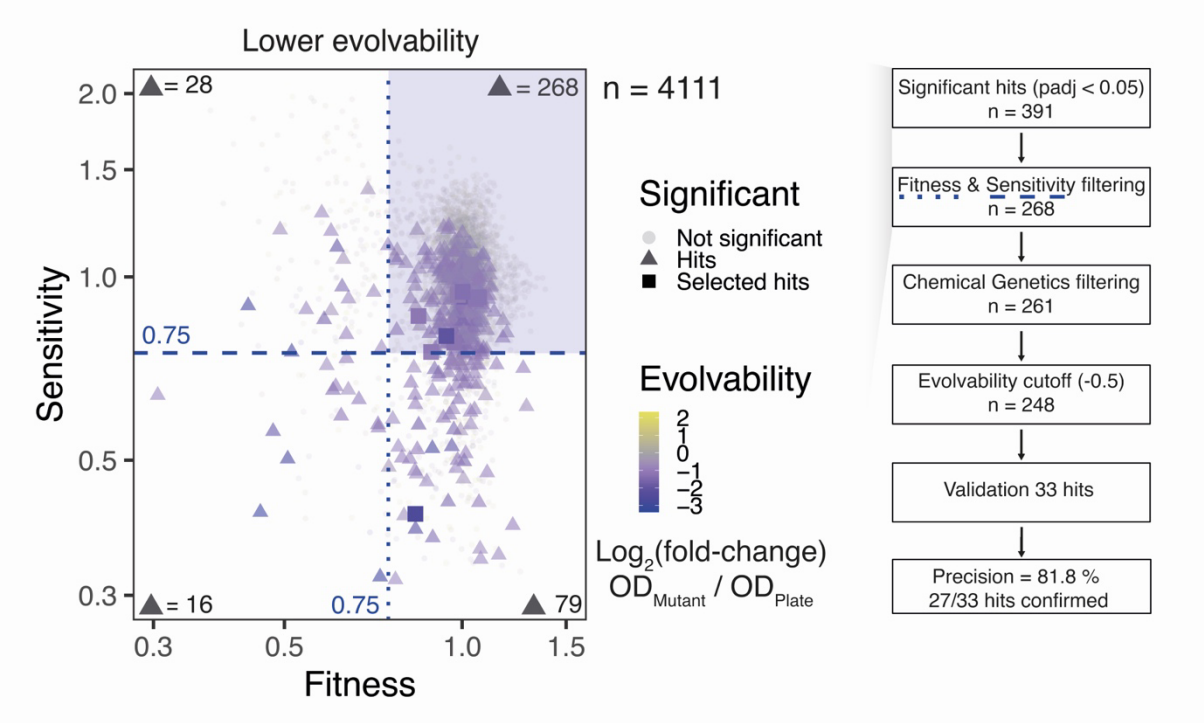

Figure 8: Identifying gene deletions with decreased cefotaxime evolvability. *Scheme of the data processing workflow to focus on epistatic interactions of resistance elements that arise during resistance evolution. Filtering out genes with decreased fitness or increased drug sensitivity identified genes with only decreased evolvability. Additional filtering steps of known suppressor mutants, chemical genetics filtering, and an effect size cut-off on evolvability reduced the final set of hits with decreased evolvability to 248. Of these 248 hits, 33 were validated with a precision of 81.8% in more replicates and larger volumes.*

To identify mutants with worse evolvability, I filtered out 123 hits that displayed low fitness or high sensitivity (Figure 8), *i.e.*, relative fitness and sensitivity lower than 0.75 based on reported decreased fitness or increased sensitivity (Nichols et al. 2011) (thresholds are indicated by blue dashed lines in Figure 8). Therefore, dark blue colored KO mutants in the top right quadrant in Figure 8 could not evolve cefotaxime resistance as well as the wildtype without exceeding the thresholds for decreased fitness or increased sensitivity towards cefotaxime. Hence, these genes are conditionally required or essential during cefotaxime resistance evolution and potentially engage in gene-gene or gene-gene-drug interactions with cefotaxime resistance genes.

As an additional filtering step, I removed seven KEIO library mutants from the final hits that contain potential compensatory mutations based on our lab database. I also confirmed the stringency of our sensitivity cut-off by testing that none of the hits displayed large negative chemical genetics scores (< -2 standard deviations) for cefoxitin and ceftazidime, two compounds from a similar drug class as cefotaxime (Nichols et al. 2011). Finally, I applied a L2FC threshold for the $OD_{595\ nm}$ at 1.5x MIC to be lower than -0.5 to prioritize hits with the highest effect sizes (Figure 8). The top 50 genes with decreased evolvability at 1.5x MIC can

be found in Supplementary Table 1. Since the experimental conditions were selected to maximize feasibility in a high-throughput setup, I probed whether the hits were condition-specific and whether compensatory mutations in the library mutants may have caused some of the observed evolvability effects.

4. Validating hits in larger population sizes confirms conserved epistasis

For the validation, I evolved cefotaxime resistance in more replicates and larger volumes in 96-well plates while keeping the 1:25 bottleneck. The resulting larger population sizes and bottlenecks allowed me to assess how condition-specific the identified 'evolvability genes' were, *i.e.*, genes required for resistance evolution (Figure 9). Therefore, the validation tests whether potential epistatic interactions between the evolvability gene KOs and the resistance trajectories that delay evolution still show an effect when rarer evolutionary trajectories are accessible. Out of the 248 genes I identified in my screen, I selected 33 functionally diverse hits for validation based on literature, gene ontology, protein complex, and functional information. For the validation experiment, I performed the experimental evolution of two independently constructed KEIO library stocks with eight biological replicates, each in 1 ml volume and 96-well plates, while keeping the concentration steps and the 1:25 dilution used in the screen (Figure 9). Testing two independent KEIO library stocks assessed the effects of potential compensatory mutations preexisting in the specific KEIO library clone used for the screen (the same mutations rarely exist in two independently constructed mutants). I labeled a hit as validated when both clones displayed a lower yield than the wildtype at 4.5x MIC determined by the BH-adjusted Wilcoxon signed-rank test. I chose the concentration of 4.5x MIC since the wildtype still grew well at 4.5x MIC in 1 ml while mutants with decreased evolvability could not grow, whereas this step was reached at 1.5x MIC in 384-well plates. This was likely caused by the larger population size and bottleneck in 1 ml volume, likely resulting in a larger diversity of the population and the increased transfer of low-frequency variants.

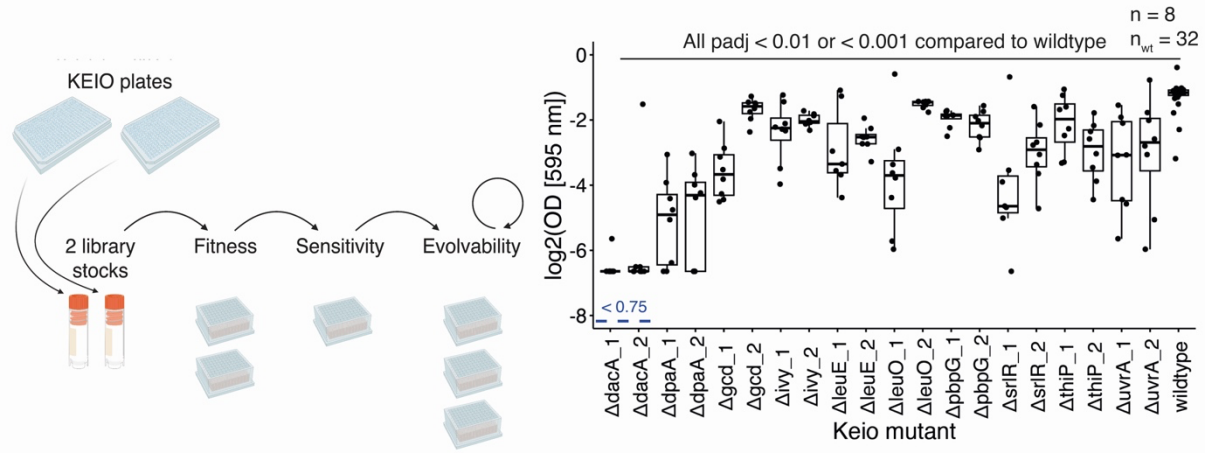

Figure 9: Validation of gene deletions with decreased evolvability in large volumes. *Validation workflow and data of two independent KEIO library clones with 8 replicates are shown for ten evolvability gene KO mutants. Antibiotic increases and bottlenecks otherwise mirrored the setup of the genome-wide screen (Figure 7). $Log_2(OD_{595\ nm})$ at 4.5x MIC is shown, and significance was assessed using the BH-adjusted Wilcoxon signed-rank test. Data for all mutants is shown in Supplementary Figure 1.*

For 27 out of 33 mutants, both independent clones could not evolve as high antibiotic resistance as the wildtype. For 5 out of 33 mutants, this was the case for one of two clones, and for one mutant, neither clone showed the expected effect. Overall, this indicated a precision of 81.8 % for my screen when using more standard experimental evolution conditions and in more replicates (Figure 9). The data for all mutants is shown in Supplementary Figure 1. For further mechanistic investigation, I selected ten evolvability gene KOs (called 'Selected Hits' in subsequent plots) spanning diverse biological processes (Δ*dacA*, Δ*dpaA*, Δ*gcd*, Δ*ivy*, Δ*leuE*, Δ*leuO*, Δ*pbpG*, Δ*srlR*, Δ*thiP* and Δ*uvrA*).

They included several cell wall related genes involved in peptidoglycan-Braun's lipoprotein (PG-Lpp) cleavage (Bahadur et al. 2021; Matthias et al. 2021) (*dpaA*), inhibition of lytic transglycosylases (LTs) (Clarke et al. 2010; Monchois et al. 2001) with a second function in mediating the folding of periplasmic proteins under stress (Lennon et al. 2015) (*ivy*), hydrolyses of D-alanyl-DAP amide bonds within murein crosslinks (Romeis & Höltje 1994) (*pbpG*). One group of genes was involved in the metabolism, including a proton-motive-force dependent leucine exporter (Kutukova et al. 2005) (*leuE*), regulation of leucine biosynthesis (Chen et al. 2005; Chen et al. 2001), stringent response (Majumder et al. 2001) and multi-drug resistance (Tomohiro et al. 2009) (*leuO*), and thiamine transport (Webb et al. 1998) (*thiP*).

Other genes were involved in oxidation-reduction, such as oxidizing glucose and feeding electrons into the respiratory chain (van Schie et al. 1985) (*gcd*), carbon utilization (Yamada &

Saier 1988; Yamada & Saier 1987) (*srlR*), as well as nucleotide excision repair (Wagner et al. 2009) and persister formation (Wilmaerts et al. 2022) (*uvrA*). Additionally, I included one mutant below the sensitivity threshold (*dacA*) that catalyzes the cleavage of the carboxy-terminal D-alanine from PG pentapeptides (Spratt & Strominger 1976; Matsuhashi et al. 1979; Sauvage et al. 2008). I included *dacA* due to its role in PG remodeling, which is functionally connected to cefotaxime that targets PG biosynthesis. The *dacA* mutant had a strong evolvability defect but was also below the sensitivity threshold I set.

To validate whether sensitivity is a good proxy for the MIC and to determine how sensitive our relative sensitivity threshold was in removing evolvability genes with increased sensitivity, I independently measured the MICs of the 27 validated evolvability genes, including *dacA*, in MHB media (Figure 10). The MIC was determined as the concentration where the background subtracted $OD_{595\ nm}$ was below 0.1 after 9 hours of growth. Four out of 28 KO mutants had a MIC 2-fold lower than the wildtype, namely *dacA* with a sensitivity lower than 0.75 and *aegA*, *chaA*, and *chaB* with a sensitivity between 0.75 and 0.85. These three mutants, *aegA*, *chaA*, and *chaB*, represent false positives that were more sensitive to cefotaxime as determined by their decreased MIC (Figure 10) but were missed by the sensitivity threshold (> 0.75) as determined from the screen data (Figure 7 and 8). Since the remaining six out of 28 with a sensitivity between 0.75 and 0.85 shared the MIC with the wildtype, the sensitivity cut-off of 0.75 was well chosen to reflect the MIC (Figure 10). In this test, I also included several controls for gene KOs providing cefotaxime resistance, such as *marR* and *waaQ* (2x MIC), as well as *ompF* and *ompR* (4x MIC), which will be discussed later.

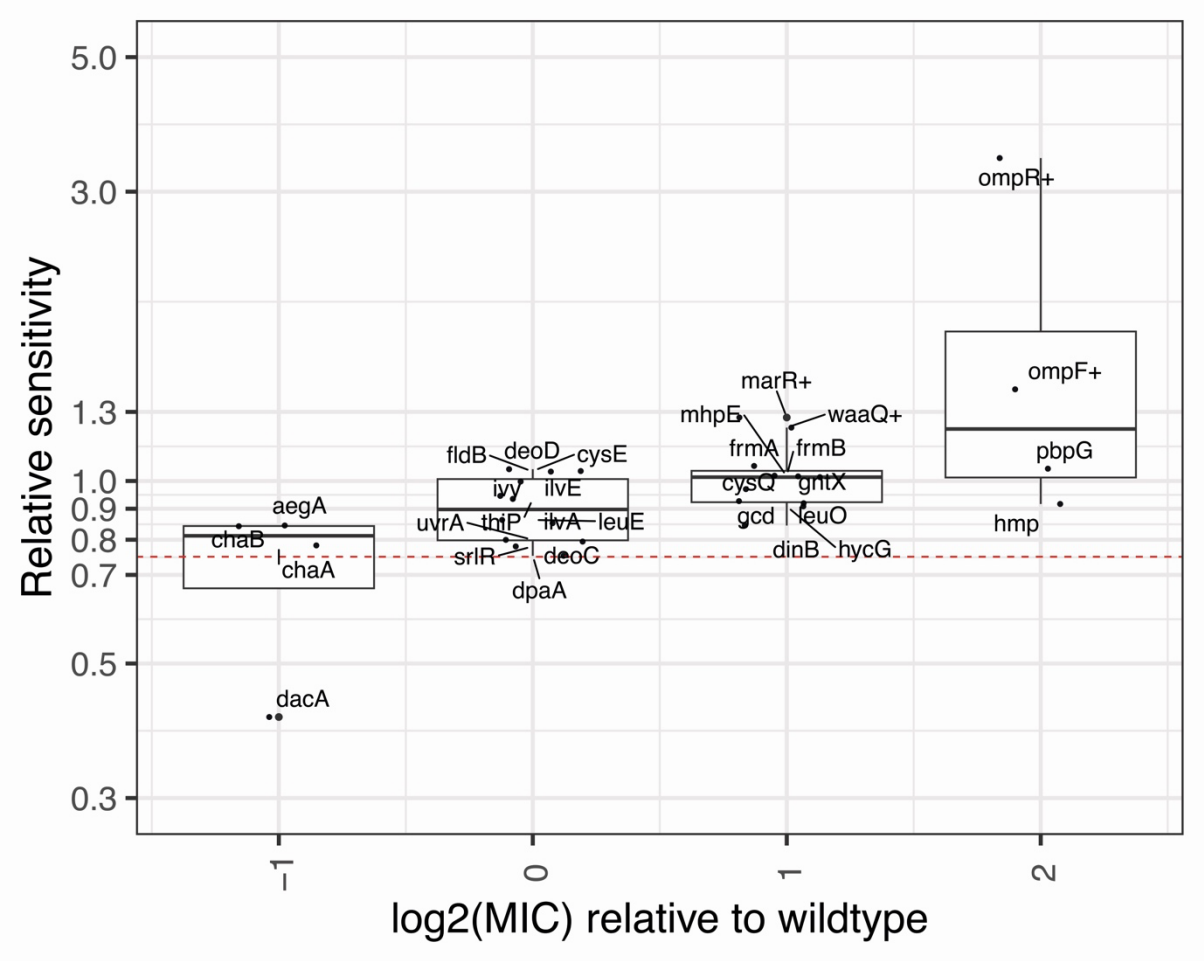

Figure 10: Cefotaxime sensitivity and MICs of evolvability gene KOs relative to the wildtype. *To assess the ability of the sensitivity filtering step to remove gene KO mutants with lower cefotaxime MIC than the wildtype, MICs were independently measured for 27 evolvability gene KO mutants plus dacA and are shown as log_2(MIC) relative to the wildtype. 0 represents mutants that show the same MIC as the wildtype, -1 represents mutants with a 2-fold lower MIC than the wildtype (more sensitive), and +1 or +2 represent mutants with a 2- or 4-fold higher MIC than the wildtype (more resistant). The MICs of mutants are compared to their sensitivity as quantified by the screen (Figures 7 and 8). Out of the 27 evolvability gene KO mutants tested, 3 with a sensitivity between 0.75 and 0.85 had a decreased MIC relative to the wildtype (more sensitive) but were missed by the sensitivity threshold (aegA, chaA, chaB), while 6 with a sensitivity between 0.75 and 0.85 had the same MIC as the wildtype. Therefore, the sensitivity cut-off was well chosen to reflect the MIC and filter out more sensitive mutants with decreased MIC. Four resistant KO mutants were added as controls and are marked with a plus sign (marR+, waaQ+, ompF+, ompR+).*

5. Identifying required cellular functions during resistance evolution

Using the described experimental and computational procedure, I identified 248 non-essential gene KOs that delay resistance evolution against cefotaxime (Figure 11). The top 50 genes with decreased evolvability at 1.5x MIC can be found in Supplementary Table 1. Resistance evolution is delayed without these genes, potentially because resistance mutations become costly or do not provide resistance anymore. These genes likely perform necessary functions during resistance evolution and constrain resistance evolution when knocked out. Since I identified those genes by quantifying OD at 1.5x MIC, they probably interact with the first-step resistance mutations evolved.

To identify common biological processes among these genes, I performed gene ontology (GO) enrichment on the significant hits with L2FC < -0.5. Although the genes represented diverse biological processes, enrichments failed to reach significance, which can be explained in multiple ways. One reason could be that this set of genes was never described together since evolvability is a biological property that has never been quantified on a genome-wide level. Another reason could be that the sensitivity or fitness filtering steps removed genes from enriched biological processes and prevented an enrichment. A final explanation could be that those genes share several common biological processes. For example, one group increases the fitness cost of resistance mutations, the second group decreases resistance levels provided by resistance mutations, and the third group decreases the mutation rate, but merging them into one list diminishes the power to identify any of those processes. Several examples can be found for the second hypothesis.

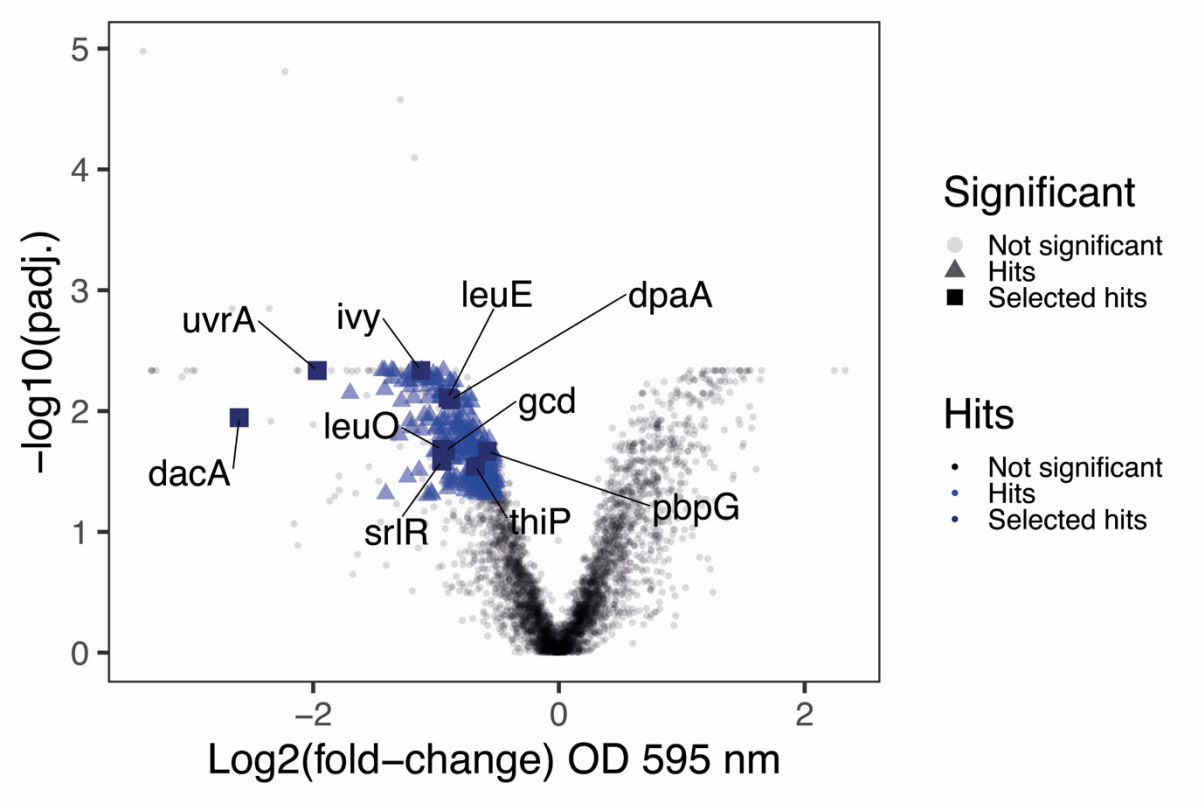

Figure 11: Hits with decreased evolvability at 1.5x MIC cefotaxime. *Hits are shown as blue triangles. Selected hits used for the follow-up experiments are labeled and shown as dark blue squares. Hits were called as shown in Figure 8 based on log_2(fold-change) <= -0.5 and padj. < 0.05, calculated from the $OD_{595\ nm}$ of all replicates for each mutant relative to its respective plate using a BH-adjusted Wilcoxon signed-rank test after filtering out mutants with decreased fitness or increased sensitivity (< 0.75).*

One expected functional group of genes required during resistance evolution was involved in cell envelope maintenance with particular emphasis on the PG. Those genes included DD-

endopeptidases *pbpG*/PBP7 (Romeis & Höltje 1994) and *dacB*/PBP4 with additional DD-carboxypeptidases activity (Matsuhashi et al. 1978; Matsuhashi et al. 1977). Another DD-carboxypeptidase *dacA*/PBP5 KO (Spratt & Strominger 1976; Matsuhashi et al. 1979; Sauvage et al. 2008) and the L,D-transpeptidase *ldtB* KO (Braun & Wolff 1970) also evolved much worse but fell below the sensitivity threshold. The murein endopeptidase *dpaA* recently described to cleave crosslinks between PG and Lpp (Matthias et al. 2021; Bahadur et al. 2021) was one of the strongest hits, as well as the periplasmic chaperone *ivy* known to inhibit LTs (Clarke et al. 2010; Monchois et al. 2001) and fold periplasmic proteins under stress (Lennon et al. 2015). The KO of the activator of amidases *actS* that activates N-acetylmuramoyl-L-alanine amidases *amiA*, *amiB*, and *amiC* (Mueller et al. 2021; Gurnani Serrano et al. 2021) evolved worse, as well as the KO of cell division coordinator *cpoB* that mediates the coordination between PG synthesis and OM constriction during cell division (Gray et al. 2015), which showed increased sensitivity on top. Regarding the cell envelope, another gene KO with delayed resistance evolution involved in LPS biosynthesis was *waaB*/*rfaB* (Qian et al. 2014).

Another functional group of genes necessary during resistance evolution performed functions in the biosynthesis of the amino acids cysteine (*cysE*, *cysK*, *cysQ*), methionine (*metE*, *metH*, *metI*, *metK*, *metN*), isoleucine (*ilvA*, *ilvE*, *ilvL*, *ilvM*), leucine (*leuO*), glycine (*glyS*) and the precursor thiamine (*thiC*, *thiE*, *thiP*, *thiQ*). Those amino acids have been connected to resistance and tolerance against cell wall targeting antibiotics *via* the stringent response and its main signaling molecule guanosine 3',5'-bispyrophosphate (ppGpp) (Rodionov & Ishiguro 1995; Wang et al. 2020). Several studies discussed the critical role of the stringent response during β-lactam treatment (Kusser & Ishiguro 1986; Pisabarro et al. 1990).

Another approach to identifying functions required for resistance evolution is to search for gene complexes, gene families, or operons of which KOs of multiple genes were hits for delayed evolution. Possibly, these genes did not result in an enrichment because genes of the operon or complex were filtered out due to their decreased fitness or increased sensitivity. One example of an operon with several evolvability genes is the *mhp* operon involved in utilizing aromatic acids as carbon and energy sources (Burlingame & Chapman 1983), of which I identified *mhpA*, *mhpC*, *mhpE*, and *mhpF* as KOs with delayed resistance evolution. Another functionally related example is the *deo* operon involved in utilizing pyrimidine deoxyribonucleoside as a carbon and energy source (Valentin-Hansen et al. 1982; Ahmad & Pritchard 1969), of which I identified *deoC* and *deoD* as hits for delayed evolution. The same applied to *rhtB* and *rhtC*,

which were both involved in the export of L-homoserine, L-homoserine lactone, and L-threonine (Eggeling & Sahm 2003; Zakataeva et al. 1999). *GcvH* and *gcvP* were both required for resistance evolution and are involved in folate biosynthesis and glycine transformation (Plamann et al. 1983). I found that both the aminopeptidase A/I *pepA* (Minh et al. 2009) and the peptidase D *pepD* (Schroeder et al. 1994), as well as the dipeptide transporters *dppD* and *dppF* (Abouhamad & Manson 1994) were hits for delayed evolution. Furthermore, two genes involved in sugar phosphate uptake, *afuB* and *afuC* (Sit et al. 2015), were required during resistance evolution, as well as *chaA* and *chaB* that encode a Na+/K+:proton antiporter contributing to growth at alkaline pH (Padan et al. 2005; Lewinson et al. 2004). Lastly, I identified glutathione-dependent formaldehyde dehydrogenases *frmA* and *frmB* (Gutheil et al. 1997) and *mobA* and *mobB* in the biosynthesis of the cofactor molybdopterin guanine dinucleotide (Johnson et al. 1991) as genes required during resistance evolution against cefotaxime.

The identified genes involved in nutrient biosynthesis, recycling, and uptake, oxidation-reduction, surviving acidic stress (*E. coli* is known to acidify the medium during long stationary growth phases), oxidative stress response, and repair of DNA or protein damage are possibly required to survive the stationary phase during the evolution experiment. As such, they could be independent of the antibiotic cefotaxime. In summary, I identified multiple genes involved in the maintenance of the PG layer and cell envelope, amino acid biosynthesis, metabolism, and oxidation-reduction that are required during cefotaxime resistance evolution, indicating that their biological function is necessary during resistance evolution and their KOs delay evolution as a result. Identifying such genes was expected since cefotaxime also targets PBP1 and 3 as part of the divisome machinery (Kjeldsen et al. 2015; Labia et al. 1980). Gene KOs with delayed evolution could either interact directly with acquired resistance elements *via* a gene-gene interaction or interact with the resistance elements in the presence of cefotaxime *via* a gene-gene-drug interaction, which I dissected during the mechanistic investigation in Chapter III. Besides identifying KOs with delayed resistance evolution, my genome-wide evolvability screen is equally powerful in identifying genes with increased evolutionary capacity, which I will discuss next.

6. Uncovering detrimental cellular functions during resistance evolution

Next, I wanted to identify genes whose absence accelerates resistance evolution, potentially because the fitness effects of resistance mutations are mitigated, or the resistance levels they provide are increased. These genes likely perform detrimental functions during resistance, accelerating resistance evolution when knocked out. In our screening dataset, I had two ways to identify KO mutants with accelerated resistance evolution: looking for better evolvers at 1.5x MIC (day 3) or 13.5x MIC (day 5). In both cases, I first filtered out KO mutants with increased resistance levels based on a sensitivity threshold of < 1.25 to focus only on evolvability and applied an effect size cut-off of > 0.5.

6.1. Investigating detrimental cellular functions at low antibiotic concentrations

First, I investigated gene KOs with higher OD at day 3 (1.5x MIC) of the experiment, the same concentration where I also identified worse evolvers, and found 299 gene KOs with increased evolvability. The top 50 genes with increased evolvability at 1.5x MIC can be found in Supplementary Table 2. The results are displayed in Figure 12. Equivalent to the worse evolvers, the better evolvers at 1.5x MIC also show most likely epistasis with the first set of resistance variants evolved under my conditions. When running a GO enrichment, I identified significant enrichments for both phospholipid transport from the *mla* operon (*mlaC*, *mlaE*, *mlaF*) (Malinverni & Silhavy 2009; Thong et al. 2016; Hughes et al. 2019) and the enterobacterial common antigen (ECA) biosynthesis process (*wecB*, wecC, *wecE*, *wecG*) (Meier-Dieter et al. 1992; Jiang et al. 2020; Meier-Dieter et al. 1990). When looking for KOs significantly increasing growth during resistance evolution in the enriched biological process, ECA biosynthesis, but lowering the effect size cut-off from >= 1 that was used for the enrichment to >= 0.75, *wecABCDEFG* KOs were significant hits and represent most of the ECA biosynthesis pathway (Meier-Dieter et al. 1992; Jiang et al. 2020; Meier-Dieter et al. 1990). This relationship can be seen in Figure 12.

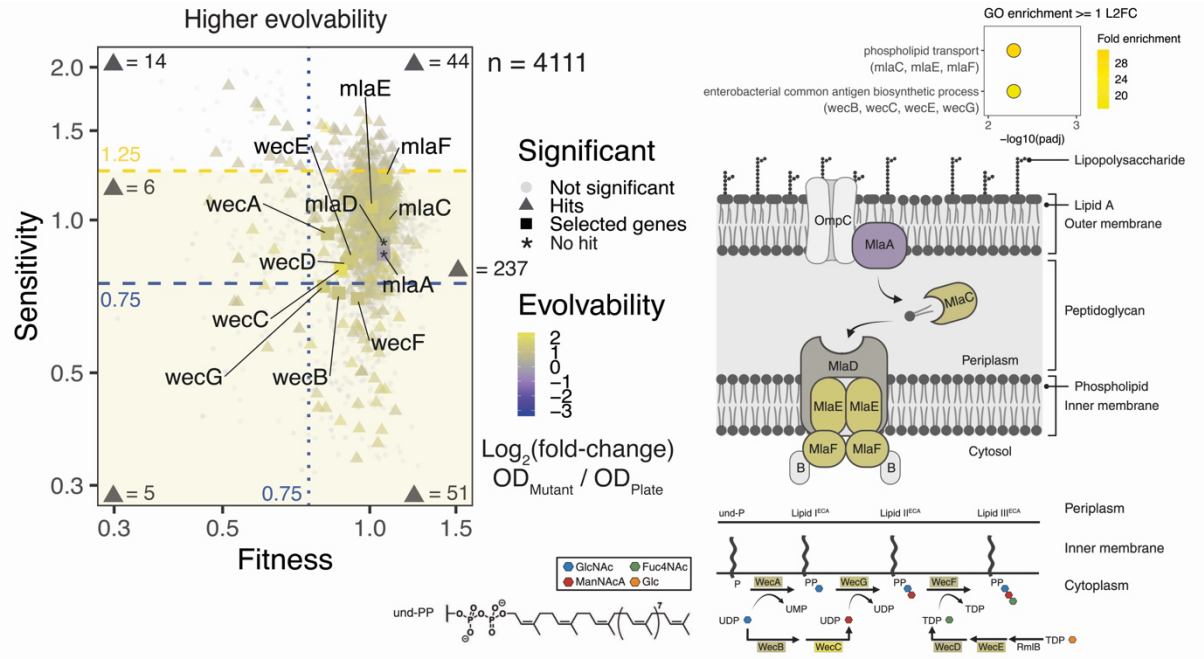

Figure 12: Identifying gene deletions with increased cefotaxime evolvability at 1.5x MIC. *Genes with increased evolvability after filtering out genes with increased resistance levels. Gene ontology enrichment reveals phospholipid transport via the mla system and enterobacterial common antigen biosynthetic process via the wec pathway as enriched among genes with increased evolvability. Selected hits identified by the enrichment are labeled. The graphic visualizes the components of the two pathways colored by their respective evolvability score.*

The *mla* system controls OM permeability and antibiotic resistance (Malinverni & Silhavy 2009; Thong et al. 2016; Hughes et al. 2019) and is controlled by the resistance regulator MarR (Sharma et al. 2017). The *wec* system is involved in ECA biosynthesis (Meier-Dieter et al. 1992; Meier-Dieter et al. 1990), and disruptions of *wecC* were reported to partially restore disrupted OM function and vancomycin resistance of mutants with increased membrane permeability, possibly by the accumulation of ECA intermediates (Jiang et al. 2020). Phospholipid transport and the ECA biosynthesis pathway negatively impact resistance evolution, and knocking them out increases cefotaxime evolvability (Figure 13).

Besides the enriched processes, I found several other processes involved in PG or cell envelope maintenance and processes where KOs of multiple members of a gene family, complex or operon, favored antibiotic resistance evolution. Those genes include lytic murein transglycosylases (LTs) *mltC*, *mltF*, and *slt* (Heidrich et al. 2002; Dijkstra & Keck 1996; Lee et al. 2013), of which the KOs increased evolvability. The fact that for *ivy*, which inhibits LTs (Clarke et al. 2010; Monchois et al. 2001), the KO decreased evolvability, while for several LTs (*mltC*, *mltF*, and *slt*), the KOs increased evolvability, speaks for a detrimental role of LTs during cefotaxime resistance evolution. Also, for *dpaA*, which cleaves PG-OM linkages

(Matthias et al. 2021; Bahadur et al. 2021), the KO decreased evolvability, while for *ldtA*, which creates such PG-OM linkages, the KO increased evolvability, suggesting a detrimental role for PG-OM linkages during cefotaxime resistance evolution. Using genes with opposing functions allowed me to pinpoint molecular functions that modulate cefotaxime AMR evolution, such as LTs and PG-OM linkages. Interestingly, also the maltose-inducible amylomaltase *malQ* that catalyzes transglycosidase reactions and the α-amylase *malS* that hydrolyzes internal 1,4-glucosidic linkages (Dippel & Boos 2005; Boos & Shuman 1998) were hits for increased evolvability. *BacA* that displays undecaprenyl pyrophosphate (Und-PP or C55-PP) phosphatase activity (Ghachi et al. 2004; Manat et al. 2015) was another process detrimental to resistance evolution and its KO increased evolvability.

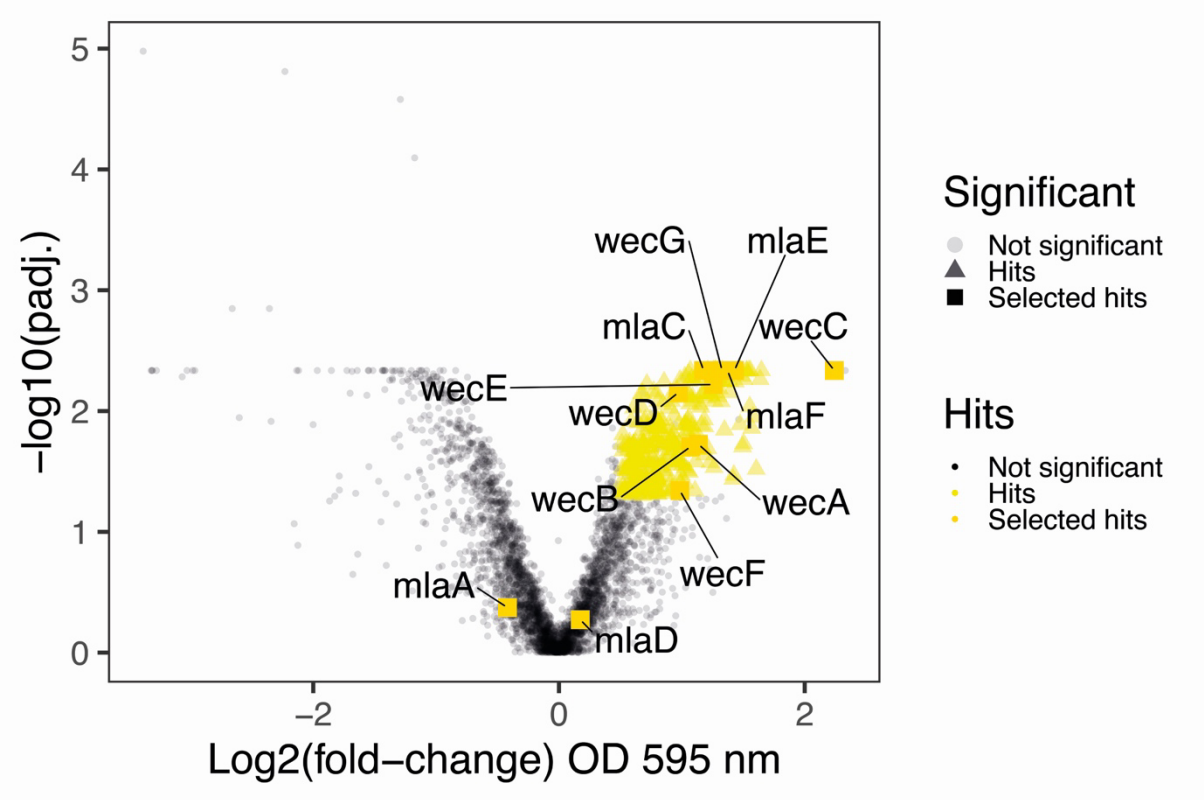

Figure 13: Hits with increased evolvability at 1.5x MIC. *Hits are shown as yellow triangles. Selected hits from the mla and wec operons are labeled and shown as dark yellow squares. The genes mlaA and mlaD are not hits but are shown as a reference because they belong to the mla operon. Hits were called as shown in Figure 12 based on log_2(fold-change) >= 0.5 and padj. < 0.05, calculated from the $OD_{595\ nm}$ of all replicates for each mutant relative to its respective plate using a BH-adjusted Wilcoxon signed-rank test after filtering out mutants with increased resistance (> 1.25).*

Several cell wall components require undecaprenyl phosphate for their synthesis. In addition, KOs of *waaD* and *waaP* involved in LPS biosynthesis (Kneidinger et al. 2002; Raetz & Whitfield 2002; Yethon et al. 1998) as well as of the endopeptidase *mepS* increased evolvability (Truong et al. 2020; Voedts et al. 2021; Singh et al. 2012). Another KO that showed a higher

yield at 1.5x MIC was *lapB*, which was described to form a complex with FtsH to degrade LpxC involved in LPS biosynthesis. LapB KO mutants show decreased LpxC degradation, and lethal LPS levels accumulate as a result (Guest et al. 2020; Shu & Mi 2022), which is why the KEIO mutant is only viable due to a *lpxC* mutation decreasing its LPS biosynthesis (Mahalakshmi et al. 2014). In addition, for multiple genes involved in flagella biosynthesis and regulation, the KOs increased evolvability, namely *flgAGJKL*, *flhB*, and *fliACKO* (Macnab 1992) as well as for the *mdo* gene family (*mdoC* and *mdoG*) responsible for osmoregulated periplasmic glucan biosynthesis (Sébastien et al. 2017).

The putrescine ABC exporter *sapB*, *sapC*, and *sapD* (Sugiyama et al. 2016) was another function where several KOs of the same complex increased evolvability. Other transporter/porin class genes were *uidB* and *uidC*, a glucuronide H+ symporter, and OM porin (Poolman et al. 1996). As part of the general stress response, both RNA polymerase sigma factor *rpoN* and *rpoS* (Dong et al. 2011; Weber et al. 2005; Zhang & Buck 2015) helped resistance evolution when knocked out, as well as *pspA* and *pspB* involved in protecting membrane integrity under stress conditions (Liu et al. 2021) and stationary-phase survival (Weiner & Model 1994; Weiner et al. 1991).

In summary, I identified several processes detrimental during resistance evolution, potentially by directly interacting with resistance elements (gene-gene interactions) or interacting with resistance elements in the presence of the drug (gene-gene-drug interaction). When such toxic processes are knocked out, the stress is relieved, and a compensatory effect is accomplished. As a result, the KO mutants evolve better than the average KO mutant. Also, for KOs to evolve better, multiple genes were identified that affect the remodeling or maintenance of PG and cell envelope. Especially phospholipid transport *via* the *mla* system and ECA biosynthesis *via* the *wec* pathway were enriched processes that accelerate resistance evolution when knocked out, highlighting that those processes contribute toxic effects during resistance evolution. Other biological processes detrimental during resistance evolution include LTs, PG-OM linkages, endopeptidases, and several transport- and stress response-associated genes.

6.2. Identifying detrimental cellular functions at high antibiotic concentrations

Besides identifying better evolving KO mutants by comparing their yield at 1.5x MIC, I also identified them based on their yield at 13.5x MIC, an antibiotic concentration at which very

few mutants could grow, after filtering by relative sensitivity < 1.25. The top 50 genes with increased evolvability at 13.5x MIC can be found in Supplementary Table 3. Since the wildtype and, therefore, most mutants could not evolve resistance mutations that support growth at this high cefotaxime concentration, I expected to find only the strongest epistatic interactions as well as DNA repair deficient mutator strains with increased mutation rates (Cox 1976; Gifford et al. 2023) among these KO mutants. When running GO enrichment on the KO mutant that evolved better at 13.5x MIC, DNA mismatch repair was enriched significantly with *mutH*, *mutS*, *mutT*, *ycjD*, *yedK*, and *uvrD* as the corresponding KOs evolving better, likely due to an increase in mutation rate (Dukan et al. 2000; Cox 1976; Gifford et al. 2023) (Figure 14). In addition, at 13.5x MIC, there were still KOs of multiple genes involved in LPS biosynthesis (*waaG*, *waaO*) (Parker et al. 1992) and in ECA biosynthesis (*wecC*) (Jiang et al. 2020) able to evolve.

Other interesting mutants able to evolve to 13.5x MIC were *fes*, the ferric enterobactin esterase that catalyzes the hydrolysis of both enterobactin and ferric enterobactin (Vinella et al. 2005; Lin et al. 2005), the accessory iron-sulfur cluster assembly gene *iscX* (Kim et al. 2014), *mpl* that acts in murein recycling and reincorporation into peptidoglycan (Mengin-Lecreulx et al. 1996) and *nlpI* that functions as a general adaptor to co-ordinate peptidoglycan hydrolases within PG biosynthetic complexes (Banzhaf et al. 2020).

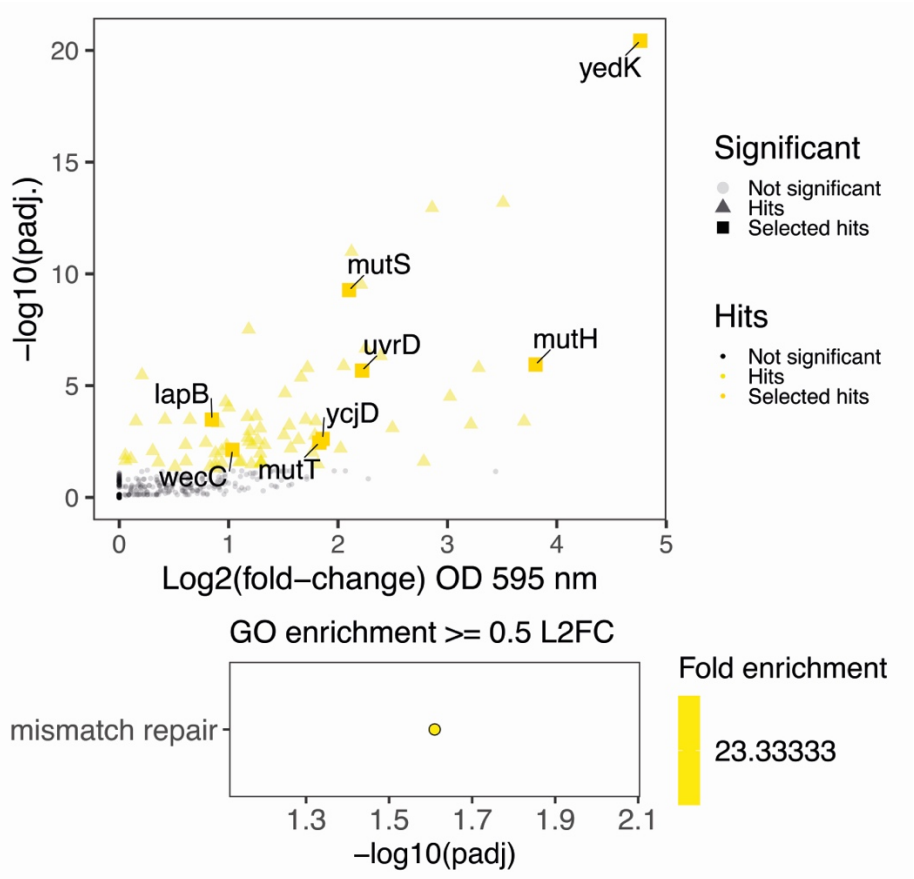

Figure 14: Hits with increased evolvability at 13.5x MIC. *Hits are shown as yellow triangles. Selected hits from the enrichment are labeled and shown as dark yellow squares. Hits were called based on log_2(fold-change) >= 0.5 and padj. < 0.05 calculated from the $OD_{595\ nm}$ of all replicates for each mutant relative to its respective plate using a BH-adjusted non-parametric Wilcoxon signed-rank test after filtering out mutants with increased resistance (> 1.25).*

Another KO that still reached growth at 13.5x MIC was *lapB*, which forms a complex together with FtsH to degrade LpxC involved in LPS biosynthesis (Guest et al. 2020; Shu & Mi 2022) and carries a *lpxC* mutation (Mahalakshmi et al. 2014). Even though the *ompC* KO did not provide high levels of resistance, it still helped to evolve up to 13.5x MIC. A biological process where several KOs were able to evolve to 13.5x MIC was riboflavin biosynthesis represented by *ribD* and *ribE* (Magalhães et al. 2008; Richter et al. 1997; Mörtl et al. 1996).

To conclude, using genome-wide experimental evolution, I identified several biological processes that shape resistance evolution by blocking existing evolutionary trajectories *via* negative epistasis or opening new ones *via* positive epistasis. These effects can allow mutants to reproducibly reach high resistance levels of >10x MIC of cefotaxime reproducibly, which is very rare for wildtype strains or most other mutants.

7. Conclusions

Processes that are required during resistance evolution are represented by KO mutants with decreased evolvability. I identified these mutants by their decreased yield at 1.5x MIC cefotaxime compared to their plate median while showing similar fitness and sensitivity as the wildtype. Mutants with decreased evolvability at 1.5x MIC cefotaxime either a) did not acquire the necessary resistance mutations, b) showed a strong fitness defect carrying resistance mutations, or c) received lower resistance levels from the same resistance mutations. Given that the antibiotic cefotaxime targets PG biosynthesis during cell division, identifying processes that tightly interact with PG biosynthesis or, generally, the cell envelope serves as a good confirmation. Examples of such processes were endopeptidases, carboxypeptidases, transpeptidases, activation of amidases, coordination of PG biosynthesis, and OM constriction. Another broader class of processes involved the metabolism, including amino acid biosynthesis, usage of aromatic acid or nucleosides as alternative carbon sources, folate biosynthesis, peptidases, and dipeptide transporters, as well as iron uptake. This finding indicates that nutrients could be limiting during resistance evolution or stationary-phase survival and that restricting the metabolism is one way to delay resistance evolution.

Even though the resistance mutations were only identified through sequencing in Chapter III, the identified gene KOs with increased or decreased evolvability provided some insights into the epistatic interactions of the major resistance trajectories that evolved during cefotaxime resistance evolution. First, the absence of enrichment for worse evolvers at 1.5x MIC could indicate that several available evolutionary trajectories, of which hits delay either one or several of them, which associates them with multiple biological processes. Here, it has to be taken into account that mutants with a decreased evolvability need to interact with all easily accessible resistance trajectories *via* epistatic interactions since they would otherwise only favor one resistance trajectory over the other without delaying resistance evolution, per se. Secondly, the abundance of mutants involved in maintaining the PG layer and the cell envelope, amino acid biosynthesis, metabolism, and oxidation-reduction suggest that those processes are required to rewire the genetic network during cefotaxime resistance evolution. They could be necessary to compensate for toxic changes in the architecture of the genetic network or to translate the resistance genotype into a resistance phenotype. The second hypothesis is supported by the fact that some of the most widespread mechanisms of cefotaxime resistance require a heavy remodeling of the cell envelope, namely the upregulation and insertion of the efflux pump

AcrAB-TolC and the downregulation of major OM porins OmpF and OmpC. These interactions I dissected after identifying the resistance mutations evolving during cefotaxime resistance evolution in Chapter III.

KOs with increased evolvability represent processes that are detrimental during resistance evolution. I identified these mutants by their higher OD at 1.5x MIC and 13.5x MIC cefotaxime than their plate median while showing similar sensitivity as the wildtype. Mutants with increased evolvability at 1.5x MIC cefotaxime likely show positive epistasis with easily accessible resistance mutations by a) acquiring them earlier, b) showing better growth in the presence of the resistance mutation than the average mutant, for example, by compensating for defects, or c) showing higher resistance levels in the presence of resistance mutations. Examples of processes with increased evolvability at 1.5x MIC cefotaxime are phospholipid transport (*mla* system), ECA biosynthesis (*wec* pathway), LPS biosynthesis, PG and cell envelope biosynthesis and maintenance, including LTs and endopeptidases, as well as flagella biosynthesis and regulation.

Mutants with increased evolvability at 13.5x MIC cefotaxime, which very few mutants accomplished, likely display a) strong positive epistasis that increases the fitness with accessible resistance mutations, b) an increased mutation rate to access evolutionary trajectories that are too rare to be frequently reached by the average mutant given the population size and the average mutation rate or c) highly increased resistance levels provided by frequent/accessible resistance mutations. Examples of processes with increased evolvability at 13.5x MIC cefotaxime were DNA mismatch repair, iron-sulfur cluster assembly, peptidoglycan recycling and coordination, LPS biosynthesis, and riboflavin biosynthesis.

Knocking out processes detrimental to resistance evolution should increase the evolvability of cefotaxime resistance. I identified such processes by both increased yield at 1.5x MIC and 13.5x MIC of cefotaxime. Both conditions represent related but also distinct readouts. While growth at 1.5x MIC focused on genetic interactions between KO mutants and easily accessible resistance trajectories under mild selection, growth at 13.5x MIC represents strong selective pressure under mutation supply rate limitation and filtered out all but the strongest beneficial effects. At 1.5x MIC cefotaxime, I identified phospholipid transport *via* the *mla* system and ECA biosynthesis *via* the *wec* pathway, as well as LTs, endopeptidases, LPS biosynthesis as well as several transport- and stress response-associated genes. At 13.5x MIC cefotaxime, on

the other hand, I identified mainly DNA repair-deficient mutants of the mut gene family, as well as genes involved in LPS biosynthesis and PG recycling and coordination. Since DNA repair-deficient mutants with increased mutation rate, also called mutator strains, showed increased evolvability against cefotaxime only at 13.5x MIC and not at 1.5x MIC, it suggests that the mutation rate was limiting at 13.5x MIC but not at 1.5x MIC cefotaxime. This is supported by the finding that most mutants could grow at 1.5x MIC, which allowed me to identify mutants with decreased evolvability in the first place. This likely indicates that resistance was evolved by acquiring loss-of-function (LOF) resistance mutations of easily-mutated resistance regulators such as *marR* or *ompR*, which have been reported for cefotaxime resistance evolution before (Schenk et al. 2022), instead of rare point mutations in the target.

In contrast to KOs increasing evolvability at only 1.5x or 13.5x MIC cefotaxime, KOs involved in the hydrolysis of enterobactin and ferric enterobactin (*fes*), whose deletion increases ppGpp levels (Vinella et al. 2005), LPS biosynthesis (*waa* genes, *lapB*), ECA biosynthesis (*wecC*) and PG recycling and remodeling (*nlpI*) increased evolvability at both 1.5x and 13.5x MIC of cefotaxime. These processes are, therefore, toxic during the resistance evolution of cefotaxime, and the resulting rewiring of the genetic network and deleting them strongly increases evolvability.

In summary, in this chapter, I used genome-scale experimental evolution to probe the rewiring of the genetic network during cefotaxime resistance evolution. By taking a global approach, I mapped the genomic landscape of cefotaxime resistance evolution and identified genes both negatively and positively interacting with the (unknown) set of resistance mutations evolving during antibiotic resistance evolution. Deletions of genes required during resistance evolution display decreased evolvability and represent targets for evolution inhibitors. In contrast, deletions of genes detrimental during resistance evolution show increased evolvability and reveal vulnerabilities and constraints the genetic network poses during resistance evolution. I uncovered several targets and vulnerabilities during cefotaxime resistance evolution, primarily in PG remodeling and LPS biosynthesis. Next, I opted to characterize in more detail how these gene deletions affect resistance evolvability and whether the identified vulnerabilities can be targeted to delay resistance evolution.

Chapter III: Dissecting epistatic interactions delaying resistance evolution

Chapter III: Dissecting epistatic interactions delaying resistance evolution

1. Summary

After measuring the impact of every non-essential gene deletion on resistance evolution rates against cefotaxime, I focused on dissecting the mechanisms behind some of the uncovered interactions. To achieve this, I employed a mixture of different methods, including whole-genome sequencing of resistant mutants and quantifying the epistatic interactions between the identified resistance elements and KO mutants with delayed resistance evolution or 'evolvability genes' in the absence and presence of cefotaxime. I identified that the evolved resistance genes interact with evolvability genes *via* both gene-gene and gene-gene-drug interactions and investigated the molecular mechanism underlying one of these interactions using quantitative genetics, high-throughput microscopy, and proteomics. Lastly, I tried to uncover the principles behind antibiotic resistance evolution by replacing genetic perturbations (gene KOs) delaying evolution with chemical perturbations (drugs) delaying evolution and the evolutionary target cefotaxime with other antibiotics from different classes with a focus on different β-lactam antibiotics. Using the acquired knowledge of genetic vulnerabilities arising during resistance evolution, I identified several drugs able to delay cefotaxime resistance. I classified the identified evolvability genes into drug-specific, drug-class-specific, and general evolvability genes based on the antibiotics against which I evolved resistance.

2. Contributions

Dr. Dimitrios Papagiannidis (EMBL) performed sample preparation, measurement, and data analysis for the mass spectrometry (MS) experiments of single and double mutants. Dr. Jiawei Sun (Stanford) introduced me to the high-throughput microscopy setup and helped me to design and perform the experiments. Dr. Ben Knapp (Stanford) introduced me to high-throughput microscopy data analysis and processing. Dr. Carlos Geert Pieter Voogdt (EMBL) and Dr. André Mateus (EMBL, now Umea) helped me plan and troubleshoot the cloning of the CRISPRi plasmid. Dr. André Mateus performed sample preparation, measurement, and data analysis for the MS validation of CRISPRi-mediated gene knockdowns. Whole-genome sequencing (WGS) analysis was performed by both Dr. Michael Knopp (EMBL) using the QIAGEN CLC Genomics workbench and by myself using *breseq* (Deatherage & Barrick 2014). I conducted all other experimental and computational work presented in this chapter. Dr. Athanasios Typas and I conceived the experimental design and method for epistatic interaction testing, MS-based proteomics, and evolution experiments. Dr. Athanasios Typas

and I discussed the data analysis and visualization of all aforementioned experiments. Dr. Kerwyn Casey Huang (Stanford) and I conceived the experimental design, method, and data analysis for high-throughput microscopy experiments and data analysis.

3. Mutations impacting drug uptake and influx arise during cefotaxime resistance evolution

To identify the major resistance evolution trajectories during experimental evolution in cefotaxime, I isolated 44 individual lineages out of 32 wildtype populations (by sampling 1-2 clones per lineage) with evolved cefotaxime resistance at 4.5x MIC from the aforementioned validation experiment in Chapter II.4. In this case, cells have been passaged without drug two times for 24 h followed by growth at 0.5x, 1.5x and 4.5x MIC of cefotaxime in 96-well plates and 1 ml total volume. I froze colony-purified lineages in glycerol stocks and determined their approximate MIC by streaking out on MHB agar plates containing different concentrations of cefotaxime (data shown in Supplementary Table 4). I extracted genomic DNA for Illumina sequencing, performed variant calling using *breseq* (Deatherage & Barrick 2014), and compared my results with variant calling performed by Dr. Michael Knopp using the QIAGEN CLC Genomics workbench.

After experimental evolution up to 4.5x MIC, clone purification, sequencing, and variant calling of 44 lineages, I identified known drug resistance elements *marR*, *ompR*, *ompF*, and *lon* as most commonly mutated in my screen (in ~82 % of the sequenced lineages) (Figure 15). An overview of all mutations can be found in Supplementary Table 4. *MarR* deletions activate the *marA*B operon and expression of efflux pumps like AcrAB-TolC (Sharma et al. 2017; Hao et al. 2014). *OmpF* encodes a major porin, which cefotaxime uses to enter the cell. *MarR* mutations also downregulate *ompF* expression *via* the small RNA *micF* (Ramani et al. 1994; Dam et al. 2017). OmpR is a major regulator of porins such as *ompF*, *ompC*, and other resistance mechanisms (Masi et al. 2022). *Lon* encodes a protease implicated in the degradation of abnormal and misfolded proteins. *Lon* mutations cause low multidrug resistance by stabilizing the Lon protease substrates MarA and SoxS, transcriptional activators of the AcrAB-TolC pump (Nicoloff & Andersson 2013).

In line with these published findings, I also found combinations of *lon* and *marR* variants, while *ompF* and *ompR* variants occur alone and without other variants in my sequenced mutants.

Furthermore, I found a loss-of-function *waaQ* variant affecting LPS biosynthesis, further increasing resistance in a *marR* variant background and a missense variant in *frdD* upstream of *ampC*, most likely upregulating β-lactamase expression, in combination with a *hycI* mutation. I found multiple other variants that most likely do not contribute to resistance, which can be found in Supplementary Table 4. Based on these sequencing results, I hypothesized that evolvability gene KOs with decreased resistance evolution against cefotaxime are less able to afford resistance variants either because of a fitness defect in the evolvability gene background or because the resistance variants cannot provide resistance anymore in the evolvability gene backgrounds. The *waaQ* mutation is especially interesting given the many LPS biosynthesis-associated genes identified to increase or decrease cefotaxime resistance evolvability in Chapter II.

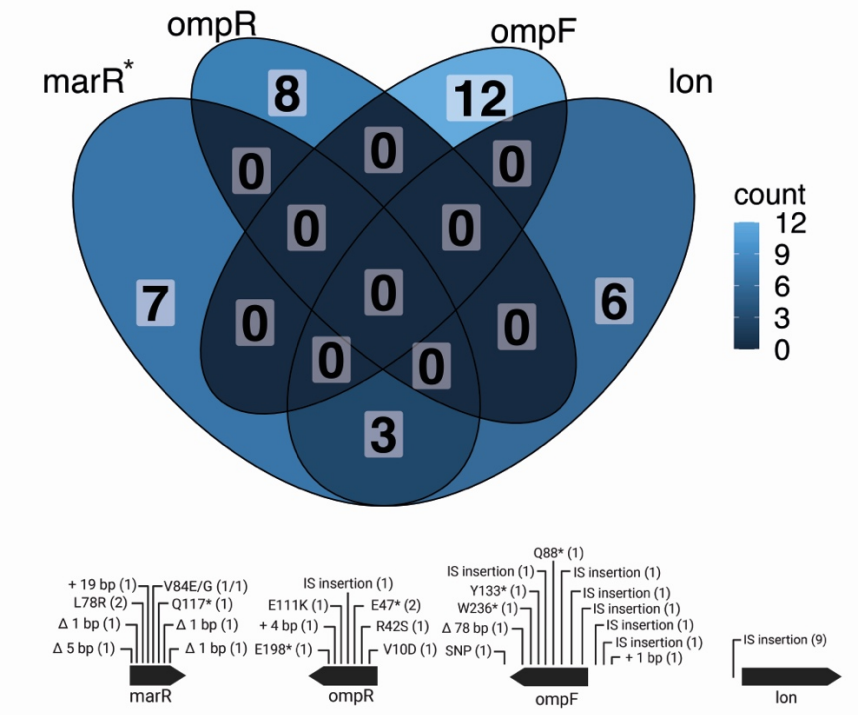

Figure 15: Cefotaxime resistance mutations identified by whole-genome sequencing. *44 lineages were isolated from 32 pools after resistance evolution up to 4.5x MIC of cefotaxime. Genomic DNA was extracted, and whole-genome sequencing was performed using paired-end Illumina sequencing. Variant calling was performed by myself using breseq (Deatherage & Barrick 2014) and CLC Genomics workbench (Qiagen) performed by Dr. Michael Knopp. Identified mutations belonging to 4 main genes, marR, ompR, ompF, and lon, are shown for all lineages. In one marR mutant, I identified an additional waaQ mutation. An overview of all mutations can be found in Supplementary Table 4.*

The mutations I identified can be separated into two mutually exclusive groups, upregulating the AcrAB-TolC pump *via marR* and *lon* and downregulating the outer membrane porins OmpF and OmpC either directly *via* mutations in *ompF* or mutations in the regulator *ompR*. Both resistance mechanisms are general and provide resistance against a diverse range of antibiotics,

including cefotaxime (Schenk et al. 2022). Based on the types of mutations identified and reported in the literature (Masi et al. 2022; Sharma et al. 2017; Norioka et al. 1986), the variants identified here represent most likely loss-of-function mutations for all four identified resistance genes. The fact that I identified two mutually exclusive trajectories to evolve cefotaxime resistance that also share features (downregulation of *ompF*, the cellular localization of both efflux pumps and porins in the cell envelope, and the reduction of intracellular drug concentration as the mechanism of resistance) has interesting implications for the epistatic interactions I identified (Darby et al. 2023). In theory, evolvability genes interacting with one of the shared features would delay both resistance trajectories.

The consistent set of sequenced mutations acquired repeatedly during experimental evolution here and in the literature (Schenk et al. 2022), as well as the high fraction of mutants being able to evolve resistance against 1.5x MIC cefotaxime, suggests that these are the mutations probed by the complete mutant library in my experimental evolution setup. Suppose both resistance trajectories can be acquired repeatedly and reproducibly given the used population size and mutation supply rate. In that case, KO mutants delaying resistance evolution that display negative epistasis with both paths are the ones that will most successfully delay resistance evolution. If only one of the common resistance trajectories showed an interaction with an evolvability gene and would be delayed, it could either delay evolution in half of the lineages or all the lineages but with half the effect size, depending on the frequency of the resistance mutations. The fact that I identified several KO mutants that show delayed evolution across replicates suggests that those mutants could interact with both the *marR* and *ompR* resistance regulators. The negative epistatic interactions of evolvability genes with both resistance pathways could be either related or independent. If related, they probably act *via* one of the shared features between the resistance mechanism mediated by *marR* and *ompR*, *i.e.*, localization in the OM, the reduction of intracellular drug concentration, or the downregulation of *ompF*. If the epistatic interactions of evolvability genes with both resistance regulators are distinct, they could also have different characteristics, one being a gene-gene and the other a gene-gene-drug interaction.

To investigate the nature of the negative epistatic interactions between evolvability genes and resistance regulators quantitatively, I decided to construct a CRISPRi system to quantitatively titrate gene expression levels of an evolvability gene in a resistance background in the absence or presence of cefotaxime.

4. CRISPRi can be used to quantify gene-gene and gene-gene-drug interactions

To investigate the mechanistic basis for the evolutionary delay, I wanted to test for direct epistatic interactions between genes required for resistance evolution against cefotaxime identified by the screen and resistance elements selected under the used resistance evolution conditions (Figure 16a). To quantitatively probe such epistatic interactions in the presence and absence of cefotaxime, I decided to construct a CRISPRi plasmid to induce and titrate genetic perturbations. I chose a plasmid backbone amenable to high-throughput conjugation, which allowed me to investigate epistatic interactions of resistance elements or antibiotic targets at a genome-wide scale, which I describe in Chapter IV.

4.1. Constructing a CRISPRi plasmid to modulate gene expression levels

First, I constructed an inducible, titratable, and conjugatable CRISPRi plasmid for the targeted knockdown of genes in *E. coli* using a catalytically inactive version of Cas9 (Qi et al. 2013). For this, I assembled components of a system previously used in the lab, namely a guide RNA scaffold from a plasmid and the gene coding for the dCas9 protein from an *E. coli* chromosome (Lawson et al. 2017; Mateus et al. 2020) with a vector backbone previously used in the lab (Bobonis et al. 2022) *via* Gibson assembly (Gibson et al. 2009). The system includes a pSC101 origin of replication (~ five copies per cell), a spectinomycin resistance cassette, an F-based origin of transfer for conjugation, and an anhydrotetracycline (aTc) inducible repressor tetR-tetO controlling dCas9 expression (Rogers et al. 2015). I showed strong inducible on-target repression on the protein level, which I confirmed using MS-based proteomics performed by Dr. André Mateus (data shown in Chapter IV).

In the next step, I cloned published guide RNAs (Rousset et al. 2021) targeting two cell wall-related evolvability gene hits of our screen (*ivy* and *dpaA*) into the CRISPRi vector pSB03_2 *via* Golden Gate cloning. Using P1 phage transduction (see detailed description in Chapter VI), I retransduced the kanamycin KO deletions of *marR*, *ompR*, and *waaQ* from the KEIO library into a clean wildtype background. Those clean deletions recapitulate the LOF mutations in resistance genes found under my evolution conditions. I then transformed my CRISPRi plasmid targeting evolvability genes into the KO mutants of resistance genes (see detailed description in Chapter VI).

4.2. Quantifying gene-gene and gene-gene-drug interaction using CRISPRi

I measured the growth of the KO mutants carrying the respective CRISPRi plasmids in the presence of cefotaxime and 0, 150, 300, or 450 ng/ml aTc inducer. Cultures were grown in 30 µl/well MHB media in 384-well plates, using a starting $OD_{595\ nm}$ of 0.01 (1:1000) dilution), as several generations were necessary to deplete the protein and observe CRISPRi-mediated effects.

I used the Bliss independence model (Bliss 1939) to quantify gene-gene interactions in the presence and absence of cefotaxime. I trimmed all growth curves at the time point where the untreated wildtype reached the highest $OD_{595\ nm}$ and determined the fitness by the area under the curve (AUC) normalizing to that of the wildtype without drug and induction. I calculated the Bliss interaction score of the gene targeted by the CRISPRi plasmid with the resistance mutant in the presence and absence of the drug (Figure 16b).

$$\varepsilon = f_{mutant_gene(_drug)} - f_{wt_gene(_drug)} \, x \, f_{mutant(_drug)}$$

Since I used three replicates for both mutant and wildtype, I calculated nine interaction scores between each replicate of mutant and wildtype, respectively. I assessed the significance of CRISPRi-induced epistasis by calculating Bliss interaction scores with and without inducer for every strain, plasmid, and drug concentration using a BH-adjusted Wilcoxon signed-rank test.

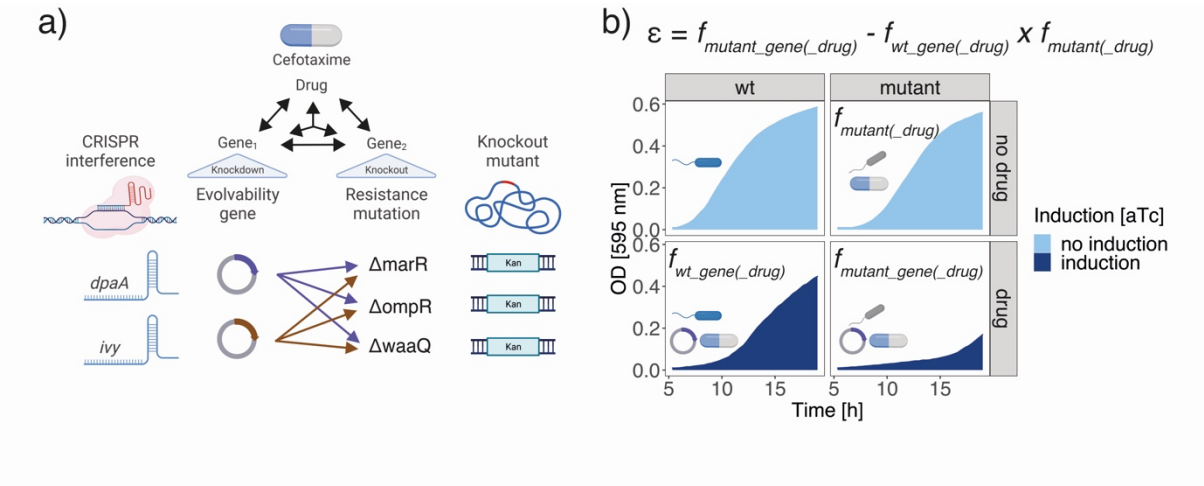

Figure 16: Epistasis of resistance elements blocks evolutionary trajectories. *a) Dissecting gene-gene and gene-gene-drug interactions between identified evolvability genes, resistance mutations, and cefotaxime. b) Gene-gene and gene-gene-drug interactions were calculated using the Bliss independence model based on the AUC of* $OD_{595\ nm}$ (Bliss 1939), *where* $\varepsilon_{Bliss} = f_{mutant_gene(_drug)} - f_{wt_gene(_drug)} \, x \, f_{mutant(_drug)}$.

I showed that there is no significant interaction between *dpaA* or *ivy* with cefotaxime (evolvability gene-drug interactions) measured by knockdown (KD) in the wildtype (Figure 17a). The absence of evolvability gene-drug interactions confirms that the identified evolvability gene KOs do not constrain resistance evolution by merely increasing drug sensitivity and validates the effectiveness of the sensitivity filtering step (Figure 10). The Bliss score at 0 µg/ml cefotaxime shows the effect of only the plasmid on wildtype growth.

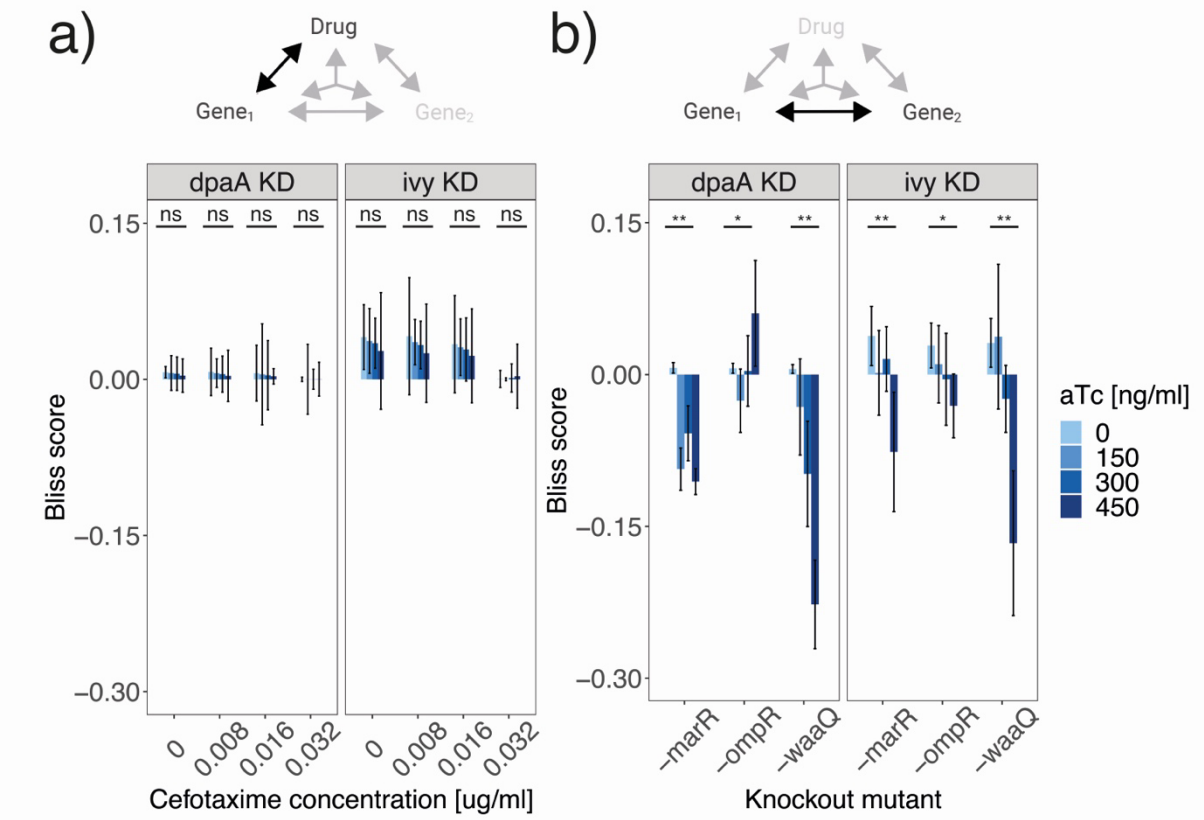

Figure 17: Quantifying gene-drug and gene-gene interactions. *a) Bliss scores between the evolvability gene knockdowns of dpaA and ivy and cefotaxime. KDs of dpaA or ivy do not increase cefotaxime sensitivity. b) Bliss scores between evolvability gene KDs dpaA and ivy in the resistance mutation KOs of marR, ompR, and waaQ. 0 aTc represents the control without induction and expected ε = 0. Error bars represent the standard deviation (n=9). Significance was calculated by comparing Bliss scores with 450ng/ml aTc and without induction by the BH-adjusted Wilcoxon signed-rank test. * padj. < 0.05, ** padj. < 0.01, *** padj. < 0.001*

Next, I measured gene-gene interactions between evolvability and resistance genes without cefotaxime. In the case of *dpaA* without cefotaxime, I saw a negative interaction with Δ*waaQ* (Δ indicating knockout) background (ε = -0.25) and with Δ*marR* (ε = -0.125) (Figure 17b). For the *ivy* KD without cefotaxime, I identified a negative interaction with Δ*waaQ* (ε = -0.2) and marginal negative interactions with Δ*ompR* or Δ*marR* (ε = ~-0.1), all scaling with CRISPRi induction levels (Figure 17b).

Finally, I measured gene-gene-drug interactions of evolvability gene KDs in resistance variant KO mutants in the presence of the drug cefotaxime. The negative gene-gene interactions between *dpaA* KD and the resistance genes Δ*marR* and Δ*waaQ* persisted in the presence of cefotaxime concentrations of 0.008 µg/ml and 0.016 ug/ml. At 0.032 µg/ml cefotaxime, the MIC of the wildtype, there is no growth in the wildtype ($f_{wt_gene_drug}$), so the Bliss score only reflects the difference between $f_{mutant_gene_drug}$ and f_{mutant_drug}. Interestingly, the *dpaA* KD reverted resistance and decreased the yield of Δ*ompR* mutants by up to ~ 52 %, visible by a decrease in the positive score upon induction (Figure 18a). The *ivy* interaction with Δ*waaQ* and Δ*marR* observed in the absence of cefotaxime stayed consistent with increasing cefotaxime concentrations of 0.008 µg/ml and 0.016 ug/ml. The Δ*ompR* interaction with the *ivy* KD scaled with increasing cefotaxime concentrations at 0.016 ug/ml and 0.032 ug/ml with the *ivy* KD decreased the yield in the presence of 0.032 µg/ml cefotaxime by up to ~40 % (Figure 18b).

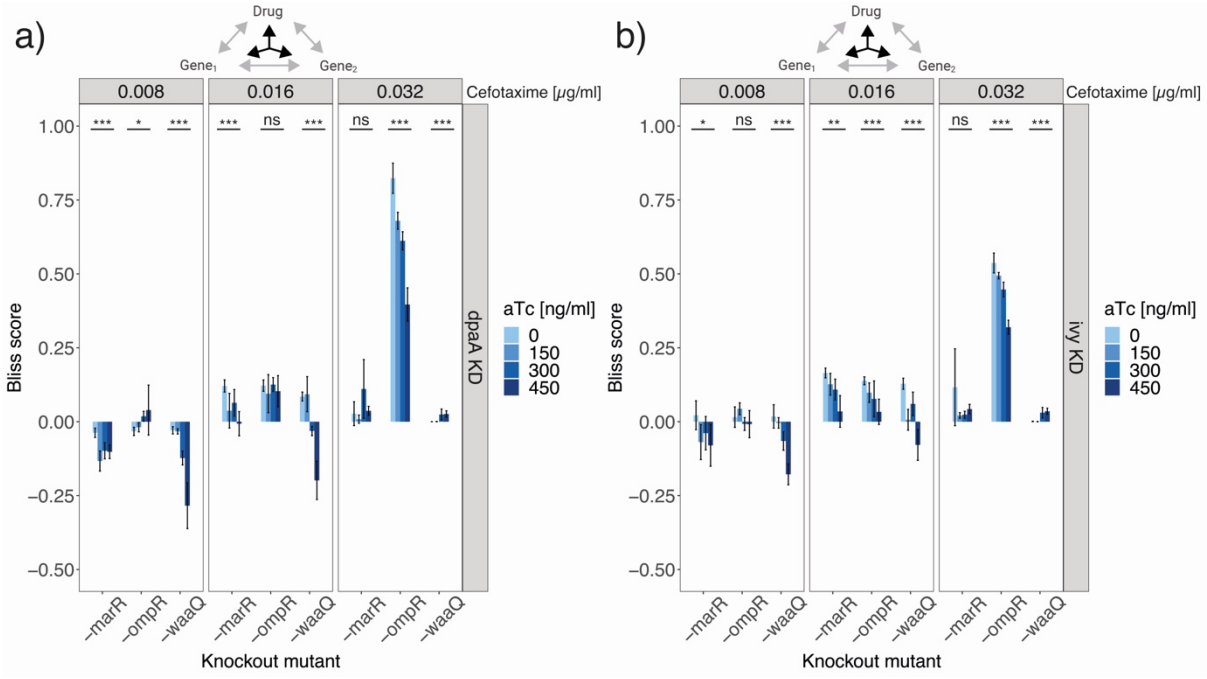

Figure 18: Quantifying gene-gene-drug interactions. *a) Bliss scores between the evolvability gene KDs of dpaA (a) and ivy (b) and the resistance KOs marR, ompR, and waaQ were quantified in the presence of the three cefotaxime concentrations 0.008, 0.016 and 0.032µg/ml. Error bars represent the standard deviation across calculated Bliss scores. Significance was calculated by comparing Bliss scores with 450ng/ml aTc and without induction by the BH-adjusted Wilcoxon signed-rank test. * padj. < 0.05, ** padj. < 0.01, *** padj. < 0.001.*

For Δ*marR*, I saw a negative gene-gene interaction with both *dpaA* and *ivy* KD in the absence of cefotaxime, which was also visible at 0.008 and 0.016 µg/ml cefotaxime but not at 0.32 µg/ml. These genetic interactions indicate that the *marR* mutants show decreased fitness when the evolvability genes *dpaA* or *ivy* are knocked down, which should negatively impact the

evolution of *marR* mutations in *dpaA* or *ivy* KO mutants. The fact that the interaction between Δ*marR* and both the *dpaA* and *ivy* KD was strongest in the absence of cefotaxime and decreased in strength with increasing cefotaxime concentration could be explained by lower growth of the Δ*marR* mutant in the presence of plasmid and cefotaxime due to leaky CRISPRi expression causing the gene-gene interaction, thereby decreasing the dynamic range to detect gene-gene-drug interactions of the *marR* mutant at 0.032 µg/ml cefotaxime.

Since Δ*waaQ* interactions with *dpaA* and *ivy* KDs were equally strong in the presence and absence of cefotaxime, it indicates a gene-gene interaction between those genes and explains why the absence of *dpaA* or *ivy* prevented *waaQ* variants from being acquired. The Δ*ompR* showed a negative interaction with the *dpaA* KD only in the presence of cefotaxime, indicating a gene-gene-drug interaction. At the same time, the negative interaction with the *ivy* KD was also visible in the absence of cefotaxime, suggesting a gene-gene interaction that could be exacerbated by cefotaxime. Therefore, the two evolvability genes *dpaA* and *ivy* might have different epistatic interactions with the resistance regulator *ompR*.

In summary, both evolvability genes (*dpaA* and *ivy*) showed negative genetic interactions with two major resistance elements for cefotaxime *marR* and *waaQ*. This shows that the evolvability gene KO mutants constrain the evolution of resistance to cefotaxime by decreasing the fitness of resistance mutants. Additionally, *dpaA* and *ivy* exhibited a conditional genetic interaction (*i.e.* gene-gene-drug interaction in the presence of cefotaxime) with *ompR*, the other resistance element. They reduce resistance levels the resistance mutation provides, thereby limiting cefotaxime resistance evolution.

To better understand the mechanistic basis for the gene-gene and gene-gene-drug interactions I identified, I first used high-throughput live microscopy of the single and double mutants of evolvability genes *dpaA* and *ivy* and the resistance regulators *marR* and *ompR* in the presence and absence of cefotaxime. The reasons for using microscopy were to identify morphological features and characteristics of the single mutants during cell growth and division and how these change in the double mutants. Furthermore, since both the evolvability genes *dpaA* and *ivy*, the resistance regulators *marR* and *ompR*, and the antibiotic cefotaxime affect cell division and the cell envelope, gene-gene or gene-gene-drug interactions may result in morphological effects.

5. Using high-throughput microscopy to dissect epistatic interactions

To investigate the mechanistic basis for the observed gene-gene and gene-gene-drug interactions, I turned to the Strain Library Imaging Protocol (SLIP) (Shi et al. 2017). This high-throughput microscopy approach allowed me to investigate single and double mutants of evolvability genes and resistance regulators with and without antibiotics. I used live imaging to identify morphological alterations during growth and cell division in the absence and presence of cefotaxime.

5.1. Live imaging reveals morphological aberrations by gene-gene interactions

To study features during live growth and division in the absence and presence of antibiotics, I grew duplicate overnight cultures of wildtype, the single KO mutants (*dpaA*, *ivy*, *marR* and *ompR*) and double KO mutants (*dpaA marR*, *ivy marR*, *dpaA ompR* and *ivy ompR*) in tubes with 5 ml MHB while rolling at 37 °C, followed by adjusting the $OD_{595\ nm}$ to 0.002 (1/5 dilution of $OD_{595\ nm}$ 0.01). I pinned these diluted cultures on an MHB agar pad without an antibiotic and grew them in the microscope chamber heated to 37 °C. I imaged 20 samples at 25 frames per position every 5 minutes for several hours. The detailed protocol can be found in Chapter VI. It should be acknowledged that all observations based on the live imaging data are of qualitative, not quantitative nature, by manually observing the outgrowth of ~250-500 cells per genotype and comparing the most extreme phenotypes. As such, they are influenced by common biases, and a more sophisticated quantification will be required to confirm all derived hypotheses in the future.

I identified morphological aberrations during growth across single and double KO mutants of the evolvability genes *dpaA* and *ivy* and resistance genes *marR* and *ompR*. I identified several morphological characteristics for the single KO mutants (Figure 19). Compared to the wildtype, I saw occasional lysis following cell division for Δ*dpaA* (Figure 19 indicated by arrows). The Δ*ivy* also showed several instances of lysis, plasmolysis, or lysis following plasmolysis (Figure 19 indicated by arrows). Plasmolysis means that the IM detaches from the cell wall and OM, which can occur upon changes in pressure and shrinking of the cytoplasmic contents and appears as a visible region of concavity in the phase signal. For the Δ*marR* mutant, I found several cells lysing, sometimes following plasmolysis, which was rarely the case for the Δ*ompR*. In addition, I identified examples of OM blebbing at midcell and outer-membrane

vesicle (OMV) release, which were frequently observed in the Δ*marR* (Figure 19 indicated by arrows).

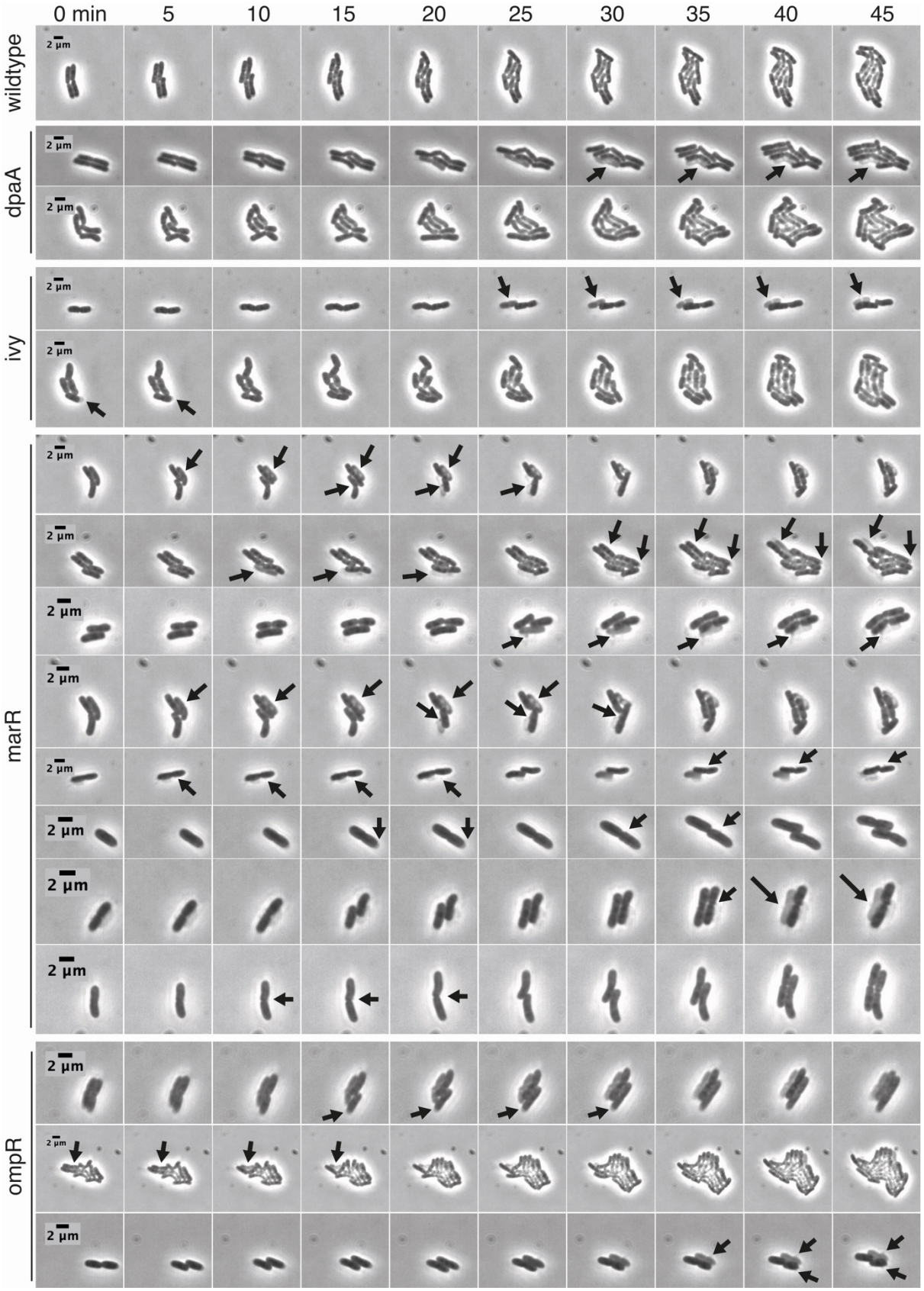

Figure 19: Live microscopy reveals single gene deletion phenotypes. *Different genotypes were grown overnight, diluted to $OD_{595\ nm}$ of 0.002, pinned on an agar plate, and imaged during live growth at 37 °C with 25 frames per position using SLIP* (Shi et al. 2017)*. Outer membrane vesicles and outer membrane blebs indicated by arrows are commonly observed in the ΔmarR and once in the ΔompR. Phase-contrast images were acquired on a Ti-E inverted microscope (Nikon Instruments) using a 100X (NA 1.40) oil immersion objective.*

Next, I wanted to compare the phenotypes of double mutants of evolvability and resistance genes (Figure 20). First, I looked at the phenotypes from the gene-gene interactions between the resistance regulator *marR* and evolvability genes *dpaA* and *ivy*. The Δ*dpaA*Δ*marR* had a tendency for lysis, plasmolysis, and lysis following plasmolysis, as well as a large plasmolysis distance relative to the overall cell length. A large plasmolysis distance, visible as a region of concavity in the phase signal located at the cell pole, suggests a large distance between the detached IM from PG and OM (Figure 20 indicated by arrows). In addition, I identified several clusters of cells with a filamentation phenotype, which was unique for the Δ*dpaA*Δ*marR* and could indicate defects in the cell division machinery.

Δ*ivy*Δ*marR* also showed a high frequency of lysis, plasmolysis, and lysis following plasmolysis, including a large plasmolysis distance (Figure 20 indicated by arrows). In addition, it also displayed a unique phenotype, interestingly the opposite of the Δ*dpaA*Δ*marR*. For several cells, asymmetric cell division led to two daughter cells with distinct morphology where one was wildtype-like while the other one was round. The round daughter cells could not grow or divide but also did not lyse in most cases. This phenotype could indicate an overactive cell division machinery, a defective elongasome, or problems of FtsZ finding the center of the cells in the Δ*ivy* when combined with the Δ*marR*.

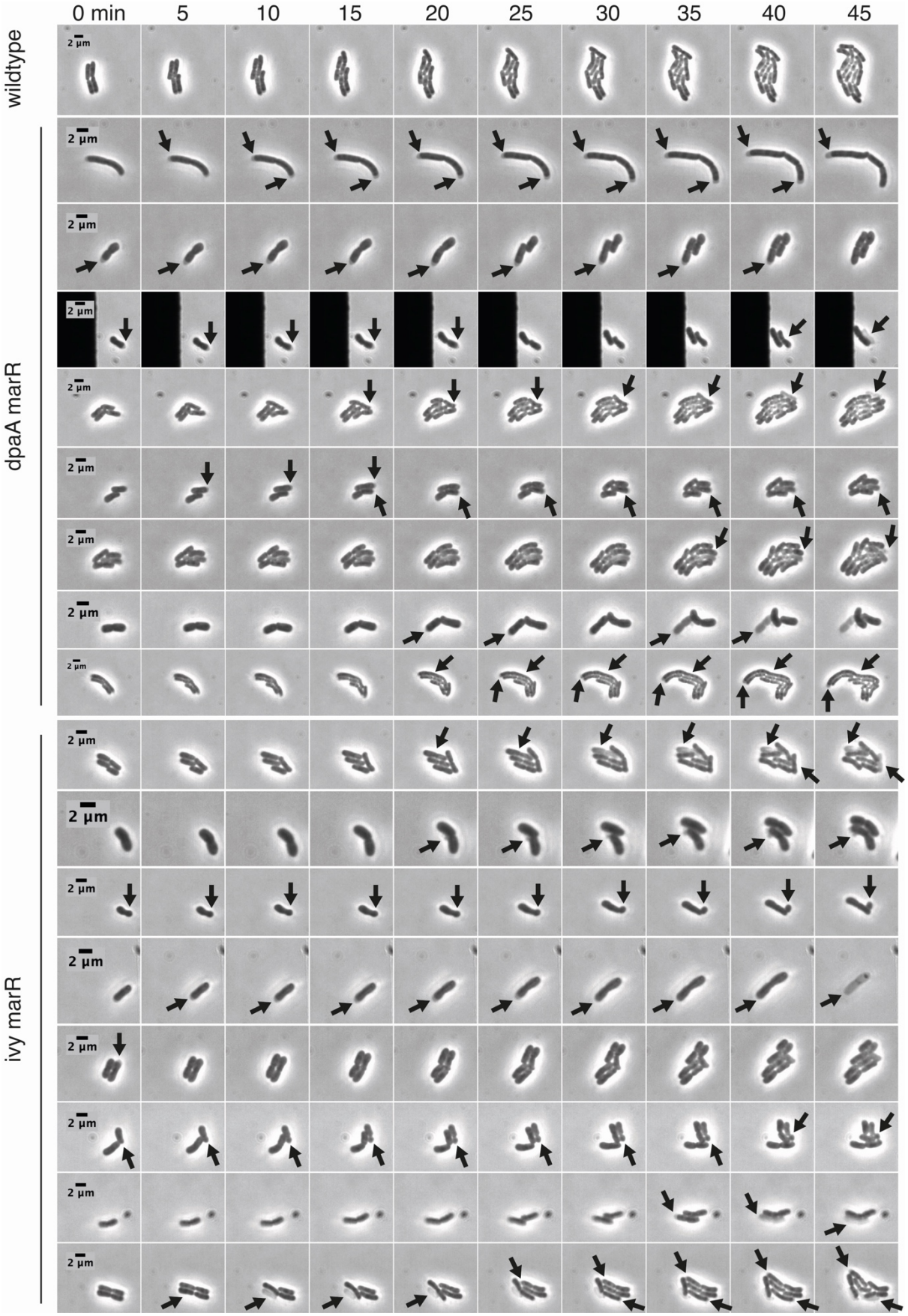
0 min
5
10
15
20
25
30
35
40
45
wildtype
dpaA marR
ivy marR
2 µm

Figure 20: Dissecting the gene-gene interactions between marR and evolvability genes using live microscopy. *Different genotypes were grown overnight, diluted to $OD_{595\ nm}$ of 0.002, pinned on an agar plate, and imaged during live growth at 37 °C with 25 frames per well using SLIP* (Shi et al. 2017)*. Phase-contrast images were acquired on a Ti-E inverted microscope (Nikon Instruments) using a 100X (NA 1.40) oil immersion objective.*

Next, I looked at the phenotypes from gene-gene interactions between the resistance regulator *ompR* and evolvability genes *dpaA* and *ivy* (Figure 21). For the Δ*dpaA*Δ*ompR* mutant, multiple clusters of cells showed the same filamentation phenotype that the Δ*dpaA* also showed in combination with the Δ*marR* (Figure 21 indicated by arrows). There were some examples of lysis, however, the frequency was lower than for the Δ*dpaA*Δ*marR*. No examples of plasmolysis were observed, mirroring the absence of a gene-gene interaction between the *dpaA* KD and *ompR* KO. For the Δ*ivy*Δ*ompR* mutant, cells were very heterogeneous, no filamentation was observed, and some cells showed a round morphology (Figure 21 indicated by arrows). These phenotypes coincided with frequent lysis, which, combined with the round morphology and the altered cell division dynamics, supported the gene-gene interaction I identified between the Δ*ivy* and Δ*ompR* in the absence of cefotaxime.

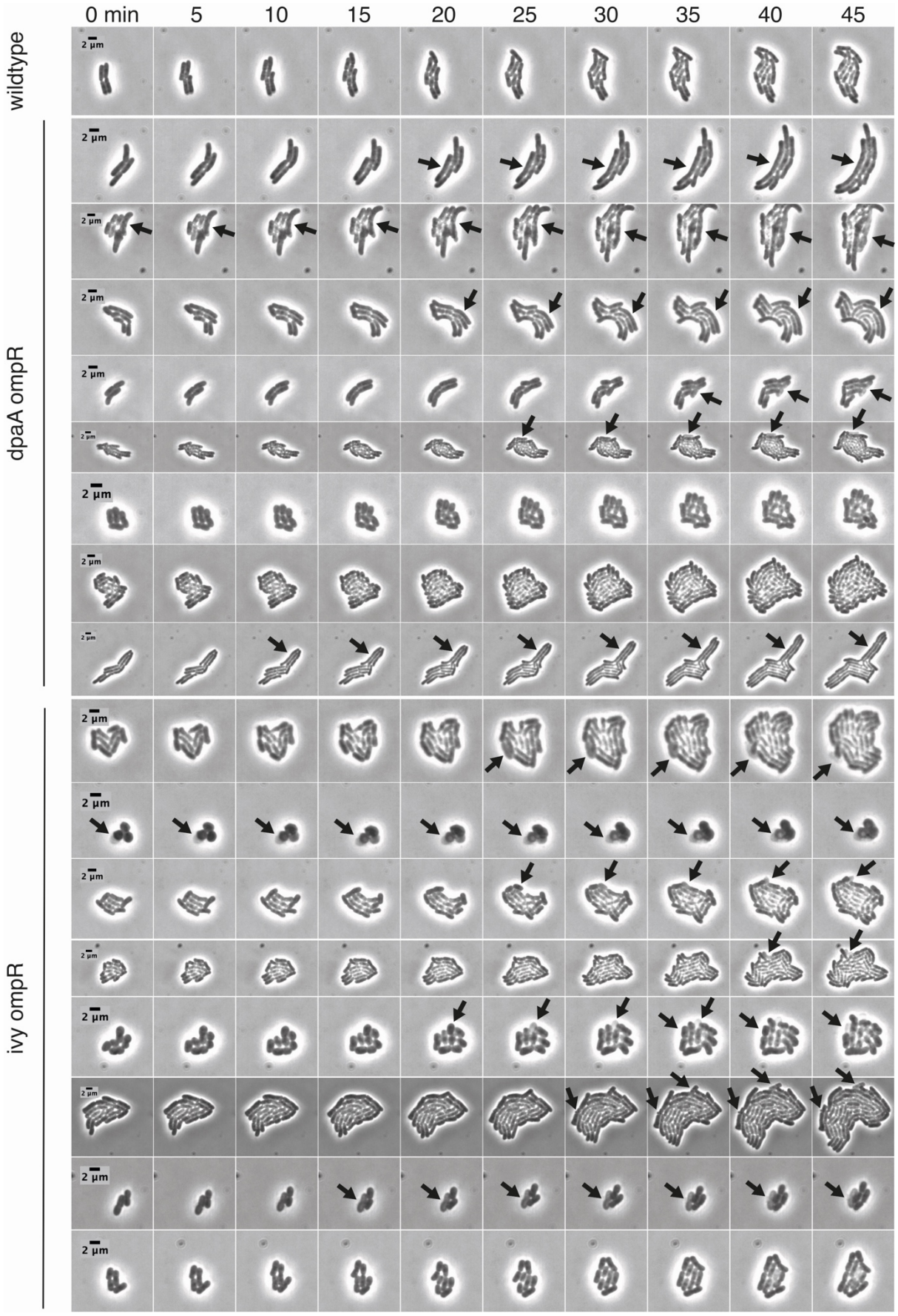
0 min
5
10
15
20
25
30
35
40
45
wildtype
dpaA ompR
ivy ompR
2 µm

Figure 21: Dissecting the gene-gene interactions between ompR and evolvability genes using live microscopy. *Different genotypes were grown overnight, diluted to $OD_{595\ nm}$ of 0.002, pinned on an agar plate, and imaged during live growth at 37 °C with 25 frames per well using SLIP* (Shi et al. 2017)*. Phase-contrast images were acquired on a Ti-E inverted microscope (Nikon Instruments) using a 100X (NA 1.40) oil immersion objective.*

While the Δ*marR* single KO mutants already displayed lysis, plasmolysis, and lysis following plasmolysis, these phenotypes appeared to be stronger and more frequent in the Δ*dpaA*Δ*marR* and Δ*ivy*Δ*marR* double KO mutants. This would confirm the observed gene-gene interactions between both evolvability genes *dpaA* or *ivy* and the resistance regulator *marR*. However, a thorough quantification of these phenotypes will be required to statistically test whether these phenotypes are indeed stronger and more frequent in the double compared to the single KO mutants.

It was reported that increased LPS levels cause OM blebbing at midcell, OMV formation, plasmolysis, and cell death in a *mlaA* GOF mutant (Sutterlin et al. 2016), which could be suppressed by mutations that reduce LPS synthesis or reduce the number of linkages between PG and OM to allow shedding of excess LPS *via* OMVs (Sutterlin et al. 2016). Since the *marR* KO directly activates the *mla* operon (Sharma et al. 2017) and also shows OM blebs at midcell, OMV formation, and plasmolysis followed by lysis (Figure 19 indicated by arrows), it could also suffer from increased LPS production and accumulation.

Since the Δ*dpaA* increases linkages between PG and OM (Bahadur et al. 2021; Matthias et al. 2021), it could prevent the compensatory shedding of excess LPS *via* OMVs and OM blebs and thereby cause the negative interaction with the *marR* KO. In support of this hypothesis is the absence of OMVs and OM blebs in the ~500 cells of the Δ*dpaA*Δ*marR* double KO mutant (Figure 20) that I observed compared to the > 10 cases I observed for the Δ*marR* KO mutant (Figure 19 indicated by arrows). A quantification of OMVs and OM blebs will be required to statistically test whether OMVs and OM blebs are more frequent in the *marR* KO than the Δ*dpaA*Δ*marR* double KO mutant. Besides this hypothesis, the interaction could also result from a different effect on cell division.

Despite the similarities of the interaction between *dpaA* and *ivy* with *marR*, there were also differences. The Δ*dpaA*Δ*marR* showed several clusters of cells that displayed filamentation. Filamentation indicates a defective cell division machinery and could be explained by a stronger connection between PG and Lpp in the Δ*dpaA* (Bahadur et al. 2021; Matthias et al.

2021). Since *dpaA* is involved in PG turnover (Bahadur et al. 2021), the Δ*dpaA* could display decreased PG turnover, which might be toxic in the Δ*marR* that requires high PG turnover to insert overexpressed efflux pumps.

In contrast, the Δ*ivy*Δ*marR* displayed the opposite phenotype. Several cells divided asymmetrically, resulting in two daughter cells with distinct morphology where one was wildtype-like while the other one was round with similar length and width, also called mini cells. The round daughter cells could not grow or divide but also did not lyse. This phenotype could indicate an overactive cell division machinery in the *ivy* KO when combined with the Δ*marR*. Besides helping to fold periplasmic proteins under stress (Lennon et al. 2015), *ivy* was also reported to inhibit lysozyme and membrane-bound lytic murein transglycosylases (Clarke et al. 2010). Overactive LT activity in the Δ*ivy* could explain the aberrant cell division phenotype. In addition, the Δ*marR* single and Δ*ivy*Δ*marR* double KO showed OM blebbing at midcell, which was also reported for a *mlaA* GOF mutant (Sutterlin et al. 2016).

For the double mutants of resistance regulator *ompR* with the evolvability genes *dpaA* and *ivy*, I observed several phenotypes, the first of which was increased cell width for both double mutants. Specific morphological features for the Δ*dpaA*Δ*ompR* double mutant were phenotypic heterogeneity, with some cells displaying filamentation. In contrast, others were round with increased width, indicating problems with both divisome and elongasome in those cells. In general, there were almost no examples of lysis in those cells, and the phenotypes were mild. For the Δ*ivy*Δ*ompR* double mutant, cell width was increased even more, and round cells, as well as lysis, were more abundant, which supports the gene-gene interaction between both genes.

Therefore, it can be hypothesized that the Δ*dpaA* induces filamentation, *i.e.*, divisome inhibition/problems, in both the Δ*marR* and Δ*ompR*. In contrast, the Δ*ivy* induces round cells with large width, *i.e.*, divisome activation or elongasome inhibition, in both the Δ*marR* and Δ*ompR*. In that regard, both evolvability genes induce opposite phenotypes in both the most prevalent resistance genes during resistance evolution. To investigate how these morphological features change in the presence of antibiotics, I decided to investigate the growth of all mutants also in the presence of cefotaxime.

5.2. Live imaging reveals resistance levels affected by gene-gene-drug interactions

To study gene-gene interactions with cefotaxime, I repeated the procedure for live imaging by growing duplicate overnight cultures of wildtype, the single KO mutants (*dpaA*, *ivy*, *marR*, and *ompR*) and double KO mutants (*dpaA marR*, *ivy marR*, *dpaA ompR*, and *ivy ompR*) in tubes with 5 ml MHB while rolling at 37 °C, followed by adjusting the $OD_{595\ nm}$ to 0.002 (1/5 dilution of $OD_{595\ nm}$ 0.01). I pinned these diluted cultures on an MHB agar pad containing 1x $MIC_{wildtype}$ of cefotaxime and grew them in the microscope chamber heated to 37 °C. I imaged 20 samples at 25 frames per position every 5 minutes for several hours. The detailed protocol can be found in Chapter VI. I identified morphological aberrations during cell division and growth in the presence of cefotaxime for single and double KO mutants of the evolvability genes *dpaA* and *ivy* in combination with the resistance regulators *marR* and *ompR*.

First, I investigated the single mutants in the presence of cefotaxime. (Figure 22). The wildtype filamented and frequently lysed after forming midcell bulges. This phenotype is expected for the divisome inhibitor cefotaxime perturbing the cell division machinery. Similarly, the Δ*dpaA* and Δ*ivy* filamented with some bulges forming and lysis (Figure 22 indicated by arrows). A high degree of heterogeneity can be observed across sensitive mutants showing phenotypes such as filamentation, filamentation leading to lysis, lysis by bursting of cells, bulging and bulging leading to lysis (Figure 22 indicated by arrows). Stochastic gene expression differences across cells could cause this stochasticity. The resistant mutants *marR* and *ompR* grew faster and showed less frequent and less severe filamentation and lysis (Figure 22 indicated by arrows), confirming their higher resistance to cefotaxime. While the Δ*marR* still showed filamentation, bulging, and lysis for some cells of each cluster (Figure 22 indicated by arrows), these phenotypes were rare in the Δ*ompR* (Figure 22), confirming its higher cefotaxime resistance levels (Figure 10).

For Δ*dpaA*Δ*marR* double mutants (Figure 23), I saw severe and frequent filamentation of cells with decreased width forming spirals, indicating exacerbated effects on the cell division machinery (Figure 23 indicated by arrows). This coincided with several cases of lysis. Filamentation induced by cefotaxime and resulting lysis were more frequent and severe in the Δ*dpaA*Δ*marR* double mutant than in the *marR* single mutant. In contrast, in the Δ*ivy*Δ*marR* double mutant, cell width was increased, and cells displayed less frequent and severe filamentation and lysis compared to the single *ivy* mutant (Figure 23 indicated by arrows), suggesting increased cefotaxime resistance and divisome activity as without cefotaxime.

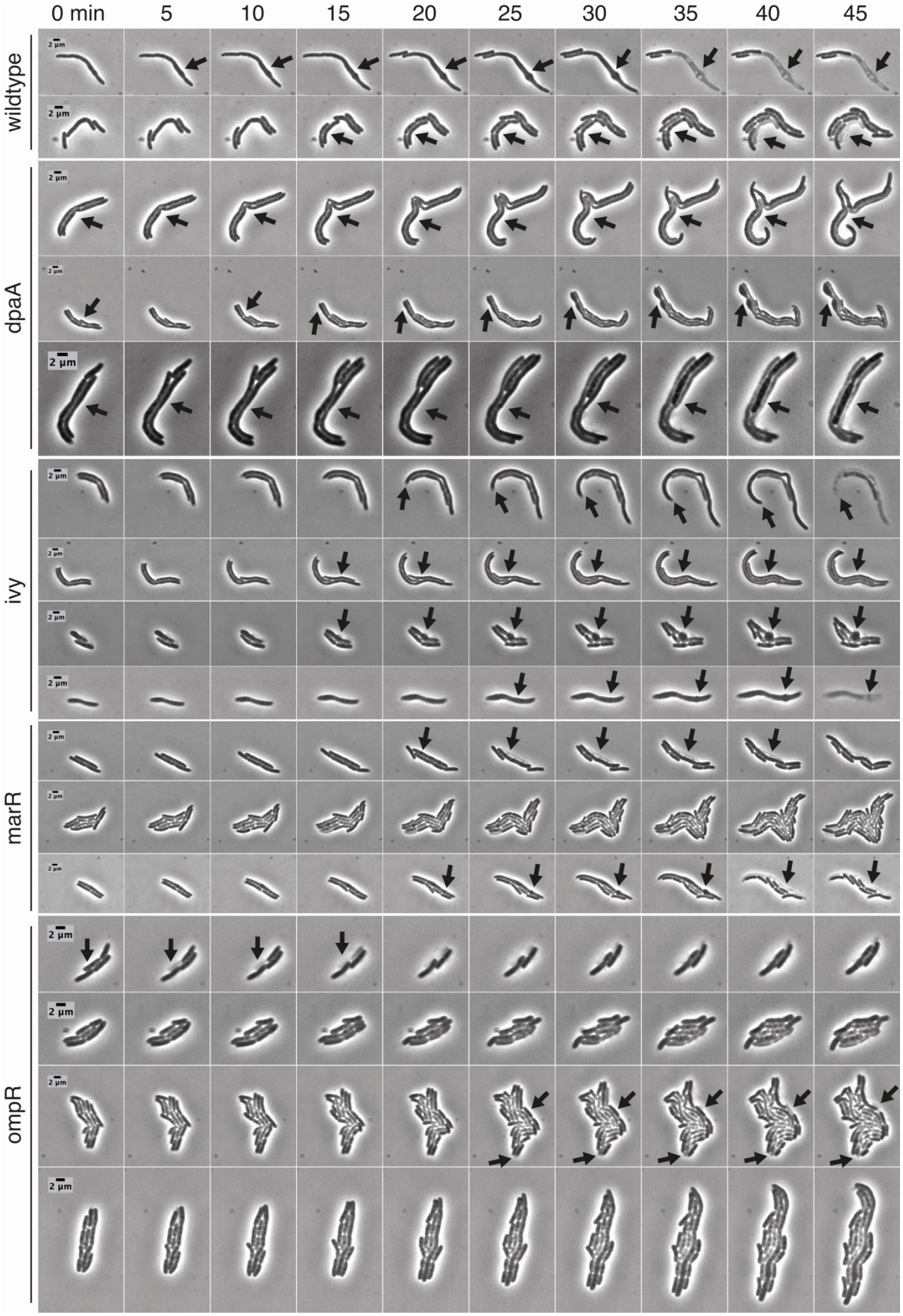
0 min
5
10
15
20
25
30
35
40
45
wildtype
dpaA
ivy
marR
ompR
2 µm

Figure 22: Live microscopy of single gene deletion mutants in the presence of cefotaxime. *Different genotypes were grown overnight, diluted to $OD_{595\ nm}$ of 0.002, pinned on an agar plate containing sub-inhibitory concentrations of cefotaxime, and imaged during live growth at 37 °C with 25 frames per position using SLIP* (Shi et al. 2017)*. Phase-contrast images were acquired on a Ti-E inverted microscope (Nikon Instruments) using a 100X (NA 1.40) oil immersion objective.*

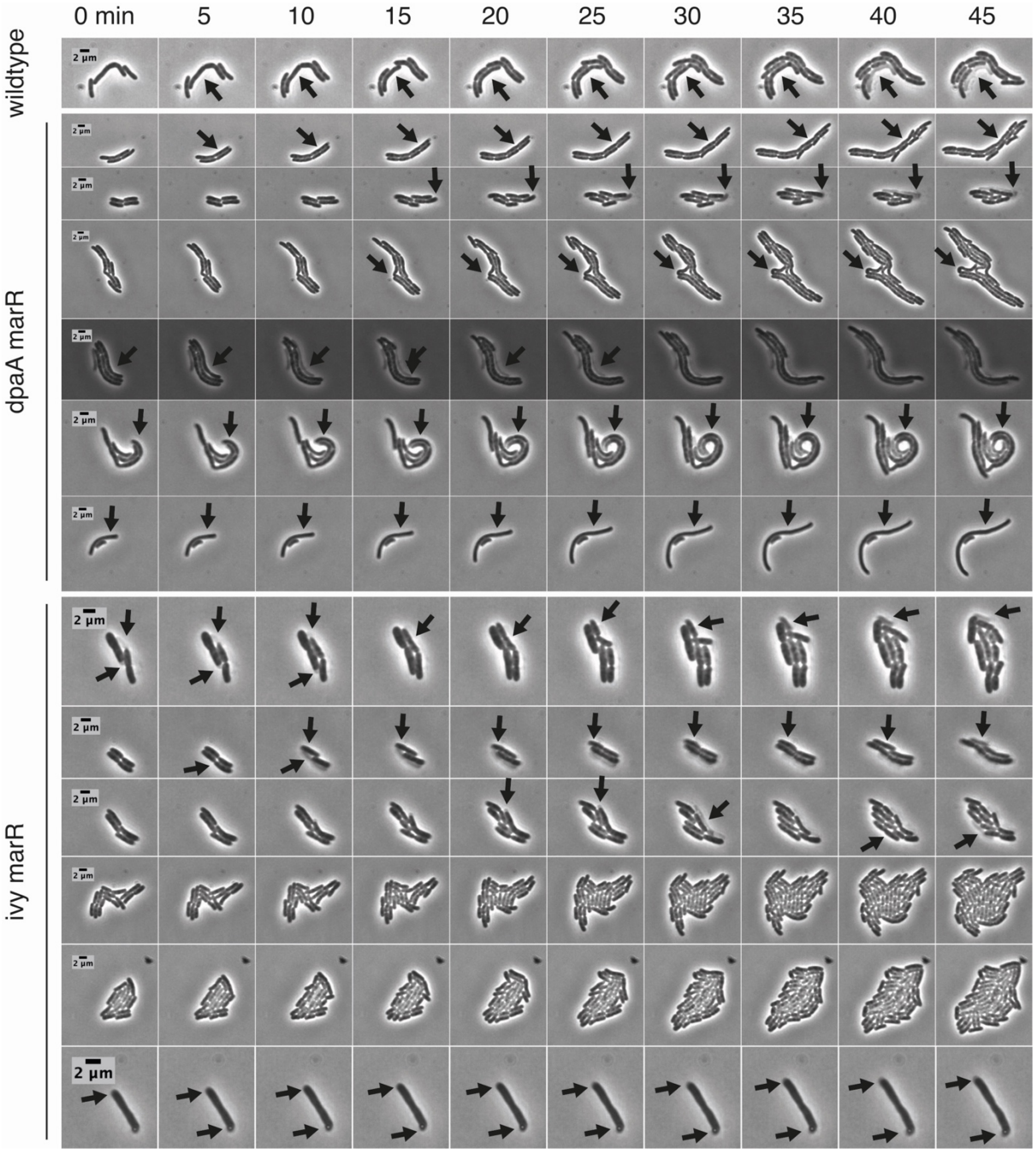

Figure 23: Dissecting gene-gene-drug interactions of *marR* in the presence of cefotaxime by live microscopy. Different genotypes were grown overnight, diluted to $OD_{595\ nm}$ of 0.002, pinned on an agar plate containing sub-inhibitory concentrations of cefotaxime, and imaged during live growth at 37 °C with 25 frames per well using SLIP (Shi et al. 2017). Phase-contrast images were acquired on a Ti-E inverted microscope (Nikon Instruments) using a 100X (NA 1.40) oil immersion objective.

The Δ*dpaA*Δ*ompR* double mutants displayed frequent filamentation, lysis, bulging, and bursting of cells, coinciding with increased cell width (Figure 24 indicated by arrows). These

phenotypes are much stronger than in the Δ*ompR* single mutant that filaments, bulges, or lysis in the presence of cefotaxime. Also, the Δ*ivy*Δ*ompR* double mutants show more filamentation, bulging, and lysis than the Δ*ompR* single mutant (Figure 24 indicated by arrows). Since both the Δ*dpaA*Δ*ompR* and Δ*ivy*Δ*ompR* showed much stronger phenotypes in the presence of cefotaxime than the Δ*ompR* single KO, it indicates that the evolvability genes *dpaA* and *ivy* constrain cefotaxime resistance evolution by increasing cefotaxime sensitivity of *ompR* mutants, mirroring the identified gene-gene-drug interaction (Figure 18).

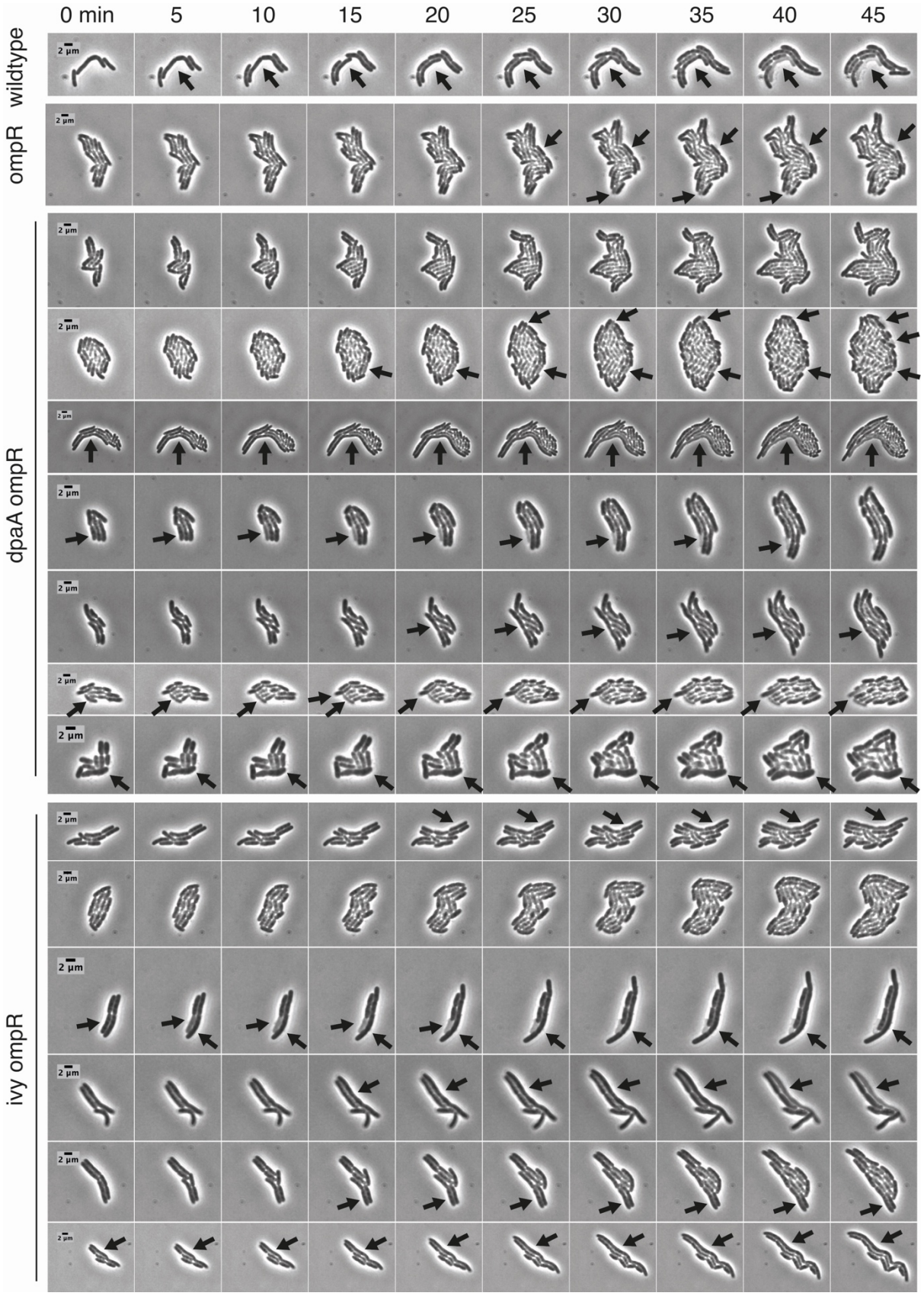

Figure 24: Dissecting gene-gene-drug interactions of ompR in the presence of cefotaxime by live microscopy. *Different genotypes were grown overnight, diluted to $OD_{595\ nm}$ of 0.002, pinned on an agar plate containing sub-inhibitory concentrations of cefotaxime, and imaged during live growth at 37 °C with 25 frames per well using SLIP* (Shi et al. 2017). *Phase-contrast images were acquired on a Ti-E inverted microscope (Nikon Instruments) using a 100X (NA 1.40) oil immersion objective.*

To conclude, I used SLIP (Shi et al. 2017) high-throughput single-cell live imaging to identify morphological features during cell growth and division that inform about the epistatic gene-gene-drug interactions. From the live microscopy data in the presence of cefotaxime, it was possible to qualitatively deduce resistance levels of specific mutants by the severity of their phenotypes. Similar to wildtype cells, *dpaA* and *ivy* filamented and lysed (with bulging or bursting and visible expulsion of cytoplasm). Those phenotypes were much milder in the resistant Δ*marR* mutants and almost nonexistent in the even more resistant Δ*ompR* mutants.

For Δ*dpaA*Δ*marR* double mutants, cells were thinner and exhibited severe filamentation, often resulting in spirals, which suggested exacerbated effects of cefotaxime on the cell division machinery in Δ*dpaA*Δ*marR* double mutants. These phenotypes coincided with frequent lysis. Since cefotaxime-induced filamentation and lysis were more severe in the Δ*dpaA*Δ*marR* double mutant than in the Δ*marR* single mutant, this suggested that without DpaA, Δ*marR* cells were less able to tolerate cefotaxime. The thin morphology and strong filamentation suggested a vulnerability of the cell division machinery in Δ*dpaA*Δ*marR* mutants exploited by cefotaxime. Since the Δ*dpaA*Δ*marR* mutants already showed filamentation in the absence of cefotaxime and cefotaxime causes filamentation in wildtype cells, both effects may synergize when combined. The increased number of PG linkages with Lpp in the absence of DpaA could be a possible explanation for the filamentation, and it could also be responsible for the synergistic interaction between the Δ*dpaA*Δ*marR* mutant and the cefotaxime effect. These findings point to why the *marR* evolutionary trajectory is detrimental for *dpaA* mutants and why *dpaA* mutants display decreased evolvability as a result.

Δ*ivy*Δ*marR* double mutant also showed frequent lysis, but in contrast to the Δ*marR* mutants, cell width was instead increased, and filamentation frequency decreased, indicating a more active divisome. This was already the case for the Δ*ivy*Δ*marR* mutants in the absence of cefotaxime, and the addition of cefotaxime only increased lysis frequency without filamentation. Since the activity of LTs is higher in Δ*ivy* mutants, this activity could rescue cell division defects caused by cefotaxime, which it does phenotypically.

The Δ*dpaA*Δ*ompR* double mutants displayed frequent filamentation, lysis, bulging, and bursting of cells, coinciding with increased cell width. Even though I observed filamentation in both the Δ*dpaA*Δ*marR* and the Δ*dpaA*Δ*ompR* double mutants, the cell width of those filaments is much larger in the Δ*ompR* than in the Δ*marR* background, suggesting an additional

effect in the Δ*ompR* double KOs. The increased frequency and severity of the phenotypes in the Δ*dpaA*Δ*ompR* mutants compared to the Δ*ompR* single mutants indicates that Δ*dpaA*Δ*ompR* mutants were much more sensitive to cefotaxime than the Δ*ompR* single mutant, confirming the gene-gene-drug interaction identified by quantifying genetic interactions. In summary, the Δ*dpaA* shows a consistent effect of inducing filamentation with both Δ*marR* and the Δ*ompR* in absence the absence of cefotaxime, potentially indicating an inhibited divisome, which is exacerbated by cefotaxime inducing filamentation and inhibiting the divisome itself. The Δ*ivy* decreased filamentation in the Δ*ivy*Δ*marR* and increased filamentation in the Δ*ivy*Δ*ompR*, both coinciding with increased cell width. This distinct phenotype of *ivy* and *dpaA* could indicate different components contributing to their epistatic interactions despite their similar genetic interactions, highlighting the need to investigate genetic interactions from multiple angles.

Even though live imaging was only used qualitatively, it allowed me to investigate the growth and division dynamics of all single and double mutants in the absence and presence of antibiotics across hundreds of cells. Showcasing severe examples of growth aberrations provides an overview of the state and common phenotypes for cells of each genotype. Without an antibiotic, wildtype cells never exhibited severe filamentation, bulging, or lysis. These phenotypes were not observed across 50 frames with several outgrowing cells per frame, *i.e.*, 250-500 cells, making them rare to occur by chance and indicative of the genotype they occur even in a small sub-population.

Live microscopy allowed me to investigate how double mutants of evolvability genes and resistance elements grow and divide compared to single mutants. This analysis revealed multiple phenotypes that arise in single and double mutants in the absence or presence of cefotaxime, informing about the underlying gene-gene and gene-gene-drug interactions. When deleted for one of the evolvability genes *dpaA* or *ivy*, both resistance elements *marR* and *ompR* mutants showed stronger phenotypes in the presence of cefotaxime. This finding confirms my hypothesis that evolvability gene KOs delay resistance evolution by blocking evolutionary paths, including those resistance genes. To zoom in closer on the molecular details of such epistatic interactions, I decided to perform MS-based proteomics on the same single and double mutant mutants of evolvability and resistance genes.

6. Using proteomics to uncover the molecular signature of epistasis

To further investigate the role of the genes I uncovered in adding constraints to the evolution of resistance to AMR, I used proteomics to quantify the protein cell state of single and double KO mutants of the evolvability (*dpaA* and *ivy*) and resistance (*marR* and *ompR*) genes. In total, I profiled exponentially growing cells of four single and four double mutants, as well as wildtype controls in MHB ($OD_{595\ nm}$ of 0.5) at 37 °C, using quantitative proteomics with the help of Dr. Dimitrios Papagiannidis, as described before (Banzhaf et al. 2020; Mateus et al. 2020). The detailed procedure can be found in Chapter VI. I will first discuss the results of the single KO mutants and then how they relate to the change in protein abundance of double KO mutants.

6.1. Proteomics analysis reveals vulnerabilities in single KO mutants

I identified several proteins whose abundance was changed in the resistance mutants *marR* KO and *ompR* KO relative to the wildtype (Figure 25). I called hits separately for essential and non-essential proteins since essential proteins showed a smaller dynamic range, as observed previously (Mateus et al. 2020). The first quality control measure was to check whether both mutants showed the effects expected and reported in the literature (Sharma et al. 2017; Yoshida et al. 2006; Norioka et al. 1986; Masi et al. 2022). As expected, the *marR* KO mutant displayed increased protein abundance for MarA, TolC, AcrA, and AcrB (*padj*. < 0.0001) and decreased abundance of OmpF, which is known to be regulated by *marR via* the small RNA micF (Dam et al. 2017; Ramani et al. 1994). As was reported, the *ompR* KO mutant showed a large decrease in protein abundance for OmpR, OmpF, and OmpC (Masi et al. 2022). Both the upregulation of the AcrAB-TolC efflux pump and the downregulation of OM porins OmpF and OmpC provide cefotaxime resistance (Schenk et al. 2022).

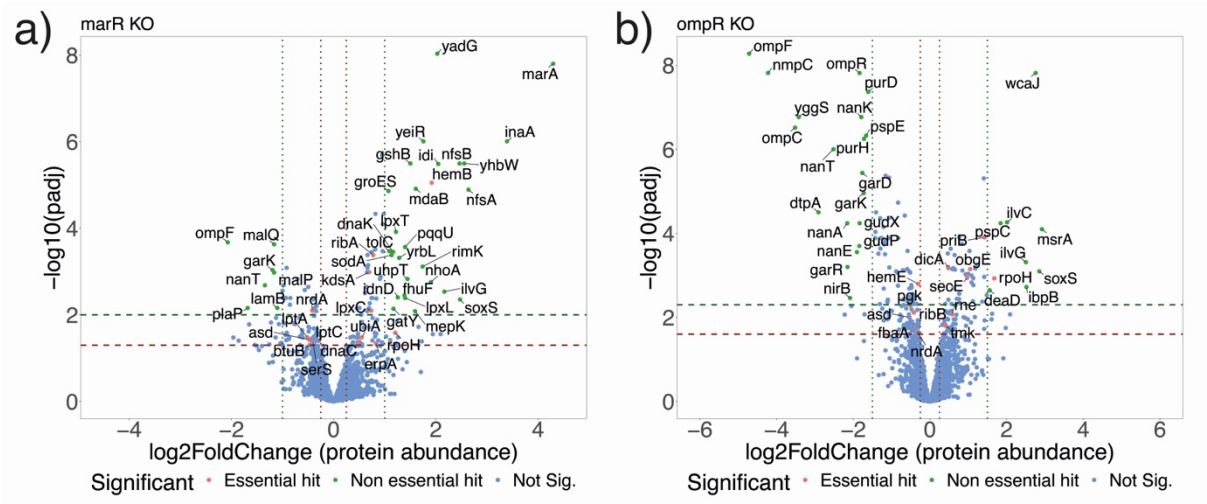

Figure 25: Mass spectrometry-based proteomics reveals protein abundance changes in marR (a) and ompR (b) deletion mutants. *Strains with different genotypes were grown overnight, diluted 1:1000, and grown until reaching the exponential phase of* $OD_{595\ nm}$ *of 0.5. Samples were measured in two replicates, and protein abundance and significance were calculated relative to the wildtype, as described before* (Banzhaf et al. 2020; Mateus et al. 2020). *Significant hits are indicated in red for essential proteins and green for non-essential proteins. Cut-offs are indicated by green and red lines for essential and non-essential proteins, respectively.*

For the *marR* KO mutant, several proteins changing in abundance were involved in LPS biosynthesis or transport. The fact that the resistant *marR* KO mutant displayed rewired LPS biosynthesis and transport is interesting, given that KOs of many genes involved in LPS biosynthesis and transport modulated resistance evolution rates against cefotaxime (Figure 12-14). Several proteins had increased abundance in the *marR* KO, including the rate-limiting essential LPS biosynthesis protein LpxC and the non-essential proteins LpxL and LpxT, suggesting that the expression of several genes of the LPS biosynthesis pathway is upregulated in *marR* KO mutants. An increase in *lpxT* expression has also been reported following sodium salicylate exposure (Pomposiello et al. 2001), which is known to activate MarA (Sulavik et al. 1995; Sharma et al. 2017), in agreement with my findings.

In the proteomics data of the *marR* KO mutant, I discovered that its essential LPS transport protein LptC is among the few essential proteins with ~20 % decreased abundance (L2FC = -0.30 relative to the wildtype). Decreased LptC levels perturb the transport of LPS from the IM to the OM (Sperandeo et al. 2006). Additional support for the significance of reduced LptC levels was observed in the decreased protein levels of LptA, which physically interacts and forms a complex with LptC (Sperandeo et al. 2011). Since the depletion of LptC and LptDE results in a decrease of LptA, it was suggested that LptA is degraded if it can not interact with LptC (IM) and LptD (OM) docking sites, thereby acting as a sensor of the correct assembly of

the Lpt complex (Sperandeo et al. 2011; Törk et al. 2023). The lower abundance of the LptA protein in the *marR* KO indicates a disruption in the assembly of the Lpt complex.

When the Lpt complex assembly is perturbed, for example, through LptC depletion, it affects the necessary transport of LPS from the IM to the OM. As a result, LPS levels increase in the IM and decrease in the outer leaflet of OM (Guest et al. 2021; Guest et al. 2020), which both cause negative effects on the cells. While LPS accumulation in the outer leaflet of the IM can be lethal (Guest et al. 2021; Guest et al. 2020), depletion of LPS in the OM results in increased sensitivity to SDS and bile salts, indicating a defective OM (Sperandeo et al. 2011; Sperandeo et al. 2006), as can be observed in available chemical genetics data for the *marR* KO mutants (Figure 26) (Nichols et al. 2011). The LPS defect in the *marR* KO seems strong, as it overcomes the upregulation of the AcrAB-TolC system, which pumps those compounds out of the cell and is upregulated in this mutant (Nichols et al. 2011).

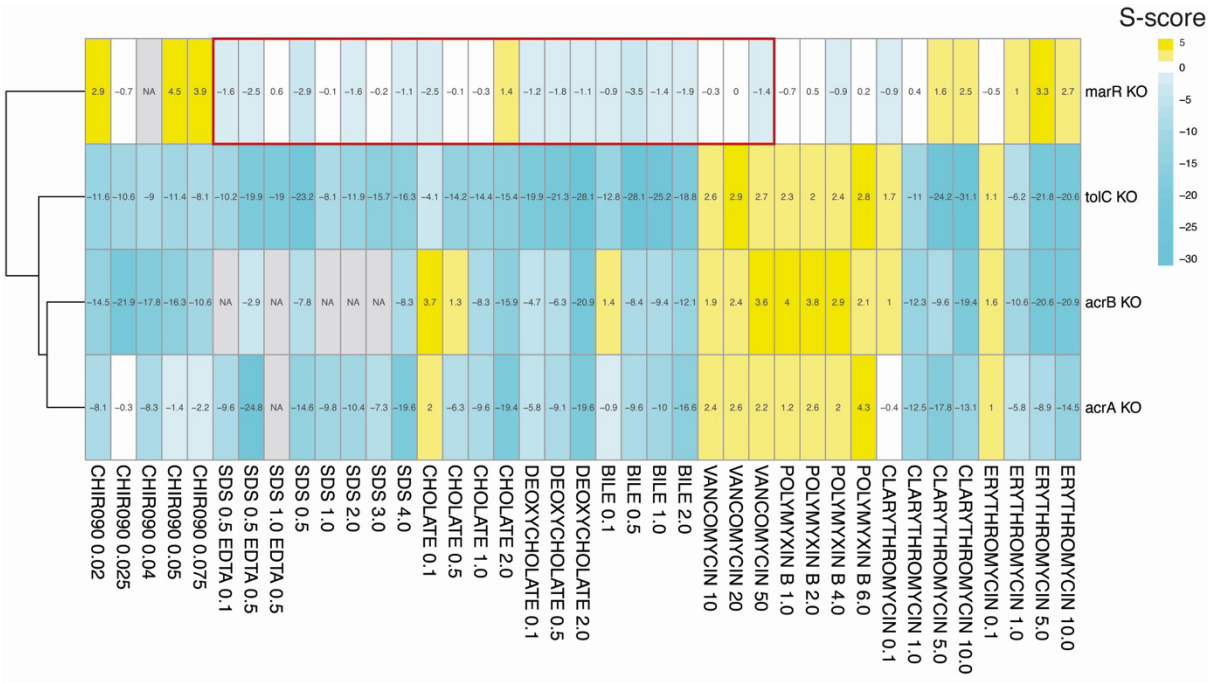

Figure 26: Chemical genetics data reveals drug sensitivities of the marR KO mutant (data from* (Nichols et al. 2011)*). *Chemical genetics S scores are shown for several membrane-active compounds in KO mutants of marR, tolC, acrA, and acrB. The increased sensitivity of the marR KO against SDS and bile salts despite the increased efflux of these compounds via an increased abundance of the AcrAB-TolC efflux pump indicates a perturbed outer membrane barrier function. Data taken from* (Nichols et al. 2011).

Accumulation of LPS in the IM upon disruption of LptA and LptC is toxic (Guest et al. 2021; Guest et al. 2020) and is signaled to the LPS production pathway in the cytoplasm (Shu & Mi 2022). Once LPS accumulates in the IM, it binds to the protein LapC. The binding of LPS to

LapC outcompetes the binding of LapB to LapC, which results in the release of LapB. The released adaptor protein LapB then delivers LpxC to FtsH and stimulates LpxC proteolysis *via* the LapB-FtsH complex (Shu & Mi 2022; Maniyeri et al. 2023; Klein et al. 2014; Nguyen et al. 2020). The essential enzyme LpxC catalyzes the first committed step in lipid A biogenesis and, therefore, represents a focal point in LPS biogenesis. Impairing LpxC degradation, for example, by *lapB* deletion results in overproduction of LPS and is lethal (Guest et al. 2021; Guest et al. 2020). However, it can be suppressed by decreasing LPS biosynthesis through an *lpxC* mutation, an Lpp deletion, or a mutant producing Lpp that can not be crosslinked to the PG (Guest et al. 2020). One explanation is that excess LPS can be removed by hypervesiculation through OMVs that are suppressed by PG-Lpp crosslinks and enhanced in Lpp mutants unable to form such crosslinks (Guest et al. 2020; Klein et al. 2014; Guest et al. 2021; Sutterlin et al. 2016). This directly relates to the negative epistasis between the *marR* KO and *dpaA* KO since the *dpaA* KO has increased PG-Lpp crosslinks (Bahadur et al. 2021; Matthias et al. 2021) and could be impairing vesiculation of excess LPS and thereby exacerbating the toxicity caused by the accumulation of LPS in the IM of *marR* KO mutants.

Another factor contributing to this phenotype is that LpxC, which should be decreased as a result of degradation by the LapB-FtsH complex upon accumulation of IM LPS in the *marR* KO, actually shows increased abundance in the *marR* KO (Figure 25a). Therefore, the *marR* KO mutant also produces more LPS in addition to its perturbed LPS transport from IM to OM. The regulatory cascade of LPS being detected in the IM is functional in *marR* KO mutants, which can be detected by elevated LapB protein levels (not significant, but L2FC = 0.48 relative to wildtype, corresponding to a 40 % increase). These findings suggest that MarA somehow interferes differently with the negative feedback of LPS production.

Such deregulation of LpxC was described in the literature for *marR* KO mutants (Maniyeri et al. 2023). LOF mutants of *lapC* lacking the periplasmic domain show elevated degradation of LpxC, which can be suppressed by *marA* and *pldA* overexpression (Maniyeri et al. 2023). Using transposon mutagenesis, the authors identified that the Mla pathway is required for the *marA*-mediated multicopy suppression of elevated LpxC degradation, which is not due to altering the LPS core or lipid A structural properties *via* the Mla pathway. The authors concluded that MarA directly regulates LpxC stability in an Mla-dependent way (Maniyeri et al. 2023). As a result, the Mla pathway could contribute to increased LpxC stability and abundance in *marR* mutants despite the aberrant accumulation of LPS in the IM due to LptA and LptC depletion. In line

with this hypothesis, Mla pathway genes are enriched among gene KOs, improving resistance evolution against cefotaxime (Figures 12 and 13). Therefore, deletions of Mla pathway genes could support *marR* mutations evolving during resistance evolution against cefotaxime by reinstating their negative LPS regulation, while deletions of LPS biosynthesis genes directly reduce LPS levels. One of the gene KOs with the highest evolvability at both 1.5x and 13.5x MIC was the *lapB* KO (Figure 12-14), which was described to carry a suppressor mutation in *lpxC* strongly reducing LPS biosynthesis (Mahalakshmi et al. 2014). Mutating *lpxC* also suppressed cell death due to excess LPS resulting in OMVs and OM blebs in *mlaA* GOF mutants (Sutterlin et al. 2016), as well as cell death due to the lethal accumulation of LPS in the IM of a *lapB* KO mutant (Guest et al. 2020).

In addition, a direct epistatic interaction has been reported between LptC-depletion and the deletion of *dpaA* (Morè et al. 2019). In contrast to deletions of ldtD and ldtE, ldtF/*dpaA* deletions showed morphological defects even when LptC levels were only mildly decreased (cells with LptC deletion supplemented with LptC from a plasmid and grown in the presence of inducer) (Morè et al. 2019). Decreasing LptC levels substantially in a *dpaA* KO (cells grown without plasmid inducer) results in strong morphological defects and cell death (Morè et al. 2019). These findings indicate a strong negative interaction between LptC depletion and *dpaA* KO. Given that *marR* KO also displayed decreased LptC (Figure 25a) levels, these findings provide another angle to explain the negative epistasis with the *dpaA* deletion.

Furthermore, one can suppress the lysis of *dpaA* KO mutants with decreased LptC levels when the cell envelope stress-induced activator of amidases *actS* is deleted (Gurnani Serrano et al. 2021). ActS activates the PG amidase AmiC and restores functional cell separation in nlpD envC mutants (Gurnani Serrano et al. 2021; Mueller et al. 2021). Authors proposed that the ability of ActS to modulate AmiC activity is somehow controlled by DpaA, potentially *via* the altered PG architecture mediated by DpaA detaching Lpp from PG (Bahadur et al. 2021; Matthias et al. 2021). Upon LptC depletion and the resulting decrease of LPS transport, DpaA indirectly affects the ActS-mediated activation of amidases. When deleting *dpaA* in such cells under LPS stress, amidases are hyperactivated by ActS and lyse the cells, which can be suppressed by deleting *actS*. Under these conditions, NlpD can partially reinstate cell separation by controlling AmiC (Gurnani Serrano et al. 2021). This provides an alternative explanation that hyperactivated amidases cause the negative epistasis between the deletion of *dpaA* in a *marR* KO background with decreased LptC levels, which constrains cefotaxime

AMR evolution. Further complementary evidence is provided by decreased evolvability of the *actS* KO mutant during cefotaxime resistance evolution, indicating a requirement for the activation of amidases during resistance evolution.

In line with existing literature, I confirmed that cefotaxime resistance in *marR* mutants is caused by increased levels of the AcrAB-TolC efflux pump and a decrease of the major outer membrane porin OmpF (Figure 25a). In addition, I identified that LPS transport from the IM to the OM is perturbed in *marR* KOs (Figure 25a), which has several consequences for the cells. First, LPS molecules that can not be transported from IM to the OM and potentially accumulate in the IM become toxic. Second, fewer LPS molecules reach the OM, which compromises OM stability and results in a defective OM, as well as an increased susceptibility to hydrophobic compounds such as SDS or bile acids. Lastly, negative regulation to decrease LPS production by degrading LpxC *via* the LapB-FtsH complex is overcome by MarA activation, stabilizing LpxC against such degradation *via* the Mla pathway.

For the *ompR* KO, I found proteins with differential protein abundance overlapping with but also distinct from the *marR* KO. Besides the downregulation of porins OmpC and OmpF, multiple pathways were downregulated in *ompR* KO mutants. Those included proteins from D-galactarate degradation (GarD, GarK, GarR), D-glucarate degradation (GudD, GudP, GudX), purine nucleotides de novo biosynthesis (PurA, PurB, PurC, PurD, PurF, PurH, PurK, PurL, PurM, PurT), pyrimidine deoxyribonucleotides de novo biosynthesis (NrdA, NrdB), maltose transport (MalF, MalG, MalK, MalP, MalQ, MalS) and N-acetylneuraminate and N-acetylmannosamine degradation (NanA, NanE, NanK, NanQ, NanT). The fact that porins play a critical role in importing nutrients could explain the strong metabolic rewiring in the *ompR* KO, which has two major porins, OmpC and OmpF, strongly downregulated. Of those proteins, only OmpF, MalQ, GarK, NanT, MalP, and NrdA showed lower abundance in the *marR* KO, representing most pathways but only with a single representatives.

Regarding genes with higher protein abundance, I found several overlaps between the *marR* and *ompR* KO. Both the transcriptional regulator SoxS and RpoH encoding the sigma factor σ32 also displayed higher protein abundance in the *ompR* KO, as well as the LPS biosynthesis protein LpxC. Lastly, PspA and PspC that protect membrane integrity under stress conditions such as heat shock or osmotic shock (Liu et al. 2021; Mehner et al. 2012; Mehta et al. 2013) were also increased in abundance in both mutants.

In summary, both the *marR* and *ompR* KOs are subject to major rewiring of the proteome, as expected for major transcriptional regulators. For the *marR* KO, this mainly affected LPS biosynthesis and transport. For the *ompR* KO, large changes happened in the carbon metabolism and nucleotide biosynthesis, likely as a consequence of both major porins being lowly expressed. For MarA, the primary gene repressed by MarR, its regulatory targets have been mapped globally using ChIP-seq and *in vitro* DNA binding (Sharma et al. 2017), and neither the LPS biosynthesis and transport genes nor the metabolism genes were direct regulatory targets of MarA. This suggests that the effect on the abundance of those proteins observed in this current work is indirect. For example, MarA was reported to stabilize LpxC *via* inducing expression of the *mla* pathway, representing a direct binding site and target (Maniyeri et al. 2023; Sharma et al. 2017).

For the two evolvability gene KO mutants *dpaA* and *ivy*, I found the following results (Figure 27). Interestingly, DpaA had lower protein abundance in the *ivy* KO mutant (Figure 27), suggesting that, at least partially, the *ivy* KO would phenocopy the *dpaA* KO. Both the *dpaA* and *ivy* KO were identified as evolvability genes required during cefotaxime evolution, both show gene-gene interactions with *marR*, and gene-gene-drug interactions with *ompR* constraining resistance evolution. Since both the *dpaA* and *ivy* KO show lower DpaA abundance, it could indicate that the absence of DpaA is driving the constraining effect on cefotaxime resistance evolution through genetic interactions with resistance regulators.

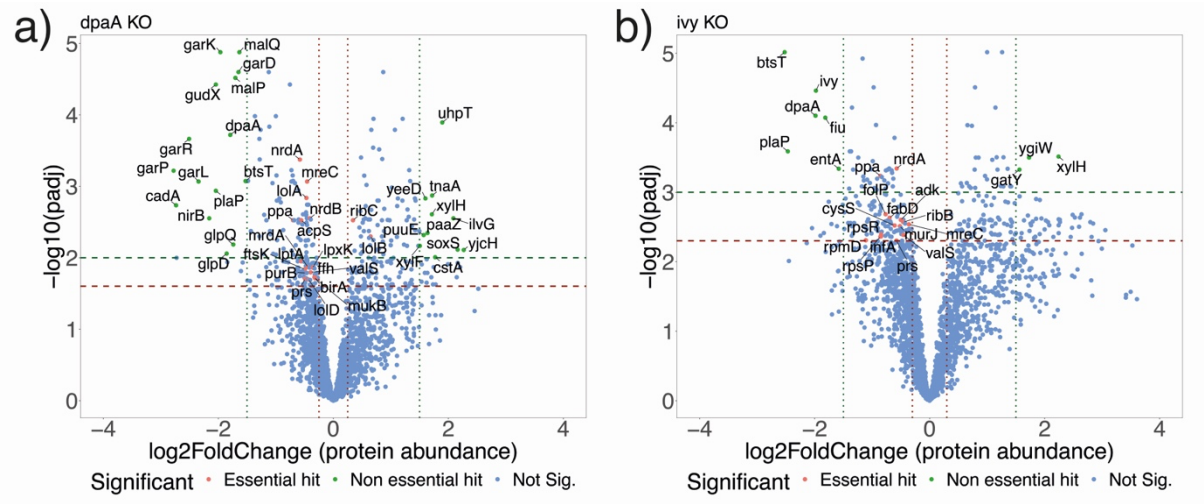

Figure 27: Proteomics reveals protein abundance changes in dpaA (a) and ivy (b) deletion mutants. *Strains with different genotypes were grown overnight, diluted 1:1000, and grown until reaching the exponential phase of* $OD_{595\ nm}$ *of 0.5. Samples were measured in two replicates, and protein abundance and significance were calculated relative to the wildtype, as described before* (Banzhaf et al. 2020; Mateus et al. 2020)*. Significant hits are indicated in red for essential proteins and green for non-essential proteins. Cut-offs are indicated by green and red lines for essential and non-essential proteins, respectively.*

Regarding essential proteins with lower abundance in the *dpaA* KO, I found LolA and LolD from the lipoprotein trafficking pathway, LptA from the LPS transport system, and LpxK involved in LPS biosynthesis. For non-essential proteins, I saw several members of galactarate and glucarate degradation, purine and pyrimidine de novo biosynthesis, and maltose transport exhibited decreased protein abundance. In contrast, fatty-acid transport and activation (FadD, FadH), LolB as part of the lipoprotein trafficking pathway, and MarA were some of the upregulated proteins in the *dpaA* KO.

For the *ivy* KO, I found multiple proteins with lower abundance in maltose transport, purine biosynthesis, the 30S ribosomal subunit (RpsH, RpsP, RpsR, RpsU), the 50S ribosomal subunit (RpmB, RpmD, RpmH), fatty-acid metabolism (FadD) and flipping lipid II across the IM (MurJ). For increased protein abundance, I also identified LolB (lipoprotein trafficking pathway), galactitol degradation proteins (GatB, GatC, GatD, GatY), as well as the chaperones (ClpB and GroES).

In summary, by mapping the proteome of the two resistance element KOs *marR* and *ompR*, as well as the two evolvability gene KOs *dpaA* and *ivy*, I can hypothesize about both their individual cell states as well as possible explanations for negative epistasis between the *dpaA* and *ivy* KO with the *marR* KO and *ompR* KO.

MarR mutations acquired through resistance evolution rewire the genetic network and create a genetic vulnerability that can be exploited by deleting one of the two evolvability genes, *dpaA* or *ivy*. The decreased cleavage of PG-Lpp crosslinks in *dpaA* KO mutants (and *ivy* KO mutants phenocopying those effects due to DpaA depletion) leads to an increased abundance of such crosslinks. One possible explanation is that the increased number of PG-Lpp linkages in *dpaA* KO mutants displays negative epistasis with *marR* KO mutants by inhibiting the shedding of excess LPS *via* OMVs. An alternative hypothesis is that uncontrolled ActS-mediated activation of amidases in *dpaA* KOs lyses the *marR* KOs with decreased LptC levels, which would also act *via* the increased amount of PG-Lpp linkages in the *dpaA* and *ivy* KO mutants. To test this hypothesis, I will measure the gene-gene interaction between the *dpaA* and *marR* KOs in the absence of multiple genes contributing to the proposed mechanism in Chapter III.7.

Besides major rewired LPS biosynthesis and transport in the *marR* KO, insights gained from the proteomics revealed metabolic remodeling in the *ompR* KO and the absence of DpaA in

both the *dpaA* and *ivy* KO mutant. Another shared feature of the *dpaA* and *ivy* KO is upregulated lipoprotein trafficking through LolB and changes in fatty-acid transport and metabolism (increased in *dpaA* KO and decreased in the *ivy* KO), which could influence the epistatic interaction through its effect on Braun's lipoprotein or Lpp, whose linkages with the OM DpaA cleaves. In the next step, I compared how the proteomic changes translate from the individual single KO mutants to the double KO mutants.

6.2. Proteomics analysis of double mutants uncovers activated stress response

To investigate the molecular basis of the epistatic interactions between evolvability and resistance genes, I compared the double KO mutants of the evolvability and resistance genes with the wildtype (Figure 28) and related these changes to the ones I measured in the single mutants.

In the *marR dpaA* double KO (Figure 28a), similarly to the *dpaA* KO, I identified an increased abundance of proteins involved in LPS biosynthesis, such as LpxA and LpxC, while the abundance of LolA, a periplasmic chaperone transporting lipoproteins from the IM to the OM (Matsuyama et al. 1995; Matsuyama et al. 1997), was decreased. Those genes were also evident in the *ompR dpaA* double mutant. This could suggest that the increased LPS biosynthesis in the *dpaA*, *ivy*, and *marR* KOs add up or synergize when combined as double mutants, potentially culminating in the observed negative genetic interaction.

Similar to the *ompR* single KO and most likely directly or indirectly regulated by OmpR (Figure 25), the *ompR dpaA* double KO showed a large decrease in several proteins involved in cellular metabolism (Figure 28c). The same can be observed in the *ompR ivy* KO (Figure 28d). In addition, both *ompR* double mutants exhibit a lower abundance of ribosome-related proteins, RpmH in the case of *ompR dpaA* and RpsP and RpsR in the case of *ompR ivy*. Lower protein abundance of the essential ribosome subunits RpsP, RpsR, and RpmD and the folate biosynthesis protein FolP were also detected in the *ivy* single KO and carried over into both the *ompR ivy* and *marR ivy* double mutants (Figure 28b and 28d). The lower expression of essential ribosome subunits in the *ompR ivy* and *marR ivy* double mutants could contribute to the negative genetic interaction between *ivy* and both resistance regulators *marR* and *ompR*. The negative gene-gene interaction with *ompR* was only observed for *ivy*, not *dpaA*.

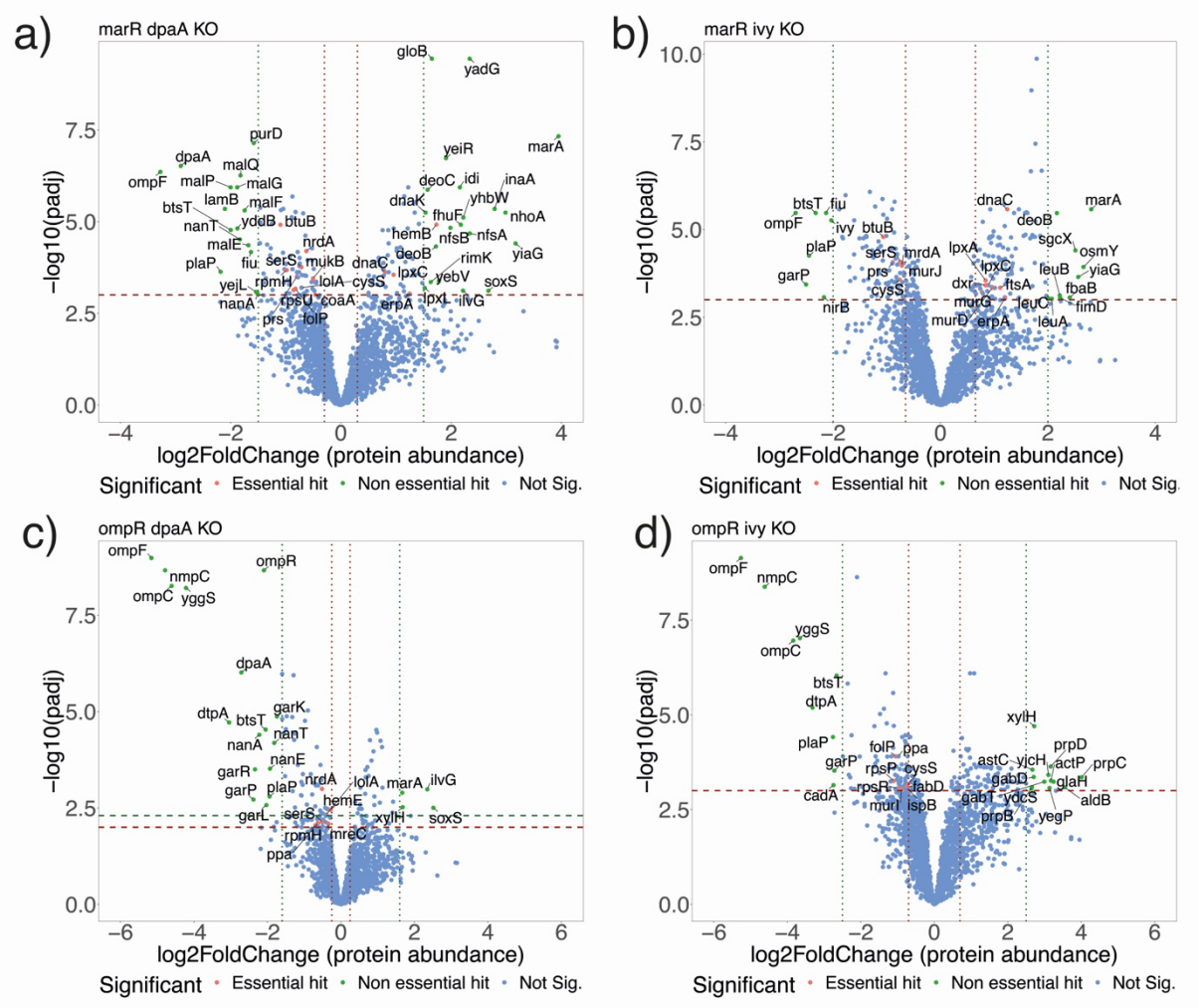

Figure 28: Using proteomics to identify the proteomic signature of gene-gene interactions in double mutants. *Strains with different genotypes were grown overnight, diluted 1:1000, and grown until reaching the exponential phase of* $OD_{595\ nm}$ *of 0.5. Samples were measured in two replicates, and protein abundance and significance were calculated relative to the wildtype, as described before* (Banzhaf et al. 2020; Mateus et al. 2020). *Significant hits are indicated in red for essential proteins and green for non-essential proteins. Cut-offs are indicated by green and red lines for essential and non-essential proteins, respectively.*

Interestingly, both the *dpaA* and *ompR* single KOs showed increased MarA protein abundance (*padj*. < 0.005), which is further increased in the *ompR dpaA* double KO (*padj*. < 0.002). This could suggest that gene-gene-drug interaction between *ompR* and the *dpaA* and *ivy* KO mutants is caused by cefotaxime further increasing the already elevated MarA levels (Hao et al. 2014; Hiniker et al. 2005) in the *ompR* KO, revealing the gene-gene interaction between MarA and the KOs of *dpaA* and *ivy* also in the *ompR* KO.

Proteome-abundance abundances of both single and double mutants of evolvability and resistance genes allowed me to track the contributions of single into double KO mutants. Interesting insights included increased LPS biosynthesis in the *marR dpaA* double KO, supporting LPS accumulation as a contributor to the negative epistatic interaction constraining

the evolution of *marR* mutations in *dpaA* KO mutants. Another relevant finding was an increased MarA level in the *ompR dpaA* double KO that functionally links *ompR* and *marR* mutations with interesting implications for the identified genetic interactions. Further increasing MarA levels in the *ompR* KO mutant, for example, through cefotaxime (Hao et al. 2014; Hiniker et al. 2005), might reveal the gene-gene interaction between MarA and *dpaA* also in the *ompR* KO mutant. Lastly, decreased levels of ribosomal subunits in the *marR ivy* and *ompR ivy* double mutants could contribute to the negative gene-gene interactions between the evolvability gene *ivy* and the resistance genes *marR* and *ompR*.

Next, I wanted to directly test epistatic interactions occurring during cefotaxime resistance evolution and further investigate genetic dependencies of the epistatic interactions between the evolvability genes *dpaA* and *ivy* with the resistance gene *marR*. Therefore, I probed their epistatic gene-gene interactions directly in an evolved mutant taken from the evolution experiment and in the absence of 17 other genes potentially contributing to the genetic interaction.

7. Breaking epistatic interactions that delay resistance evolution

To closely resemble epistatic interactions present during cefotaxime resistance evolution, I also measured genetic interactions directly in a cefotaxime resistance mutant lineage from the validation experiment (Chapter III.4.2). Thereby, I tested whether epistatic interactions are causing the evolutionary delay in clean genetic KOs as well as in resistant lineages evolved under the conditions that carry these variants.

Additional evidence supporting the deregulated toxic overproduction of LPS in the *marR* KO is that one sequenced *marR* KO mutant (Evo 25b) acquired a potentially compensatory mutation in LPS biosynthesis. This IS-element insertion in *waaQ*, at the beginning of the LPS biosynthesis operon, likely perturbed LPS biosynthesis to compensate for the toxicity of the *marR* deletion this strain carried. Following my hypothesis that the gene-gene interaction of the *marR* KO with the *dpaA* KO is caused by decreased LPS transport from IM to OM and deregulated LPS production resulting in the LPS accumulation in the IM, a compensatory mutation decreasing LPS production should, therefore, also prevent the gene-gene interaction of the *marR* KO with the *dpaA* KO. This negative interaction was reverted in the evolved strain Evo25b carrying a *waaQ* insertion on top of the *marR* deletion upon *dpaA* KD (Figure 29),

measured as in Chapter III 4.2. in the absence of cefotaxime. However, this was not the case for the *ivy* KD, which still showed negative epistasis in the evolved mutant, indicating that the epistatic interaction between *ivy* KO and *marR* KO has additional components besides the absence of DpaA in the *ivy* KO.

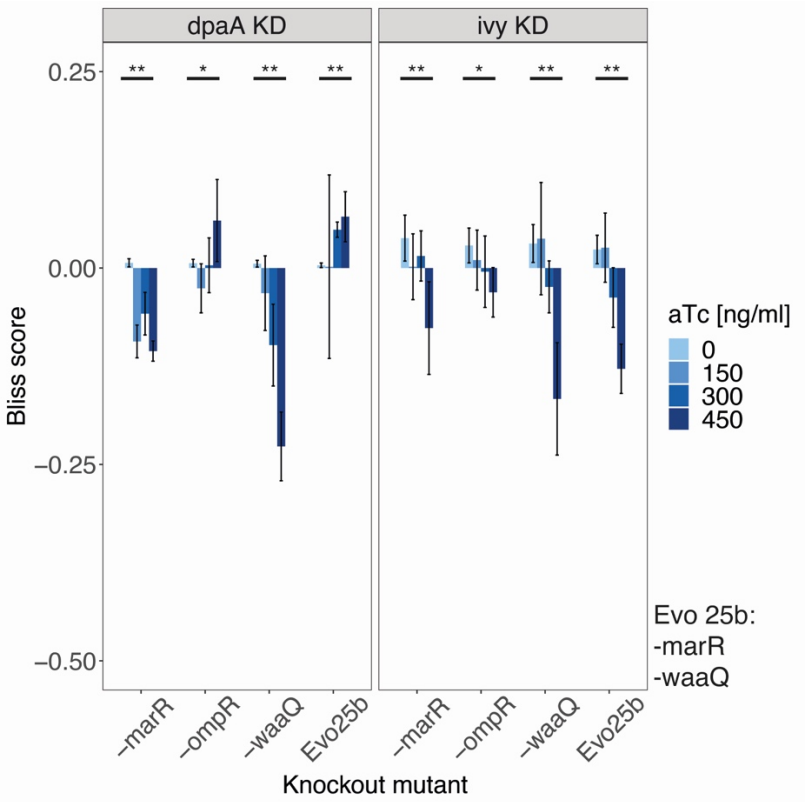

Figure 29: Measuring gene-gene interactions in an evolved cefotaxime-resistant mutant. *Bliss interaction scores between evolvability gene KDs dpaA and ivy in the evolved resistant mutant Evo25b carrying a marR and waaQ deletion. The negative gene-gene interaction between the dpaA KD and the marR KO is reverted by the additional deletion of waaQ, while the negative gene-gene interaction between the ivy KD and the marR KO still occurs in the evolved mutant. Error bars represent the standard deviation across calculated Bliss scores. Significance was calculated by comparing Bliss scores with 450ng/ml aTc and without induction by the BH-adjusted Wilcoxon signed-rank test. * padj. < 0.05, ** padj. < 0.01, *** padj. < 0.001.*

In order to test my hypothesis about the mechanism underlying the identified gene-gene interaction between the evolvability gene *dpaA* and the resistance gene *marR*, I tested the potential dependence on several genes by measuring gene-gene interactions in their absence (Figure 30). I picked the genes with positive evolvability scores and functional association with the evolvability gene *dpaA*, the resistance element *marR*, or my proposed mechanism for the epistatic interaction.

Since increased expression of *acrA*, *acrB*, and *tolC* encoding the efflux pump AcrAB-TolC and decreased expression of the genes *ompC* and *ompF* encoding OM porins are associated with

the resistance mechanism of the resistance gene *marR* (Schenk et al. 2022), I included them. For the evolvability gene *dpaA* that cleaves crosslinks between PG and Lpp, I chose *ldtA*, which creates such crosslinks and because the KO showed a positive evolvability score. MepK and MepS are endopeptidases, while MltC and MltF are lytic murein transglycosylases, which I included due to their increased evolvability scores and involvement in cleaving PG crosslinks in the cell envelope. I chose KOs of *mla* genes because they are required for the stabilization of LpxC by MarA and for removing misplaced PLs in the outer leaflet of the OM, which potentially accumulate there due to decreased LPS levels in the OM. Both *mla* and *wec* genes were enriched among better-evolving KOs. Another reason to include *wec* genes was that deletions of *wecC* were reported to partially restore disrupted outer membrane function and vancomycin resistance of *tol-pal* mutants by accumulating ECA intermediates (Jiang et al. 2020). LpxT showed increased evolvability when knocked out, increased protein levels in the *marR* KO, and is involved in LPS biosynthesis. I picked it since decreasing LPS biosynthesis could rescue the LPS deregulation if it contributes to the epistatic interaction. YtfK is a stringent response regulator activated under phosphate and fatty acid starvation conditions, its KO evolved better and was reported to show decreased accumulation of (p)ppGpp (Germain et al. 2019).

To test the effect of those genes on the gene-gene interaction between *dpaA* and *marR*, I first flipped out the kanamycin resistance cassette of the *marR* and *ompR* KO mutants using FLP recombinase encoded by the pCP20 plasmid (Datsenko & Wanner 2000). I replaced 17 genes, potentially affecting the epistatic interactions, in a wildtype, *marR*, and *ompR* KO background with a kanamycin resistance cassette using P1 transduction. All strains, including controls for single *marR*, *ompF*, *ompR*, and *waaQ*, were grown in liquid LB medium, arrayed in a 96-well plate, pinned to a solid LB medium agar plate, and the CRISPRi plasmid knocking down *dpaA* or *ivy* was conjugated at a density of 96 per LB agar plate with a conjugation donor spread as a lawn. After conjugation on double selection for spectinomycin and kanamycin, single and double KO mutants carrying the plasmid were transferred to liquid LB medium, grown overnight at 37 °C, and frozen in 20 % glycerol. The detailed protocol can be found in Chapter VI.

For the growth assay, each gene deletion of interest in a wildtype, *marR*, and *ompR* KO background was grown in liquid LB medium at 37 °C in triplicates, diluted about 1:1000 until $OD_{595\,nm}$ of 0.01, incubated shaking at 1000 rpm at 37 °C during which growth was monitored

by $OD_{595\ nm}$ in the presence and absence of 450 ng/ml aTc inducer for 24 h. Bliss scores were calculated as for the *dpaA* KD in the *marR* KO background in the absence of the antibiotic (Figure 17b) with the difference that the Bliss score without inducer was subtracted from the Bliss score with inducer, which calculates the change of Bliss score upon CRISPRi induction and DpaA depletion in every *marR* double KO mutant. The change in Bliss score was then compared with the *marR* single KO mutant to answer whether the *marR dpaA* gene-gene interaction was altered in the absence of an extra gene. This analysis should account for potential interactions between the extra gene deletion and the *marR* KO.

More specifically, I trimmed all growth curves at the time point when the untreated wildtype reached the highest $OD_{595\ nm}$ and determined the fitness by the area under the curve (AUC) relative to the AUC of the wildtype without induction. I calculated the Bliss interaction score of a mutant (single or double KO) carrying a CRISPRi plasmid by the fitness of the respective mutant with inducer ($f_{mutant_drug_gene}$) minus the fitness of the wildtype with inducer ($f_{wt_drug_gene}$) multiplied by the fitness of the mutant without inducer (f_{mutant}). I subtracted Bliss scores without induction from the Bliss scores with induction to arrive at the change of Bliss score upon CRISPRi induction and DpaA depletion.

$$\Delta\varepsilon = (f_{mutant_gene_induced} - f_{wt_gene_induced} \times f_{mutant_uninduced}) - (f_{mutant_gene_uninduced} - f_{wt_gene_uninduced} \times f_{mutant_uninduced})$$

Since I used three replicates for both mutant and wildtype, I calculated nine interaction scores between each replicate of mutant and wildtype, respectively. I assessed the significance by comparing the change in Bliss score between the *marR* single KO and all *marR* double KOs using the BH-adjusted Wilcoxon signed-rank test. The data is intrinsically noisy, given the biological variation resulting from perturbing three distinct genes in every strain and the technical variation of the high-throughput format, including experimentally adjusting 72 $OD_{595\ nm}$ values. Nevertheless, several gene KOs affected the gene-gene interaction between the *marR* KO and *dpaA* KD.

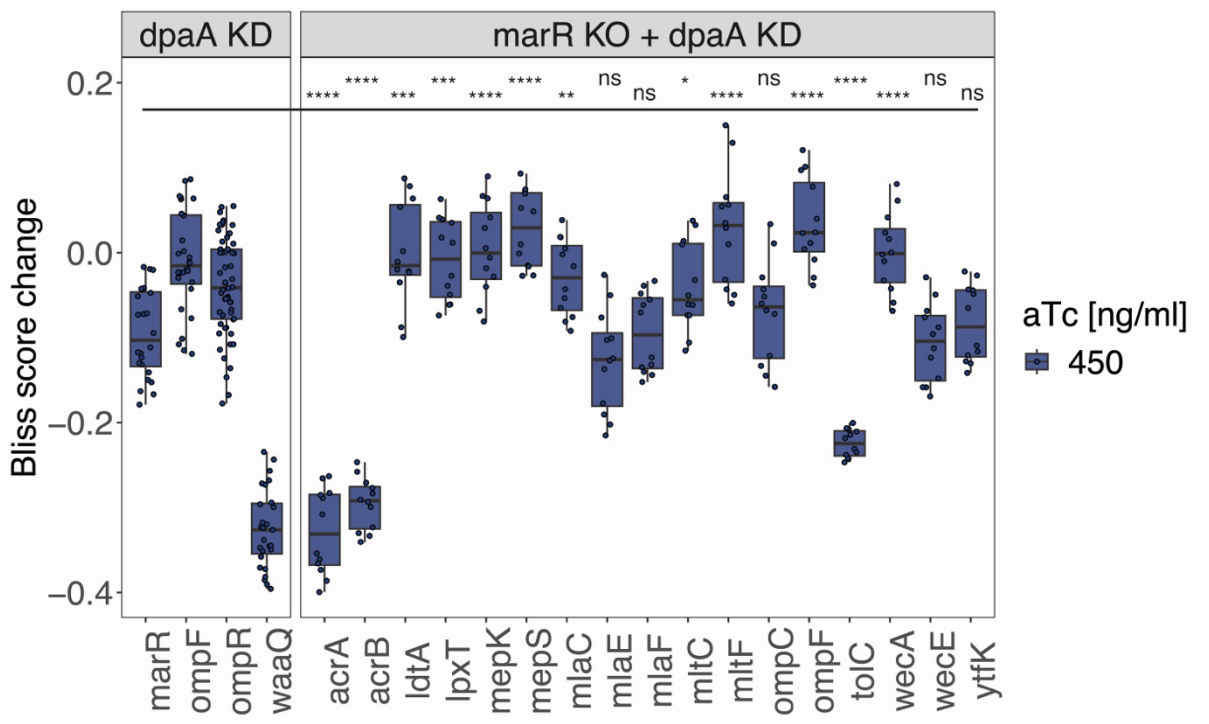

Figure 30: Measuring gene-gene-gene interactions reverting epistasis between dpaA and marR. *Measurement of Bliss score change of the gene-gene interaction between the dpaA KD and the marR KO in the absence of 17 KOs potentially affecting the strength of the interaction. Significance was calculated by comparing Bliss scores with 450ng/ml aTc between the marR single KO and all 17 marR double KO mutants by the BH-adjusted Wilcoxon signed-rank test. Several KOs such as ldtA, lpxT, mepK, mepS, mlaC, mltC, mltF, ompF, and wecA decreased the interaction, while acrA, acrB, and tolC increased the interaction. * padj. < 0.05, ** padj. < 0.01, *** padj. < 0.001.*

For the three genes encoding the AcrAB-TolC efflux pump, KOs increased the gene-gene interaction between the *marR* KO and *dpaA* KD. Since the upregulation of these efflux pump components is usually the major effect associated with *marR* KO and the resulting increase in MarA protein abundance (protein abundance of AcrA, AcrB and TolC increased in the *marR* KO *padj*. < 0.0005, Figure 25a) (Sharma et al. 2017), it was surprising that the gene-gene interaction increases upon KO of any of the three efflux pump components AcrA, AcrB and TolC. One possible explanation independent of the actual mechanism of the gene-gene interaction is that in the absence of the complete efflux pump, the intracellular aTc and, therefore, the *dpaA* KD levels are increased. Another explanation is that given the unstable cell envelope in *marR* KO mutants with potentially mislocalized LPS, the large machinery of the efflux pump spanning IM, periplasm including PG and OM contributes to the stability of the cell envelope, which is removed upon deletion.

KOs of several genes leading to increased evolvability reduced or prevented the gene-gene interaction (Figure 30). The gene-gene interaction was prevented in the *ldtA* KO, which creates fewer crosslinks between PG and Lpp, thereby directly counteracting the effect of the *dpaA*

KD, which cleaves fewer crosslinks. By cleaving m-DAP^3 - D-ala^4 crosslinks and linking m-DAP^3 to Braun's lipoprotein, *ldtA* anchors Lpp to PG and contributes to cell envelope stability (Braun & Wolff 1970; Magnet et al. 2007). Furthermore, KOs of the two endopeptidases *mepK* and *mepS* prevented the gene-gene interaction between *marR* and *dpaA*. Endopeptidase activity contributes to murein incorporation and PG expansion during bacterial growth and cell elongation. While *mepK* cleaves 3-3 crosslinks, *mepS* cleaves D-ala^4 - m-DAP^3 and m-DAP^3 - m-DAP^3 crosslinks in PG (Chodisetti & Reddy 2019). MepS also influences the cell division process by interfering with the activation of PG biogenesis by the divisome during septum formation (Truong et al. 2020). Both endopeptidases contribute to PG expansion and biosynthesis anchor Lpp to the PG by providing available m-DAP^3 that can be crosslinked to Lpp. Their deletion could counteract the *dpaA* KO by reducing the amount of crosslinked PG-Lpp. Another relevant observation is that MepK protein abundance was increased in the *marR*, *ompR*, and *dpaA* single KO mutants.

In addition, deletions of the two membrane-bound lytic murein transglycosylases perturbed the gene-gene interaction, with *mltF* showing a more substantial effect than *mltC*. Both LTs cleave the β-1,4 glycosidic PG bond between MurNAc and GlcNAc, performing a critical function in PG turnover (Lee et al. 2013; Dijkstra & Keck 1996). Since both *mltC* and *mltF* KO mutants evolved better during resistance evolution against cefotaxime (Chapter II.6.1.) and both genes were required for the gene-gene interaction between *dpaA* and *marR* (Figure 30), the PG cleavage they mediate was detrimental.

Also, deleting *lpxT* of the LPS biosynthesis pathway prevented the gene-gene interaction, further corroborating the hypothesis that the aberrant accumulation of LPS in the *marR* KO contributes to the observed gene-gene interaction. By transferring a phosphate group from Und-PP to the lipid A-core oligosaccharide (Touzé et al. 2008), LpxT enhances the negative charge of LPS and contributes to the recycling of Und-P required for PG and LPS biosynthesis (Egan et al. 2020). Increased *lpxT* expression has also been reported due to sodium salicylate exposure (Pomposiello et al. 2001), known to activate MarA (Sulavik et al. 1995; Sharma et al. 2017), which could indicate that the *lpxT* KO interrupts the direct and indirect regulation of LPS biosynthesis *via* MarA and the resulting gene-gene interaction with *dpaA* in the *marR* KO.

Of the three KOs from the *mla* pathway for phospholipid trafficking, only the *mlaC* KO reduced the *marR* interaction with *dpaA* (Figure 30). Since the *marA*-mediated stabilization of LpxC is

dependent on the *mla* pathway and, more specifically, *mlaC* and *mlaD* (Maniyeri et al. 2023), the fact that only *mlaC* disrupted the interaction suggests that toxicity is caused by the aberrant accumulation of LPS due to toxic LpxC activity resulting from its stabilization.

Without *wecA*, the gene-gene interaction between *marR* and *dpaA* was removed. The *wec* system is involved in ECA biosynthesis, and disruptions of *wecC* were reported to partially restore disrupted OM function and vancomycin resistance of mutants with increased membrane permeability, possibly by the accumulation of ECA intermediates (Jiang et al. 2020). I also tested the *wecC* KO for its effect on the gene-gene interaction (data not shown), but it could not be assessed due to the SL with the *marR* KO mutant even in the absence of aTc depleting *dpaA* levels. As a result, the *wecC* function was required in the *marR* KO background or the ECA intermediates, the *wecC* KO was reported to accumulate, reverted the negative genetic interaction. Lastly, the gene-gene interaction between *dpaA* and *marR* was tested in backgrounds with the major OM porins *ompC* and *ompF* deleted. Even though *marR* mutations downregulate *ompF via* the small RNA micF (Ramani et al. 1994; Dam et al. 2017), deleting *ompF* still reversed the gene-gene interaction. This effect could indicate toxicity between remaining OmpF and DpaA, or it can be explained by the *ompF* deletion reducing intracellular aTc levels and thereby decreasing the apparent gene-gene interaction. However, the *ompC* deletion did not affect the gene-gene interaction.

In summary, I illuminated the genetic dependencies of the gene-gene interaction between *dpaA* and *marR*, which delays resistance evolution against cefotaxime. While deletions of components of the major efflux pump AcrAB-TolC exacerbated the interaction, growth could be rescued in multiple ways. LdtA, *mepK*, and *mepS* KOs most likely reversed the interaction by decreasing PG-Lpp crosslinks, thereby counteracting the *dpaA* KO. LpxT and *mlaC* reversed the interaction's *marR* function, possibly by reducing LPS biosynthesis directly or indirectly by interrupting the MarA-mediated stabilization of LpxC. WecA contributes to ECA and O-antigen polysaccharide biosynthesis by catalyzing the transfer of GlcNAc-1-phosphate onto Und-P to form Und-P-P-GlcNAc (Rick et al. 1994). That inability of *wecA* mutants to synthesize LPS 08-side chains and ECA (Meier-Dieter et al. 1992) could explain why it prevents the gene-gene interaction by limiting LPS biosynthesis. MltF also interacts with GlcNAc by cleaving the β-1,4 glycosidic bond with MurNAc (Lee et al. 2013; Dijkstra & Keck 1996). The decrease of DpaA increases the amount of PG-Lpp linkages and, as a result, the rigidity of the cell envelope. LTs are a major component in PG turnover, and the *mltF* function

seems to directly contribute to the gene-gene interaction, potentially by contributing to lysis under cell envelope stress. The same was reported for amidases activated in *dpaA* KO mutants under LptC-depleted conditions, which is the case for the *marR* KO. The strong lysis phenotype of *dpaA* KO mutants during LptC-depletion could be rescued by deleting the activator of amidases *actS* (Mueller et al. 2021; Gurnani Serrano et al. 2021), which could be another interesting gene to test for its impact on the epistatic interaction of *dpaA* and *marR*. In the next step, I wanted to use the insights I gained on the rewired genetic network during cefotaxime resistance evolution to delay resistance evolution using different small molecules. Small molecules inhibiting evolution are preferred over the genetic targets from a translational angle since they could be applied in combination therapy with antibiotics as evolution inhibitors.

8. Using identified genetic vulnerabilities to delay resistance evolution with drugs

Using the identified genetic vulnerabilities during cefotaxime resistance evolution, I delayed resistance using different small molecules I selected in a hypothesis-driven manner. To probe perturbed outer membrane function against hydrophobic molecules of LptC-depleted cells, reflected by the increased sensitivity to SDS and bile acids for the *marR* KO in chemical genetics data (Nichols et al. 2011), I selected vancomycin and the macrolide clarithromycin. I included polymyxin B since it targets LPS in the inner and outer membranes, and I suspect LPS to be mislocalized in *marR* KO mutants.

Since the *marR* KO affects outer membrane function and permeability *via* the *mla* pathway (Sharma et al. 2017) and several KOs of *mla* genes increased resistance to mecillinam, erythromycin, clarithromycin, vancomycin, and polymyxin B (Nichols et al. 2011), elevated *mla* expression in *marR* KOs should increase sensitivity against those compounds. This potential susceptibility provided a rationale to include mecillinam, clarithromycin, and vancomycin.

The other compounds I selected from the acquired evolvability dataset after combining it with available chemical genetics data (Nichols et al. 2011). I filtered for less effective drugs (increased S-score) in evolvability gene KO backgrounds. In the presence of such drugs, cells need to decrease the expression of evolvability genes, which would contribute to surviving the drug, but decreasing their expression delays resistance evolution. To test this inferred collateral sensitivity, I chose procaine because of its positive interaction with the *hycG* and *dacA* KOs,

cefsulodin and trimethoprim by their positive interaction with the *pbpG* KO, and sulfamethizole by its positive interaction with the chaB KO. For all drugs, several concentrations were tested with the cefotaxime experimental evolution protocol in 96-well plates with the succession of MHB media, MHB media, 0.5x, 1.5x, 4.5x, and 13.5x MIC of cefotaxime while adding the extra drug at a constant sub-inhibitory concentration starting at the 0.5x MIC of cefotaxime for all following days (Figure 31).

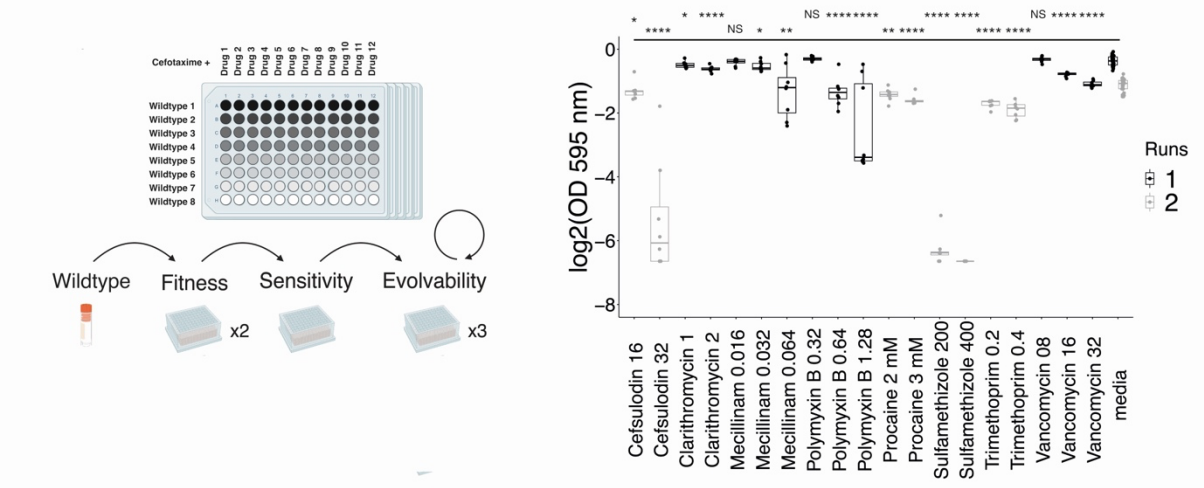

Figure 31: Delay cefotaxime resistance evolution with small molecules. *Workflow and results of small molecules delaying cefotaxime resistance evolution at sub-inhibitory concentrations in a concentration-dependent manner. All drug concentrations are shown in µg/ml except procaine in mM. Two runs were measured on two plate readers, explaining the different wildtype baselines. $Log_2(OD_{595\ nm})$ after growth in 4.5x MIC of cefotaxime is shown, and significance is assessed by the BH-adjusted Wilcoxon signed-rank test. * padj. < 0.05, ** padj. < 0.01, *** padj. < 0.001.*

By comparing sensitivity, *i.e.*, yield in the presence of 0.5x MIC of cefotaxime divided by yield without cefotaxime, with the sensitivity in the presence of the extra drugs, I chose drug concentrations where none of the drugs showed a relative sensitivity of less than 0.75, so none inhibited growth in the unevolved wildtype in the presence of 0.5x MIC cefotaxime. This measure should account for both inhibition by the extra drug and synergistic interactions of the extra drug with cefotaxime. Results from two different runs are depicted in gray and originate from data acquired by two plate readers. Drugs delaying resistance evolution were identified by the BH-adjusted Wilcoxon signed-rank test relative to the wildtype of its respective run at 4.5x MIC of cefotaxime. Multiple testing correction was performed, including all tests of both runs.

From run 1, I identified that clarithromycin, mecillinam, polymyxin B, and vancomycin delayed cefotaxime resistance evolution at non-inhibitory concentrations in a concentration-

dependent way. The fact that for both mecillinam and polymyxin B at the highest concentration, only some mutants could not evolve cefotaxime resistance indicated that the drugs blocked at least one but not all of the evolutionary trajectories. The effect sizes for decreased $OD_{595\ nm}$ were much larger than for clarithromycin. Vancomycin consistently delayed resistance evolution with a large effect size for all mutants in a concentration-dependent manner. In the second experiment, I identified that procaine and trimethoprim delayed the onset of cefotaxime resistance with small effect sizes. In contrast, the effect sizes for cefsulodin and sulfamethizole were much larger and entirely prevented growth in some mutants for cefsulodin and all mutants for sulfamethizole. It should be noted that besides the drugs shown here (Figure 31), I also tested buflomedil, cefoxitin, clenbuterol, clorgyline, cloxacillin, copper, desipramine, dibucaine, erythromycin, estradiol-17 beta, methotrexate, paraquat, suloctidil, ticagrelor, vatalanib using similar reasoning and concentrations inhibiting growth to a similar degree, which did not delay resistance evolution against cefotaxime (data not shown). The fact that many drugs could not delay cefotaxime resistance evolution suggests that the delay of cefotaxime resistance evolution mediated by the compounds shown (Figure 31) can not merely be explained by their inhibiting effect on growth.

While vancomycin, cefsulodin, and mecillinam target PG biosynthesis in the cell envelope, clarithromycin is a macrolide targeting the ribosome. Sulfamethizole (sulfonamide class of antimicrobials) and trimethoprim target tetrahydrofolate (THF) biosynthesis with sulfamethizole showing specificity for FolP and trimethoprim for FolA. The abundance of the essential protein FolP was decreased in the *ivy* single KO and all four double KOs of evolvability genes *dpaA* and *ivy* with the resistance genes *marR* and *dpaA* (*padj*. < 0.05). In existing chemical genetics data, both drugs showed correlated responses across KO mutants and differences (Nichols et al. 2011). While *glyA* KO mutants of the serine hydroxymethyltransferase were only sensitive to trimethoprim, *gcvP*, *gcvH*, and *gcvT* KO mutants of the glycine cleavage were only sensitive to sulfonamides. Both represent alternative branches of the pathway that synthesize 5,10-methylene THF from THF (Nichols et al. 2011). The fact that cefotaxime resistance evolution was delayed more by sulfamethizole than trimethoprim could indicate that the glycine cleavage pathway is conditionally essential during the resistance evolution. This hypothesis is supported by the fact that both *gcvH* and *gcvP* KOs represent bona fide hits for significantly delayed resistance evolution with unchanged fitness and sensitivity. At the same time, *glyA* and *gcvT* KOs evolved as the wildtype. This example shows the power of reverse genetics of genome-wide KO mutant libraries. Another explanation

could be that sulfonamides targeting FolP induce metabolic inhibition similar to the *ivy* KO, resulting in a more complete barrier to evolution.

Since the drugs vancomycin, polymyxin B, and clarithromycin all delayed resistance evolution against cefotaxime but target distinct processes, their structural similarities as large molecules suggested their uptake might be facilitated. Clarithromycin targets the ribosome, polymyxin B targets LPS molecules in the outer and inner membrane, and vancomycin targets PG biosynthesis. The more substantial effect of polymyxin B and vancomycin than clarithromycin suggests that their targets in the cell envelope might synergize with increased uptake. According to my hypothesis, LPS is transported less from the IM to the OM in *marR* mutants, and LPS aberrantly accumulates in the IM while getting depleted in the OM. This could enhance polymyxin B action by perturbing the already reduced number of LPS molecules in the OM to a critical level or increasing the number of targets and the amount of targeted surface in the IM. Vancomycin forms hydrogen bonds with the D-alanine-D-alanine peptide motif of PG precursor lipid II and inhibits polymerization and transglycosylation of the PG cell wall (Johnson et al. 1990; Boneca & Chiosis 2003). The mechanism could synergize with the inhibition of the PG biosynthesis mediated by cefotaxime but only in resistant mutants such as *marR* or the *ompR* due to their rewired cell envelope.

Also, the state of the OM affects the uptake of the β-lactams mecillinam and cefsulodin. While KOs of several *mla* genes that facilitate retrograde PL transport from the outer leaflet of the OM to the IM (Malinverni & Silhavy 2009) increase sensitivity against cefsulodin, they increase resistance against mecillinam (Nichols et al. 2011). MarA directly controls the expression of the *mla* system to regulate outer membrane permeability (Sharma et al. 2017), and KOs of *mla* genes sensitize against hydrophobic molecules such as clarithromycin (Sharma et al. 2017). In cells where LPS is depleted from the outer leaflet of the OM, phospholipids have a higher tendency to flip from the inner to the outer leaflet of the OM (Benn et al. 2021), which makes the *mla* system critical in such a state, and provides an explanation why the *mla* system is activated in the *marR* KO. Even though the exact mechanisms for drugs that delayed resistance evolution against cefotaxime are still unclear and must be further investigated, they represent a good starting point for identifying potent evolution inhibitors. The fact that I selected them based on the genetic vulnerabilities I identified during resistance evolution against cefotaxime using the genome-wide KO library underlines the value of performing

genome-wide reverse genetics screens for interrogating complex phenotypes such as antibiotic resistance evolution.

Finally, I wanted to assess the specificity of evolvability genes by testing their impact on the resistance evolution of different antibiotics with an emphasis on β-lactams to dissect structure target relationships. The aim is to investigate whether the absence of these genes only constrains cefotaxime resistance evolution or whether they delay resistance evolution more generally.

9. Evolvability genes delay the evolution of resistance to other antibiotics

To investigate how general the identified evolvability genes are, I tested whether they can also delay resistance evolution against other antibiotics targeting the same, similar, or distinct cellular processes. I selected 9 gene KOs with decreased evolvability (Chapter II.5.) and confirmed by the validation experiment (Chapter II.4.). I evolved resistance in these KO mutants in 8 replicates against 12 other antibiotics primarily targeting cell wall biosynthesis to dissect structure-target relationships, as well as gentamicin and tetracycline targeting translation *via* the 30S ribosomal subunit and trimethoprim targeting folate biosynthesis. I evolved resistance in 1 ml MHB and 96-well plates with 1:25 bottleneck and the same resistance steps as for cefotaxime (media, media, 0.5x, 1.5x, 4.5x, and 13.5x MIC). I assessed evolvability using the BH-adjusted Wilcoxon signed-rank test relative to the wildtype at 1.5x MIC except for cefotaxime, cefsulodin, and piperacillin, which were scored at 4.5x MIC, based on the highest concentration at which the wildtype still grows to high yield (Figure 32).

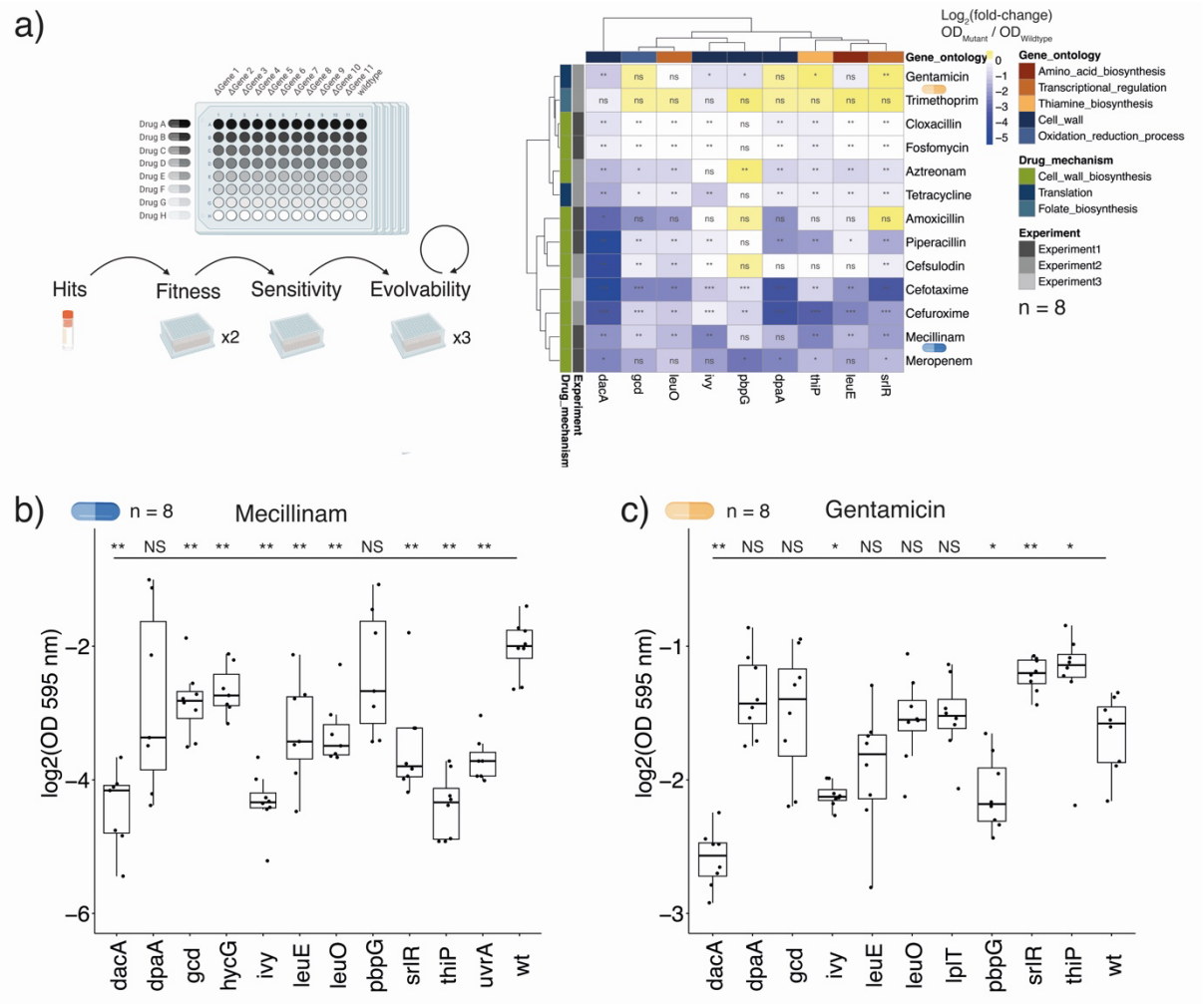

Figure 32: Resistance evolution of cefotaxime evolvability genes against multiple antibiotics. *a) Workflow and evolvability heat map of cefotaxime evolvability genes evolved against a panel of 12 antibiotics targeting different cellular processes, emphasizing cell wall targeting antibiotics. b) Resistance evolution of evolvability gene KOs against the cell wall targeting antibiotic mecillinam is shown. c) Resistance evolution of evolvability KOs against the aminoglycoside gentamicin is shown. For A-C), $log_2(OD_{595\ nm})$ after growth in 1.5x MIC drug (except for cefsulodin and piperacillin at 4.5x MIC) is shown, and significance is calculated by BH-adjusted Wilcoxon signed-rank test. * padj. < 0.05, ** padj. < 0.01, *** padj. < 0.001.*

I discovered that all gene KOs delaying resistance evolution against cefotaxime also delay resistance against cefuroxime, sharing both targets PBP1a and 3, indicating a high functional overlap. There are multiple genes delaying resistance of the other PBP3 targeting antibiotics piperacillin and aztreonam, such as *dacA*, *gcd*, *leuO*, *dpaA*, *leuE*, *srlR*, and *thiP*, even though they represent different chemical classes ureidopenicillin and monobactams. Compared to cefotaxime and cefuroxime, *pbpG* promotes resistance evolution against aztreonam and does not affect piperacillin resistance evolution.

Several genes delaying cefotaxime resistance evolution also delayed resistance evolution against mecillinam targeting the elongasome such as *dacA*, *gcd*, *leuO*, *ivy*, *leuE*, *srlR*, and *thiP* (Figure 32). Mecillinam was unaffected by *dpaA*, which delayed the resistance evolution of all

PBP3-targeting drugs cefotaxime, cefuroxime, piperacillin, and aztreonam, suggesting an interaction with PBP3 being targeted. An alternative explanation is that the *dpaA* KO is less affected by mecillinam, which was visible by the decreased abundance of PBP2 in the proteomics data (*padj*. < 0.02), indicating less dependence.

There was a smaller overlap between cefotaxime and cefsulodin targeting PBP1b and includes mostly metabolism-related processes such as *gcd*, *leuO*, *srlR*, *dacA*, and *ivy* related to the cell wall, indicating a lower functional overlap between cefotaxime and cefsulodin. This finding has to be set in perspective to the ability of cefsulodin to delay cefotaxime resistance evolution at sub-inhibitory concentrations. The conservation of evolvability factors with amoxicillin targeting PBP4 was even lower and included only *dacA*, indicating distinct targets or resistance mechanisms.

Cloxacillin and fosfomycin shared highly similar profiles and were affected by all genes except *pbpG* but displayed small effect sizes. Fosfomycin affects the cell wall by limiting the biosynthesis of PG precursors, while cloxacillin targets multiple PBPs. Their shared pleiotropic effect on the cell wall might explain their concordant resistance profile.

Trimethoprim targets folate biosynthesis and represents a useful negative control since none of the genes significantly delayed resistance evolution against it. The other non cell wall-targeting antibiotics, gentamicin and tetracycline, target translation but represent different chemical classes, tetracyclines and aminoglycosides. Three cell wall-related genes, *dacA*, *ivy*, and *pbpG*, also delayed the resistance evolution of gentamicin, while *srlR* and *thiP* promoted resistance evolution. Tetracycline, instead, was affected by *dacA*, *gcd*, *leuO*, *ivy*, *dpaA*, *leuE*, *srlR*, and *thiP* and thereby shares a high overlap with cefotaxime. Despite the small sample size in my subset, the fact that evolvability factors are more conserved within the drug class β-lactams than with other drug classes points towards either A) a structural or functional specificity of the evolvability factors I identified instead of just growth inhibition as a mechanism to delay resistance evolution or B) a stronger growth dependence of β-lactams than other drug classes during resistance evolution, which could be explained by the fact that β-lactams only kill actively growing bacteria.

These insights allowed me to distinguish between genes only conditional-essential during cefotaxime and cefuroxime resistance evolution, such as *pbpG*, genes conditional-essential

during resistance evolution of the PBP3 targeting antibiotics (cefotaxime, cefuroxime, piperacillin, and aztreonam) plus tetracycline, such as *dpaA* and genes conditional-essential during resistance evolution against both cell wall targeting antibiotics and the ribosome targeting antibiotic tetracycline such as *ivy*, *gcd*, *leuO*, *leuE*, *srlR*, and *thiP*.

Based on these findings, some genes are more likely target-dependent, such as *dpaA*, potentially indicating that gene-gene-drug interactions between resistance elements, evolvability factors, and antibiotics are causing the evolutionary delay. Tetracycline represents a specific case since the AcrAB-TolC efflux pump exports it, and therefore, it selects for efflux-promoting *marR* mutations (Alekshun & Levy 1999; Sharma et al. 2017; Lukačišinová et al. 2020) that, in addition, directly interact with *dpaA*. Therefore, *dpaA* has a dual function in delaying resistance evolution of both PBP3 targeting antibiotics (Bahadur et al. 2021) and against antibiotics where *marR* deletions provide resistance.

For gene KOs affecting resistance evolution against antibiotics targeting diverse processes within and outside the cell envelope, the mechanism is more likely based on epistatic interactions with general resistance elements such as *marR*, *ompR*, and *ompF*. The ability of genes involved in metabolism and oxidation-reduction to delay resistance evolution against most antibiotics tested likely indicates that common resistance mechanisms, such as the decrease in porins, put additional constraints on the import of nutrients and, therefore, affect metabolism. Such constraints can materialize as gene-gene interactions causing SL or gene-gene-drug interactions, *i.e.*, by preventing the actualization of resistance variants into functional resistance phenotypes. In the cases of *dpaA* and *ivy*, I verified both gene-gene and gene-gene-drug interactions by CRISPRi experiments (Figures 17b and 18). An alternative explanation is that general evolvability genes affect stationary phase survival, independent of the antibiotic. In summary, the evolvability genes I identified using high-throughput experimental evolution represent novel targets to delay resistance evolution against multiple antibiotics or to resensitize populations by specifically targeting resistant lineages utilizing SL.

10. Conclusions

In Chapter III, I used a combination of genetics, genomics, proteomics, high-throughput microscopy for phenotypic profiling, and evolution experiments to dissect the mechanistic basis of epistatic interactions delaying resistance evolution. Furthermore, I wanted to

investigate whether evolvability genes are conditional essential during resistance evolution due to their gene-gene and gene-gene-drug interaction with resistance genes.

I first sequenced the genome of 34 wildtype clones after cefotaxime resistance evolution (Figure 15). The sequencing revealed two mutually exclusive resistance trajectories reported before (Schenk et al. 2022). One resistance trajectory was characterized by mutations in the resistance regulator *marR*, increasing *marA* expression, and, optionally, mutations in the *lon* protease, additionally stabilizing MarA. The other resistance trajectory displayed mutations in the outer membrane porin regulator *ompR*, decreasing porin expression or directly in one of the porins OmpF. The *marR* resistance trajectory mediates cefotaxime resistance by upregulating the efflux pump AcrAB-TolC ((Sharma et al. 2017; Hao et al. 2014) and downregulating the porin *ompF via* the small RNA micF (Dam et al. 2017; Ramani et al. 1994). The *ompR* resistance trajectory, on the other hand, provides cefotaxime resistance by decreasing drug influx through the porins OmpF and OmpC (Masi et al. 2022).

As a result, to delay resistance evolution against cefotaxime under our conditions, evolvability gene KOs must delay both evolutionary trajectories with shared and distinct features. The decrease of intracellular drug concentration by either increasing drug influx or decreasing drug efflux was shared, as well as the downregulation of the outer membrane porin OmpF. Differences between the evolutionary trajectories boiled down to the different regulons affected by *marR* and *ompR* mutation. Even though *marR* and *ompR* deletions are often reduced to affecting only efflux pump and porin expression, respectively, deletions of both regulators change the expression of tens of genes, thereby complicating further mechanistic analysis. Lastly, measuring delayed evolution against two divergent evolutionary trajectories created an interesting interplay between competing lineages within each population. Blocking one mutational path entirely by epistasis while leaving the other unaffected would select the alternative path and result in normal growth, which is why the decreased yield in evolvability gene deletion mutants can only be achieved by affecting all resistance trajectories, given that they both occur frequently.

Next, I wanted to test whether evolvability genes interact with resistance regulators in the presence or absence of cefotaxime (Figure 16). I developed an approach to quantify gene-gene and gene-gene-drug interactions directly from liquid growth by using an inducible and titratable CRISPRi plasmid I constructed. Using this system, I identified gene-gene interactions

of the evolvability genes *dpaA* and *ivy* with the resistance regulator *marR* and LPS gene *waaQ* (Figure 17b), a gene-gene interaction between *ivy* and the resistance regulator *ompR* (Figure 17b), as well as gene-gene-drug interactions of *dpaA* and *ivy* with *ompR* in the presence of cefotaxime (Figure 18a and 18b). Both *dpaA* and *ivy* interact with *marR via* a gene-gene and with *ompR via* a gene-gene-drug interaction, pointing towards different processes of the two respective resistance regulons interacting with *dpaA* and *ivy.*

Unidirectional or bidirectional dependence can explain negative gene-gene interactions between *dpaA* and *marR* deletions. One example of such an interaction would be one protein directly or indirectly processing a toxic byproduct of the other protein's function. Even though *marR* resistance is mainly mediated by upregulating efflux pumps, it regulates various genes (Sharma et al. 2017), each of which can be the source of the epistatic interaction with *dpaA*. Negative gene-gene-drug interactions between *dpaA* and *ompR* can be summarized as the dependence of the *ompR* resistance mechanism on *dpaA* function. The *dpaA* deletion can either directly interfere with the *ompR* resistance mechanism or increase sensitivity orthogonal to the *ompR* resistance mechanism in the rewired genetic network of the *ompR* mutant, for example, by providing a new route for drug influx despite porins getting downregulated. To learn more about the nature of the gene-gene and gene-gene-drug interactions, I used high-throughput microscopy to observe phenotypic and morphological characteristics of both single and double mutants of evolvability and resistance genes in the absence and presence of cefotaxime during growth and division.

In addition, comparing the different phenotypes made it possible to qualitatively assess drug sensitivity and severity of the gene-gene and gene-gene-drug interactions. A single *marR* mutant showed a frequent release of OMVs and OM blebs at midcell (Figure 19). The double mutants of evolvability genes *dpaA* or *ivy* and the resistance regulator *marR* did not show OMVs and OM blebs anymore, but therefore, a high frequency and severity of the phenotypes lysis, plasmolysis followed by lysis and plasmolysis distance (Figure 20).

A similar phenotype of OMVs, OM blebs at midcell, plasmolysis, and lysis was previously reported for a *mlaA* GOF mutation and linked to increased LPS biosynthesis, LPS accumulation, and phospholipid depletion leading to cell death (Sutterlin et al. 2016). One explanation for the cell death phenotype was that the OM is destabilized by increased levels of LPS biosynthesis, resulting in the production of OMVs and midcell blebs at cell division sites

(Sutterlin et al. 2016), which I also observed in the *marA* KO mutant (Figure 19). OM blebbing at midcell and OMV release was reported as a way to shed overabundant LPS and is increased in cells with a reduced amount of crosslinks between PG and Lpp in the OM such as an *lpp* KO or LOF mutants (Guest et al. 2020). In the literature, the cell death phenotype could be suppressed by decreasing crosslinks between PG and Lpp to shed excess LPS by increased OM vesiculation or by directly reducing LPS biosynthesis through *lpxC* mutations (Sutterlin et al. 2016; Guest et al. 2020; Klein et al. 2014). The fact that the *dpaA* KO has an increased amount of such PG-Lpp linkages (Bahadur et al. 2021; Matthias et al. 2021) could indicate that it exacerbates the *marR* phenotype by preventing OM vesiculation to shed excess LPS.

One explanation why the *marR* KO could show increased LPS biosynthesis was reported as a result of increased MarA abundance in a *marR* KO mutant (Maniyeri et al. 2023) that stabilized the rate-limiting protein in LPS biosynthesis LpxC by protecting it from negative regulation *via* LapB-FtsH-mediated proteolysis (Guest et al. 2020; Nguyen et al. 2020; Mahalakshmi et al. 2014; Guest et al. 2021). Furthermore, MarA directly activates the *mla* operon to regulate OM permeability (Sharma et al. 2017). In line with those findings, the GOF mutant of *mlaA* has been associated with the OMVs, OM blebs plasmolysis, and lysis phenotypes (Sutterlin et al. 2016). In addition, the *mlaA* GOF was also reported to stabilize LpxC (Sutterlin et al. 2016) as MarA does (Maniyeri et al. 2023) and could explain the high degree of similarity between the *mlaA* GOF and the *marR* KO phenotypes. Lastly, introducing an *lpxC* mutation that decreases LPS biosynthesis suppressed the death phenotype in the *mlaA* GOF mutant (Sutterlin et al. 2016). One of the KO mutants that showed the highest evolvability scores at both 1.5x MIC and 13.5x MIC in my genome-wide evolvability screen (Chapter II) was the *lapB* KO. *LapB* is an essential gene, and its growth is only possible due to a compensatory *lpxC* mutation reducing LPS biosynthesis (Mahalakshmi et al. 2014), corroborating the hypothesis that LPS overproduction constrains resistance evolution against cefotaxime and can be used to decrease or increase evolvability.

Since the *dpaA* deletion causes an increased amount of crosslinks between the PG and Lpp, it potentially exacerbates the toxic accumulation of LPS by preventing OMV release and OM blebs, whose absence I observed in *dpaA* and *dpaA marR* mutants in the live microscopy data (Figure 19 and 20). However, despite observing the presence or absence of such vesicles or blebs in hundreds of cells, this provides only complementary qualitative evidence and no definitive proof of the proposed hypothesis.

In the published *mlaA* GOF mutant, lipids from the IM replaced lipids lost from the OM by vesiculation to shed LPS, which results in IM shrinkage, decrease of the cytoplasmic volume, and increase of the cytoplasmic density (Sutterlin et al. 2016). The high cytoplasmic concentration leads to plasmolysis followed by lysis, which can be explained by the mechanical rupture of the IM, resulting in cell death (Sutterlin et al. 2016). Since following my hypothesis, the *dpaA* KO would prevent such OMV release in *marR* mutants and conserve phospholipids, the observed plasmolysis, lysis and cell death in the *marR dpaA* double mutant would result out of the lethal LPS accumulation as was reported for the *lapB* deletion (Guest et al. 2021; Nguyen et al. 2020; Guest et al. 2020; Shu & Mi 2022), and not out of the depletion of phospholipids leading to rupture of the IM as for the *mlaA* GOF mutant (Sutterlin et al. 2016).

Deletion of the *mla* operon and the *wec* pathway increased cefotaxime evolvability, which both affect lipid homeostasis and transport in the cell envelope and are located in the inner and outer leaflets of the IM. The *mla* system is regulated by *marR* and controls OM permeability and antibiotic resistance by transporting PL mislocated in the outer leaflet of the OM back to the inner membrane (Sharma et al. 2017). The *wec* system is involved in ECA biosynthesis, and disruptions of *wecC* were reported to partially restore disrupted OM function and vancomycin resistance of mutants with increased membrane permeability, possibly by the accumulation of ECA intermediates (Jiang et al. 2020). Since all KOs of *wec* pathway genes increased cefotaxime evolvability, the accumulation of ECA intermediates, including novel diacylglycerol pyrophosphoryl (DAG-PP)-linked species (Jiang et al. 2020), could replenish a limiting factor.

Besides the shared phenotypes between Δ*dpaA* and Δ*ivy*, the Δ*dpaA* also displayed unique features such as filamentation with both the Δ*marR* (Figure 20) and the Δ*ompR* (Figure 21), suggesting a defective divisome. This phenotype could be explained by increased linkages between PG and Lpp in Δ*dpaA* mutants perturbing cell division (Bahadur et al. 2021; Matthias et al. 2021). Since cefotaxime targets the divisome and causes filamentation, filamentation of the Δ*dpaA* in both the Δ*marR* and Δ*ompR* background already without cefotaxime potentially synergizes with the addition of cefotaxime. It could explain delayed cefotaxime resistance evolution *via marR* and *ompR* in the *dpaA* KO. The fact that filamentation arose in the Δ*dpaA* when combined with both the Δ*marR* (Figure 20) and Δ*ompR* (Figure 21) suggests that it is caused by one of the features shared between both resistance regulators, such as the downregulation of the outer membrane porin OmpF.

Also, the Δ*ivy* showed a unique characteristic when combined with the Δ*marR* (Figure 20) and the Δ*ompR* (Figure 21). Firstly, cell width was increased, and many cells with a round morphology were observed (Figures 20 and 21), indicating a defective elongasome or overactive divisome, which is expected to antagonize with the divisome inhibition mediated by cefotaxime. In several cases, asymmetric cell division was observed, which resulted in one wildtype-like cell and one round cell with a similar length as width (Figure 20). These round daughter cells could not grow or divide but did not lyse. Ivy was reported to fold periplasmic proteins under stress (Lennon et al. 2015) and inhibit lysozyme and LTs (Clarke et al. 2010). Therefore, the absence of Ivy could result in overactive LTs contributing to cell division or lysis.

For live microscopy in the presence of cefotaxime, the first phenotype that can be observed across genotypes is cefotaxime sensitivity (Figure 22). Cefotaxime sensitivity can be identified by the frequency and severity of cefotaxime-induced morphological aberrations such as filamentation, bulging, and lysis. While the KO mutants of the evolvability genes *dpaA* or *ivy* were as sensitive as the wildtype, the resistant mutant *marR* was less affected by growing on cefotaxime, and drug phenotypes were almost undetected in the KO mutant of the resistant mutant Δ*ompR* (Figure 22). Deleting *dpaA* or *ivy* on top of the resistant Δ*marR* or Δ*ompR* backgrounds exacerbated their existing cefotaxime-induced phenotypes and added new ones (Figures 23 and 24). Therefore, deleting *dpaA* and *ivy* increased cefotaxime sensitivity in both resistant backgrounds, corroborating the identified gene-gene-drug interactions.

The Δ*dpaA* showed strong filamentation and lysis in both the Δ*dpaA*Δ*marR* and Δ*dpaA*Δ*ompR* double mutants in the presence of cefotaxime (Figures 23 and 24). Since both Δ*dpaA* double mutants showed filamentation in the absence of cefotaxime and cefotaxime induces filamentation in wildtype cells, both effects may synergize by affecting the divisome. While filamenting cells of the Δ*dpaA*Δ*marR* double mutants showed a thin morphology with a small width (Figure 23), filamenting cells but also non-filamenting cells of the Δ*dpaA*Δ*ompR* double mutants showed an increased width often coinciding with bulging and bursting of cells (Figure 24), coinciding with an increase in cell width. Both the Δ*dpaA*Δ*marR* and Δ*dpaA*Δ*ompR* double mutants showed stronger phenotypes (Figures 23 and 24) than the Δ*marR* and Δ*ompR* single mutants (Figure 22) in the presence of cefotaxime, reflecting their increased cefotaxime sensitivity in the absence of *dpaA*. Based on these findings, I can hypothesize that both the Δ*dpaA*Δ*marR* and Δ*dpaA*Δ*ompR* double KO mutants already show cell division defects

without cefotaxime (Figures 20 and 21) that are exacerbated by cefotaxime (Figures 23 and 24), revealing the phenotype of the *dpaA* gene-gene-drug interaction. These observations support the finding that the *dpaA* KO mutant constrains cefotaxime resistance evolution by increasing cefotaxime sensitivity in *marR* and *ompR* KO mutants.

The Δ*ivy*Δ*marR* phenotype appears almost opposite to the Δ*dpaA* phenotype in the presence of cefotaxime (Figure 23). The Δ*ivy*Δ*marR* mutants show increased cell width and decreased cell length, with little filamentation, even in the presence of cefotaxime that induces filamentation by inhibiting the divisome. This phenotype is similar to the one both Δ*ivy* double mutants showed in the absence of cefotaxime (Figures 20 and 21) and visibly counteracts the cefotaxime-induced filamentation. Based on these findings, I can hypothesize that both the Δ*ivy*Δ*marR* mutants already show overactive cell division or cell elongation defects that change or even counteract cefotaxime (Figure 23), revealing the potential phenotype of the *ivy* gene-gene interaction. For Δ*ivy*Δ*ompR* mutants, filamentation was increased (Figure 24) compared to the single Δ*ompR* (Figure 22), leading to increased cefotaxime sensitivity in Δ*ompR* and underlining their gene-gene-drug interaction constraining resistance evolution.

To investigate the molecular mechanisms of gene-gene interactions in more detail, I performed proteomics analysis of the described single and double KO mutants with the help of Dr. Dimitrios Papagiannidis. I confirmed the reported abundance changes for the different KO mutants. One critical insight I gained was that DpaA protein abundance is decreased to similar levels in the *dpaA* and *ivy* KO mutants (Figure 27), suggesting direct or indirect regulation of DpaA *via* Ivy and explaining the high degree of similarity of phenotypes of both mutants across genetic and evolution experiments. One possible explanation could be the folding of DpaA by the chaperone Ivy. For the *ompR* KO, major changes in the metabolic network were detected, such as the lower abundance of multiple proteins from the pathways performing D-galactarate degradation, D-glucarate degradation, purine nucleotides *de novo* biosynthesis, pyrimidine deoxyribonucleotides *de novo* biosynthesis, maltose transport and N-acetylneuraminate and N-acetylmannosamine degradation (Figure 25b).

For the *marR* KO, the protein abundance quantification revealed a rewiring of the genetic network regarding LPS biosynthesis and transport. LPS biosynthesis proteins LpxC, LpxL, and LpxT showed increased abundance, while the LPS transport machinery proteins LptA and LptC decreased (Figure 25a). Together, both effects could result in the LPS accumulating in the IM,

as was reported before, for LptC depletion (Sperandeo et al. 2011; Guest et al. 2021). LapC senses the accumulating LPS in the IM and should trigger proteolysis of LpxC *via* LapB-FtsH (Shu & Mi 2022; Guest et al. 2020; Nguyen et al. 2020). However, this negative autoregulation of LPS biosynthesis mediated by proteolysis of LpxC could be prevented in the *marR* KO by direct stabilization and increased abundance of LpxC by MarA *via* the Mla system (Maniyeri et al. 2023). This hypothesis is based on the finding that LOF mutants of *lapC* show elevated degradation of LpxC, which can be suppressed by *marA* or *pldA* overexpression in an Mla pathway-dependent manner (Maniyeri et al. 2023). This reported finding possibly explains why the KO of several genes of the *mla* pathway increased cefotaxime evolvability (Figures 12 and 13).

This rewired cellular state of deregulated LPS biosynthesis and decreased transport from the IM to the OM can have multiple consequences for the cells. Firstly, LPS accumulates in the IM, which can be lethal (Guest et al. 2021; Guest et al. 2020). Secondly, less LPS reaches the OM, resulting in a compromised barrier function of the OM and increased sensitivity to SDS and bile salts (Sperandeo et al. 2006; Sperandeo et al. 2011), which can be seen in available chemical genetics data for the *marR* KO (Figure 26) (Nichols et al. 2011). As a result, more phospholipids flip from the inner to the outer leaflet of the OM to fill holes created by the depleted LPS (Benn et al. 2021), which could deplete phospholipids from the IM, ultimately resulting in its rupture and cell death, as it was reported for the *mlaA* GOF (Sutterlin et al. 2016).

Overproduction and accumulation of LPS in the IM, for example, by impaired LpxC degradation in a *lapB* KO mutant, is suppressed in mutants that can not crosslink their PG with the Lpp in their OM, which can be achieved by deleting *lpp* or using a mutant *lpp* that can not be crosslinked to the PG (Guest et al. 2021; Klein et al. 2014; Guest et al. 2020). This phenomenon was explained by shedding excess LPS utilizing hypervesiculation through OMVs, which is prevented by PG-Lpp crosslinks. The *dpaA* KO and the *ivy* KO that phenocopies decreased DpaA levels display increased PG-Lpp crosslinks (Bahadur et al. 2021; Matthias et al. 2021). As a result, both mutants could prevent the shedding of excess LPS *via* vesiculation, thereby exacerbating the toxic accumulation of LPS in the IM in the *marR* KO and resulting in SL. Additional evidence that toxic LPS production affects the *marR* KO mutant and is exacerbated by the *dpaA* KO was provided by a) the finding that one *marR* KO evolved a potentially compensatory mutation in *waaQ*, decreasing LPS biosynthesis levels and

increasing resistance levels and b) increased evolvability at 1.5x and 13.5x MIC for the *lapB* KO (Figures 12 and 13) with reduced *lpxC* activity and LPS biosynthesis.

Suppose the gene-gene interaction between the *dpaA* and *marR* KOs is caused by the increased LPS levels in *marR*. In that case, the potentially compensatory *waaQ* mutation decreasing LPS biosynthesis should abolish the gene-gene interaction, which it did for the *dpaA* KO but, interestingly, not for the *ivy* KO (Figure 29). That suggests that the *ivy* KO has an additional gene-gene interaction with *marR* that adds upon the loss of DpaA in the *ivy* KO that already interacts with *marR*, thereby making *ivy* a dual evolvability gene. The additional interactions of *ivy* are supported by the fact that it shows both gene-gene and gene-gene-drug interactions with *marR* and *ompR*, which was not the case for the *dpaA* KO.

As an alternative explanation for the negative epistasis between *dpaA* and *marR*, a strong negative epistatic interaction was reported between the *dpaA* KO and decreased LptC levels (Morè et al. 2019), which I also detected in the *marR* KO by proteomics (Figure 25a). This SL was dependent on the activator of amidases ActS, whose ability to activate AmiA, AmiB, and AmiC was indirectly controlled by DpaA in cells under LPS stress through LptC depletion (Gurnani Serrano et al. 2021). When LptC levels are depleted in a background missing *dpaA*, uncontrolled activation of amidases *via* ActS results in cell lysis (Mueller et al. 2021; Gurnani Serrano et al. 2021).

The gene-gene-drug interaction between the resistance regulator *ompR* and the evolvability genes *dpaA* and *ivy* in the presence of cefotaxime remains elusive. One possibility is that *dpaA* and *ivy* exacerbate the nutrient limitation that is caused by the decreased abundance of major porins, which is supported by the other metabolism and oxidation-reduction related evolvability genes (Chapter II.5.). Another possibility is that due to the decreased abundance of major outer membrane porins OmpF and OmpC, there is an increased demand for LPS, which can be identified by an increased LpxC protein abundance. When adding cefotaxime, MarR senses the liberation of membrane-bound copper and activates MarA (Hao et al. 2014; Hiniker et al. 2005), which results in the described gene-gene interactions with *dpaA*. If cefotaxime evokes the same gene-gene interaction in the *ompR* KO as in the *marR* KO, this could explain the similar phenotypes of the *dpaA* KO causing filamentation and lysis and the *ivy* KO decreasing filamentation and causing round cells with increased cell width, in both the

marR and *ompR* double mutants during live microscopy. However, more experiments are needed to uncover the mechanism of the identified gene-gene-drug interaction.

To pinpoint the molecular basis for the observed gene-gene interaction, I measured the gene-gene interaction between *dpaA* and *marR* in the absence of several genes, either increasing evolvability when knocked out or hypothesized to be involved in the proposed mechanism (Figure 30). Several of the gene deletions affected the gene-gene interaction between *dpaA* and *marR*. Gene deletion mutants of the genes encoding the AcrAB-TolC efflux pump increased the strength of the gene-gene interaction, which could be explained by increased intracellular inducer concentration or by stabilizing the cell envelope through the efflux pump. The gene *ldtA* KO creates fewer crosslinks between PG and Lpp (Braun & Wolff 1970; Magnet et al. 2007) and, therefore, possibly counteracts the effect of the *dpaA* KO, creating more crosslinks and abolishes the gene-gene interaction between *dpaA* and *marR*. I also observed suppression of the gene-gene interaction in the absence of the endopeptidases *mepK* and *mepS*. Both cleave *m*-DAP[3] crosslinks in the PG (Chodisetti & Reddy 2019) and thereby provide available *m*-DAP[3] that can be used to crosslink PG with Lpp in the OM, suggesting that *mepK* and *mepS* also suppress the gene-gene interaction by limiting the amount of PG-Lpp crosslinks and reversing the phenotype of the *dpaA* deletion. *MepK* and *mepS* also contribute to murein incorporation and PG expansion during bacterial growth, elongation, and division (Truong et al. 2020), which could serve as another possibility to counteract the epistatic interaction. In addition, MepK showed higher protein abundance in the *marR* KO mutant (Figure 25a).

Other genes involved in PG turnover and remodeling that weakened the gene-gene interaction were the two membrane-bound lytic murein transglycosylases, *mltF* and *mltC*, with *mltF* showing a more substantial effect than *mltC*. Both contribute to PG turnover by mediating the cleavage of the β-1,4 glycosidic PG bond between MurNAc and GlcNAc (Dijkstra & Keck 1996; Lee et al. 2013), thereby potentially contributing to further destabilization of the cell envelope. LTs could also directly contribute to the lysis phenotype, which was already reported for amidases under LptC-depleted conditions like in the *marR* KO when *dpaA* is deleted on top (Gurnani Serrano et al. 2021; Mueller et al. 2021).

Also, the lipid biosynthesis gene *lpxT* suppressed the gene-gene interaction, which points towards the toxic overproduction and accumulation of LPS, possibly in the IM, as a source of or contributor to the negative epistasis. LpxT transfers a phosphate group from Und-PP to the

lipid A-core oligosaccharide and contributes to the negative charge of LPS, as well as to the recycling of Und-P needed for PG and LPS biosynthesis (Touzé et al. 2008). LpxT protein abundance was also increased in the *marR* KO mutant, which was reported due to sodium salicylate exposure (Pomposiello et al. 2001), known to activate MarA (Sharma et al. 2017). Of the three gene KOs from the *mla* pathway for phospholipid trafficking from the OM back to the IM, only *mlaC* prevented the interaction. Since *mlaC* is responsible for reintegrating PLs back into the inner membrane (Hughes et al. 2019; Ekiert et al. 2017), the fact that its deletion prevents the gene-gene interactions supports the hypothesis of aberrant accumulation of LPS in the IM or the depletion of PLs in the OM. Furthermore, *mlaC* was required for the MarA-mediated stabilization of LpxC against degradation in *marR* KO mutants, thereby directly contributing to LPS biosynthesis (Maniyeri et al. 2023).

The *wecA* deletion suppressed the interaction between *dpaA* and *marR*, potentially by accumulating ECA intermediates that were reported to restore defective OM function and vancomycin resistance in mutations with perturbed OM barrier function (Jiang et al. 2020). Lastly, the deletion of *ompF* coding for the OM porin either prevented the gene-gene interaction by interacting with *marR* or *dpaA* or by preventing the influx of the inducer (Moya-Torres et al. 2014) and, therefore, *dpaA* depletion. In contrast, the *ompC* deletion did not affect the gene-gene interaction.

In summary, KOs of *ldtA*, *mepK*, and *mepS* most likely reversed the gene-gene interaction of *dpaA* and *marR* by preventing the accumulation of PG-Lpp crosslinks and counteracting the result of the *dpaA* deletion. Deletions of *lpxT*, *mlaC*, and *wecA* were likely suppressing the gene-gene interaction by reducing LPS biosynthesis or contributing to the stability of the cell envelope.

Next, I wanted to use the genetic vulnerabilities I uncovered using genome-wide resistance evolution and target them with small molecules to delay resistance evolution. Out of the small molecules I selected and tested for their ability to delay cefotaxime resistance evolution, cefsulodin, clarithromycin, mecillinam, polymyxin B, procaine, sulfamethizole, trimethoprim, and vancomycin were able to delay cefotaxime resistance evolution in a dose-dependent manner at sub-inhibitory concentrations (Figure 31).

Since LptC is reduced in the *marR* KO (Figure 25a), the outer leaflet of the OM lacks LPS molecules to ensure proper OM barrier function. This lack of LPS could explain the increased uptake of bulky molecules such as vancomycin and clarithromycin due to perturbed OM function, ultimately inhibiting growth and delaying evolution. Polymyxin B could delay evolution since it targets LPS molecules in the inner and outer membrane (Sabnis et al. 2021), which is mislocalized in *marR* mutants that evolve during cefotaxime resistance evolution. MarR directly regulates the *mla* operon (Sharma et al. 2017), uses it to stabilize LpxC against degradation (Maniyeri et al. 2023), and KOs of several *mla* genes increase resistance against mecillinam, clarithromycin, erythromycin, vancomycin and polymyxin B (Nichols et al. 2011). Since the *marA*-dependent upregulation of the *mla* operon in evolved *marR* mutants could cause sensitivity against mecillinam and clarithromycin, I also included them in the experiment.

The other drugs, cefsulodin, procaine, sulfamethizole, and trimethoprim, were selected because evolvability gene KOs display increased resistance levels against them in available chemical genetics data (Nichols et al. 2011). Therefore, cells should decrease the expression of such genes to survive drug exposure and thereby decrease their own evolvability against cefotaxime. I chose procaine because of its positive interaction with the *hycG* and *dacA* KOs, sulfamethizole because of its positive interaction with the *chaB* KO, and cefsulodin and trimethoprim because of their positive interaction with *pbpG*.

While effect sizes were small for clarithromycin and procaine, the effect sizes for cefsulodin, mecillinam, polymyxin B, trimethoprim, sulfamethizole, and vancomycin were much larger. For both mecillinam and polymyxin B, at least one but not all evolutionary trajectories were blocked, which suggests that they only prevented the evolution of at least one but not all resistance elements. In contrast, the delay in cefotaxime resistance evolution is similar for all clones evolving in the presence of cefsulodin, sulfamethizole, trimethoprim, and vancomycin. It is interesting to observe differences between sulfamethizole and trimethoprim, both of which target THF biosynthesis. Zooming in further revealed that trimethoprim targets FolA while sulfonamides target FolP. Besides the high correlation of sensitivity of both drugs across many KO mutants, mutants from the glycine cleavage pathway *gcvP*, *gcvH*, and *gcvT* are only sensitive to sulfonamides (Nichols et al. 2011). The fact that cefotaxime resistance evolution was delayed more by sulfamethizole than trimethoprim suggests that glycine cleavage could be conditional essential during cefotaxime resistance evolution, which was indeed the case. In

the acquired dataset for KO mutants with decreased evolvability, I found that both *gcvH* and *gcvP* KOs display delayed resistance evolution against cefotaxime with fitness and sensitivity mirroring that of the wildtype.

Since the drugs vancomycin, polymyxin B, and clarithromycin all target distinct processes but share a similar bulky structure, they likely delay cefotaxime resistance evolution by showing increased uptake through the perturbed cell envelope. The same could be true for the b-lactams mecillinam and cefsulodin, which are both affected by the presence of *mla* genes (Nichols et al. 2011).

Lastly, I wanted to test how drug-specific the identified evolvability genes are. To assess this systematically, I evolved 9 KO mutants with decreased evolvability against cefotaxime against 12 different antibiotics targeting cell wall biosynthesis, translation, or folate biosynthesis (Figure 32a). As expected, all genes that delayed cefotaxime resistance evolution also delayed resistance evolution against cefuroxime, sharing both targets and high structural similarity. The second highest overlap was with the other PBP3 targeting antibiotic piperacillin, sharing eight evolvability genes, and aztreonam, sharing seven evolvability genes, even though they belong to different drug classes, ueridopenicillins, and monobactams. Mecillinam shared seven evolvability genes with cefotaxime (Figure 32b), even though it targets the elongasome instead of the divisome. Since both drugs target PG biosynthesis but during either elongation of division, the fact that two evolvability genes involved in PG biosynthesis, linkage or cleavage, *dpaA* and *pbpG*, are not shared between both drugs could indicate a target dependence for these two genes. The other evolvability genes were more likely to act in a target-independent manner by interacting with general resistance mechanisms such as decreased porin abundance limiting nutrient availability or increased efflux pups constraining nutrients and taking up energy.

For cefsulodin, *gcd*, *leuO*, *srlR*, *dacA*, and *ivy* delayed resistance evolution, which is interesting given that cefsulodin also delays cefotaxime resistance evolution when added at subinhibitory concentrations. Despite the concordance of their resistance trajectories, part of the cefsulodin response or resistance mechanism displays collateral sensitivity with cefotaxime. Amoxicillin only shared *dacA* as a gene delaying resistance evolution with cefotaxime. Cloxacillin and fosfomycin both target PG precursors and showed a high overlap with cefotaxime evolvability genes but small effect sizes. Trimethoprim evolution was not affected by any of the evolvability gene KOs. For gentamicin, *dacA*, *ivy*, and *pbpG* delay resistance evolution (Figure 32c), while

for tetracycline, the overlap includes all evolvability genes except *pbpG*. The high overlap between cefotaxime and tetracycline can be explained by the fact that *marR* resistance is most likely delayed by those genes and also represents the major resistance element providing tetracycline resistance *via* upregulation of the AcrAB-TolC efflux pump (Alekshun & Levy 2007; Alekshun & Levy 1999; Lukačišinová et al. 2020). To conclude, I identified genes conditional-essential during only cefotaxime and cefuroxime resistance evolution, resistance evolution of PBP3 targeting antibiotics, and resistance evolution of antibiotics against which *marR* provides resistance since these genes interact with *marR*. The last class was comprised of genes that affected resistance evolution against multiple antibiotics from different classes targeting various processes, which are more likely to represent general evolvability genes interacting with general processes during resistance evolution.

In this chapter, I used the different methods of quantitative genetics, genomics, proteomics, and qualitative live imaging to dissect the interactions between evolvability and resistance genes that constrain cefotaxime resistance evolution. Even though several hypotheses about the mechanisms underlying such gene-gene and gene-gene-drug interactions were supported by different experiments, it remains an open question whether the studied effects are of correlated or causal nature. While a further characterization using biochemistry could answer some of the remaining open questions, a more detailed characterization might not be necessary to conclude that the identified evolvability genes represent promising targets for evolution inhibitors. Furthermore, deletion of the identified evolvability genes delayed antibiotics against different antibiotics, and the insights gained were used successfully to identify and validate several antibiotics delaying resistance evolution against cefotaxime.

Chapter IV: Global epistasis of antibiotic targets and resistance genes

Chapter IV: Global epistasis of antibiotic targets and resistance genes

1. Summary

Sustainable drug treatments should incorporate the evolutionary potential for resistance development and delay or prevent resistance evolution. In the previous chapters, I evolved resistance in a genome-wide KO library, identified evolvability genes conditional-essential during resistance evolution, and discovered that the absence of such genes delayed resistance evolution *via* gene-gene and gene-gene-drug interactions. Since performing experimental evolution of a genome-wide KO library over six days is time-, labor- and cost-intensive and can not be scaled to multiple antibiotics easily, this chapter aims to develop and benchmark a more scalable approach to quantify epistatic interactions between an antibiotic drug target or resistance gene with all non-essential genes. To achieve this, I quantified global gene-gene interactions by conjugating the CRISPRi plasmid I developed in Chapter II, knocking down the essential antibiotic target and resistance gene *parC* into the KEIO library of non-essential KO mutants using high-throughput conjugation on plates. I measured the impact of the CRISPRi-mediated KD on every non-essential KO mutant in high-density arrayed microbial colonies by imaging and colony quantification using Iris (Kritikos et al. 2017). I identified several known and novel non-essential genes that increase or decrease the essentiality of *parC via* epistasis interactions. This approach represents a faster, cheaper, and more scalable approach to measuring global epistasis of resistance elements or antibiotic targets that can be easily scaled to a few genes in the absence or presence of an antibiotic per experiment.

2. Contributions

Dr. Carlos Geert Pieter Voogdt (EMBL) and Dr. André Mateus (EMBL, now Umea) helped me to design and optimize the CRISPRi plasmid and the experimental workflow. Dr. André Mateus performed the mass spectrometry-based proteomics of the CRISPRi plasmid targeting different genes. I conducted all other experimental and computational work presented in this chapter. Dr. Athanasios Typas and I conceived the experimental design and method for preliminary testing and the genome-wide screen. Dr. Athanasios Typas and myself discussed the pipeline for data analysis and visualization.

3. Measuring global epistasis of antibiotic targets and resistance genes

Mapping global epistasis during antibiotic resistance evolution in Chapter II revealed that resistance evolution can be modulated by gene-gene or gene-gene-drug interactions between

resistance genes and non-essential genes. In this chapter, I present an orthogonal approach to measure epistasis of antibiotic targets or resistance genes with all non-essential genes based on high-density bacterial colony arrays that are more scalable, cost- and time-efficient. Targeting negative epistatic interactions or SL between an essential drug target or resistance gene and a non-essential gene can put additional constraints on the essential gene and make it more difficult to overcome a stressor via suppressor mutations, thereby possibly increasing the efficacy and sustainability of the treatment. As an alternative approach to Chapters II and III, this chapter aims to measure global epistasis by the KD of antibiotic resistance genes to identify genetic vulnerabilities that can be targeted to delay resistance evolution. Another possibility is to measure the global epistasis of antibiotic targets instead of resistance genes. Measuring the global epistasis of an antibiotic target can reveal both negative and positive epistatic interactions that can be used to increase the effectiveness of the antibiotic (by exploiting negative epistasis) or for the identification of possible resistance genes (positive epistasis) (Figure 33).

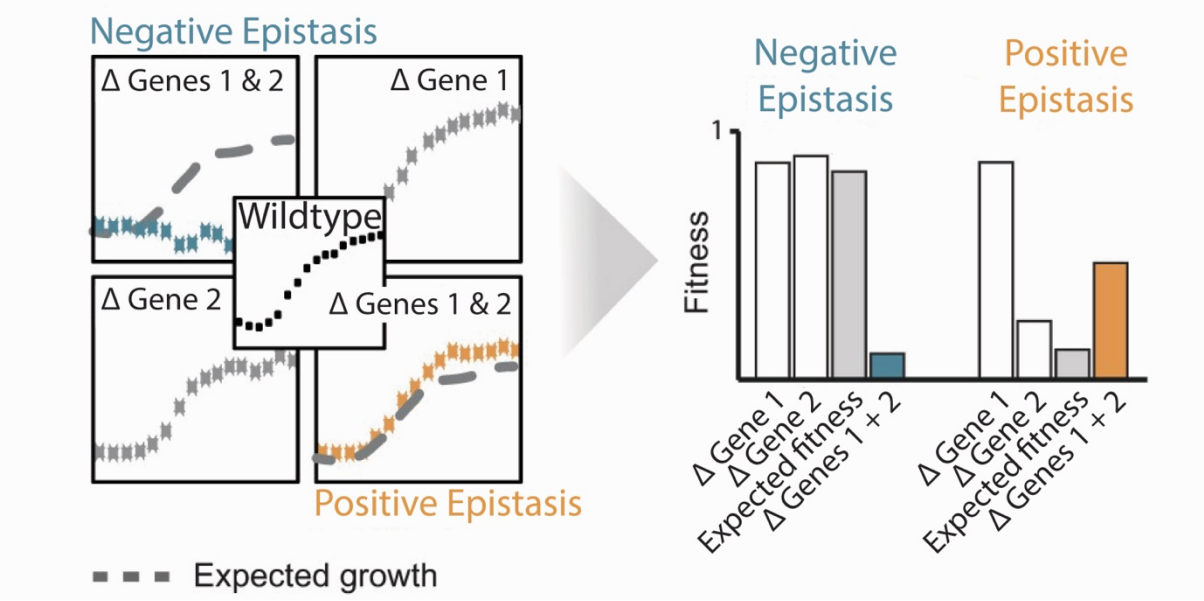

Figure 33: Quantifying epistatic interactions. *Two genetic perturbations show negative epistasis when fitness in the presence of both perturbations is lower than expected, and positive epistasis when fitness in the presence of both perturbations is higher than expected following the Bliss independence model* (Bliss 1939)*. Figure adapted from* (Brochado et al. 2018)*.*

3.1. Preliminary testing identified the optimal conditions to quantify epistasis

ParC is one of the targets and resistance genes of the commonly used fluoroquinolone antibiotic ciprofloxacin. To determine which genes might be epistatically interacting with *parC*, I inserted a guide RNA (gRNA) targeting *parC* (Rousset et al. 2021) into the CRISPRi

plasmid pSB03_2 (Chapter III.3.1). As a negative control, I repeated all steps with a non-targeting scrambled gRNA to identify the potential toxicity of the system. The ability to be transferred *via* conjugation makes this CRISPRi system amenable to high-throughput conjugation into pooled or arrayed genome-wide knockout or transposon libraries, as described before, with other plasmids (Typas et al. 2008).

Additionally, I cloned published gRNAs (Rousset et al. 2021) targeting several other essential and non-essential genes into the CRISPRi vector pSB03_2 via Golden Gate cloning and assessed growth effects by spot assay using a tenfold dilution series starting at $OD_{595\ nm}$ of 0.1 (Figure 34a). As expected, KDs of essential genes coding for proteins of the ribosome (RplI, RplA, RpsA), RNA polymerase (RpoB), DNA gyrase (GyrA), and DNA topoisomerase IV (ParC) reduced colony-forming unit (CFU) counts by several orders of magnitude (Figure 34a). Also, the KD of the non-essential gene coding for a subunit of the ATP synthase F_1 (AtpA) and of the global chaperone (DnaK) reduced viability visible by a reduction of CFUs and opacity in the case of *atpA* KD. FolA coding for dihydrofolate reductase is known to be essential, but no loss of viability was observed when this gene was targeted by KD, potentially because reducing folate biosynthesis has less effect in rich media.

To confirm CRISPRi-mediated transcriptional repression on the protein level, I used MS-based proteomics performed by Dr. André Mateus on several non-essential KDs (Figure 34b). Strong and specific CRISPRi-mediated KD was confirmed for all targeted genes marked in red with *folA* and *ompF* representing examples of highly specific KDs (Figure 34b). Proteins with lower abundance other than the targeted protein are often part of the same operon, which results in their CRISPRi-mediated transcriptional repression since CRISPRi has polar effects and the entire targeted operon is silenced (Peters et al. 2016). Since DnaK folds hundreds of other proteins (Aguilar-Rodríguez et al. 2016; Calloni et al. 2012), the decreased abundance of other proteins upon DnaK depletion could be explained by the degradation of unfolded or misfolded proteins or negative transcriptional feedback.

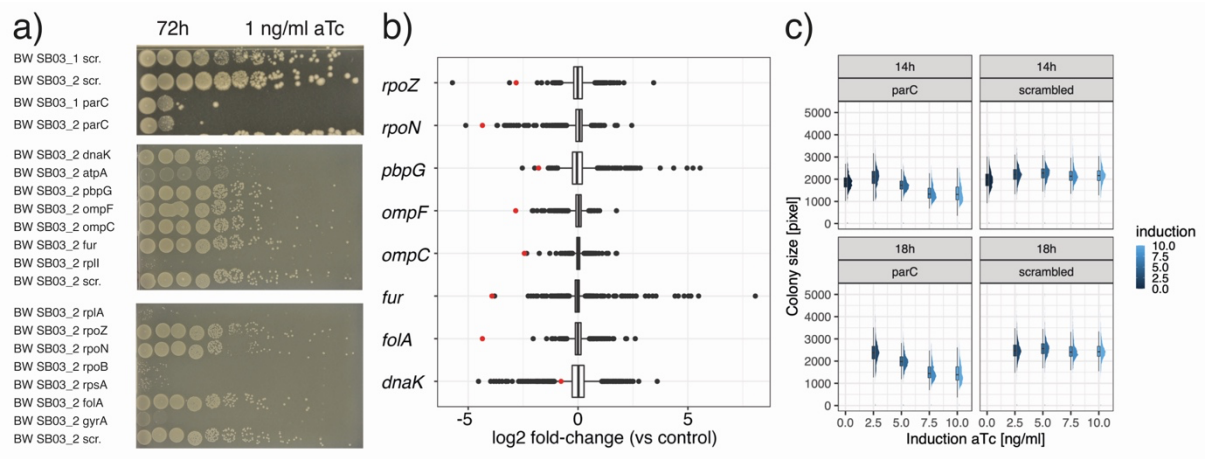

Figure 34: CRISPRi-mediated KDs specifically reduce CFUs, protein abundance, and* colony *size. *a) KDs of essential genes reduce the CFUs by several orders of magnitude measured by spot assay of a 10-fold dilution series. Spot assays were grown for 72 h on 1 ng/ml anhydrotetracycline (aTc). b) KDs translate to a target-specific depletion of protein abundance. Targeted genes are marked in red. Other proteins with reduced abundance are part of the same operon or depend on the abundance of the targeted protein, as in the case of the chaperone dnaK. c) KD of the essential gene parC encoding a subunit of the DNA topoisomerase IV reduces the* colony *size of 1536 KO mutants in a dose-dependent manner.*

Next, I conjugated the plasmid carrying the *parC*-targeting gRNA and a control plasmid carrying a scrambled gRNA into 1536 KEIO mutants using high-throughput conjugation on plates and quantified the effects of different induction levels on colony size (Figure 34c). For conjugation, I transformed the conjugation proficient donor strain (BW25113 pseudoHfr::(trp bla (-) (Typas et al. 2008)) with the plasmid and spread it on agar plates without selection and dried it for 2 hours, after which I pinned a 1536-mutant KEIO plate on top. After 14 hours of overnight conjugation, I pinned colonies onto selective plates and incubated overnight to select for kan- and spec-resistant transconjugants and removal of the donor (kan sensitive). After a second overnight selection on kan and spec, I pinned the colonies on plates with 0, 2.5, 5, 7.5, and 10 ng/ml of anhydrotetracycline (aTc), providing different induction levels.

Induction levels required to see growth effects on colony size were much higher than those required to see effects on spot assays (1 ng/ml) due to the higher resolution of the spot assay, which allows for the measurement of $\log_{10}$ differences in colony numbers. I took pictures after 14 h and 18 h and quantified colony sizes and opacity using IRIS (Kritikos et al. 2017). The detailed protocol can be found in Chapter VI. This proof of principle confirmed titratable CRISPRi induction and specific *parC* repression by the constructed plasmid pSB03_2, resulting in decreased colony size and opacity correlating with induction levels (Figure 34c). Furthermore, it revealed that 10 ng/ml of aTc induction reduced colony size by ~ 40 % in the *parC* KD, which is optimal for detecting both negative and positive epistasis.

A small colony size reduction upon KD decreases the dynamic range to detect positive epistasis, *i.e.*, less than average colony size reduction. In contrast, a large colony size reduction decreases the dynamic range to detect negative epistasis, *i.e.*, more than average colony size reduction. Furthermore, since changes in colony size and opacity are more difficult to detect in smaller colonies, higher inducer concentrations and the resulting smaller colonies decrease the resolution to detect both positive and negative epistasis.

In high-density colony arrays, colony size and opacity are highly correlated, but since bacteria grow both in area and height, three-dimensional growth is better depicted by summing brightness values across all pixels within the colony bounds, also called colony integral opacity. Since opacity shows a better dynamic range and recapitulates growth more accurately, especially for smaller colonies than colony size, I used it for all further quantification of epistasis (Kritikos et al. 2017).

3.2. Quantifying global epistasis of the DNA topoisomerase IV

In the next step, I repeated the same workflow with the whole KEIO library, including ~ 4,000 single-gene KOs (Baba et al. 2006; Yamamoto et al. 2009) with 4 colonies per mutant across 2 plates using a 1,536 format and 10 ng/ml aTc induction. I took pictures after 14, 18, and 22 h of growth and quantified colony sizes and opacity using IRIS (Kritikos et al. 2017). 1 out of 6 KEIO plates corresponding to $1/6^{th}$ of the KEIO mutants had to be discarded due to a technical problem, *i.e.*, the plate was not dry enough for the conjugation step. The Pearson correlation of opacity across technical and biological replicates was above 0.8 for all plates (Figure 35a).

Technical replicates correspond to the same colonies pinned on a different plate, while biological replicates are two different stocks of each gene deletion pinned on the same plate. I calculated the relative *parC*-inhibition of a single KO mutant by first dividing the opacity value of that mutant carrying a *parC*-targeting guide by the opacity of that mutant carrying a scrambled guide. This value was then divided by the median opacity of all mutants on the same plate carrying a *parC*-targeting guide divided by the opacity of all mutants carrying a scrambled guide. This median *parC*-inhibition value was around 0.6 – 0.7, corresponding to a 30 – 40 % decrease in colony size and opacity upon *parC* KD (Figure 35b). Lastly, I calculated Log_2(fold-change) and significance (BH-adjusted Wilcoxon signed-rank test) of relative *parC*-inhibition

so that hits represented non-essential KOs that are significantly more or less affected by *parC* KD than all other KOs on their respective plate, indicating epistatic interactions (Figure 35c).

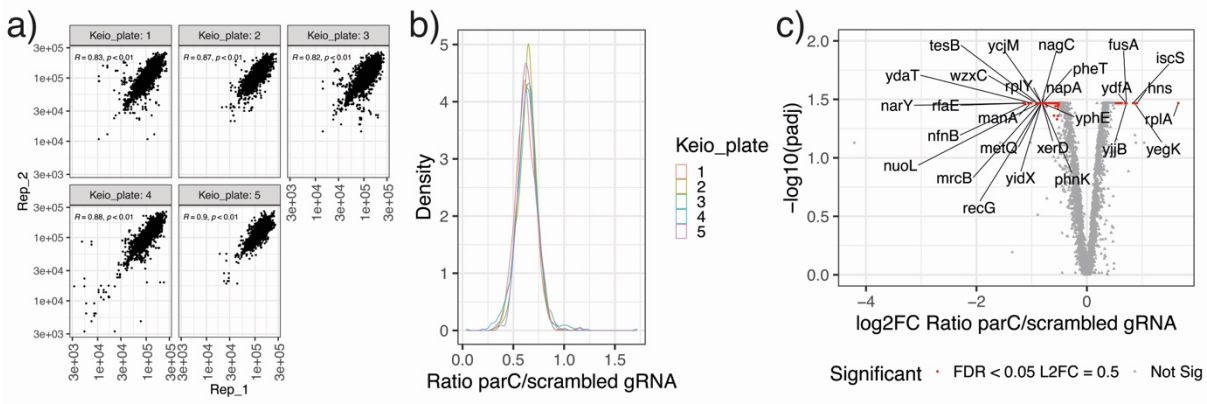

Figure 35: Global epistasis of antibiotic target and resistance gene parC with >80 % of non-essential gene KOs. *a) Gene-wise Pearson correlation across technical and biological replicates is larger than 0.8 across KEIO plates. b) Plate-wise distribution of* colony *opacity of a single KO mutant in the presence of the parC-targeting guide divided by the opacity of that mutant carrying a scrambled guide is shown. c) Log_2(fold-change) and significance (BH-adjusted Wilcoxon signed-rank test) of the opacity of a single KO mutant in the presence of the parC-targeting divided by scrambled guide relative to the median opacity of all genes of their respective plate carrying a parC-targeting guide divided by a scrambled guide. Hits are labeled based on the padj. significance cut-off <0.05 and effect size cut-off of 0.5.*

Hits with strong negative epistasis are in line with negative epistatic interaction partners of *parC* previously identified by thermal stability measured by MS and validated using a two-component CRISPRi system by spot assay such as *phoP* (Mateus et al. 2020). The *phoP* KO affects the thermal stability of ParC, and *phoP* KO cells cannot tolerate ParC depletion, indicating a genetic interaction (Mateus et al. 2020), which I confirmed by global epistatic interaction screening (Figure 36). Gene KOs with negative epistasis with the *parC* KD (*padj.* < 0.05 and Log_2(fold-change) < -0.25) were enriched for the gene ontology term DNA binding (1.9-fold enrichment and 0.014 BH-adjusted *p-value*). It fits the expectation that in KO mutants of non-essential DNA binding genes encoding subunits of the DNA helicase IV (*helD*), DNA topoisomerase IV (*parE)*, ATP-dependent DNA helicase (*recG)*, RNA polymerase (*rpoZ),* DNA polymerase (*umuD*) and flap endonuclease (*ygdG*/ExoIX), the depletion of the DNA topoisomerase IV subunit encoded by *parC* has a stronger impact relative to the plate median. Therefore, these genes increase the essentiality of *parC*. Furthermore, multiple transcription factors and genes involved in the response to DNA damage were among the gene KOs exhibiting negative epistasis with the *parC* KD.

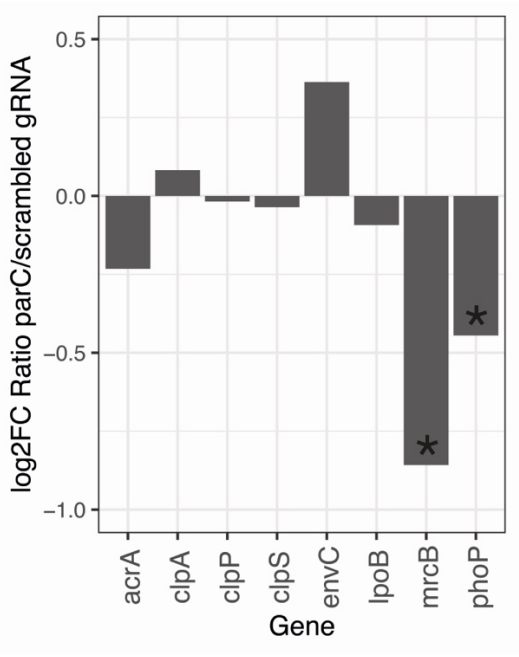

Figure 36: Global epistasis method recapitulates known interaction partners of parC. *Epistatic interactions of genes previously tested for their interaction with parC are shown* (Mateus et al. 2020)*. Hits recapitulate gene KOs that show negative epistasis with parC, identified by decreased parC thermostability and confirmed by spot assay* (Mateus et al. 2020)*. Log_2(fold-change) and significance (BH-adjusted Wilcoxon signed-rank test) of the opacity of a single KO mutant in the presence of the parC-targeting divided by scrambled guide relative to the median opacity of all genes of their respective plate carrying a parC-targeting guide divided by a scrambled guide is shown. The used significance cut-off was padj. < 0.05.*

3.2. Next steps to systematically test antibiotic targets and resistance genes

The following steps include repeating this workflow with additional essential or non-essential gene KDs that either represent resistance regulators, such as *marR*, antibiotic resistance genes, such as the porins *ompC* and *ompF* or antibiotic targets, such as the ribosomal genes (*rplI*, *rplA*, *rpsA*), RNA polymerase (*rpoB*) and DNA gyrase (*gyrA*). I will select target gene KDs and respective inducer concentrations based on the decrease in colony size and opacity upon KD to determine the dynamic range of epistatic interactions I can detect. A reduction of ~ 40 % in colony size and opacity, such as for the *parC* KD at 10 ng/ml aTc, represents optimal conditions because both an increased and a decreased reduction in colony size relative to the plate median can be detected.

The preliminary method presented here opens many opportunities for modification and adaptation. In order to test not only for gene-gene interactions but also for gene-gene-drug interactions, one could measure gene-gene interactions in the absence and presence of an antibiotic in the plate as it has been done systematically (Nichols et al. 2011). This would probe not only how non-essential gene deletions affect the essentiality of the essential KD but also how this affects sensitivity to the corresponding antibiotic.

An even more scalable, time- and cost-efficient approach would be to conjugate the CRISPRi plasmid into a pooled barcoded KO or transposon library of *E. coli* and measure positive and negative epistasis of different KO or transposon mutants in the pool. Barcode sequencing can be used to estimate every mutant's abundance and infer fitness (Levy et al. 2015; Nguyen Ba et al. 2019; Venkataram et al. 2016; Kinsler et al. 2020; Wetmore et al. 2015). Based on this count data, epistasis can be inferred from the decrease in fitness carrying an essential gene targeting guide versus a scrambled guide. It is probably more sensible to create the pooled and barcoded transposon or KO library first and then conjugate the CRISPRi plasmid. Performing the methodology *vice versa* would allow suppressor mutants of the CRISPRi plasmid to arise during the library preparation that requires several growth phases, and transposon mutants in the CRISPRi plasmid would outcompete other mutants. This approach could be scaled up to tens of essential resistance genes and antibiotic targets. Each CRISPRi plasmid will be constructed, conjugated into a pooled transposon library, and grown in an individual well. This will be followed by a barcode PCR with indexed primers and multiplexed barcode sequencing as fitness readout. Preliminary experiments to create transposon mutants (Hualan et al. 2018) in a *rpoB* KD strain carrying the functional pSB03_2 plasmid were already successful and identified several transposon mutants that suppressed essentiality of *rpoB* (data not shown).

Since antibiotic targets are, by definition, essential genes, target mutations of such genes rarely represent LOF but rather point mutations. Therefore, mapping the global epistasis of the CRISPRi KD of the essential gene might not fully recapitulate the global epistasis of point mutations in an essential antibiotic target. An alternative approach for measuring the global epistasis of a point mutation in an essential antibiotic target could be to fully KD the native essential antibiotic target on the chromosome using CRISPRi and provide an alternative mutated version of the essential antibiotic target from the plasmid.

Lastly, I will quantify the epistatic interactions of clinical resistance genes such as extended-spectrum β-lactamases (ESBL) on a plasmid (Darphorn et al. 2021). I will conjugate the resistance plasmid carrying the ESBL into the pooled or arrayed KEIO collection and either measure gene-gene interactions of the resistance gene with all non-essential genes by growing in media without antibiotic or measure gene-gene-drug interactions of the resistance gene with all non-essential genes growing in media containing antibiotic, thereby measuring resistance levels provided by the plasmid in the absence of non-essential genes.

I will use a subset of KDs exhibiting negative epistasis to quantify suppressor frequency in SL pairs of essential KD and non-essential KOs. Therefore, I will compare suppressor counts measured by CFUs of an essential gene KD in the wildtype background and the SL non-essential KO background. Using the measured suppressor frequency across different knockdowns in the wildtype I can estimate a background mutation rate of the plasmid. To filter out suppressors carrying a mutation in the CRISPRi plasmid, I will conjugate suppressors with a fresh plasmid carrying a different resistance marker and measure the effects on growth by the fresh plasmid in liquid. To filter out suppressors with a mutation in the sgRNA binding site on the chromosome, I will sequence this site for the remaining suppressors in the last step. This will enable the identification of potential non-essential targets or pathways to increase antibiotic effectiveness and delay resistance evolution.

4. Conclusions

In summary of Chapter IV, I developed a quantitative method to measure global epistasis between an essential or non-essential gene and all non-essential genes, thereby illuminate the cell's genetic wiring. This method is based on a single CRISPRi plasmid amenable to high-throughput conjugation and can be induced and titrated. The CRISPRi-mediated transcriptional repression translates to a strong and target-specific protein depletion, which I confirmed using MS-based proteomics with the help of Dr. Andre Mateus. This target-specific modulation of gene expression can likely be extended to other genes and strains and opens up various applications ranging from epistatic interactions, as visualized in Chapters II and III, to targeted strain depletion and antibiotic potentiation. Another application arises from adding multiple sgRNAs to the CRISPRi plasmid targeting multiple essential or non-essential genes, allowing epistatic measurements to be further multiplexed.

I used this tool to probe genome-wide epistasis of the antibiotic target and resistance element of ciprofloxacin *parC* encoding the DNA topoisomerase IV subunit A. I uncovered both known negative interaction partners (Mateus et al. 2020), such as *phoP*, and unknown negative and positive interaction partners that either decrease or increase the essentiality of *parC*. Essentiality has been shown in yeast to be an evolvable quantitative property that depends on the environment (Liu et al. 2015), and here, I modulate essentiality by altering the genetic background in a systematic, gene-wise manner.

In the next steps, I will use the assay to probe genome-wide epistasis of other essential antibiotic targets and resistance genes with non-essential genes in arrayed KO libraries. While negative epistasis, *i.e.*, more colony size reduction in a given genetic background, can be measured when knocking down essential or non-essential genes, positive epistasis, *i.e.*, less colony size reduction in a given genetic background, can only be quantified in essential genes where the KD reduces colony size by 30-40 %. One way to overcome this limitation is by adding an antibiotic to the plates that reduces colony sizes by a similar margin.

Identified non-essential genes showing SL with antibiotic targets represent targets to increase antibiotic effectivity by increasing the essentiality of the essential gene targeted by an antibiotic. One could search for molecules leveraging the SL of the antibiotic target and use them in combination with the antibiotic to increase the selective pressure. Non-essential genes showing SL with resistance genes represent targets to specifically prevent growth in resistant clones and diminish their evolutionary potential to develop antibiotic resistance. Targeting the SL partner gene of a primary resistance mechanism with a small molecule should inhibit existing mutants and prevent new mutants from carrying this resistance gene.

One open question that arises from quantifying the global epistasis of the genetic network is the degree of species-specificity and how it relates to gene essentiality (Rousset et al. 2021). CRISPRi KD of the same essential gene in transposon libraries of multiple *E. coli* strains or other bacterial species could answer this question systemantically. Targeting the SL partner gene of a primary resistance mechanism that only exists in *E. coli* should inhibit resistance evolution in a species-specific manner while sparing other species of the microbial community, such as the human gut microbiome. On the other hand, shared SL partner genes could be targeted to remove resistant clones from diverse species of the community and select against resistant elements in a community-wide manner.

Upon identification of SL interactions of the essential gene with non-essential genes, I plan to quantify suppressor frequencies of essential KDs in wildtype and SL KO backgrounds to reveal genetic interactions necessary for survival and evolvability upon essential gene perturbation. Thereby, I will test the hypothesis that, given a negative epistatic pair of an essential and a non-essential gene in *E. coli*, fewer suppressor mutants will arise for the essential gene in the synthetically lethal non-essential gene KO background than in a wildtype background. This represents the final test of whether probing genome-wide gene-gene or gene-gene-drug

interactions with the method presented in Chapter IV is equivalent to the method for measuring the impact of every gene KO on resistance evolution rates I presented in Chapters II and III. I envision systematically mapping ways in which bacteria rewire essentiality following antibiotic exposure and evolve resistance across multiple antibiotic targets, resistance genes, and strains to identify unique and shared genetic vulnerabilities.

Chapter V: Discussion and outlook

Chapter V: Discussion and outlook

This thesis extends the current understanding of how the genetic network shifts during resistance evolution through two orthogonal ways: 1) systematically mapping the impact of every non-essential gene on antibiotic resistance evolution and 2) quantifying the global epistasis of antibiotic resistance genes and targets. For both genome-wide approaches, the design, analysis, validation, and mechanistic characterization have been described in this thesis.

1. Genome-wide experimental evolution

1.1. Brief recap of results

Sustainable drug treatments should incorporate the evolutionary potential for resistance development. However, the current understanding of how the genetic network rewires during antibiotic resistance evolution is limited, and no methods exist to measure evolvability on a genome-wide scale. To address this unsolved need, I developed a method to map the impact of every non-essential gene KO on AMR evolvability. In order to perform this experiment, I first needed to develop a high-throughput experimental evolution method that allowed me to perform ~24.000 evolution experiments, *i.e.*, ~4,000 KO mutants in 6 replicates. Therefore, I systematically tested different experimental evolution conditions and antibiotics to arrive at the optimal conditions. Under those conditions, I evolved antibiotic resistance against the commonly used antibiotic cefotaxime in the genome-wide KO library of *E. coli.*

This experiment revealed several non-essential gene KOs that decreased or increased cefotaxime evolvability when knocked out. Mutants with decreased evolvability were identified by their lower $OD_{595\ nm}$ at 1.5x after filtering out KO mutants with decreased fitness or increased drug sensitivity. Mutants with increased evolvability, on the other hand, I found by their higher OD at 1.5x and 13.5x MIC after filtering out KO mutants with increased resistance. While GO enrichment analysis could not identify any enrichments for gene KOs with decreased evolvability, I identified phospholipid transport (*mla* system) and enterobacterial common antigen biosynthetic process (*wec* pathway) as enriched among gene KOs with increased evolvability at 1.5x MIC and mismatch repair (*mut* genes) as enriched among gene KOs with increased evolvability at 13.5x MIC. In addition, I validated 33 gene KOs delaying resistance evolution identified by high-throughput experimental evolution under standard experimental evolution conditions in more replicates with a precision of 81.8 %. Furthermore, I benchmarked my cefotaxime sensitivity cut-off calculated from growth in 0.5x

MIC cefotaxime relative to growth without cefotaxime with the widely used MIC measurement. They aligned well and that the sensitivity cut-off effectively removed KO mutants with increased cefotaxime sensitivity from the dataset of mutants with decreased evolvability.

1.1. Measuring genome-wide evolvability reveals global epistasis

In this project, I performed experimental resistance evolution in the absence of every non-essential gene in an arrayed format to understand how antibiotic resistance evolves, how this process is shaped by epistasis, how the genetic network rewires during resistance, and what vulnerabilities and dependencies arise as a result. While KO libraries were already used in reverse genetics experiments to assess fitness (*i.e.*, gene-gene interactions between the absence of a non-essential gene and an otherwise wildtype genetic background) and drug sensitivity (*i.e.*, gene-drug interactions between the absence of a non-essential gene and an otherwise wildtype genetic background in the presence of a drug), neither one nor both are sufficient to predict evolvability. In my experimental setup, evolvability as a property quantifies how acquiring a resistance mutation and thereby changing the genetic background alters these interactions. The absence of a non-essential gene can engage in gene-gene interactions or gene-gene-drug interactions with the resistant genetic background or in both. By calculating evolvability based on yield, I integrate all possible interactions between the absence of a non-essential gene, the resistant genetic background, and the drug to assess the degree of (conditional) essentiality of the non-essential gene during antibiotic resistance evolution.

The high-throughput experimental evolution protocol I developed allowed me to quantify fitness, drug sensitivity, and evolvability on a genome-wide level. This multi-modal information is critical to disentangle the lower evolvability from the confounders fitness and sensitivity by leveraging their orthogonality. As a result, I could track how the epistatic landscape changes during resistance evolution, *i.e.*, how resistance mutations interact with non-essential genes in the presence and absence of the antibiotic. Gene KO mutants with decreased fitness already engage in indispensable gene-gene interactions before evolution, while mutants with increased sensitivity already engage in gene-drug interactions with the antibiotic before evolution. By filtering out mutants with decreased fitness or increased sensitivity, I identified evolvability genes that only became conditional-essential through indispensable gene-gene or gene-gene-drug interactions forming during resistance evolution and the accompanying

rewiring of the genetic network. Such genes represent novel targets to block evolution or specifically target resistant subpopulations without affecting the wildtype.

Besides the comprehensiveness of acquiring genome-wide evolvability information, this represents a novel concept of our approach compared to conventional methods measuring gene-drug (Nichols et al. 2011), gene-gene interactions (Typas et al. 2008), or evolvability as a function of fitness and sensitivity (Lukačišinová et al. 2020). From the genome-wide dataset, I conclude that evolvability, sensitivity, and fitness represent orthogonal properties within our thresholds. However, mutants must also display reduced fitness or increased sensitivity to decrease evolvability to a minimum. While other studies have already quantified the impact of a pre-selected subset of ~100 KO mutants on the ability to evolve antibiotic resistance (Lukačišinová et al. 2020), using an unbiased genome-wide approach has several advantages. Such advantages include the capability to identify unexpected genes and uncover novel functions, the ability to map complete genetic modules and pathways implicated in the phenotype of interest supported by GO enrichment analysis, increased statistical robustness, and the option to align and compare the genome-wide dataset with other datasets acquired using the same KO library. Examples are chemical genetics or metabolomics datasets also acquired using the *E. coli* KEIO collection (Fuhrer et al. 2017; Campos & Zampieri 2019; Nichols et al. 2011). Furthermore, genome-wide datasets provide a valuable tool for the research community, allowing unlimited opportunities for follow-ups and hypothesis-driven research in the future.

Lastly, the evolutionary potential and genomic plasticity are still enigmatic properties of biological systems that represent both a great risk to humanity in the form of microbial or cancer drug resistance but also a great opportunity given the diverse use cases in how directed evolution has been applied to engineer properties in an unbiased manner. Studying how gene deletions delay or accelerate evolution can give us unprecedented insights into how we can mitigate risks and take advantage of such properties. In the next part, I will discuss what I learned about cefotaxime resistance evolution by evolving a genome-wide KO library.

1.2. Genomic landscape of cefotaxime resistance evolution

By evolving cefotaxime resistance in the absence of every non-essential gene, I took a global view of the resistance evolution process and how it interacts with the genetic network. KO mutants that evolve worse occur in genes that perform necessary functions during cefotaxime

resistance evolution. Those mutants either later or not at all acquire the necessary resistance mutation (mutation rate), they showed a fitness defect with the resistance mutation (gene-gene interaction), or they reduced resistance levels provided by resistance mutations (gene-gene-drug interaction). I identified mutants evolving worse by comparing yield at 1.5x MIC, and most KO mutants evolve resistance against 1.5x or 4.5x MIC of the antibiotic, which suggests that mutation rate is not limiting for mutants with decreased evolvability. Hence, I most likely selected single-step high-rate small-effect SVs that cause LOF of resistance regulators and provide resistance by efflux pump upregulation and porin downregulation, as it was reported before (Schenk et al. 2022).

As a result, it is likely that gene KO mutants with decreased evolvability delay evolution by gene-gene or gene-gene-drug interactions with this first set of single-step resistance mutations than by affecting the mutation rate. Evolvability at 1.5x MIC can, therefore, be reduced to epistasis with the first set of single-step mutations evolving during cefotaxime resistance evolution. This has the positive effect that the epistasis I measure is with a set of single-step mutations, which makes it easier to investigate specific gene-gene and gene-gene-drug interactions on a molecular level. Furthermore, since high-rate, low-benefit mutations often start the evolutionary trajectory and are followed by other mutations, blocking evolution at the first step presents the most promising translational angle. Lastly, in the case that evolvability can be reduced to direct gene-gene or gene-gene-drug interactions with the first set of single-step mutations, it opens the possibility to characterize evolvability with alternative approaches based on high-density colony arrays that were described in Chapter IV and can be scaled to multiple antibiotics.

Since the antibiotic cefotaxime used targets PG biosynthesis during cell division, it fits the expectation that several of the evolvability genes required during cefotaxime resistance evolution were involved in remodeling the cell envelope. Examples were endo-, carboxy- and transpeptidases, and genes involved in PG biosynthesis, OM constriction, and the regulation of amidases. Another class of processes was involved amino acid, peptide, iron, and carbon utilization and metabolism. Those processes were required for the successful evolution of cefotaxime resistance and, therefore, represent targets for cefotaxime evolution inhibitors, which I explored in Chapter III.8.

KO mutants that evolve better represent harmful processes during the resistance evolution of cefotaxime. Characteristics for such better evolving KO mutants include that they acquire the required variants faster (mutation rate), they show faster growth with the resistance mutation (gene-gene interaction), or higher resistance levels with the resistance mutation (gene-gene-drug interaction). Since most mutants can evolve resistance against 1.5x MIC, the mutation rate is likely not limiting at this antibiotic concentration. Therefore, mutants with increased yield probably accelerate resistance evolution by positive gene-gene or gene-gene-drug interactions with resistance elements. Such processes were involved in LPS biosynthesis, phospholipid transport, ECA biosynthesis, flagella biosynthesis, and regulation, as well as PG and cell envelope biosynthesis and remodeling *via* endopeptidases and LTs. KO mutants with increased evolvability at 13.5x MIC showed several overlaps with mutants that display increased evolvability at 1.5x MIC, but also differences. Since few mutants evolved resistance up to 13.5x MIC, the mutation rate becomes limiting at this condition, suggesting that the high-rate small-effect LOF mutations of resistance regulators did not provide enough resistance to grow at 13.5x MIC and were replaced by low-rate large-effect target mutations (Schenk et al. 2022). Supporting this hypothesis, I found that gene KOs with higher evolvability at 13.5x MIC were enriched for DNA mismatch repair, suggesting that they represent a mutator phenotype with a higher mutation rate (Schofield & Hsieh 2003; Cox 1976; Gifford et al. 2023). In addition, there were several genes from the processes of LPS biosynthesis, PG coordination and remodeling, iron-sulfur cluster assembly, and riboflavin biosynthesis.

In summary, by quantifying both decreased and increased evolvability at 1.5x MIC cefotaxime under mutation rate-saturated conditions, I systematically mapped both positive and negative epistasis of every non-essential gene deletion with the most common resistance mutations at this concentration. Those resistance mutations are most likely high-rate, low-benefit mutations given the high probability of growing at 1.5x MIC and the low probability of growing at 13.5x MIC. An interesting side effect of this way of measuring gene-gene and gene-gene-drug interactions with unknown resistance trajectories is that, most likely, several distinct resistance mutations exist. Therefore, measuring lower yield in a mutant at 1.5x MIC entails interactions with multiple competing resistance mutations, given that multiple ones exist and occur with a high enough probability to be commonly observed.

The fact that cefotaxime targets PG biosynthesis and that I identified genes involved in PG and cell envelope remodeling among genes with both negative and positive effects on resistance

evolvability suggests that those genes delayed resistance evolution by gene-gene-drug interactions. At 13.5x MIC, where the mutation rate becomes limiting, I found genes that increased evolvability by increasing the mutation rate following the expectation. However, several genes were not involved in DNA mismatch repair but in LPS biosynthesis and PG remodeling among better evolvers at 13.5x MIC, some of which overlapped with better evolvers at 1.5x MIC and indicated strong positive epistasis with resistance elements. As for any experiment, and even more so for high-throughput experiments, there were several compromises I had to make when designing and performing these experiments, which I will discuss next.

1.3. Shortcomings and potential pitfalls

In order to achieve the throughput needed to perform arrayed experimental evolution at the scale of a genome-wide KO library in several replicates, I had to accept several compromises and limitations. For every experimental evolution setup, the results are condition-dependent, which also applies here. The first potential shortcoming relates to the liquid volume used for the evolution experiment. While many experimental evolution studies use volumes between 1 and 100 ml, the need to use 384-well plates restricted the maximum volume to 150 µl. This will decrease the population size by up to 3 orders of magnitude and, therefore, limit the type of accessible mutations, for example, by preventing the evolution of rare point mutations in the antibiotic target. As a result, gene KOs with decreased evolvability potentially only restrict evolution in small populations and lose their effect in larger populations and larger bottlenecks when more low-frequency mutations are accessible and transferred. To test this condition-specificity, I performed a validation experiment of 33 KO mutants with decreased evolvability. I confirmed that 81.8 % also delayed resistance evolution in ~10x larger volumes, population sizes, and bottlenecks by evolving two independent KEIO clones in more replicates. This experiment also revealed that the decreased evolvability is not caused by compensatory mutations known to be present in large-scale libraries such as the KEIO collection for many mutants.

One shortcoming is that due to the scale of the experimental approach, only one antibiotic could be tested for gene KOs affecting its evolvability, so the findings could only be relevant for cefotaxime. To address this limitation, I examined in Chapter III.9 whether the identified evolvability gene KOs also delay the resistance evolution of other antibiotics. Indeed, many of

the identified evolvability genes were required during the resistance evolution of other antibiotics of the same and even different classes. In addition, I applied the insights I identified in Chapters II and III that gene-gene and gene-gene-drug interactions can delay resistance evolution to develop an orthogonal method to identify such epistatic interactions in Chapters III that can be easily scaled to tens of antibiotics by using high-density colony arrays instead of liquid cultures.

Another limitation due to the scale of the approach is the need to use one antibiotic concentration for all KO mutants, even though the pre-existing fitness and sensitivity of different KOs could limit the ability to evolve cefotaxime resistance and skew the evolvability results. In the case of decreased fitness, a KO mutant that grows at a slower growth rate reaches lower population sizes after 24 h, limiting its potential for resistance evolution. A mutant with higher cefotaxime sensitivity will be subjected to a higher selective pressure than the other KO mutants. Therefore, the common high-rate low-benefit mutations might not be sufficient to allow growth at 1.5x MIC. Another study addressed this challenge by keeping the growth rate constant for every mutant using an automated robotic setup (Lukačišinová et al. 2020).

Since this is impossible when working with around 4500 individual wells at a time, I employed a strategy to filter out KO mutants with decreased fitness or increased sensitivity. This allowed me to focus on mutants that show only decreased evolvability while sharing the fitness and sensitivity of the wildtype. Since the employed filtering step was based on arbitrary thresholds based on the fitness and sensitivity distributions, as well as known mutants with decreased MICs, it could be that my thresholds missed mutants with decreased fitness or increased sensitivity. To address this potential pitfall, I performed a benchmarking of my sensitivity filtering step with the widely used MIC measurement for 27 mutants. I found that they agreed well in filtering out mutants with increased sensitivity. In addition, testing evolvability under the same conditions for all mutants allowed me to dissect the relationship between fitness and evolvability, as well as between sensitivity and evolvability, in more detail. Besides the expected case of mutants with decreased fitness or increased sensitivity showing lower evolvability, opposite cases exist, where despite decreased fitness or increased sensitivity, some mutants still showed increased evolvability. *Vice versa*, some mutants with increased fitness or decreased sensitivity also showed decreased evolvability, underlining the need to measure fitness, sensitivity, and evolvability for every mutant to assess resistance evolution comprehensively.

Lastly, when considering an infection context, the ability to evolve resistance will always depend on fitness and sensitivity, and determining absolute evolvability at a constant concentration across all mutants gives us a better estimate of the impact of potent targets to delay resistance evolution. In this translational case, identifying a target that decreases both resistance and evolvability might be advantageous, which I can dissect using the described approach.

1.4. Conclusion and outlook

The described protocol represents the first example of experimental evolution using an arrayed genome-wide KO library. As a result, the biological property of evolvability I characterized on a genome-wide scale represents a novel angle to quantify evolution. By measuring it early in the evolution experiment, I reduced evolvability to epistasis with the first set of single-step resistance mutations. This allowed me to interrogate the epistatic landscape of this confined set of pioneer resistance mutations on a molecular level in Chapter III by characterizing interactions with resistance mutations and identifying drugs to delay resistance evolution.

The presented method can be easily adapted to quantify evolvability against other selective pressures. I have already tested 18 antibiotics under the high-throughput experimental evolution conditions employed for the screen, and both gentamicin and nitroxoline are valid candidates. The limiting factor in scaling the method to multiple antibiotics is the high number of liquid transfers requiring robotic systems and automation. However, given that the optimal antibiotic concentration to quantify evolvability can be adjusted to 1.5x MIC, as in this study, it is possible to shorten the experimental duration and the required number of liquid transfers from 7 to 3. This substantially increases feasibility and decreases the time- and resource-requirements. Since gene KOs with delayed evolvability identified by experimental evolution (Chapter II) delayed resistance evolution based on direct epistatic interactions with resistance elements (Chapter III), it opens the possibility for alternative approaches measuring global epistasis of resistance elements that are more scalable, such as the method described in Chapter IV. In principle, mutants with the largest decrease or increase in evolvability could also be identified by evolving a pooled barcoded *E. coli* KO library and applying the same filtering thresholds for fitness and sensitivity. However, this would limit the measurement resolution compared to the arrayed approach since competition will select mutants with fast growth rates

and increased antibiotic resistance during every transfer. Pooled approaches were discussed in more detail in Chapter IV.4.

Lastly, the approach presented here makes the resistance evolution process more tangible by illuminating parts of the genetic network that can delay or accelerate it. By characterizing the epistatic dependencies accompanying the rewiring of the genetic network during cefotaxime resistance evolution, I identified several gene-gene and gene-gene-drug interactions that delay resistance evolution and arrived at a list of potential targets that can be used to delay, stop, or revert resistance evolution.

2. Epistatic interactions delaying resistance evolution

2.1. Brief recap of results

To uncover the mechanistic basis for epistatic interactions delaying resistance evolution, I first sequenced resistance mutants I evolved under my experimental evolution setup. As hypothesized, I identified single-step high-rate, low-benefit LOF mutations of the resistance regulators *marR* and *ompR*. MarR provides resistance by upregulating efflux pumps such as AcrAB-TolC (Sharma et al. 2017) and downregulating the porin *ompF* (Ramani et al. 1994), while *ompR* downregulates the porins *ompF* and *ompC* (Yoshida et al. 2006a). I also identified LOF mutations directly in *ompF* and in *lon* that stabilize *marA* (Nicoloff & Andersson 2013). Furthermore, I found an example of a *waaQ* variant affecting LPS biosynthesis, further increasing resistance in a mutant carrying already a *marR* mutation.

Next, I constructed a CRISPRi plasmid that can be induced, titrated, and conjugated. I used it to measure gene-gene and gene-gene-drug interactions between the resistance elements *marR* and *ompR* and two evolvability genes, *dpaA* and *ivy*, both of which were hits with decreased evolvability. DpaA cleaves crosslinks between PG and Lpp (Bahadur et al. 2021; Matthias et al. 2021), while the periplasmic chaperone *ivy* was reported to fold periplasmic proteins under protein stress and to inhibit lytic transglycosylases, as well as lysozyme (Lennon et al. 2015; Clarke et al. 2010; Monchois et al. 2001). Using evolvability gene KDs in resistance gene KO backgrounds in the absence of cefotaxime, I identified gene-gene interactions between the evolvability gene *dpaA* and the resistance genes *marR* and *waaQ* and of the evolvability gene *ivy* with the resistance genes *marR*, *ompR*, and *waaQ*. By testing interactions in the presence

of cefotaxime, I identified gene-gene-drug interactions between the evolvability genes *dpaA ivy* and the resistance gene *ompR*.

To assess morphological changes during cell growth and division, I followed the single and double mutants of evolvability and resistance genes in the absence and presence of cefotaxime using live microscopy. First, I will discuss observed phenotypes in the absence of cefotaxime.

For the *marR* KO, I identified several examples of lysis, plasmolysis followed by lysis, OMV release, and OM blebbing, mostly at midcell. For both the *marR* double mutants with *dpaA* and *ivy*, I observed multiple examples of plasmolysis, plasmolysis followed by lysis, and a large plasmolysis distance. In addition, the *dpaA marR* double mutant showed several cases of filamentation, while the *ivy marR* double mutant showed several cases of round cells unable to grow and divide. As for the *dpaA* and *ivy* single mutants in the presence of cefotaxime, this points towards inhibited cell division in the *dpaA* KO and overactive cell division or inhibited cell elongation in the *ivy* KO. The same observation was revealed in the double mutants of *ompR* with *dpaA* and *ivy*. The *dpaA ompR* double mutants showed frequent and strong filamentation, while the *ivy ompR* double mutants showed some filamentation and increased cell width. Both phenotypes often coincided with lysis.

Finally, I observed live growth and cell division in the presence of cefotaxime. Cefotaxime inhibits the divisome and, therefore, induces filamentation. This was confirmed by a strong filamentation phenotype, often resulting in lysis in the wildtype, *dpaA*, and *ivy* KO mutants. Interestingly, while the *dpaA marR* double KO mutant showed a high frequency and strong phenotype of filamentation in the presence of cefotaxime, the *ivy marR* double KO mutant showed little filamentation, mirroring the results without cefotaxime. Both the *dpaA ompR* and the *ivy ompR* double mutants showed more filamentation and large cell width, indicating increased cefotaxime sensitivity of the *ompR* KO in the absence of the evolvability genes. This increased sensitivity of the *ompR* KO explains the identified gene-gene-drug interaction and supports the constraining effects evolvability genes have *dpaA* and *ivy* have on cefotaxime resistance evolution.

Live growth of all single and double mutants in the absence and presence of cefotaxime suggest that *dpaA* KO mutants are very susceptible to decreased cell division, often leading to filamentation, which can be revealed in the double mutants of *dpaA* with either *marR* or *ompR*

in the absence of cefotaxime. Adding cefotaxime, a cell division inhibitor itself, further exacerbates the inhibition of cell division and the resulting filamentation phenotype in both the *dpaA marR* and the *dpaA ompR* double mutants. Interestingly, the opposite effect can be observed for the *ivy* KO mutant. Even though the *ivy* single KO mutants show filamentation in the presence of cefotaxime, in *ivy marR* double mutants, it seems to be counteracting the inhibition of cell division and rarely shows filamentation, but rather an increased cell width and decreased cell length. This increase in cell width instead of cell length and the absence of filamentation in *ivy* double mutants is observed in the absence and even in the presence of cefotaxime, which causes filamentation.

Next, I next used MS-based proteomics of the single and double mutants to investigate the molecular characteristics of the interactions I identified between resistance and evolvability genes. First, the experiment confirmed several expected changes, such as that OmpC and OmpF protein levels were increased in the *ompR* KO, and MarA was increased in the *marR* KO mutant, leading to increased AcrAB-TolC and decreased OmpF abundance. In addition, MarA protein abundance was also increased in both the *dpaA* and *ompR* single KOs and further increased in the *ompR dpaA* double KO. An unexpected finding was that DpaA abundance was as low in the *ivy* KO mutant as in the *dpaA* KO mutant, explaining the high concordance between both phenotypes.

Besides the expected changes in protein abundance, I also identified several unexpected changes in protein abundance in *marR* KO mutants, affecting its LPS biosynthesis and transport. The protein abundance of the two essential proteins, LptA and LptC, parts of the LPS transport machinery transporting LPS from the inner to the outer membrane, was decreased. In addition, I found that three LPS biosynthesis proteins showed increased abundance, namely the essential and rate-limiting protein LpxC, and the non-essential proteins LpxL and LpxT. This was interesting since many genes decreasing or increasing cefotaxime evolvability were involved in LPS biosynthesis or transport.

Furthermore, one sequenced *marR* mutant evolved a *waaQ* deletion on top, which decreased LPS biosynthesis levels and increased cefotaxime resistance in that mutant. To test whether the reduction in LPS biosynthesis also affects the gene-gene interaction with *dpaA* and *ivy*, I quantified epistasis using the same CRISPRi plasmid directly in the evolved mutant. I

discovered that the gene-gene interaction with *dpaA* was indeed reversed while the gene-gene interaction with *ivy* was still present.

Following the same principle, I measured the gene-gene interaction between *dpaA* and *marR* in the absence of 17 genes I deleted on top of *marR*. I selected genes based on positive evolvability at 1.5x MIC scores, indicating positive epistasis and functional connections to either *dpaA* or *marR*. Out of 17 gene KOs tested, nine were able to decrease or prevent the gene-gene interaction between *dpaA* and *ivy*, while three KO mutants increased the strength of the interaction. While *acrA*, *acrB*, and *tolC* deletions increased the strength of the gene-gene interaction, *ldtA*, *lpxT*, *mepK*, *mepS*, *mlaC*, *mltC*, *mltF*, *ompF*, and *wecA* decreased the strength of the interaction or prevented it entirely.

Next, I wanted to investigate whether I could use the genetic vulnerabilities I identified to delay cefotaxime resistance evolution using small molecules. Those small molecules I selected based on functional association with evolvability genes or identified susceptibilities of the *marR* mutants. I tested 8 drugs with 2-3 concentrations per drug, at which they did not inhibit growth in the presence of 0.5x MIC cefotaxime to exclude inhibited evolution due to synergistic drug effects inhibiting growth. Several of the tested drugs were able to delay cefotaxime resistance evolution in a dose-dependent manner at non-inhibiting concentrations, with cefsulodin, mecillinam, polymyxin B, sulfamethizole, and trimethoprim showing the strongest effects.

Last, I wanted to test whether the evolvability genes I identified also delayed resistance evolution against antibiotics of the same, similar, or distinct classes. I selected 9 antibiotics and evolved them against 12 antibiotics (excluding cefotaxime) and found that some evolvability genes are cefotaxime specific, while others are drug class specific or general evolvability genes among the antibiotics I tested. The number of shared evolvability genes was the highest for cefuroxime, piperacillin, mecillinam, and aztreonam.

2.2. Mechanistic insights into epistatic gene-gene and gene-gene-drug interactions

Evolving cefotaxime resistance under the conditions I used required an early single-step high-rate low-benefit LOF mutation of either *marR*, providing resistance by increasing drug efflux and decreasing uptake, or *ompR*, providing higher resistance levels by decreasing drug uptake. Acquiring those mutations has a high probability, which is why most KO mutants grew up to

1.5x MIC in low volumes under high-throughput conditions and up to 4.5x MIC in larger volumes under the validation conditions.

Since both the *dpaA* KO and the *ivy* KO display lower evolvability, they must interact with both *marR* and *ompR* through gene-gene or gene-gene-drug interactions. Blocking just one of the two resistance trajectories with similar probability would still allow growth or even favor growth with the alternative variant, not resulting in decreased evolvability. This hypothesis was confirmed by directly measuring a gene-gene interaction between the resistance gene *marR* and *waaQ*, and a gene-gene-drug interaction between the resistance gene *ompR* with both evolvability genes *dpaA* and *ivy*.

To characterize these interactions phenotypically, I characterized single and double mutants of resistance and evolvability genes in the absence and presence of cefotaxime using imaging to track growth and cell division. Findings point towards susceptibility of the genetic network of the *dpaA* KO mutant against inhibition of cell division and filamentation mediated by cefotaxime treatment, for example, by a vulnerable or inhibited divisome. Therefore, *dpaA* KO susceptible to cell division inhibition may synergize with cefotaxime inhibiting cell division, which is only revealed when *marR* or *ompR* are deleted on top. In contrast, microscopy data points towards resistance of the genetic network of the *ivy* deletion mutants against inhibition of cell division and filamentation mediated by cefotaxime treatment when *marR* is deleted on top, for example, by an overactive divisome or inhibited elongasome. Therefore, the *ivy* mutant seems to antagonize with the inhibition of cell division and the resulting filamentation caused by cefotaxime, which is only revealed when *marR* is deleted on top.

Next, I characterized the proteome of the different single and double KO mutants. Besides confirming that all mutants are correct and resistance is indeed provided by upregulating efflux pumps or downregulating porins, proteomics revealed that the *ivy* KO phenocopies the *dpaA* KO by showing equally low *dpaA* levels. A possible explanation is that since Ivy is a periplasmic chaperone folding proteins under stress of the cell envelope, it could also fold DpaA. In the absence of *ivy*, DpaA can not be folded correctly and is degraded as a result. Furthermore, proteomics revealed decreased LPS transport from the IM to the OM and increased LPS biosynthesis in the *marR* KO mutants, potentially revealing a susceptibility that explains the negative and positive epistasis modulating resistance evolvability.

A decreased abundance of LptA/LptC, as I identified in the *marR* KO mutant, can lead to the toxic accumulation of LPS in the inner membrane (Shu & Mi 2022; Guest et al. 2020; Nguyen et al. 2020; Klein et al. 2014) and depletion of LPS in the outer leaflet of the outer membrane, which can perturb the OM barrier function and result in OM permeability (Sperandeo et al. 2006; Sperandeo et al. 2011). The increased OM permeability leading to sensitivity against SDS, bile salts, cholate, deoxycholate, and vancomycin can be observed in the *marR* KO mutant in available chemical genetics data (Nichols et al. 2011). This finding is counterintuitive, given that the major effect associated with the *marR* KO is an upregulation of the AcrAB-TolC efflux pump that pumps out the compounds. Since deletions of *acrA*, *acrB*, and *tolC* increase sensitivity towards SDS, bile salts, cholate, and deoxycholate, their upregulation in the *marR* KO should render it resistant against those compounds. The fact that the *marR* KO is still more sensitive points towards a disruption of the OM barrier function, leading to an influx that overshadows the increased efflux.

The second effect of perturbed LPS transport from the IM to the OM is the potential accumulation of LPS in the IM. Accumulating LPS in the IM activates a negative feedback loop mediated by LapC to decrease LPS biosynthesis by triggering degradation of the rate-limiting protein LpxC *via* the LapB-FtsH complex (Shu & Mi 2022; Guest et al. 2021; Klein et al. 2014; Guest et al. 2020). However, my proteomics findings that the protein abundance of LptA/LptC is depleted and LpxC/LpxL/LpxT is increased are inconsistent with this reported negative feedback loop.

This indicates that the *marR* somehow deregulates LPS biosynthesis by interrupting the negative feedback loop. Since the protein abundance of LapB is ~40 % increased compared to the wildtype, LPS accumulation at the IM is correctly sensed in the *marR* KO mutant. Therefore, the deregulation of LPS biosynthesis must happen differently. Indeed, MarA was described in the literature to directly stabilize LpxC against LapB-FtsH-mediated proteolysis in a Mla pathway-dependent way by testing a *lapC* LOF mutants with elevated LapB-FtsH activity (Maniyeri et al. 2023). This provides a possible explanation for why KO mutants of the Mla system increased cefotaxime evolvability, potentially by interrupting the toxic stabilization of LpxC in *marR* KO mutants. Another KO mutant with an increased evolvability score at both 1.5x MIC and 13.5x MIC was the *lapB* KO mutant known to carry a suppressor mutation in LpxC, reducing its LPS biosynthesis (Mahalakshmi et al. 2014). Lastly, the fact

that one *marR* KO mutant evolved an additional *waaQ* deletion that increased its resistance levels supports the hypothesis of toxic overproduction of LPS in the *marR* KO.

Mutants showing a toxic overproduction of LPS were reported to release excess LPS by OM vesicles and OM blebs at midcell, which I also observed for the *marR* KO mutant using live microscopy. Suppressor mutations of such phenotypes either directly reduced LPS biosynthesis, *e.g.*, by *lpxC* mutations, or by increasing the release of excess LPS *via* OM vesicles and OM blebs by decreasing the amount of PG-Lpp crosslinks (Sutterlin et al. 2016; Guest et al. 2020; Nguyen et al. 2020). Since DpaA cleaves such crosslinks and the *dpaA* KO has an increased abundance of such crosslinks (Bahadur et al. 2021; Matthias et al. 2021), it is possible that it prevents the shedding of excess LPS in the *marR* KO mutant and thereby exacerbates the toxic accumulation of LPS. In line with this hypothesis, I did not observe any OMVs and OM blebs in the *marR dpaA* double KO using live microscopy. Another experiment supporting this hypothesis is that in the evolved *marR* KO mutant with the *waaQ* deletion and decreased LPS biosynthesis, the gene-gene interaction with *dpaA* was reverted. Interestingly, despite the high concordance of the *dpaA* and *ivy* phenotypes across genetic tests and the absence of the DpaA protein in the *ivy* KO mutant, the *marR* KO mutant with the *waaQ* deletion did not revert the gene-gene interaction with *ivy*, indicating that it is based on a different mechanism or is influenced by additional factors. Also, the microscopy data indicates different effects of the evolvability genes *dpaA* and *ivy* on the resistance genes *marR* and *ompR*.

To further investigate genetic dependencies of the gene-gene interaction between *marR* and *dpaA*, I probed it in the absence of 17 other genes related to the proposed mechanism. Ways to disrupt the gene-gene interaction between *dpaA* and *marR* included deletions of a) *ldtA* that anchors Lpp to PG, suggesting a decreased amount of Lpp-PG crosslinks in the KO, b) *lpxT* involved in LPS biosynthesis with decreased LPS production in the KO and c) *mlaC* that stabilizes LpxC against degradation in *marR* KO mutants, suggesting that the deletion likely leads to decreased LpxC levels and decreased LPS production. Other gene deletions reverting the interaction were *mepK* and *mepS*. MepK also showed higher protein abundance in the *marR* KO, and both are endopeptidases that contribute to murein incorporation and PG remodeling. One possible explanation is that by their cleavage, they create available *m*-DAP[3] that can be used to crosslink the PG to Lpp in the OM. Therefore, they could indirectly reduce the number of PG-Lpp crosslinks. The *wecA* deletion also reverted the gene-gene interaction. Genes of the *wec* pathway were reported to restore disrupted OM barrier function and vancomycin resistance

in mutants with perturbed reduced OM barrier function by accumulating ECA intermediates (Jiang et al. 2020).

The two LTs, *mltC* and *mltF*, also decreased the gene-gene interaction, with *mltF* having a stronger effect than *mltC*. Both gene KOs show increased evolvability, indicating that their PG cleavage is detrimental during resistance evolution and contributes to the gene-gene interaction between *marR* and *dpaA*. KOs of the three genes that are part of the AcrAB-TolC efflux pump increased the strength of the interaction. However, this effect is possibly caused by reduced efflux of the CRISPRi inducer aTc, which would result in stronger transcriptional repression of *dpaA* in these strains. The opposite could be the case for the *ompF* KO, which allows reduced aTc entry and thereby prevents the transcriptional repression of *dpaA*.

Based on the evidence I described, acquiring a *marR* mutation rewires the genetic network and can result in several vulnerabilities, such as the toxic overproduction of LPS, PG-Lpp crosslinks, LT activity and an increased OM permeability. In the next step, I harnessed these vulnerabilities by targeting them with antibiotics to delay cefotaxime resistance evolution. Adding several antibiotics at sub-inhibitory concentrations delayed cefotaxime resistance evolution. The strongest effects were exerted by cefsulodin, mecillinam, polymyxin B, sulfamethizole, trimethoprim, and vancomycin. Cefsulodin, mecillinam, and vancomycin target PG biosynthesis, polymyxin B targets LPS, while trimethoprim and sulfamethizole target folate biosynthesis.

Since the OM barrier function prevents vancomycin entry and is possibly perturbed in *marR* KO mutants, lineages evolving *marR* mutations could display an increased influx of vancomycin and their evolutionary trajectory ends. This is supported by the increased sensitivity of the *marR* KO against vancomycin in available chemical genetics data (Nichols et al. 2011). Since I suspect an LPS imbalance in *marR* KO mutants and polymyxin B targets LPS, the evolutionary delay could be caused by a synergy of polymyxin B with the already perturbed LPS localization in *marR* KO mutants. Mecillinam and cefsulodin target PG biosynthesis and delay cefotaxime resistance evolution, possibly by targeting genetic vulnerabilities in cell wall remodeling that arise in *marR*- or *ompR*-resistant mutants. Mecillinam targets PBP2 as part of the elongasome, and both *marR* and *ompR* mutants showed an increase in cell length and width after mecillinam exposure quantified by microscopy. Cefsulodin targets PBP1b, 7, and 8 instead. While PBP1b is synthetically lethal with PBP3

targeted by cefotaxime (García del Portillo & de Pedro 1990), PBP7, also called *pbpG*, is a *bona fide* evolvability gene, whose inhibition by cefsulodin could explain the decreased evolvability again cefotaxime.

Trimethoprim and sulfamethizole target different branches of folate biosynthesis, namely FolA and FolP, respectively. The stronger inhibition of evolution by sulfamethizole than trimethoprim could be caused by the fact that glycerine cleavage mutants *gcvH* and *gcvP* are only sensitive to sulfonamides, not trimethoprim, and *bona fide* hits with decreased evolvability against cefotaxime. Even though the molecular mechanism of how those compounds inhibit cefotaxime resistance evolution was not confirmed, the approach represents a proof-of-concept that evolution inhibitors can be identified from genome-wide resistance evolution data by targeting the uncovered genetic vulnerabilities. Thereby, they cement a path towards effective evolution inhibitors able to delay or revert antibiotic resistance.

Lastly, I investigated how generalizable the identified evolvability genes were by evolving them against diverse antibiotics from the same, similar, or distinct antibiotic subclasses and classes. While some evolvability genes were specific for cefotaxime, others delayed evolution based on the target or resistance mechanism of the antibiotic. One sensible signature identified is that resistance evolution of antibiotics that evolve *marR* resistance mutations such as cefotaxime, cefuroxime, and tetracycline are delayed by *dpaA* and *ivy* that show negative epistasis with *marR*. A final set of evolvability genes delayed evolution against a set of antibiotics that did not share any apparent features and, therefore, represented general evolvability genes under the used conditions. Such general evolvability factors most likely interact with general resistance mechanisms such as porins preventing drug influx. This hypothesis is supported by the finding that multiple general evolvability genes were involved in the metabolism, potentially exacerbating the nutrient limitation in strains with decreased nutrient availability due to decreased porins abundance.

In conclusion, I used various method including quantitative genetics, genomics, high-throughput imaging and proteomics to characterize the mechanisms behind epistatic interactions delaying resistance evolution. Despite the diverse set of experiments, there are still many open questions, mainly caused by the pleiotropic effects of resistance regulators such as *marR* and *ompR* targeting many different sets of genes involved in diverse processes.

For the *marR* KO mutant, I uncovered decreased LPS transport from IM to OM coupled with deregulated and increased LPS biosynthesis by proteomics. This potentially manifests as perturbed OM barrier function due to LPS depletion, supported by an independent chemical genetics dataset (Nichols et al. 2011). The observation that OM barrier function is perturbed during cefotaxime resistance evolution is supported by the finding that KO mutants of the *wec* pathway, known to restore OM barrier function and vancomycin sensitivity by accumulating ECA intermediates (Jiang et al. 2020), were enriched among gene KOs with increased evolvability. A second phenotype observed in the *marR* KO is the shedding of excess LPS, possibly accumulating in the IM, *via* OMVs and OM blebs, supported by live microscopy data. Additional evidence for a toxic accumulation of LPS during cefotaxime resistance evolution is provided by the increased evolvability of several LPS biosynthesis KO mutants, with the *lapB* KO carrying an *lpxC* mutation representing the strongest example. In addition, genetic evidence identified a direct role of MarA in stabilizing LpxC against degradation in a Mla dependent way (Maniyeri et al. 2023), which provides a possible explanation for the deregulated levels of LpxC, as well as the enrichment of *mla* gene KOs among genes with increased evolvability. Furthermore, a *marR* KO evolved a *waaQ* deletion, reducing its LPS biosynthesis, which further increased its resistance levels and reduced the gene-gene interaction with *dpaA* but not with *ivy*.

Shedding of excess LPS *via* OMVs and OM blebs is dependent on the abundance of PG-Lpp crosslinks, and mutations decreasing the amount of crosslinks increase this phenotype (Sutterlin et al. 2016; Guest et al. 2020; Nguyen et al. 2020). Since the *dpaA* KO mutant was reported to increase the abundance of PG-Lpp crosslinks (Bahadur et al. 2021; Matthias et al. 2021), it could prevent the formation of OMVs and OM blebs and exacerbate LPS accumulation. This hypothesis is supported by the absence of OMVs and OM blebs in *marR dpaA* mutants from the live microscopy experiment, as well as reversion of the gene-gene interaction between *marR dpaA* mutant in KO mutants that decrease the amount of PG-Lpp crosslinks or decrease LPS biosynthesis. However, there is no definitive proof that the negative epistasis between *dpaA* and *marR* is caused by or only correlated with LPS levels and PG-Lpp crosslinks.

For the gene-gene interaction between *marR* and *ivy*, the same interaction should occur as between *marR* and *dpaA*, given that the *ivy* KO phenocopies a *dpaA* KO. However, the fact that the evolved *marR waaQ* mutant reverted the gene-gene interaction only with *dpaA* and not

with *ivy* indicates that the *ivy* KO has additional components contributing to the interaction. One possible explanation could be *ivy*'s pleiotropic effects as a chaperone folding diverse periplasmic proteins under membrane stress, and by its secondary function as an inhibitor of LTs (Lennon et al. 2015; Clarke et al. 2010). The result that KOs of the two LTs *mltC* and *mltF* disrupted the gene-gene interaction between *dpaA* and *marR*, that both KOs also showed increased evolvability, as well as the fact that LTs are more active in the KO of the LT inhibitor *ivy*, points towards a role of LTs in the interaction between *marR* and *ivy.* This interaction of overactive LTs could act on top of the *dpaA marR* interaction also present in the *ivy marR* KO and is supported by live microscopy data where *ivy marR* mutants displayed a round morphology, increased cell width, and no filamentation even in the presence of cefotaxime that inhibits the divisome and causes filamentation in most genotypes. The same observation of round cells without filamentation in the presence of cefotaxime was also made for the *ivy ompR* mutant. It could explain why the *ompR* mutant only showed a gene-gene interaction with *ivy* but not *dpaA*.

Generally, the gene-gene-drug interactions between the evolvability genes *dpaA* and *ivy* with the resistance regulator *ompR* are even more challenging to decipher, given their tripartite nature. One possible explanation is that MarA protein abundance is also decreased in *dpaA* and *ompR* single, as well as the *dpaA ompR* double KO. Adding cefotaxime liberates membrane-bound copper and further activates MarA (Hao et al. 2014; Hiniker et al. 2005), which could result in the same gene-gene interactions observed between *dpaA*/*ivy* and *marR*. However, more experiments are needed to explain the identified gene-gene-drug interactions.

Another exciting line of research would be whether the gene-gene-drug interactions are drug-dependent and whether other antibiotics could replace cefotaxime. One angle to answer this question is by evolving cefotaxime evolvability genes against different antibiotics from the same, similar, or distinct classes targeting the same, similar, or distinct processes. While some evolvability genes were drug-dependent, others were more pleiotropic in their constraining impact on antibiotic resistance evolution. While gene-gene interactions between evolvability and resistance genes only depend on the resistance mechanism, gene-gene-drug interactions are more likely to depend on the target or structure of the antibiotics. The fact that multiple evolvability genes with functions involved in the metabolism and oxidation-reduction delayed resistance evolution against antibiotics with diverse structures targeting different processes suggests that those genes interact with multi-drug resistance elements, *e.g.*, by exacerbating the

nutrient limitation in porin-depleted strains or the high energy consumption in strains with high efflux pumps activity. Both represent primising targets for broad-spectrum resistance evolution inhibitors.

In summary, characterizing the genomic landscape of the multi-drug resistance regulators *marR* and *ompR* not only elevates our understanding of cefotaxime resistance evolution but can be transferred to many antibiotics from various classes against resistance evolves through those genes. This is supported by the finding that multiple evolvability genes not only delay resistance evolution against cefotaxime but also against other antibiotics from the same or different classes targeting the same, similar, or distinct cellular processes. Finally, this also applies to the resistance evolution inhibitors I identified using the uncovered genetic vulnerabilities arising during resistance evolution. Since cefotaxime resistance evolution mainly selects for *marR* and *ompR* under the used conditions, the identified evolution inhibitors selecting against those resistance elements should be equally able to delay the resistance evolution of other antibiotics that evolve antibiotic resistance through the same genes *marR* and *ompR*.

2.3. Shortcomings and potential pitfalls

When investigating the molecular mechanism behind the identified gene-gene and gene-gen-drug interactions, there were several potential shortcomings and compromises. At many steps throughout the mechanistic investigation, decisions had to be taken to follow up on specific subsets of the identified hits. Based on 248 identified and 27 validated evolvability genes, I decided to test *dpaA* and *ivy* for their interactions with the most common resistance genes, *marR* and *ompR*. These are not representative of all evolvability genes I identified but should be viewed as examples of how evolvability genes can be identified and how their interactions with resistance genes can be deciphered using different methods. Fortunately, the evolvability genes *dpaA* and *ivy* showed both types of interactions with resistance elements, which I predicted to be possible. However, these findings may or may not generalize to the other evolvability genes I identified.

The first potential shortcoming is that *dpaA* or *ivy* might delay cefotaxime resistance evolution by decreasing fitness or increasing antibiotic sensitivity instead of decreasing evolvability. If

so, the effect is negligible given the test of *dpaA* and *ivy* KDs in a wildtype background at different cefotaxime concentrations.

One limitation of the quantitative CRISPRi experiments to measure gene-gene-drug interactions is that the fitness of the wildtype in the presence of 1x MIC of cefotaxime is 0. Therefore, the Bliss score is out of its dynamic range and represents the decrease in resistance levels upon gene KD. Nevertheless, this quantifies what can be defined as a gene-gene-drug interaction, but the CRISPRi effect might be overestimated because the wildtype KD contribution is not considered. However, this contribution should be negligible compared to the 40 and 52 % reduction in absolute fitness in the presence of the drug. Furthermore, increased sensitivity of the *ompR* KO in combination with the *dpaA* and *ivy* was evident in the live microscopy data in the presence of cefotaxime, confirming the gene-gene-drug interaction.

Another potential pitfall could be to overinterpret the qualitative live microscopy data I acquired concerning counting and comparing the occurrence and severity of mutant- or drug-induced phenotypes such as plasmolysis, lysis, filamentation, OMVs, or OM blebs. On the one hand, the microscopy data was used here in a purely qualitative manner, meaning a quantitative comparison such as the phenotype of mutant X is stronger or occurs with higher frequency than in mutant Y lacks a statistical foundation and is unjustified without proper quantification of such phenomena. On the other hand, looking at hundreds of single cells and comparing the severity and frequency of phenotypes does allow a semi-quantitative characterization of the most extreme phenotypes. Even though it is possible that a wildtype might show strong filamentation, plasmolysis, lysis, and OM blebs in the absence of any chemical or genetic perturbation, it was not observed once among 100s of single cells, so it is highly unlikely given the used conditions. Therefore, I think all comparisons are justified in this study. However, their status as qualitative measures should be acknowledged when interpreting the data, and future studies will need to implement more sophisticated quantification to back the hypotheses with statistical tests.

One shortcoming arises from quantifying gene-gene-gene interactions between *marR* and *dpaA* and the absence of several other genes. I compared the classical Bliss score quantification (Bliss 1939; Brochado et al. 2018) with different approaches able to quantify higher-order interactions (Russ & Kishony 2018; Tekin et al. 2018), but in the end decided to use the classical Bliss score change between the presence and absence of inducer. The reason is that, ultimately, I am

interested in how the gene-gene interaction between *dpaA* and *marR* changes based on the genetic background. By using the standard Bliss score, I might neglect contributions the additional KO might have on *dpaA* or on *marR*. However, in practice, accounting for all single and dual interactions to predict the triple gene-gene-gene interaction led to a multiplicative accumulation of multiple noise measurements and resulted in all scores being highly positive. Furthermore, even though many of the gene KOs that were tested for their effect on the gene-gene interaction between *marR* and *dpaA* were selected based on their positive evolvability score and, therefore, supposedly positive epistasis with *marR*, this does not necessarily mean that the null hypothesis is that they revert the gene-gene interaction between *marR* and *dpaA*. For example, a KO that shows positive epistasis with *marR* by overcoming transcriptional inhibition will still not mitigate the effect of a translation inhibitor.

Regarding the small molecules able to delay cefotaxime resistance evolution, it has to be acknowledged that at this moment, there is no evidence to show that the compounds delay resistance evolution based on the reasons I selected them for or any other reason. These molecules must be tested rigorously before moving them forward as evolution inhibitors. However, the experiment still represents a proof of concept that novel evolution inhibitors can be identified based on the catalog of evolvability genes and genetic vulnerabilities of resistance genes I described here. Also, for the evolvability genes delaying resistance evolution against antibiotics targeting the same, similar, or distinct processes, I identified different degrees of pleiotropy of evolution inhibitors among my small sample set, but the molecular mechanisms of those interactions must be further characterized.

Lastly, regarding the molecular mechanism I describe for the gene-gene interaction between *marR* and *dpaA,* with some limitations also for *marR* and *ivy*, several shortcomings have to be considered. Besides the proteomic data that LPS transport is reduced and LPS biosynthesis is increased, I only have indirect evidence based on qualitative observations of OMVs and OM blebs using live microscopy, increased sensitivity to bile salts and SDS in available chemical genetics data, and the finding that LPS biosynthesis reducing deletions and deletions in the Mla pathway increase resistance evolvability. None of them provides definitive proof that LPS is accumulating in the inner membrane or depleted in the OM. Another question is, even if LPS accumulates in the IM, how would it be shed *via* OMVs and OM blebs through the OM? One possible explanation could be hemifusion, *i.e.*, direct contact between IM and OM, which was described before to allow direct exchange of PL between IM and OM in mutants with increased

LPS biosynthesis (Sutterlin et al. 2016). Another experiment to clarify this interaction would be isolating and characterizing OMVs for their LPS content in *marR* and *marR dpaA* KO mutants by western blot (Guest et al. 2020; Nguyen et al. 2020). However, this would not answer whether the amount of OMVs and OM blebs is decreased in the *marR dpaA* KO versus the *marR* KO. The question of the LPS localization across IM and OM and LPS accumulation could be answered by performing a western blot for the LPS content of the IM and OM fractions across different mutants.

2.4. Conclusion and outlook

In conclusion, I used a various approaches to characterize genetic vulnerabilities arising during antibiotic resistance evolution of the multi-drug resistance regulators *marR* and *ompR* in the presence of cefotaxime. As multi-drug resistance regulators, targeting these genes with epistatic gene-gene or gene-gene-drug interactions provides an angle to delay antibiotic resistance evolution, potentially against all antibiotics against which they provide resistance. First, I identified evolvability genes that present targets to delay antibiotic resistance by phenotypic screening. In the next step, I characterized how these evolvability genes interact with resistance genes by gene-gene and gene-gene-drug interactions. Even though the identified evolvability genes represent targets to delay antibiotic resistance evolution potentially against diverse antibiotics, for many of them, chemicals inhibiting the proteins encoded by these genes might not exist. Hence, I used the insights into genetic vulnerabilities of resistance genes and how they can be exploited genetically to find and validate several chemical evolution inhibitors of cefotaxime.

I found various evolvability genes from processes such as cell wall remodeling, amino acid biosynthesis, oxidation-reduction, and carbon metabolism required for cefotaxime resistance evolution. Investigating the gene-gene interaction between the evolvability genes *dpaA* and the resistance gene *marR* revealed that the increased number of PG-Lpp crosslinks in the *dpaA* KO possibly exacerbates the toxic deregulation of LPS transport and biosynthesis in *marR* mutants by preventing the shedding of excess LPS *via* compensatory OMVs and OM blebs. Inhibiting DpaA with copper could be one way to translate this uncovered SL of the *marR* KO with too many PG-Lpp linkages into an evolution inhibitor (Peters et al. 2018). Alternatively, the depletion of LPS in the OM leads to an increased OM permeability in *marR* mutants, which results in increased susceptibility against compounds whose diffusion through the OM is

usually prevented by LPS, such as SDS, bile acids, and vancomycin. Applying those insights to delay resistance evolution revealed that vancomycin can delay cefotaxime resistance evolution in a dose-dependent manner at sub-inhibitory concentrations. Targeting vulnerabilities of resistance elements should not only be a way to delay resistance evolution but also to target resistant subpopulations and resensitize populations.

This approach of characterizing genetic vulnerabilities of resistance genes and targeting them with antibiotics to delay resistance evolution represents the essence of this project. However, since the first step of identifying genetic vulnerabilities of resistance evolution by experimental evolution of a genome-wide KO library is very time and resource-intensive, I developed an orthogonal approach to identify such genetic vulnerabilities that can be scaled to multiple antibiotic resistance genes or targets in Chapter III.

3. Global epistasis of antibiotic targets and resistance elements

3.1. Brief recap of results

In Chapter III, I developed a novel method to quantify the global epistasis of essential genes by measuring epistatic interactions with all non-essential gene KOs. This method is based on conjugating the CRISPRi plasmid I constructed in Chapter II into the genome-wide KO library of *E. coli* using high-throughput conjugation on plates. Knocking down an essential gene in all non-essential KO backgrounds allows me to quantify global epistasis and the degree of essentiality of the essential gene across all non-essential gene deletion backgrounds by measuring colony size and opacity in high-density colony arrays.

First, I cloned guide RNAs targeting several antibiotic resistance genes and targets into the CRISPRi plasmid and quantified the reduction in CFUs using a spot assay based on a 10-fold dilution series. As expected, the CRISPRi KD of the essential genes coding for the ribosome (RplI, RplA, RpsA), RNA polymerase (RpoB), DNA gyrase (GyrA) and DNA topoisomerase IV (ParC), as well as KDs of the two non-essential genes encoding a global chaperone (*dnaK*) and the ATP synthase F_1 (AtpA) reduced CFUs, colony opacity or both. I also assessed the specificity of the CRISPRi-mediated transcriptional repression and confirmed target-specific depletion on the protein level using MS-based proteomics performed by Dr. Andre Mateus. Other proteins with decreased abundance are encoded by genes on the same operon as the target

gene, which are also silenced due to the polar effects of CRISPRi silencing the whole operon (Peters et al. 2016; Peters et al. 2015).

For the next step, I selected the *parC* plasmid, since the KD decreased CFUs and *parC* represents both an antibiotic resistance gene and target of ciprofloxacin, conjugated it into one KEIO plate (1536-format) and measured colony size at different inducer levels. The colony size measurement revealed a concentration-dependent decrease in colony size upon transcriptional repression of *parC* without an increase in CRISPRi toxicity when using a scrambled guide RNA. The reduction in colony size at the highest inducer concentration represents an optimal reduction to detect both positive and negative epistasis.

Next, I conjugated the CRISPRi-plasmid knocking down *parC* into the complete genome-wide KO library to measure the global epistasis of *parC*. The replicate Pearson correlation across biological and technical replicates was between 0.8 and 0.9, and the colony size was reduced by 30 to 40 % in all plates. Epistasis with *parC* was quantified by a stronger or weaker reduction in opacity relative to the average opacity reduction upon *parC* KD. Gene KO with negative epistasis, *i.e.*, larger than average reduction in opacity, were enriched for the GO term DNA binding as expected for the transcriptional repression of *parC* encoding a DNA topoisomerase IV subunit. Among hits with negative epistasis, I found a subunit of the DNA topoisomerase IV (*parE)*, ATP-dependent DNA helicase (*recG)*, DNA helicase IV (*helD*), RNA polymerase (*rpoZ),* DNA polymerase (*umuD*) and flap endonuclease (*ygdG*/ExoIX). Furthermore, the results aligned with a previous study that identified non-essential gene KOs exhibiting negative epistasis with ParC by their negative effect on the thermal stability of ParC (Mateus et al. 2020). The *phoP* KO reduced ParC thermal stability and showed negative epistasis measured by spot assay in the previous study (Mateus et al. 2020), and its negative epistasis was recapitulated using the global approach I described here.

3.2. A novel method to measure global epistasis of essential genes

The method described here allows me to measure quantitative interactions of any gene with all non-essential genes in *E. coli*. However, the information acquired will be limited by the dynamic range of the colony size and opacity reduction, which depends on the essentiality of the targeted gene, the guide RNA and the inducer concentration used, and the duration of growth before measuring colony sizes and opacity. As discussed in Chapter IV, opacity has a

higher dynamic range and, therefore, better represents 3D growth on high-density colony arrays and should, therefore, be used for all quantifications (Kritikos et al. 2017). To improve understandability, I will still use 'colony size' to describe considerations when designing the assay, but they equally apply to opacity measurements. Performing the assay at conditions that lead to no colony size reduction upon KD maximizes the dynamic range to detect negative epistasis, *i.e.*, larger than average reduction in colony size, while minimizing the dynamics range to detect positive epistasis, *i.e.*, smaller than average reduction in colony size. Performing the assay at conditions that lead to 80 % colony size reduction reverses these trends and can only identify positive but not negative epistasis.

To measure global epistasis, an average colony size reduction of 30-40 %, as shown in the *parC* KD, represents optimal conditions to identify both negative and positive epistasis. Another important consideration is that the dynamic range to measure changes in colony size decreases in small colonies, so total colony sizes in the assay should range from around 40 to 100 %. Therefore, the average colony size reduction by *parC* KD to around 60 to 70 % represents an optimal dynamic range to detect both negative and positive epistasis. Besides the condition-dependent essentiality of the targeted gene, inducer concentrations and the guide RNA can be modified to achieve an optimal average colony size reduction. Recent approaches such as mismatch CRISPRi (Hawkins et al. 2020) allow transcriptional repression to be titrated by introducing mismatches into the guide RNA. Another option to modify this assay is to perform it in different growth media or the presence of an antibiotic, thereby extending its use case from measuring gene-gene to measuring gene-gene-drug interactions. This would allow the knocking down of non-essential genes without colony size reduction since the dynamic range colony size could be titrated using the antibiotic. The method can then quantify resistance levels provided by endogenous or exogenous resistance elements in the presence of the antibiotic across every non-essential gene KO background.

This method reveals the entirety of positive and negative interactions with all non-essential genes, which can be described as its global epistasis. Applied to an antibiotic resistance gene, negative epistasis interaction partners represent targets to delay or revert resistance evolution. In contrast, positive interaction partners can be used to compensate for the essential resistance gene KD and accelerate evolution. Therefore, the epistatic interaction score measured here can be compared to the evolvability score calculated in Chapter II. However, resistance evolution, as performed in Chapter II, integrates both gene-gene and gene-gene-drug interactions of a

non-essential KO with all available resistance trajectories and under competition in the presence of the antibiotic. Only if no available resistance trajectories can grow will the absence of growth be observed. As a result, to fully reproduce this complex phenotype of delayed resistance evolution, it would be necessary to perform the global epistasis method described here with *marR* against all non-essential genes in the absence and presence of cefotaxime and with *ompR* against all non-essential genes in the absence and presence of cefotaxime, followed by integrating all four assays into one final evolvability score. One solution could be to integrate both approaches by first measuring global epistasis with the method presented here for multiple antibiotic resistance genes, followed by assessing the impact of shared genes with negative epistasis on experimental evolution rates in liquid culture. as described in Chapter II.

The method described here can also be used to measure the global epistasis of antibiotic targets. Non-essential gene KOs exhibiting negative epistasis with an antibiotic target represent vulnerabilities in the genetic network during antibiotic treatment that can be used to increase antibiotic effectiveness. Gene KOs showing positive epistasis represent likely suppressor mutations and resistance genes compensating for the genetic or chemical depletion of the essential antibiotic target. Furthermore, epistasis of clinical resistance plasmids carrying ESBLs (Periasamy et al. 2020), and other endogenous or exogenous resistance elements with all non-essential genes can be measured in the absence or presence of an antibiotic.

While global epistasis of clinical resistance elements in the absence of antibiotics assesses the fitness cost of the resistance elements in every non-essential gene KO background, performing the assay in the presence of the corresponding or other antibiotics quantifies the resistance levels provided by the resistance element in every non-essential gene KO background. Identified genes that interact with clinical resistance elements transferred *via* HGT represent targets to slow down or prevent the spread of clinical resistance elements by exacerbating their fitness cost or decreasing their resistance levels. Another assay adaptation would be to multiplex the CRISPRi KD by including multiple gRNAs on the plasmid, as it is already common practice in other areas (McCarty et al. 2020). This would allow to KD not just one but several essential or non-essential genes in all non-essential KO backgrounds. The method presented here could be applied to investigate the genomic landscape of drug-drug interactions by KD of one antibiotic target in the presence of an antibiotic targeting a different protein. In such a case, non-essential gene KOs with negative epitasis represent genes exacerbating the interaction, for example, by causing a synergy. In contrast, genes with positive epistasis

suppress the interaction, for example, by causing an antagonism, thereby allowing the mapping of global epistasis of the drug-drug interaction. Non-essential gene KOs that negatively interact with the KD of an antibiotic target can be compared to non-essential gene KOs that negatively interact with the corresponding antibiotic by using available data of the same KO library probed in the presence of many different antibiotics (Nichols et al. 2011). Lastly, conjugating the CRISPRi plasmid into a pooled barcoded KO or transposon library allows the investigation of global epistasis of the essential KD across tens of essential genes and drug conditions by using barcode sequencing as a readout to quantify fitness and epistasis.

Essentiality is a condition-dependent, quantitative, and evolvable property, and ~9 % of essential gene deletions in yeast can be overcome by adaptive evolution. (Rancati et al. 2018; Liu et al. 2015). An interesting theoretical question arises based on the new method described here and the results it produces. Will knocking down an essential gene in an SL non-essential KO background result in a lower suppressor frequency for the essential gene? By titrating transcriptional repression of essential genes in a genome-wide KO library of non-essential genes, the method described here can identify such SL between an essential KD and non-essential KO backgrounds. Thereby, they increase the essentiality of the essential gene and possibly also the difficulty of overcoming the essential gene KD *via* suppressor mutations.

To measure suppressor frequency, wildtype and SL KO backgrounds carrying the CRISPRi plasmid must be plated on the inducer, and CFUs must be quantified. However, since inactivating the CRISPRi plasmid represents an easy way to overcome the stress on the essential gene, I have to devise a high-throughput method to distinguish suppressors of the CRISPRi plasmid from suppressors carrying chromosomal mutations. I performed the first preliminary tests by conjugating a second CRISPRi plasmid carrying a different resistance marker into suppressor mutants of a CRISPRi KD of an essential gene. By measuring liquid growth across different inducer concentrations, suppressors of the first plasmid showed growth corresponding to single plasmid CRISPRi KD from the second plasmid at different inducer concentrations, while chromosomal suppressors showed dual plasmid KD levels compensated by the chromosomal suppressor mutation. In order to answer whether SL increases essentiality and reduces the amount of suppressor mutations, I will quantify suppressor frequencies of only chromosomal suppressors in the wildtype and several SL KO backgrounds in the future.

Lastly, besides measuring colony size and opacity after 14, 18, and 22 h of growth, it is also possible to measure growth curves of up to 7500 colonies arrayed on 5 1536-plates from the colony size and opacity increase over time using a single conventional scanner placed in an incubator. This would be an interesting addition to the described experimental workflow since colony growth curves give an estimate of lag phase, growth rate, and final yield, thereby allowing the dissection of genetic interactions at an even higher resolution.

3.3. Shortcomings and potential pitfalls

The described method based on high-density colony arrays comes with the usual challenges associated with such plate-based assays (Kritikos et al. 2017; Typas et al. 2008; Nichols et al. 2011). Regarding the pinning of colonies across plates, the transferred cell mass is uneven, which can result in uneven colony sizes despite an identical growth rate. Hence, having biological and technical replicates, and a targeting and non-targeting CRISPRi plasmid with a scrambled guide RNA is essential to estimate the biological and technical noise of the assay. Since the dynamic range of colony size and opacity is limited, the assay settings must be precisely adapted and optimized for each essential gene KD. However, this decrease in resolution is outweighed by the increased throughput and scalability.

The fact that not all gene KOs previously identified to show negative epistasis with *parC* or reported to affect the thermostability of *parC* (Mateus et al. 2020) were confirmed with the presented approach could have several explanations. First, while stabilization or destabilization of proteins as a feature may be correlated with genetic interactions, effects on thermal stability do not always result in genetic interactions and *vice versa*, as was also pointed out in the former study (Mateus et al. 2020). Reasons for the discrepancy between genetic interactions of *parC* in the previous study (Mateus et al. 2020) compared to this study could be either explained by the different CRISPRi systems used or by the difference between measuring genetic interactions by CFU versus colony size. Both represent correlated distinct fitness, viability, and growth proxies.

Whether the identified non-essential gene KO mutants with negative epistasis with resistance genes really represent targets to delay antibiotic resistance evolution as identified by phenotypic screening in Chapters II and III has to be validated first. Many antibiotics target multiple genes, and resistance can arise through multiple genes, which suggests that the effect

of an antibiotic on the genetic network can most likely not be accurately reproduced by a single gene KD. Introducing multiple gRNAs to repress transcription of all genes targeted by an antibiotic or providing resistance against an antibiotic could mimic the antibiotic effect or resistance evolution more closely. However, even then, the repression of every gene could be different due to different CRISPRi efficiencies and the differences between transcriptional repression *via* CRISPRi versus binding of the protein by the antibiotic.

3.4. Conclusion and outlook

Despite its limitations, the method presented here allows us to characterize the global epistasis of essential genes systematically and, therefore, represents a substantial advance in studying the plasticity of genetic networks. In particular, I developed this approach to systematically characterize epistatic interactions of antibiotic resistance genes and targets to understand the properties of the genetic network during antibiotic treatment and resistance evolution. Performing the described methodology for multiple antibiotic resistance genes and targets in the absence and presence of antibiotics will allow us to find common and unique vulnerabilities of the genetic network. Evolvability genes whose KOs show SL with multiple antibiotic resistance genes represent potential targets for evolution inhibitors and can be compared with the evolvability genes identified in Chapter II. Gene deletions negatively interacting with antibiotic targets can be targeted using antibiotic potentiators to increase antibiotic effectiveness, while gene deletions positively interacting with antibiotic targets give us insights into potential resistance trajectories to overcome the stress on an essential gene. Linking the global epistasis data with the quantification of suppressor frequencies will allow us to systematically map how essentiality translates to suppressor frequency and thereby answer critical questions about evolvability and the plasticity of genetic networks.

4. Final remarks

Antibiotic resistance is one of the major challenges faced by humanity. While in the 20th century, our efforts to develop novel antibiotics have outpaced the rate with which antibiotics became irrelevant due to widespread antibiotic resistance, we are now facing the turning point of this trajectory for many major antibiotic classes. One explanation is that developing novel antibiotics is becoming increasingly difficult and, therefore, more expensive. In contrast, antibiotic resistance develops at a constant, if not accelerating, pace due to widespread and increasing use across the globe. Given the current economic system, it will be impossible to

develop antibiotics with novel mechanisms of action at some point in the not-too-distant future. Therefore, identifying alternative approaches to delay, prevent, or revert antibiotic resistance evolution for existing antibiotics is imperative and currently represents the only solution. To develop such approaches, we need to elevate our understanding of how the genetic network is constructed, how it changes during antibiotic treatment and resistance evolution, and which vulnerabilities arise during this process. This thesis provides two complementary methods that can be used to map the plasticity of the genetic network during antibiotic resistance evolution on a genome-wide scale and at molecular resolution.

While genome-wide experimental evolution has never been performed, the approach presented in Chapter II is feasible to be performed with several other antibiotics, given that the experimental conditions are chosen to shorten the experimental evolution to three days per antibiotic. The yield-based readout allows for competition among resistance trajectories in the presence of the antibiotic and, therefore, integrates the entirety of gene-gene and gene-gene-drug interactions. Therefore, it mimics closely how a non-essential gene deletion affects the plasticity of the complete genetic network during resistance evolution and how it interacts with the main resistance trajectories by gene-gene and gene-gene-drug interactions.

In Chapter III, I have shown how such gene-gene and gene-gene-drug interactions between evolvability genes and resistance elements can be dissected using quantitative genetics, proteomics, HT imaging, and HT experimental evolution across multiple genes and drugs. Even though there are still many open questions, Chapter III describes a set of approaches that can be used to illuminate genetic interactions shaping evolutionary processes.

The method described in Chapter IV focuses on the entirety of epistatic interactions of one resistance gene or antibiotic target and, therefore, zooms closer into the genetic network surrounding such a gene. While interactions of a single resistance gene can not replace the complex readout of experimental evolution, I showed in Chapter III that one gene-gene interaction of a major resistance gene does provide a certain degree of predictability to delay resistance evolution as a whole. Therefore, both approaches represent complementary readouts.

Identifying evolvability genes and networks of synthetic lethality and inhibiting these with single drugs or drug combinations potentially paves the way for a new class of anti-evolution drugs. For the first time, this systematically tackles the underlying challenge posed by

resistance evolution on a genome-wide level, as opposed to the development of new growth inhibitors, against which resistance is eventually bound to develop (Ortmayr et al. 2022). The systematic genome-wide mapping of genes conditional-essential during antibiotic resistance evolution could yield combinatorial strategies of antibiotics and resistance inhibitors, with a strong potential to drive discoveries in other important related fields, such as resistance evolution in cancer (Russo et al. 2019). The platforms I developed to acquire genome-wide evolvability information can be applied to any chemical stress and any unicellular bacteria or fungi for which arrayed knockout, overexpression, or transposon libraries are available. The data acquired in this project gives us access to unprecedented information about the genetic dependencies underlying resistance evolution and the accompanying rewiring of the genetic network. Therefore, it approaches one of the most fundamental biological processes from a systematic and genome-wide angle with potential implications for all evolutionary processes, such as resistance, epistasis, and evolvability. The presented approaches and the increased level of understanding of how evolution can be dissected and targeted can facilitate future research and contribute to the arms race against antibiotic resistance evolution.

Chapter VI: Experimental procedures

Chapter VI: Experimental procedures

1. List of primers and plasmids

All plasmids, primers, and oligos used in this thesis are mentioned hereafter, including a description and reference for plasmids (Table 1), as well as sequence and use for primers and oligos (Table 2).

Table 1: All plasmids used in the study. *Plasmids, including their source or reference and a description of their use.*

Plasmid name	Description	Source / Reference
pJB37	pSB101 origin of replication, F-based origin of transfer, Spectinomycin resistance	(Bobonis et al. 2022)
pgRNA	Constitutive expression SpeI promoter guide RNA scaffold	(Qi et al., 2013)
pSB01	Gibson assembly of 1. pSC101 origin of replication, F- based origin of transfer, aadA spectinomycin resistance cassette from pJB37 (Bobonis et al. 2022), 2. Constitutive expression SpeI promotor guide RNA scaffold from pgRNA (Qi et al., 2013) and 3. Inducible repressor tetR-tetO under strong ProB promoter controlling dCas9 expression from chromosomal dCas9 expression cassette in BW25113 (Lawson et al., 2017; Mateus et al., 2020)	this study
pSB02	pSB01 with BsaI cutting site removed	this study
pSB03_1	pSB02 with second BsaI cutting site removed version 1	this study
pSB03_2	pSB02 with second BsaI cutting site removed version 2	this study
pCP20	FLP recombinase, Ampicillin and Chloramphenicol resistance	(Datsenko et al., 2000)

Table 2: All oligos and primers used in the study. *The oligo name, identifier of the primer, sequence, and function are listed.*

Primer name	Sequence	Use
Gibson assembly plasmid construction		
Gibson_pdCas9_FWD	attgtctgattcgttaccaaGGACCAAAACGAAAAAAGACG	Constructing the CRISPRi plasmid pSB01
Gibson_pdCas9_REV	tgctttttttgCTGCAGggggagagcgttcaccgacaaac	Constructing the CRISPRi plasmid pSB01
Gibson_pJB37_FWD	aggactgagctagctgtcaaagtaaagccctcgctagatt	Constructing the CRISPRi plasmid pSB01
Gibson_pJB37_REV	GTCTTTTTTCGTTTTGGTCCttggtaacgaatcagacaattg	Constructing the CRISPRi plasmid pSB01
Gibson_psgRNA_FWD	cgctctcccccCTGCAGcaaaaaaagcaccgactcggtgcc	Constructing the CRISPRi plasmid pSB01
Gibson_psgRNA_REV	aatctagcgagggctttactttgacagctagctcagtcct	Constructing the CRISPRi plasmid pSB01
Gibson_BsaI1_Backbone_FWD	tggctggcgaacgagcgcaatcgtcaggcattggcggcct	Constructing the CRISPRi plasmid pSB02
Gibson_BsaI1_Backbone_REV	tgggtcgatgtttgatgttagatgttacgcagcagggcagt	Constructing the CRISPRi plasmid pSB02
Gibson_BsaI1_Insert_FWD	ctgccctgctgcgtaacatctaacatcaaacatcgacccacggc	Constructing the CRISPRi plasmid pSB02
Gibson_BsaI1_Insert_REV	aggccgccaatgcctgacgattgcgctcgttcgccagcca	Constructing the CRISPRi plasmid pSB02
Gibson_BsaI2_partA_FWD_1	AAACCGTTGTGGaCTCCCTGAATATAGC	Constructing the CRISPRi plasmid pSB03_1
Gibson_BsaI2_partA_FWD_2	ACCGTTGTGGTCaCCCTGAATATAGCC	Constructing the CRISPRi plasmid pSB03_2
Gibson_BsaI2_partA_REV_fixed	atcttcgagccagccacgatcgac	Constructing the CRISPRi plasmids pSB03_1 and _2
Gibson_BsaI2_partB_FWD_fixed	gtcgatcgtggctggctcgaagatac	Constructing the CRISPRi plasmids pSB03_1 and _2
Gibson_BsaI2_partB_REV_1	TATTCAGGGAGtCCACAACGGTTTC	Constructing the CRISPRi plasmid pSB03_1
Gibson_BsaI2_partB_REV_2	TATATTCAGGGtGACCACAACGGT	Constructing the CRISPRi plasmid pSB03_2
Sequence pSB03		
Seq1_1	cgattacttcgccaactatt	Sequencing pSB03_2
Seq2_1	ttgtttcatcaagccttacg	Sequencing pSB03_2
Seq3_1	gatatttaaaaaagcggtgtcg	Sequencing pSB03_2
Seq4_1	cagttaaagcatcgtgtagt	Sequencing pSB03_2
Seq5_1	ctcaattggtctaggtgatttt	Sequencing pSB03_2
Seq6_1	ctaatgagacgaatctgatcg	Sequencing pSB03_2
Seq7_1	ctaatttttgttgacactctatcg	Sequencing pSB03_2
Seq8_1	attgctttgtcattgggttt	Sequencing pSB03_2
Seq9_1	gctttatgagtattttacggtttat	Sequencing pSB03_2
Seq10_1	caaagaattaggaagtcagattct	Sequencing pSB03_2
Seq11_1	tcgaaactaatggggaaact	Sequencing pSB03_2
Seq12_1	cgtctacaaaagaagttttagatg	Sequencing pSB03_2
Seq13_2	aaggttctggaccagttg	Sequencing pSB03_2
Seq14_2	ctgttgagctgtaacaagtt	Sequencing pSB03_2
Seq15_2	aatctctatatttgccttgtgag	Sequencing pSB03_2
Seq16_2	atcttccaatacgcaacct	Sequencing pSB03_2
Seq17_2	ggaagaatcgtatttgttatctaca	Sequencing pSB03_2
Seq18_2	aattccttattatgttggtccatt	Sequencing pSB03_2
Seq19_2	ggtacctaccatgatttgct	Sequencing pSB03_2
Seq20_2	ctaaattagtttctgacttccga	Sequencing pSB03_2
Seq21_2	aaacggatgctggctag	Sequencing pSB03_2
Seq22_2	gacaaaccaatacgtgaacaa	Sequencing pSB03_2
Confirm gene deletions		
marR_KO_fwd	CCCTGCAACTAATTACTTGCCAGG	Confirm gene deletion of marR by PCR
marR_KO_rev	CGTCTGGACATCGTCATACCT	Confirm gene deletion of marR by PCR
ompR_KO_fwd	tgaacttcgtggcgagaagc	Confirm gene deletion of ompR by PCR
ompR_KO_rev	caaattgttgcgaacctttggga	Confirm gene deletion of ompR by PCR
ivy_long_KO_fwd	GCAGTTGCCTTAGCGCAG	Confirm gene deletion of ivy by PCR
ivy_long_KO_rev	TGCGCAGTATTAACGTTGATGACTTTGA	Confirm gene deletion of ivy by PCR
dpaA_KO_fwd	ctggcaaaagattatgccaggc	Confirm gene deletion of dpaA by PCR
dpaA_KO_rev	gcgtgtgtaaccgttttatcaagga	Confirm gene deletion of dpaA by PCR
tolC_KO_fwd	ttgaggcacattaacgccctatg	Confirm gene deletion of tolC by PCR
tolC_KO_rev	ggtaaatacccatcagaatagaggatgg	Confirm gene deletion of tolC by PCR
50bp_acrA_KO_fwd	catgatgataatggcgatcacccacg	Confirm gene deletion of acrA by PCR
50bp_acrA_KO_rev	agcacgacgataatataaacgcagcaatgg	Confirm gene deletion of acrA by PCR
100bp_acrA_KO_fwd	ccggcggtgcaatcgtag	Confirm gene deletion of acrA by PCR
100bp_acrA_KO_rev	cgaggatgtgttggcgcg	Confirm gene deletion of acrA by PCR
150bp_acrA_KO_fwd	cgataacctgtgtcaccgtgtcc	Confirm gene deletion of acrA by PCR
150bp_acrA_KO_rev	gcccagcgaggtggatg	Confirm gene deletion of acrA by PCR
acrB_KO_fwd	atccgtggttaatactggttttcgtatg	Confirm gene deletion of acrB by PCR
acrB_KO_rev	gctgcagaaagtgcgtcctg	Confirm gene deletion of acrB by PCR
actS_KO_fwd	cttgggaagctctcgttctacc	Confirm gene deletion of actS by PCR
actS_KO_rev	cttcccttgccaaatgaaattaacctc	Confirm gene deletion of actS by PCR
ldtA_KO_fwd	cagtcggtagaacggcgga	Confirm gene deletion of ldtA by PCR
ldtA_KO_rev	gggcgaacttgctgccagtaatattg	Confirm gene deletion of ldtA by PCR
lpxT_KO_fwd	gctgatttccagcagcgaagc	Confirm gene deletion of lpxT by PCR
lpxT_KO_rev	ttgagtgaaacgcatgcaatccattcatttac	Confirm gene deletion of lpxT by PCR
mepK_KO_fwd	gtcgtaataattagcatgattgggggcga	Confirm gene deletion of mepK by PCR
mepK_KO_rev	atcgaccagtgcggcca	Confirm gene deletion of mepK by PCR
mepS_KO_fwd	gcgttagtccacagatttggcctt	Confirm gene deletion of mepS by PCR
mepS_KO_rev	gcctggatcaagacgcggaa	Confirm gene deletion of mepS by PCR
mlaC_KO_fwd	gcaggtaatccccttcaccgc	Confirm gene deletion of mlaC by PCR
mlaC_KO_rev	ggtcagttcctttacggtagtaaaggcg	Confirm gene deletion of mlaC by PCR
mltF_KO_fwd	ggctgtaataagttgccatctggcg	Confirm gene deletion of mltF by PCR
mltF_KO_rev	ccgggtatgaatcaccgagtggaaatta	Confirm gene deletion of mltF by PCR
wecA_KO_fwd	GCTGGCATGTTATGCAATTTGCATATCAAATGG	Confirm gene deletion of wecA by PCR
wecA_KO_rev	agccccatgccaataatccatagctt	Confirm gene deletion of wecA by PCR

Primer name	Sequence	Use
CRISPRi guide RNAs		
GG_PARC_FWD	CCTAGCATCTGGTCTCATAGTCCAAACCGCGACATCAGCGC	Guide RNA for targeted CRISPRi knockdown of parC
GG_PARC_REV	GTAATCCGATGGTCTCCAAACGCGCTGATGTCGCGGTTTGG	Guide RNA for targeted CRISPRi knockdown of parC
GG_DNAK_FWD	CCTAGCATCTGGTCTCATAGTAGTTTCACCATCCTGGGTAT	Guide RNA for targeted CRISPRi knockdown of dnaK
GG_DNAK_REV	GTAATCCGATGGTCTCCAAACATACCCAGGATGGTGAAACT	Guide RNA for targeted CRISPRi knockdown of dnaK
GG_ATPA_FWD	CCTAGCATCTGGTCTCATAGTATCGGTAATGGAGATTACGT	Guide RNA for targeted CRISPRi knockdown of atpA
GG_ATPA_REV	GTAATCCGATGGTCTCCAAACACGTAATCTCCATTACCGAT	Guide RNA for targeted CRISPRi knockdown of atpA
GG_PBPG_FWD	CCTAGCATCTGGTCTCATAGTAATAAAGAAACTCGAAATTT	Guide RNA for targeted CRISPRi knockdown of pbpG
GG_PBPG_REV	GTAATCCGATGGTCTCCAAACAAATTTCGAGTTTCTTTATT	Guide RNA for targeted CRISPRi knockdown of pbpG
GG_OMPF_FWD	CCTAGCATCTGGTCTCATAGTGTTGATGATGTAGTCAACAT	Guide RNA for targeted CRISPRi knockdown of ompF
GG_OMPF_REV	GTAATCCGATGGTCTCCAAACATGTTGACTACATCATCAAC	Guide RNA for targeted CRISPRi knockdown of ompF
GG_OMPC_FWD	CCTAGCATCTGGTCTCATAGTCTACCAGCAGAGCTGGGACC	Guide RNA for targeted CRISPRi knockdown of ompC
GG_OMPC_REV	GTAATCCGATGGTCTCCAAACGGTCCCAGCTCTGCTGGTAG	Guide RNA for targeted CRISPRi knockdown of ompC
GG_FUR_FWD	CCTAGCATCTGGTCTCATAGTGCACTGACGTGATGGTTGTC	Guide RNA for targeted CRISPRi knockdown of fur
GG_FUR_REV	GTAATCCGATGGTCTCCAAACGACAACCATCACGTCAGTGC	Guide RNA for targeted CRISPRi knockdown of fur
GG_RPLI_FWD	CCTAGCATCTGGTCTCATAGTTAACGTTTACCTGATCACCC	Guide RNA for targeted CRISPRi knockdown of rplI
GG_RPLI_REV	GTAATCCGATGGTCTCCAAACGGGTGATCAGGTAAACGTTA	Guide RNA for targeted CRISPRi knockdown of rplI
GG_RPLA_FWD	CCTAGCATCTGGTCTCATAGTTACACGCCTTTCGCCTGAGT	Guide RNA for targeted CRISPRi knockdown of rplA
GG_RPLA_REV	GTAATCCGATGGTCTCCAAACACTCAGGCGAAAGGCGTGTA	Guide RNA for targeted CRISPRi knockdown of rplA
GG_RPOZ_FWD	CCTAGCATCTGGTCTCATAGTCATCTGACGAGCGCGACGCG	Guide RNA for targeted CRISPRi knockdown of rpoZ
GG_RPOZ_REV	GTAATCCGATGGTCTCCAAACCGCGTCGCGCTCGTCAGATG	Guide RNA for targeted CRISPRi knockdown of rpoZ
GG_RPON_FWD	CCTAGCATCTGGTCTCATAGTGCATCGAGCGGCAGCTCTTC	Guide RNA for targeted CRISPRi knockdown of rpoN
GG_RPON_REV	GTAATCCGATGGTCTCCAAACGAAGAGCTGCCGCTCGATGC	Guide RNA for targeted CRISPRi knockdown of rpoN
GG_RPOB_FWD	CCTAGCATCTGGTCTCATAGTCTTACGAATACGTTTTTTCT	Guide RNA for targeted CRISPRi knockdown of rpoB
GG_RPOB_REV	GTAATCCGATGGTCTCCAAACAGAAAAAACGTATTCGTAAG	Guide RNA for targeted CRISPRi knockdown of rpoB
GG_RPSA_FWD	CCTAGCATCTGGTCTCATAGTCGCCACGAACGATAGAACCC	Guide RNA for targeted CRISPRi knockdown of rpsA
GG_RPSA_REV	GTAATCCGATGGTCTCCAAACGGGTTCTATCGTTCGTGGCG	Guide RNA for targeted CRISPRi knockdown of rpsA
GG_FOLA_FWD	CCTAGCATCTGGTCTCATAGTGCGTTTAAACCAGGCGAGAT	Guide RNA for targeted CRISPRi knockdown of folA
GG_FOLA_REV	GTAATCCGATGGTCTCCAAACATCTCGCCTGGTTTAAACGC	Guide RNA for targeted CRISPRi knockdown of folA
GG_GYRA_FWD	CCTAGCATCTGGTCTCATAGTGACGGATCAGTTCGATGATC	Guide RNA for targeted CRISPRi knockdown of gyrA
GG_GYRA_REV	GTAATCCGATGGTCTCCAAACGATCATCGAACTGATCCGTC	Guide RNA for targeted CRISPRi knockdown of gyrA
GG_IVY_FWD	CCTAGCATCTGGTCTCATAGTCGTTGCGAGCCACAGTCATG	Guide RNA for targeted CRISPRi knockdown of ivy
GG_IVY_REV	GTAATCCGATGGTCTCCAAACCATGACTGTGGCTCGCAACG	Guide RNA for targeted CRISPRi knockdown of ivy
GG_DPAA_FWD	CCTAGCATCTGGTCTCATAGTGAAGATCTGGATGTAGACAG	Guide RNA for targeted CRISPRi knockdown of dpaA
GG_DPAA_REV	GTAATCCGATGGTCTCCAAACCTGTCTACATCCAGATCTTC	Guide RNA for targeted CRISPRi knockdown of dpaA
GG_DACA_FWD	CCTAGCATCTGGTCTCATAGTCATGATACGAGCGGAAAAAA	Guide RNA for targeted CRISPRi knockdown of dacA
GG_DACA_REV	GTAATCCGATGGTCTCCAAACTTTTTTCCGCTCGTATCATG	Guide RNA for targeted CRISPRi knockdown of dacA
GG_PBPG_FWD	CCTAGCATCTGGTCTCATAGTAATAAAGAAACTCGAAATTT	Guide RNA for targeted CRISPRi knockdown of pbpG
GG_PBPG_REV	GTAATCCGATGGTCTCCAAACAAATTTCGAGTTTCTTTATT	Guide RNA for targeted CRISPRi knockdown of pbpG
GG_MARR_FWD	CCTAGCATCTGGTCTCATAGTAATTTCATTGAACAGATCGC	Guide RNA for targeted CRISPRi knockdown of marR
GG_MARR_REV	GTAATCCGATGGTCTCCAAACGCGATCTGTTCAATGAAATT	Guide RNA for targeted CRISPRi knockdown of marR
GG_OMPR_FWD	CCTAGCATCTGGTCTCATAGTTCGAACCTGGAAGCCTTGTT	Guide RNA for targeted CRISPRi knockdown of ompR
GG_OMPR_REV	GTAATCCGATGGTCTCCAAACAACAAGGCTTCCAGGTTCGA	Guide RNA for targeted CRISPRi knockdown of ompR
GG_OMPF_FWD	CCTAGCATCTGGTCTCATAGTGTTGATGATGTAGTCAACAT	Guide RNA for targeted CRISPRi knockdown of ompF
GG_OMPF_REV	GTAATCCGATGGTCTCCAAACATGTTGACTACATCATCAAC	Guide RNA for targeted CRISPRi knockdown of ompF
GG_FRDD_FWD	CCTAGCATCTGGTCTCATAGTCCGAAGAGGCCCCAGAATAC	Guide RNA for targeted CRISPRi knockdown of frdD
GG_FRDD_REV	GTAATCCGATGGTCTCCAAACGTATTCTGGGGCCTCTTCGG	Guide RNA for targeted CRISPRi knockdown of frdD
GG_ASPC_FWD	CCTAGCATCTGGTCTCATAGTCAGAATCGGGTCGGCAGGAG	Guide RNA for targeted CRISPRi knockdown of aspC
GG_ASPC_REV	GTAATCCGATGGTCTCCAAACCTCCTGCCGACCCGATTCTG	Guide RNA for targeted CRISPRi knockdown of aspC
GG_LON_FWD	CCTAGCATCTGGTCTCATAGTGCTTGATGTAGCCTTCGAAC	Guide RNA for targeted CRISPRi knockdown of lon
GG_LON_REV	GTAATCCGATGGTCTCCAAACGTTCGAAGGCTACATCAAGC	Guide RNA for targeted CRISPRi knockdown of lon

2. List of strains used in this work

All strains used in this study are mentioned hereafter, including their genotype, reference, and description. All strains used in this study were constructed by myself in an *E. coli* K12 BW 25113 background, with the exception of the first two strains (Table 3).

Table 3: All bacterial strains used in this work. *Identifier, genetic background, and reference for the source are indicated.*

Strains	Genotype	Source or Reference	Description
E. coli K12 BW 25113			
NT5000	intC::tetR-dcas9-aadA lacY::ypet-cat araB::T7 RNAP-tetA ΔaraB	(Lawson et al., 2017; Mateus et al., 2020)	Chromosomal dCas9 expression cassette, TetR repressor protein expressed by strong ProB promoter, aadA gene product confers resistance to Spectinomycin
CAG 60056	pseudoHfr::(trp bla (-))	(Typas et al., 2008)	~43 kb HindIII fragment of F (entire transfer region) integrated into the trp locus and linked to an ampicillin marker
NT6001	ΔmarR::kan	this study	E. coli K12 BW 25113 with marR gene replaced by kanamycin resistance
NT6002	ΔompR::kan	this study	E. coli K12 BW 25113 with ompR gene replaced by kanamycin resistance
NT6003	ΔwaaQ::kan	this study	E. coli K12 BW 25113 with waaQ gene replaced by kanamycin resistance
NT6004	ΔtolC::kan	this study	E. coli K12 BW 25113 with tolC gene replaced by kanamycin resistance
NT6005	ΔacrA::kan	this study	E. coli K12 BW 25113 with acrA gene replaced by kanamycin resistance
NT6006	ΔacrB::kan	this study	E. coli K12 BW 25113 with acrB gene replaced by kanamycin resistance
NT6007	ΔompC::kan	this study	E. coli K12 BW 25113 with ompC gene replaced by kanamycin resistance
NT6008	ΔompF::kan	this study	E. coli K12 BW 25113 with ompF gene replaced by kanamycin resistance
NT6009	ΔdpaA::kan	this study	E. coli K12 BW 25113 with dpaA gene replaced by kanamycin resistance
NT6010	Δivy::kan	this study	E. coli K12 BW 25113 with ivy gene replaced by kanamycin resistance
NT6011	ΔdacA::kan	this study	E. coli K12 BW 25113 with dacA gene replaced by kanamycin resistance
NT6012	ΔpbpG::kan	this study	E. coli K12 BW 25113 with pbpG gene replaced by kanamycin resistance
NT6013	ΔbacA::kan	this study	E. coli K12 BW 25113 with bacA gene replaced by kanamycin resistance
NT6014	ΔlapA::kan	this study	E. coli K12 BW 25113 with lapA gene replaced by kanamycin resistance
NT6015	ΔldtA::kan	this study	E. coli K12 BW 25113 with ldtA gene replaced by kanamycin resistance
NT6016	ΔlpoA::kan	this study	E. coli K12 BW 25113 with lpoA gene replaced by kanamycin resistance
NT6017	ΔlpoB::kan	this study	E. coli K12 BW 25113 with lpoB gene replaced by kanamycin resistance
NT6018	ΔlpxL::kan	this study	E. coli K12 BW 25113 with lpxL gene replaced by kanamycin resistance
NT6019	ΔlpxT::kan	this study	E. coli K12 BW 25113 with lpxT gene replaced by kanamycin resistance
NT6020	ΔmepK::kan	this study	E. coli K12 BW 25113 with mepK gene replaced by kanamycin resistance
NT6021	ΔmepS::kan	this study	E. coli K12 BW 25113 with mepS gene replaced by kanamycin resistance
NT6022	ΔmlaC::kan	this study	E. coli K12 BW 25113 with mlaC gene replaced by kanamycin resistance
NT6023	ΔmlaE::kan	this study	E. coli K12 BW 25113 with mlaE gene replaced by kanamycin resistance
NT6024	ΔmlaF::kan	this study	E. coli K12 BW 25113 with mlaF gene replaced by kanamycin resistance
NT6025	ΔmltC::kan	this study	E. coli K12 BW 25113 with mltC gene replaced by kanamycin resistance
NT6026	ΔmltF::kan	this study	E. coli K12 BW 25113 with mltF gene replaced by kanamycin resistance
NT6027	ΔnlpI::kan	this study	E. coli K12 BW 25113 with nlpI gene replaced by kanamycin resistance
NT6028	ΔompW::kan	this study	E. coli K12 BW 25113 with ompW gene replaced by kanamycin resistance
NT6029	ΔwecA::kan	this study	E. coli K12 BW 25113 with wecA gene replaced by kanamycin resistance
NT6030	ΔwecC::kan	this study	E. coli K12 BW 25113 with wecC gene replaced by kanamycin resistance
NT6031	ΔwecE::kan	this study	E. coli K12 BW 25113 with wecE gene replaced by kanamycin resistance
NT6032	Δslt::kan	this study	E. coli K12 BW 25113 with slt gene replaced by kanamycin resistance
NT6033	ΔuidB::kan	this study	E. coli K12 BW 25113 with uidB gene replaced by kanamycin resistance
NT6034	ΔuidC::kan	this study	E. coli K12 BW 25113 with uidC gene replaced by kanamycin resistance
NT6035	ΔytfK::kan	this study	E. coli K12 BW 25113 with ytfK gene replaced by kanamycin resistance
NT6036	ΔmarR:: ΔdpaA::kan	this study	E. coli K12 BW 25113 with marR gene deletion (FRT site scar) and dpaA gene replaced by kanamycin resistance
NT6037	ΔmarR:: Δivy::kan	this study	E. coli K12 BW 25113 with marR gene deletion (FRT site scar) and ivy gene replaced by kanamycin resistance
NT6038	ΔmarR:: ΔbacA::kan	this study	E. coli K12 BW 25113 with marR gene deletion (FRT site scar) and bacA gene replaced by kanamycin resistance
NT6039	ΔmarR:: ΔlapA::kan	this study	E. coli K12 BW 25113 with marR gene deletion (FRT site scar) and lapA gene replaced by kanamycin resistance
NT6040	ΔmarR:: ΔldtA::kan	this study	E. coli K12 BW 25113 with marR gene deletion (FRT site scar) and ldtA gene replaced by kanamycin resistance
NT6041	ΔmarR:: ΔlpoA::kan	this study	E. coli K12 BW 25113 with marR gene deletion (FRT site scar) and lpoA gene replaced by kanamycin resistance
NT6042	ΔmarR:: ΔlpoB::kan	this study	E. coli K12 BW 25113 with marR gene deletion (FRT site scar) and lpoB gene replaced by kanamycin resistance
NT6043	ΔmarR:: ΔlpxL::kan	this study	E. coli K12 BW 25113 with marR gene deletion (FRT site scar) and lpxL gene replaced by kanamycin resistance
NT6044	ΔmarR:: ΔlpxT::kan	this study	E. coli K12 BW 25113 with marR gene deletion (FRT site scar) and lpxT gene replaced by kanamycin resistance
NT6045	ΔmarR:: ΔmepK::kan	this study	E. coli K12 BW 25113 with marR gene deletion (FRT site scar) and mepK gene replaced by kanamycin resistance
NT6046	ΔmarR:: ΔmepS::kan	this study	E. coli K12 BW 25113 with marR gene deletion (FRT site scar) and mepS gene replaced by kanamycin resistance
NT6047	ΔmarR:: ΔmlaC::kan	this study	E. coli K12 BW 25113 with marR gene deletion (FRT site scar) and mlaC gene replaced by kanamycin resistance
NT6048	ΔmarR:: ΔmlaE::kan	this study	E. coli K12 BW 25113 with marR gene deletion (FRT site scar) and mlaE gene replaced by kanamycin resistance
NT6049	ΔmarR:: ΔmlaF::kan	this study	E. coli K12 BW 25113 with marR gene deletion (FRT site scar) and mlaF gene replaced by kanamycin resistance
NT6050	ΔmarR:: ΔmltC::kan	this study	E. coli K12 BW 25113 with marR gene deletion (FRT site scar) and mltC gene replaced by kanamycin resistance
NT6051	ΔmarR:: ΔmltF::kan	this study	E. coli K12 BW 25113 with marR gene deletion (FRT site scar) and mltF gene replaced by kanamycin resistance
NT6052	ΔmarR:: ΔnlpI::kan	this study	E. coli K12 BW 25113 with marR gene deletion (FRT site scar) and nlpI gene replaced by kanamycin resistance
NT6053	ΔmarR:: ΔompW::kan	this study	E. coli K12 BW 25113 with marR gene deletion (FRT site scar) and ompW gene replaced by kanamycin resistance
NT6054	ΔmarR:: ΔwecA::kan	this study	E. coli K12 BW 25113 with marR gene deletion (FRT site scar) and wecA gene replaced by kanamycin resistance
NT6055	ΔmarR:: ΔwecC::kan	this study	E. coli K12 BW 25113 with marR gene deletion (FRT site scar) and wecC gene replaced by kanamycin resistance
NT6056	ΔmarR:: ΔwecE::kan	this study	E. coli K12 BW 25113 with marR gene deletion (FRT site scar) and wecE gene replaced by kanamycin resistance
NT6057	ΔmarR:: Δslt::kan	this study	E. coli K12 BW 25113 with marR gene deletion (FRT site scar) and slt gene replaced by kanamycin resistance
NT6058	ΔmarR:: ΔuidB::kan	this study	E. coli K12 BW 25113 with marR gene deletion (FRT site scar) and uidB gene replaced by kanamycin resistance
NT6059	ΔmarR:: ΔuidC::kan	this study	E. coli K12 BW 25113 with marR gene deletion (FRT site scar) and uidC gene replaced by kanamycin resistance
NT6060	ΔmarR:: ΔytfK::kan	this study	E. coli K12 BW 25113 with marR gene deletion (FRT site scar) and ytfK gene replaced by kanamycin resistance
NT6061	ΔompR:: ΔdpaA::kan	this study	E. coli K12 BW 25113 with ompR gene deletion (FRT site scar) and dpaA gene replaced by kanamycin resistance
NT6062	ΔompR:: Δivy::kan	this study	E. coli K12 BW 25113 with ompR gene deletion (FRT site scar) and ivy gene replaced by kanamycin resistance
NT6063	ΔompR:: ΔbacA::kan	this study	E. coli K12 BW 25113 with ompR gene deletion (FRT site scar) and bacA gene replaced by kanamycin resistance
NT6064	ΔompR:: ΔlapA::kan	this study	E. coli K12 BW 25113 with ompR gene deletion (FRT site scar) and lapA gene replaced by kanamycin resistance
NT6065	ΔompR:: ΔldtA::kan	this study	E. coli K12 BW 25113 with ompR gene deletion (FRT site scar) and ldtA gene replaced by kanamycin resistance
NT6066	ΔompR:: ΔlpoA::kan	this study	E. coli K12 BW 25113 with ompR gene deletion (FRT site scar) and lpoA gene replaced by kanamycin resistance
NT6067	ΔompR:: ΔlpoB::kan	this study	E. coli K12 BW 25113 with ompR gene deletion (FRT site scar) and lpoB gene replaced by kanamycin resistance
NT6068	ΔompR:: ΔlpxL::kan	this study	E. coli K12 BW 25113 with ompR gene deletion (FRT site scar) and lpxL gene replaced by kanamycin resistance
NT6069	ΔompR:: ΔlpxT::kan	this study	E. coli K12 BW 25113 with ompR gene deletion (FRT site scar) and lpxT gene replaced by kanamycin resistance
NT6070	ΔompR:: ΔmepK::kan	this study	E. coli K12 BW 25113 with ompR gene deletion (FRT site scar) and mepK gene replaced by kanamycin resistance
NT6071	ΔompR:: ΔmepS::kan	this study	E. coli K12 BW 25113 with ompR gene deletion (FRT site scar) and mepS gene replaced by kanamycin resistance
NT6072	ΔompR:: ΔmlaC::kan	this study	E. coli K12 BW 25113 with ompR gene deletion (FRT site scar) and mlaC gene replaced by kanamycin resistance
NT6073	ΔompR:: ΔmlaE::kan	this study	E. coli K12 BW 25113 with ompR gene deletion (FRT site scar) and mlaE gene replaced by kanamycin resistance
NT6074	ΔompR:: ΔmlaF::kan	this study	E. coli K12 BW 25113 with ompR gene deletion (FRT site scar) and mlaF gene replaced by kanamycin resistance
NT6075	ΔompR:: ΔmltC::kan	this study	E. coli K12 BW 25113 with ompR gene deletion (FRT site scar) and mltC gene replaced by kanamycin resistance
NT6076	ΔompR:: ΔmltF::kan	this study	E. coli K12 BW 25113 with ompR gene deletion (FRT site scar) and mltF gene replaced by kanamycin resistance
NT6077	ΔompR:: ΔnlpI::kan	this study	E. coli K12 BW 25113 with ompR gene deletion (FRT site scar) and nlpI gene replaced by kanamycin resistance
NT6078	ΔompR:: ΔompW::kan	this study	E. coli K12 BW 25113 with ompR gene deletion (FRT site scar) and ompW gene replaced by kanamycin resistance
NT6079	ΔompR:: ΔwecA::kan	this study	E. coli K12 BW 25113 with ompR gene deletion (FRT site scar) and wecA gene replaced by kanamycin resistance
NT6080	ΔompR:: ΔwecC::kan	this study	E. coli K12 BW 25113 with ompR gene deletion (FRT site scar) and wecC gene replaced by kanamycin resistance
NT6081	ΔompR:: ΔwecE::kan	this study	E. coli K12 BW 25113 with ompR gene deletion (FRT site scar) and wecE gene replaced by kanamycin resistance
NT6082	ΔompR:: Δslt::kan	this study	E. coli K12 BW 25113 with ompR gene deletion (FRT site scar) and slt gene replaced by kanamycin resistance
NT6083	ΔompR:: ΔuidB::kan	this study	E. coli K12 BW 25113 with ompR gene deletion (FRT site scar) and uidB gene replaced by kanamycin resistance
NT6084	ΔompR:: ΔuidC::kan	this study	E. coli K12 BW 25113 with ompR gene deletion (FRT site scar) and uidC gene replaced by kanamycin resistance
NT6085	ΔompR:: ΔytfK::kan	this study	E. coli K12 BW 25113 with ompR gene deletion (FRT site scar) and ytfK gene replaced by kanamycin resistance

Strains	Genotype	Source or Reference	Description
E. coli K12 BW 25113			
NT6086	pSB03_2 scrambled gRNA	this study	E. coli K12 BW 25113 with CRISPRi plasmid pSB03_2 with a scrambled non-targeting gRNA
NT6087	pSB03_2 dpaA gRNA	this study	E. coli K12 BW 25113 with CRISPRi plasmid pSB03_2 with dpaA targeting gRNA
NT6088	pSB03_2 ivy gRNA	this study	E. coli K12 BW 25113 with CRISPRi plasmid pSB03_2 with ivy targeting gRNA
NT6089	pSB03_2 dacA gRNA	this study	E. coli K12 BW 25113 with CRISPRi plasmid pSB03_2 with dacA targeting gRNA
NT6090	pSB03_2 pbpG gRNA	this study	E. coli K12 BW 25113 with CRISPRi plasmid pSB03_2 with pbpG targeting gRNA
NT6091	pSB03_2 parC gRNA	this study	E. coli K12 BW 25113 with CRISPRi plasmid pSB03_2 with parC targeting gRNA
NT6092	pSB03_2 dnaK gRNA	this study	E. coli K12 BW 25113 with CRISPRi plasmid pSB03_2 with dnaK targeting gRNA
NT6093	pSB03_2 atpA gRNA	this study	E. coli K12 BW 25113 with CRISPRi plasmid pSB03_2 with atpA targeting gRNA
NT6094	pSB03_2 ompF gRNA	this study	E. coli K12 BW 25113 with CRISPRi plasmid pSB03_2 with ompF targeting gRNA
NT6095	pSB03_2 ompC gRNA	this study	E. coli K12 BW 25113 with CRISPRi plasmid pSB03_2 with ompC targeting gRNA
NT6096	pSB03_2 fur gRNA	this study	E. coli K12 BW 25113 with CRISPRi plasmid pSB03_2 with fut targeting gRNA
NT6097	pSB03_2 rplI gRNA	this study	E. coli K12 BW 25113 with CRISPRi plasmid pSB03_2 with rplI targeting gRNA
NT6098	pSB03_2 rplA gRNA	this study	E. coli K12 BW 25113 with CRISPRi plasmid pSB03_2 with rplA targeting gRNA
NT6099	pSB03_2 rpoZ gRNA	this study	E. coli K12 BW 25113 with CRISPRi plasmid pSB03_2 with rpoZ targeting gRNA
NT6100	pSB03_2 rpoN gRNA	this study	E. coli K12 BW 25113 with CRISPRi plasmid pSB03_2 with rpoN targeting gRNA
NT6101	pSB03_2 rpoB gRNA	this study	E. coli K12 BW 25113 with CRISPRi plasmid pSB03_2 with rpoB targeting gRNA
NT6102	pSB03_2 rpsA gRNA	this study	E. coli K12 BW 25113 with CRISPRi plasmid pSB03_2 with rpsA targeting gRNA
NT6103	pSB03_2 folA gRNA	this study	E. coli K12 BW 25113 with CRISPRi plasmid pSB03_2 with folA targeting gRNA
NT6104	pSB03_2 gyrA gRNA	this study	E. coli K12 BW 25113 with CRISPRi plasmid pSB03_2 with gyrA targeting gRNA
NT6105	pSB03_2 marR gRNA	this study	E. coli K12 BW 25113 with CRISPRi plasmid pSB03_2 with marR targeting gRNA
NT6106	pSB03_2 ompR gRNA	this study	E. coli K12 BW 25113 with CRISPRi plasmid pSB03_2 with ompR targeting gRNA
NT6107	pSB03_2 frdD gRNA	this study	E. coli K12 BW 25113 with CRISPRi plasmid pSB03_2 with frdD targeting gRNA
NT6108	pSB03_2 aspC gRNA	this study	E. coli K12 BW 25113 with CRISPRi plasmid pSB03_2 with aspC targeting gRNA
NT6109	pSB03_2 lon gRNA	this study	E. coli K12 BW 25113 with CRISPRi plasmid pSB03_2 with lon targeting gRNA
NT6110	ΔmarR::kan pSB03_2 dpaA gRNA	this study	E. coli K12 BW 25113 with marR gene replaced by kanamycin resistance and CRISPRi targeting dpaA
NT6111	ΔompR::kan pSB03_2 dpaA gRNA	this study	E. coli K12 BW 25113 with ompR gene replaced by kanamycin resistance and CRISPRi targeting dpaA
NT6112	ΔwaaQ::kan pSB03_2 dpaA gRNA	this study	E. coli K12 BW 25113 with waaQ gene replaced by kanamycin resistance and CRISPRi targeting dpaA
NT6113	Evo 25b ΔmarR:: ΔwaaQ:: pSB03_2 dpaA gRNA	this study	E. coli K12 BW 25113 evolved against cefotaxime (marR and waaQ deletions) with CRISPRi targeting dpaA
NT6114	ΔtolC::kan pSB03_2 dpaA gRNA	this study	E. coli K12 BW 25113 with tolC gene replaced by kanamycin resistance and CRISPRi targeting dpaA
NT6115	ΔacrA::kan pSB03_2 dpaA gRNA	this study	E. coli K12 BW 25113 with acrA gene replaced by kanamycin resistance and CRISPRi targeting dpaA
NT6116	ΔacrB::kan pSB03_2 dpaA gRNA	this study	E. coli K12 BW 25113 with acrB gene replaced by kanamycin resistance and CRISPRi targeting dpaA
NT6117	ΔompC::kan pSB03_2 dpaA gRNA	this study	E. coli K12 BW 25113 with ompC gene replaced by kanamycin resistance and CRISPRi targeting dpaA
NT6118	ΔompF::kan pSB03_2 dpaA gRNA	this study	E. coli K12 BW 25113 with ompF gene replaced by kanamycin resistance and CRISPRi targeting dpaA
NT6119	ΔbacA::kan pSB03_2 dpaA gRNA	this study	E. coli K12 BW 25113 with bacA gene replaced by kanamycin resistance and CRISPRi targeting dpaA
NT6120	ΔlapA::kan pSB03_2 dpaA gRNA	this study	E. coli K12 BW 25113 with lapA gene replaced by kanamycin resistance and CRISPRi targeting dpaA
NT6121	ΔldtA::kan pSB03_2 dpaA gRNA	this study	E. coli K12 BW 25113 with ldtA gene replaced by kanamycin resistance and CRISPRi targeting dpaA
NT6122	ΔlpoA::kan pSB03_2 dpaA gRNA	this study	E. coli K12 BW 25113 with lpoA gene replaced by kanamycin resistance and CRISPRi targeting dpaA
NT6123	ΔlpoB::kan pSB03_2 dpaA gRNA	this study	E. coli K12 BW 25113 with lpoB gene replaced by kanamycin resistance and CRISPRi targeting dpaA
NT6124	ΔlpxL::kan pSB03_2 dpaA gRNA	this study	E. coli K12 BW 25113 with lpxL gene replaced by kanamycin resistance and CRISPRi targeting dpaA
NT6125	ΔlpxT::kan pSB03_2 dpaA gRNA	this study	E. coli K12 BW 25113 with lpxT gene replaced by kanamycin resistance and CRISPRi targeting dpaA
NT6126	ΔmepK::kan pSB03_2 dpaA gRNA	this study	E. coli K12 BW 25113 with mepK gene replaced by kanamycin resistance and CRISPRi targeting dpaA
NT6127	ΔmepS::kan pSB03_2 dpaA gRNA	this study	E. coli K12 BW 25113 with mepS gene replaced by kanamycin resistance and CRISPRi targeting dpaA
NT6128	ΔmlaC::kan pSB03_2 dpaA gRNA	this study	E. coli K12 BW 25113 with mlaC gene replaced by kanamycin resistance and CRISPRi targeting dpaA
NT6129	ΔmlaE::kan pSB03_2 dpaA gRNA	this study	E. coli K12 BW 25113 with mlaE gene replaced by kanamycin resistance and CRISPRi targeting dpaA
NT6130	ΔmlaF::kan pSB03_2 dpaA gRNA	this study	E. coli K12 BW 25113 with mlaF gene replaced by kanamycin resistance and CRISPRi targeting dpaA
NT6131	ΔmltC::kan pSB03_2 dpaA gRNA	this study	E. coli K12 BW 25113 with mltC gene replaced by kanamycin resistance and CRISPRi targeting dpaA
NT6132	ΔmltF::kan pSB03_2 dpaA gRNA	this study	E. coli K12 BW 25113 with mltF gene replaced by kanamycin resistance and CRISPRi targeting dpaA
NT6133	Δnlpl::kan pSB03_2 dpaA gRNA	this study	E. coli K12 BW 25113 with nlpl gene replaced by kanamycin resistance and CRISPRi targeting dpaA
NT6134	ΔompW::kan pSB03_2 dpaA gRNA	this study	E. coli K12 BW 25113 with ompW gene replaced by kanamycin resistance and CRISPRi targeting dpaA
NT6135	ΔwecA::kan pSB03_2 dpaA gRNA	this study	E. coli K12 BW 25113 with wecA gene replaced by kanamycin resistance and CRISPRi targeting dpaA
NT6136	ΔwecC::kan pSB03_2 dpaA gRNA	this study	E. coli K12 BW 25113 with wecC gene replaced by kanamycin resistance and CRISPRi targeting dpaA
NT6137	ΔwecE::kan pSB03_2 dpaA gRNA	this study	E. coli K12 BW 25113 with wecE gene replaced by kanamycin resistance and CRISPRi targeting dpaA
NT6138	Δslt::kan pSB03_2 dpaA gRNA	this study	E. coli K12 BW 25113 with slt gene replaced by kanamycin resistance and CRISPRi targeting dpaA
NT6139	ΔuidB::kan pSB03_2 dpaA gRNA	this study	E. coli K12 BW 25113 with uidB gene replaced by kanamycin resistance and CRISPRi targeting dpaA
NT6140	ΔuidC::kan pSB03_2 dpaA gRNA	this study	E. coli K12 BW 25113 with uidC gene replaced by kanamycin resistance and CRISPRi targeting dpaA
NT6141	ΔytfK::kan pSB03_2 dpaA gRNA	this study	E. coli K12 BW 25113 with uidC gene replaced by kanamycin resistance and CRISPRi targeting dpaA
NT6142	ΔmarR:: ΔtolC::kan pSB03_2 dpaA gRNA	this study	E. coli K12 BW 25113 with marR deletion (FRT site scar), tolC gene replaced by kanamycin resistance and CRISPRi targeting dpaA
NT6143	ΔmarR:: ΔacrA::kan pSB03_2 dpaA gRNA	this study	E. coli K12 BW 25113 with marR deletion (FRT site scar), acrA gene replaced by kanamycin resistance and CRISPRi targeting dpaA
NT6144	ΔmarR:: ΔacrB::kan pSB03_2 dpaA gRNA	this study	E. coli K12 BW 25113 with marR deletion (FRT site scar), acrB gene replaced by kanamycin resistance and CRISPRi targeting dpaA
NT6145	ΔmarR:: ΔompC::kan pSB03_2 dpaA gRNA	this study	E. coli K12 BW 25113 with marR deletion (FRT site scar), ompC gene replaced by kanamycin resistance and CRISPRi targeting dpaA
NT6146	ΔmarR:: ΔompF::kan pSB03_2 dpaA gRNA	this study	E. coli K12 BW 25113 with marR deletion (FRT site scar), ompF gene replaced by kanamycin resistance and CRISPRi targeting dpaA
NT6147	ΔmarR:: ΔbacA::kan pSB03_2 dpaA gRNA	this study	E. coli K12 BW 25113 with marR deletion (FRT site scar), bacA gene replaced by kanamycin resistance and CRISPRi targeting dpaA
NT6148	ΔmarR:: ΔlapA::kan pSB03_2 dpaA gRNA	this study	E. coli K12 BW 25113 with marR deletion (FRT site scar), lapA gene replaced by kanamycin resistance and CRISPRi targeting dpaA
NT6149	ΔmarR:: ΔldtA::kan pSB03_2 dpaA gRNA	this study	E. coli K12 BW 25113 with marR deletion (FRT site scar), ldtA gene replaced by kanamycin resistance and CRISPRi targeting dpaA
NT6150	ΔmarR:: ΔlpoA::kan pSB03_2 dpaA gRNA	this study	E. coli K12 BW 25113 with marR deletion (FRT site scar), lpoA gene replaced by kanamycin resistance and CRISPRi targeting dpaA
NT6151	ΔmarR:: ΔlpoB::kan pSB03_2 dpaA gRNA	this study	E. coli K12 BW 25113 with marR deletion (FRT site scar), lpoB gene replaced by kanamycin resistance and CRISPRi targeting dpaA
NT6152	ΔmarR:: ΔlpxL::kan pSB03_2 dpaA gRNA	this study	E. coli K12 BW 25113 with marR deletion (FRT site scar), lpxL gene replaced by kanamycin resistance and CRISPRi targeting dpaA
NT6153	ΔmarR:: ΔlpxT::kan pSB03_2 dpaA gRNA	this study	E. coli K12 BW 25113 with marR deletion (FRT site scar), lpxT gene replaced by kanamycin resistance and CRISPRi targeting dpaA
NT6154	ΔmarR:: ΔmepK::kan pSB03_2 dpaA gRNA	this study	E. coli K12 BW 25113 with marR deletion (FRT site scar), mepK gene replaced by kanamycin resistance and CRISPRi targeting dpaA
NT6155	ΔmarR:: ΔmepS::kan pSB03_2 dpaA gRNA	this study	E. coli K12 BW 25113 with marR deletion (FRT site scar), mepS gene replaced by kanamycin resistance and CRISPRi targeting dpaA
NT6156	ΔmarR:: ΔmlaC::kan pSB03_2 dpaA gRNA	this study	E. coli K12 BW 25113 with marR deletion (FRT site scar), mlaC gene replaced by kanamycin resistance and CRISPRi targeting dpaA
NT6157	ΔmarR:: ΔmlaE::kan pSB03_2 dpaA gRNA	this study	E. coli K12 BW 25113 with marR deletion (FRT site scar), mlaE gene replaced by kanamycin resistance and CRISPRi targeting dpaA
NT6158	ΔmarR:: ΔmlaF::kan pSB03_2 dpaA gRNA	this study	E. coli K12 BW 25113 with marR deletion (FRT site scar), mlaF gene replaced by kanamycin resistance and CRISPRi targeting dpaA
NT6159	ΔmarR:: ΔmltC::kan pSB03_2 dpaA gRNA	this study	E. coli K12 BW 25113 with marR deletion (FRT site scar), mltC gene replaced by kanamycin resistance and CRISPRi targeting dpaA
NT6160	ΔmarR:: ΔmltF::kan pSB03_2 dpaA gRNA	this study	E. coli K12 BW 25113 with marR deletion (FRT site scar), mltF gene replaced by kanamycin resistance and CRISPRi targeting dpaA
NT6161	ΔmarR:: Δnlpl::kan pSB03_2 dpaA gRNA	this study	E. coli K12 BW 25113 with marR deletion (FRT site scar), nlpl gene replaced by kanamycin resistance and CRISPRi targeting dpaA
NT6162	ΔmarR:: ΔompW::kan pSB03_2 dpaA gRNA	this study	E. coli K12 BW 25113 with marR deletion (FRT site scar), ompW gene replaced by kanamycin resistance and CRISPRi targeting dpaA
NT6163	ΔmarR:: ΔwecA::kan pSB03_2 dpaA gRNA	this study	E. coli K12 BW 25113 with marR deletion (FRT site scar), wecA gene replaced by kanamycin resistance and CRISPRi targeting dpaA
NT6164	ΔmarR:: ΔwecC::kan pSB03_2 dpaA gRNA	this study	E. coli K12 BW 25113 with marR deletion (FRT site scar), wecC gene replaced by kanamycin resistance and CRISPRi targeting dpaA
NT6165	ΔmarR:: ΔwecE::kan pSB03_2 dpaA gRNA	this study	E. coli K12 BW 25113 with marR deletion (FRT site scar), wecE gene replaced by kanamycin resistance and CRISPRi targeting dpaA
NT6166	ΔmarR:: Δslt::kan pSB03_2 dpaA gRNA	this study	E. coli K12 BW 25113 with marR deletion (FRT site scar), slt gene replaced by kanamycin resistance and CRISPRi targeting dpaA
NT6167	ΔmarR:: ΔuidB::kan pSB03_2 dpaA gRNA	this study	E. coli K12 BW 25113 with marR deletion (FRT site scar), uidB gene replaced by kanamycin resistance and CRISPRi targeting dpaA
NT6168	ΔmarR:: ΔuidC::kan pSB03_2 dpaA gRNA	this study	E. coli K12 BW 25113 with marR deletion (FRT site scar), uidC gene replaced by kanamycin resistance and CRISPRi targeting dpaA
NT6169	ΔmarR:: ΔytfK::kan pSB03_2 dpaA gRNA	this study	E. coli K12 BW 25113 with marR deletion (FRT site scar), ytfK gene replaced by kanamycin resistance and CRISPRi targeting dpaA

Strains	Genotype	Source or Reference	Description
E. coli K12 BW 25113			
NT6170	ΔompR:: ΔtolC::kan pSB03_2 dpaA gRNA	this study	E. coli K12 BW 25113 with ompR deletion (FRT site scar), tolC gene replaced by kanamycin resistance and CRISPRi targeting dpaA
NT6171	ΔompR:: ΔacrA::kan pSB03_2 dpaA gRNA	this study	E. coli K12 BW 25113 with ompR deletion (FRT site scar), acrA gene replaced by kanamycin resistance and CRISPRi targeting dpaA
NT6172	ΔompR:: ΔacrB::kan pSB03_2 dpaA gRNA	this study	E. coli K12 BW 25113 with ompR deletion (FRT site scar), acrB gene replaced by kanamycin resistance and CRISPRi targeting dpaA
NT6173	ΔompR:: ΔompC::kan pSB03_2 dpaA gRNA	this study	E. coli K12 BW 25113 with ompR deletion (FRT site scar), ompC gene replaced by kanamycin resistance and CRISPRi targeting dpaA
NT6174	ΔompR:: ΔompF::kan pSB03_2 dpaA gRNA	this study	E. coli K12 BW 25113 with ompR deletion (FRT site scar), ompF gene replaced by kanamycin resistance and CRISPRi targeting dpaA
NT6175	ΔompR:: ΔbacA::kan pSB03_2 dpaA gRNA	this study	E. coli K12 BW 25113 with ompR deletion (FRT site scar), bacA gene replaced by kanamycin resistance and CRISPRi targeting dpaA
NT6176	ΔompR:: ΔlapA::kan pSB03_2 dpaA gRNA	this study	E. coli K12 BW 25113 with ompR deletion (FRT site scar), lapA gene replaced by kanamycin resistance and CRISPRi targeting dpaA
NT6177	ΔompR:: ΔldtA::kan pSB03_2 dpaA gRNA	this study	E. coli K12 BW 25113 with ompR deletion (FRT site scar), ldtA gene replaced by kanamycin resistance and CRISPRi targeting dpaA
NT6178	ΔompR:: ΔlpoA::kan pSB03_2 dpaA gRNA	this study	E. coli K12 BW 25113 with ompR deletion (FRT site scar), lpoA gene replaced by kanamycin resistance and CRISPRi targeting dpaA
NT6179	ΔompR:: ΔlpoB::kan pSB03_2 dpaA gRNA	this study	E. coli K12 BW 25113 with ompR deletion (FRT site scar), lpoB gene replaced by kanamycin resistance and CRISPRi targeting dpaA
NT6180	ΔompR:: ΔlpxL::kan pSB03_2 dpaA gRNA	this study	E. coli K12 BW 25113 with ompR deletion (FRT site scar), lpxL gene replaced by kanamycin resistance and CRISPRi targeting dpaA
NT6181	ΔompR:: ΔlpxT::kan pSB03_2 dpaA gRNA	this study	E. coli K12 BW 25113 with ompR deletion (FRT site scar), lpxT gene replaced by kanamycin resistance and CRISPRi targeting dpaA
NT6182	ΔompR:: ΔmepK::kan pSB03_2 dpaA gRNA	this study	E. coli K12 BW 25113 with ompR deletion (FRT site scar), mepK gene replaced by kanamycin resistance and CRISPRi targeting dpaA
NT6183	ΔompR:: ΔmepS::kan pSB03_2 dpaA gRNA	this study	E. coli K12 BW 25113 with ompR deletion (FRT site scar), mepS gene replaced by kanamycin resistance and CRISPRi targeting dpaA
NT6184	ΔompR:: ΔmlaC::kan pSB03_2 dpaA gRNA	this study	E. coli K12 BW 25113 with ompR deletion (FRT site scar), mlaC gene replaced by kanamycin resistance and CRISPRi targeting dpaA
NT6185	ΔompR:: ΔmlaE::kan pSB03_2 dpaA gRNA	this study	E. coli K12 BW 25113 with ompR deletion (FRT site scar), mlaE gene replaced by kanamycin resistance and CRISPRi targeting dpaA
NT6186	ΔompR:: ΔmlaF::kan pSB03_2 dpaA gRNA	this study	E. coli K12 BW 25113 with ompR deletion (FRT site scar), mlaF gene replaced by kanamycin resistance and CRISPRi targeting dpaA
NT6187	ΔompR:: ΔmltC::kan pSB03_2 dpaA gRNA	this study	E. coli K12 BW 25113 with ompR deletion (FRT site scar), mltC gene replaced by kanamycin resistance and CRISPRi targeting dpaA
NT6188	ΔompR:: ΔmltF::kan pSB03_2 dpaA gRNA	this study	E. coli K12 BW 25113 with ompR deletion (FRT site scar), mltF gene replaced by kanamycin resistance and CRISPRi targeting dpaA
NT6189	ΔompR:: Δnlpl::kan pSB03_2 dpaA gRNA	this study	E. coli K12 BW 25113 with ompR deletion (FRT site scar), nlpI gene replaced by kanamycin resistance and CRISPRi targeting dpaA
NT6190	ΔompR:: ΔompW::kan pSB03_2 dpaA gRNA	this study	E. coli K12 BW 25113 with ompR deletion (FRT site scar), ompW gene replaced by kanamycin resistance and CRISPRi targeting dpaA
NT6191	ΔompR:: ΔwecA::kan pSB03_2 dpaA gRNA	this study	E. coli K12 BW 25113 with ompR deletion (FRT site scar), wecA gene replaced by kanamycin resistance and CRISPRi targeting dpaA
NT6192	ΔompR:: ΔwecC::kan pSB03_2 dpaA gRNA	this study	E. coli K12 BW 25113 with ompR deletion (FRT site scar), wecC gene replaced by kanamycin resistance and CRISPRi targeting dpaA
NT6193	ΔompR:: ΔwecE::kan pSB03_2 dpaA gRNA	this study	E. coli K12 BW 25113 with ompR deletion (FRT site scar), wecE gene replaced by kanamycin resistance and CRISPRi targeting dpaA
NT6194	ΔompR:: Δslt::kan pSB03_2 dpaA gRNA	this study	E. coli K12 BW 25113 with ompR deletion (FRT site scar), slt gene replaced by kanamycin resistance and CRISPRi targeting dpaA
NT6195	ΔompR:: ΔuidB::kan pSB03_2 dpaA gRNA	this study	E. coli K12 BW 25113 with ompR deletion (FRT site scar), uidB gene replaced by kanamycin resistance and CRISPRi targeting dpaA
NT6196	ΔompR:: ΔuidC::kan pSB03_2 dpaA gRNA	this study	E. coli K12 BW 25113 with ompR deletion (FRT site scar), uidC gene replaced by kanamycin resistance and CRISPRi targeting dpaA
NT6197	ΔompR:: ΔytfK::kan pSB03_2 dpaA gRNA	this study	E. coli K12 BW 25113 with ompR deletion (FRT site scar), ytfK gene replaced by kanamycin resistance and CRISPRi targeting dpaA
NT6198	ΔmarR::kan pSB03_2 ivy gRNA	this study	E. coli K12 BW 25113 with marR gene replaced by kanamycin resistance and CRISPRi targeting ivy
NT6199	ΔompR::kan pSB03_2 ivy gRNA	this study	E. coli K12 BW 25113 with ompR gene replaced by kanamycin resistance and CRISPRi targeting ivy
NT6200	ΔwaaQ::kan pSB03_2 ivy gRNA	this study	E. coli K12 BW 25113 with waaQ gene replaced by kanamycin resistance and CRISPRi targeting ivy
NT6201	Evo 25b ΔmarR:: ΔwaaQ:: pSB03_2 ivy gRNA	this study	E. coli K12 BW 25113 evolved against cefotaxime (marR and waaQ deletions) with CRISPRi targeting ivy
NT6202	ΔtolC::kan pSB03_2 ivy gRNA	this study	E. coli K12 BW 25113 with tolC gene replaced by kanamycin resistance and CRISPRi targeting ivy
NT6203	ΔacrA::kan pSB03_2 ivy gRNA	this study	E. coli K12 BW 25113 with acrA gene replaced by kanamycin resistance and CRISPRi targeting ivy
NT6204	ΔacrB::kan pSB03_2 ivy gRNA	this study	E. coli K12 BW 25113 with acrB gene replaced by kanamycin resistance and CRISPRi targeting ivy
NT6205	ΔompC::kan pSB03_2 ivy gRNA	this study	E. coli K12 BW 25113 with ompC gene replaced by kanamycin resistance and CRISPRi targeting ivy
NT6206	ΔompF::kan pSB03_2 ivy gRNA	this study	E. coli K12 BW 25113 with ompF gene replaced by kanamycin resistance and CRISPRi targeting ivy
NT6207	ΔbacA::kan pSB03_2 ivy gRNA	this study	E. coli K12 BW 25113 with bacA gene replaced by kanamycin resistance and CRISPRi targeting ivy
NT6208	ΔlapA::kan pSB03_2 ivy gRNA	this study	E. coli K12 BW 25113 with lapA gene replaced by kanamycin resistance and CRISPRi targeting ivy
NT6209	ΔldtA::kan pSB03_2 ivy gRNA	this study	E. coli K12 BW 25113 with ldtA gene replaced by kanamycin resistance and CRISPRi targeting ivy
NT6210	ΔlpoA::kan pSB03_2 ivy gRNA	this study	E. coli K12 BW 25113 with lpoA gene replaced by kanamycin resistance and CRISPRi targeting ivy
NT6211	ΔlpoB::kan pSB03_2 ivy gRNA	this study	E. coli K12 BW 25113 with lpoB gene replaced by kanamycin resistance and CRISPRi targeting ivy
NT6212	ΔlpxL::kan pSB03_2 ivy gRNA	this study	E. coli K12 BW 25113 with lpxL gene replaced by kanamycin resistance and CRISPRi targeting ivy
NT6213	ΔlpxT::kan pSB03_2 ivy gRNA	this study	E. coli K12 BW 25113 with lpxT gene replaced by kanamycin resistance and CRISPRi targeting ivy
NT6214	ΔmepK::kan pSB03_2 ivy gRNA	this study	E. coli K12 BW 25113 with mepK gene replaced by kanamycin resistance and CRISPRi targeting ivy
NT6215	ΔmepS::kan pSB03_2 ivy gRNA	this study	E. coli K12 BW 25113 with mepS gene replaced by kanamycin resistance and CRISPRi targeting ivy
NT6216	ΔmlaC::kan pSB03_2 ivy gRNA	this study	E. coli K12 BW 25113 with mlaC gene replaced by kanamycin resistance and CRISPRi targeting ivy
NT6217	ΔmlaE::kan pSB03_2 ivy gRNA	this study	E. coli K12 BW 25113 with mlaE gene replaced by kanamycin resistance and CRISPRi targeting ivy
NT6218	ΔmlaF::kan pSB03_2 ivy gRNA	this study	E. coli K12 BW 25113 with mlaF gene replaced by kanamycin resistance and CRISPRi targeting ivy
NT6219	ΔmltC::kan pSB03_2 ivy gRNA	this study	E. coli K12 BW 25113 with mltC gene replaced by kanamycin resistance and CRISPRi targeting ivy
NT6220	ΔmltF::kan pSB03_2 ivy gRNA	this study	E. coli K12 BW 25113 with mltF gene replaced by kanamycin resistance and CRISPRi targeting ivy
NT6221	Δnlpl::kan pSB03_2 ivy gRNA	this study	E. coli K12 BW 25113 with nlpI gene replaced by kanamycin resistance and CRISPRi targeting ivy
NT6222	ΔompW::kan pSB03_2 ivy gRNA	this study	E. coli K12 BW 25113 with ompW gene replaced by kanamycin resistance and CRISPRi targeting ivy
NT6223	ΔwecA::kan pSB03_2 ivy gRNA	this study	E. coli K12 BW 25113 with wecA gene replaced by kanamycin resistance and CRISPRi targeting ivy
NT6224	ΔwecC::kan pSB03_2 ivy gRNA	this study	E. coli K12 BW 25113 with wecC gene replaced by kanamycin resistance and CRISPRi targeting ivy
NT6225	ΔwecE::kan pSB03_2 ivy gRNA	this study	E. coli K12 BW 25113 with wecE gene replaced by kanamycin resistance and CRISPRi targeting ivy
NT6226	Δslt::kan pSB03_2 ivy gRNA	this study	E. coli K12 BW 25113 with slt gene replaced by kanamycin resistance and CRISPRi targeting ivy
NT6227	ΔuidB::kan pSB03_2 ivy gRNA	this study	E. coli K12 BW 25113 with uidB gene replaced by kanamycin resistance and CRISPRi targeting ivy
NT6228	ΔuidC::kan pSB03_2 ivy gRNA	this study	E. coli K12 BW 25113 with uidC gene replaced by kanamycin resistance and CRISPRi targeting ivy
NT6229	ΔytfK::kan pSB03_2 ivy gRNA	this study	E. coli K12 BW 25113 with ytfK gene replaced by kanamycin resistance and CRISPRi targeting ivy
NT6230	ΔmarR:: ΔtolC::kan pSB03_2 ivy gRNA	this study	E. coli K12 BW 25113 with marR deletion (FRT site scar), tolC gene replaced by kanamycin resistance and CRISPRi targeting ivy
NT6231	ΔmarR:: ΔacrA::kan pSB03_2 ivy gRNA	this study	E. coli K12 BW 25113 with marR deletion (FRT site scar), acrA gene replaced by kanamycin resistance and CRISPRi targeting ivy
NT6232	ΔmarR:: ΔacrB::kan pSB03_2 ivy gRNA	this study	E. coli K12 BW 25113 with marR deletion (FRT site scar), acrB gene replaced by kanamycin resistance and CRISPRi targeting ivy
NT6233	ΔmarR:: ΔompC::kan pSB03_2 ivy gRNA	this study	E. coli K12 BW 25113 with marR deletion (FRT site scar), ompC gene replaced by kanamycin resistance and CRISPRi targeting ivy
NT6234	ΔmarR:: ΔompF::kan pSB03_2 ivy gRNA	this study	E. coli K12 BW 25113 with marR deletion (FRT site scar), ompF gene replaced by kanamycin resistance and CRISPRi targeting ivy
NT6235	ΔmarR:: ΔbacA::kan pSB03_2 ivy gRNA	this study	E. coli K12 BW 25113 with marR deletion (FRT site scar), bacA gene replaced by kanamycin resistance and CRISPRi targeting ivy
NT6236	ΔmarR:: ΔlapA::kan pSB03_2 ivy gRNA	this study	E. coli K12 BW 25113 with marR deletion (FRT site scar), lapA gene replaced by kanamycin resistance and CRISPRi targeting ivy
NT6237	ΔmarR:: ΔldtA::kan pSB03_2 ivy gRNA	this study	E. coli K12 BW 25113 with marR deletion (FRT site scar), ldtA gene replaced by kanamycin resistance and CRISPRi targeting ivy
NT6238	ΔmarR:: ΔlpoA::kan pSB03_2 ivy gRNA	this study	E. coli K12 BW 25113 with marR deletion (FRT site scar), lpoA gene replaced by kanamycin resistance and CRISPRi targeting ivy
NT6239	ΔmarR:: ΔlpoB::kan pSB03_2 ivy gRNA	this study	E. coli K12 BW 25113 with marR deletion (FRT site scar), lpoB gene replaced by kanamycin resistance and CRISPRi targeting ivy
NT6240	ΔmarR:: ΔlpxL::kan pSB03_2 ivy gRNA	this study	E. coli K12 BW 25113 with marR deletion (FRT site scar), lpxL gene replaced by kanamycin resistance and CRISPRi targeting ivy
NT6241	ΔmarR:: ΔlpxT::kan pSB03_2 ivy gRNA	this study	E. coli K12 BW 25113 with marR deletion (FRT site scar), lpxT gene replaced by kanamycin resistance and CRISPRi targeting ivy
NT6242	ΔmarR:: ΔmepK::kan pSB03_2 ivy gRNA	this study	E. coli K12 BW 25113 with marR deletion (FRT site scar), mepK gene replaced by kanamycin resistance and CRISPRi targeting ivy
NT6243	ΔmarR:: ΔmepS::kan pSB03_2 ivy gRNA	this study	E. coli K12 BW 25113 with marR deletion (FRT site scar), mepS gene replaced by kanamycin resistance and CRISPRi targeting ivy
NT6244	ΔmarR:: ΔmlaC::kan pSB03_2 ivy gRNA	this study	E. coli K12 BW 25113 with marR deletion (FRT site scar), mlaC gene replaced by kanamycin resistance and CRISPRi targeting ivy
NT6245	ΔmarR:: ΔmlaE::kan pSB03_2 ivy gRNA	this study	E. coli K12 BW 25113 with marR deletion (FRT site scar), mlaE gene replaced by kanamycin resistance and CRISPRi targeting ivy
NT6246	ΔmarR:: ΔmlaF::kan pSB03_2 ivy gRNA	this study	E. coli K12 BW 25113 with marR deletion (FRT site scar), mlaF gene replaced by kanamycin resistance and CRISPRi targeting ivy
NT6247	ΔmarR:: ΔmltC::kan pSB03_2 ivy gRNA	this study	E. coli K12 BW 25113 with marR deletion (FRT site scar), mltC gene replaced by kanamycin resistance and CRISPRi targeting ivy
NT6248	ΔmarR:: ΔmltF::kan pSB03_2 ivy gRNA	this study	E. coli K12 BW 25113 with marR deletion (FRT site scar), mltF gene replaced by kanamycin resistance and CRISPRi targeting ivy
NT6249	ΔmarR:: Δnlpl::kan pSB03_2 ivy gRNA	this study	E. coli K12 BW 25113 with marR deletion (FRT site scar), nlpI gene replaced by kanamycin resistance and CRISPRi targeting ivy
NT6250	ΔmarR:: ΔompW::kan pSB03_2 ivy gRNA	this study	E. coli K12 BW 25113 with marR deletion (FRT site scar), ompW gene replaced by kanamycin resistance and CRISPRi targeting ivy
NT6251	ΔmarR:: ΔwecA::kan pSB03_2 ivy gRNA	this study	E. coli K12 BW 25113 with marR deletion (FRT site scar), wecA gene replaced by kanamycin resistance and CRISPRi targeting ivy
NT6252	ΔmarR:: ΔwecC::kan pSB03_2 ivy gRNA	this study	E. coli K12 BW 25113 with marR deletion (FRT site scar), wecC gene replaced by kanamycin resistance and CRISPRi targeting ivy
NT6253	ΔmarR:: ΔwecE::kan pSB03_2 ivy gRNA	this study	E. coli K12 BW 25113 with marR deletion (FRT site scar), wecE gene replaced by kanamycin resistance and CRISPRi targeting ivy
NT6254	ΔmarR:: Δslt::kan pSB03_2 ivy gRNA	this study	E. coli K12 BW 25113 with marR deletion (FRT site scar), slt gene replaced by kanamycin resistance and CRISPRi targeting ivy
NT6255	ΔmarR:: ΔuidB::kan pSB03_2 ivy gRNA	this study	E. coli K12 BW 25113 with marR deletion (FRT site scar), uidB gene replaced by kanamycin resistance and CRISPRi targeting ivy
NT6256	ΔmarR:: ΔuidC::kan pSB03_2 ivy gRNA	this study	E. coli K12 BW 25113 with marR deletion (FRT site scar), uidC gene replaced by kanamycin resistance and CRISPRi targeting ivy
NT6257	ΔmarR:: ΔytfK::kan pSB03_2 ivy gRNA	this study	E. coli K12 BW 25113 with marR deletion (FRT site scar), ytfK gene replaced by kanamycin resistance and CRISPRi targeting ivy

Strains	Genotype	Source or Reference	Description
E. coli K12 BW 25113			
NT6258	ΔompR::ΔtolC::kan pSB03_2 ivy gRNA	this study	E. coli K12 BW 25113 with ompR deletion (FRT site scar), tolC gene replaced by kanamycin resistance and CRISPRi targeting ivy
NT6259	ΔompR::ΔacrA::kan pSB03_2 ivy gRNA	this study	E. coli K12 BW 25113 with ompR deletion (FRT site scar), acrA gene replaced by kanamycin resistance and CRISPRi targeting ivy
NT6260	ΔompR::ΔacrB::kan pSB03_2 ivy gRNA	this study	E. coli K12 BW 25113 with ompR deletion (FRT site scar), acrB gene replaced by kanamycin resistance and CRISPRi targeting ivy
NT6261	ΔompR::ΔompC::kan pSB03_2 ivy gRNA	this study	E. coli K12 BW 25113 with ompR deletion (FRT site scar), ompC gene replaced by kanamycin resistance and CRISPRi targeting ivy
NT6262	ΔompR::ΔompF::kan pSB03_2 ivy gRNA	this study	E. coli K12 BW 25113 with ompR deletion (FRT site scar), ompF gene replaced by kanamycin resistance and CRISPRi targeting ivy
NT6263	ΔompR::ΔbacA::kan pSB03_2 ivy gRNA	this study	E. coli K12 BW 25113 with ompR deletion (FRT site scar), bacA gene replaced by kanamycin resistance and CRISPRi targeting ivy
NT6264	ΔompR::ΔlapA::kan pSB03_2 ivy gRNA	this study	E. coli K12 BW 25113 with ompR deletion (FRT site scar), lapA gene replaced by kanamycin resistance and CRISPRi targeting ivy
NT6265	ΔompR::ΔldtA::kan pSB03_2 ivy gRNA	this study	E. coli K12 BW 25113 with ompR deletion (FRT site scar), ldtA gene replaced by kanamycin resistance and CRISPRi targeting ivy
NT6266	ΔompR::ΔlpoA::kan pSB03_2 ivy gRNA	this study	E. coli K12 BW 25113 with ompR deletion (FRT site scar), lpoA gene replaced by kanamycin resistance and CRISPRi targeting ivy
NT6267	ΔompR::ΔlpoB::kan pSB03_2 ivy gRNA	this study	E. coli K12 BW 25113 with ompR deletion (FRT site scar), lpoB gene replaced by kanamycin resistance and CRISPRi targeting ivy
NT6268	ΔompR::ΔlpxL::kan pSB03_2 ivy gRNA	this study	E. coli K12 BW 25113 with ompR deletion (FRT site scar), lpxL gene replaced by kanamycin resistance and CRISPRi targeting ivy
NT6269	ΔompR::ΔlpxT::kan pSB03_2 ivy gRNA	this study	E. coli K12 BW 25113 with ompR deletion (FRT site scar), lpxT gene replaced by kanamycin resistance and CRISPRi targeting ivy
NT6270	ΔompR::ΔmepK::kan pSB03_2 ivy gRNA	this study	E. coli K12 BW 25113 with ompR deletion (FRT site scar), mepK gene replaced by kanamycin resistance and CRISPRi targeting ivy
NT6271	ΔompR::ΔmepS::kan pSB03_2 ivy gRNA	this study	E. coli K12 BW 25113 with ompR deletion (FRT site scar), mepS gene replaced by kanamycin resistance and CRISPRi targeting ivy
NT6272	ΔompR::ΔmlaC::kan pSB03_2 ivy gRNA	this study	E. coli K12 BW 25113 with ompR deletion (FRT site scar), mlaC gene replaced by kanamycin resistance and CRISPRi targeting ivy
NT6273	ΔompR::ΔmlaE::kan pSB03_2 ivy gRNA	this study	E. coli K12 BW 25113 with ompR deletion (FRT site scar), mlaE gene replaced by kanamycin resistance and CRISPRi targeting ivy
NT6274	ΔompR::ΔmlaF::kan pSB03_2 ivy gRNA	this study	E. coli K12 BW 25113 with ompR deletion (FRT site scar), mlaF gene replaced by kanamycin resistance and CRISPRi targeting ivy
NT6275	ΔompR::ΔmltC::kan pSB03_2 ivy gRNA	this study	E. coli K12 BW 25113 with ompR deletion (FRT site scar), mltC gene replaced by kanamycin resistance and CRISPRi targeting ivy
NT6276	ΔompR::ΔmltF::kan pSB03_2 ivy gRNA	this study	E. coli K12 BW 25113 with ompR deletion (FRT site scar), mltF gene replaced by kanamycin resistance and CRISPRi targeting ivy
NT6277	ΔompR::Δnlpl::kan pSB03_2 ivy gRNA	this study	E. coli K12 BW 25113 with ompR deletion (FRT site scar), nlpI gene replaced by kanamycin resistance and CRISPRi targeting ivy
NT6278	ΔompR::ΔompW::kan pSB03_2 ivy gRNA	this study	E. coli K12 BW 25113 with ompR deletion (FRT site scar), ompW gene replaced by kanamycin resistance and CRISPRi targeting ivy
NT6279	ΔompR::ΔwecA::kan pSB03_2 ivy gRNA	this study	E. coli K12 BW 25113 with ompR deletion (FRT site scar), wecA gene replaced by kanamycin resistance and CRISPRi targeting ivy
NT6280	ΔompR::ΔwecC::kan pSB03_2 ivy gRNA	this study	E. coli K12 BW 25113 with ompR deletion (FRT site scar), wecC gene replaced by kanamycin resistance and CRISPRi targeting ivy
NT6281	ΔompR::ΔwecE::kan pSB03_2 ivy gRNA	this study	E. coli K12 BW 25113 with ompR deletion (FRT site scar), wecE gene replaced by kanamycin resistance and CRISPRi targeting ivy
NT6282	ΔompR::Δslt::kan pSB03_2 ivy gRNA	this study	E. coli K12 BW 25113 with ompR deletion (FRT site scar), slt gene replaced by kanamycin resistance and CRISPRi targeting ivy
NT6283	ΔompR::ΔuidB::kan pSB03_2 ivy gRNA	this study	E. coli K12 BW 25113 with ompR deletion (FRT site scar), uidB gene replaced by kanamycin resistance and CRISPRi targeting ivy
NT6284	ΔompR::ΔuidC::kan pSB03_2 ivy gRNA	this study	E. coli K12 BW 25113 with ompR deletion (FRT site scar), uidC gene replaced by kanamycin resistance and CRISPRi targeting ivy
NT6285	ΔompR::ΔytfK::kan pSB03_2 ivy gRNA	this study	E. coli K12 BW 25113 with ompR deletion (FRT site scar), ytfK gene replaced by kanamycin resistance and CRISPRi targeting ivy

3. Bacterial growth conditions

Unless indicated otherwise, *E. coli* was grown in LB Lennox liquid media or on LB-agar plates at 37 °C. LB Lennox liquid media and LB agar plates were prepared by the EMBL media kitchen. For selection conditions, the antibiotic and concentration are indicated. Standard concentrations used on plates and in liquid cultures were 100 µg/ml ampicillin, 10-20 µg/ml chloramphenicol, 100 µg/ml spectinomycin, and 50 µg/ml kanamycin. For storage, bacterial stocks were grown overnight and stored at -80 °C in the presence of 20 % glycerol. Liquid cultures were inoculated from single colonies after streaking out from the glycerol stock on LB plates with or without selection. On plates, strains were stored at 4 °C for up to 1 week maximum. Antibiotics and other chemicals were purchased from Sigma, except for cefotaxime (MP Biomedicals). Stocks were prepared according to the supplier's recommendations, using water as the preferred solvent, and kept at -30 °C until used.

4. Electroporation

To create electrocompetent cells, an overnight culture was diluted 1:100 into 50 ml LB and grown for 2-3 h while shaking at 150 rpm in the incubator at 37 °C to reach the exponential phase (OD 0.2 - 0.4). The culture was centrifuged at 4,000 rpm and 4 °C for 10 minutes, and the supernatant was discarded. This procedure was repeated 3 times with 20 ml ice cold water containing 10 % glycerol on ice to wash the cells. After the last wash, the cells were resuspended in 550 µl water with 10 % glycerol and split into 5 Eppendorf tubes containing 100 µl each.

In the next step, 0.2 µl of plasmid were added to each tube and kept on ice for 5 minutes. The whole 100 µl of cells with plasmid were transferred into a pre-cooled electroporation cuvette (0.1 cm electrode gap, BioRad, cat. nr. 1652089) and electroporated with 1.8 kV for 5 ms using a BioRad GenePulser Xcell electroporator. Using a glass Pasteur pipette, 1 ml LB Lennox media was added immediately, the suspension was transferred into a glass tube and grown for 1 h while rolling at 37 °C. The culture was then plated onto agar plates containing the appropriate antibiotic corresponding to the electroporated plasmid and grown overnight at 37 °C.

5. Transforming non-competent cells using Transformation and Storage Solution (TSS)

To prepare 200 ml of 2x TSS buffer, 20 mg of PEG 8000 and 5 ml of 1 M $MgCl_2$ were added to 190 ml of LB Lennox media. After filter sterilizing using a 0.22 µm filter (Merck, cat. nr. SLMP025SS), 10 ml of DMSO were added. To grow the recipient cells, single colonies were used to inoculate 2 ml of LB Lennox media. Cells were grown while rolling at 37 °C until the culture was slightly turbid and in exponential phase (OD 0.2 – 0.4). In a pre-cooled Eppendorf tube, 200 µl of the recipient culture were mixed with 200 µl of 2x TSS buffer and 0.5 µl of plasmid on ice. After 30 minutes of incubation on ice, cells were transferred to 37 °C while rolling for 1 hour. The culture was then plated onto agar plates containing the appropriate antibiotic corresponding to the transformed plasmid and grown overnight at 37 °C.

6. P1 phage transduction

6.1. Preparation of the P1 lysate

The donor strain was streaked out on a plate, and a single colony was used to inoculate 5 ml of LB Lennox media. After overnight growth rolling at 37 °C, the culture was diluted 1:100 into fresh 5 ml of LB Lennox media and grown until the culture was slightly turbid (OD 0.3 – 0.8) rolling at 37 °C. Using a glass Pasteur pipette, 1 drop of $CaCl_2$ and 2 drops of P1 lysate were added. The P1 lysate added should be a lysis product from the used wildtype strain, which was *E. coli* K12 BW 25113 here. Lysis was performed between 2-8 hours and was indicated by debris at the walls of the glass tube and an opaque culture. In the next step, the P1-lysed culture was transferred to a 15 ml Falcon tube, 400 µl of chloroform were added, and the tube was vortexed for 30 seconds. The lysate was centrifuged at 4,000 rpm for 10 minutes, transferred

into a fresh 15 ml Falcon tube, 100 µl of chloroform were added, the tube was vortexed for 15 seconds and stored at 4 °C.

6.2. P1 transduction

First, the transduction recipient was streaked out, and a single colony was used to inoculate 5 ml of LB Lennox media for overnight growth while rolling at 37 °C. The culture was transferred to a 15 ml Falcon tube and centrifuged at 4,000 rpm for 10 minutes. The supernatant was discarded, and the pellet was resuspended in 2 ml of LB Lennox media containing 10 mM of $MgSO_4$ and 5 mM of $CaCl_2$. Next, 200 µl of the cell suspension were transferred into a glass tube, and 2 drops of undiluted P1 lysate were added using a glass Pasteur pipette. The culture was grown for 30 mins while rolling at 37 °C, after which 200 µl of 1 M Sodium Citrate and 600 µl of 2x YT medium were added. After 1 h rolling at 37 °C, the transduction volume was plated onto agar plates containing the appropriate antibiotic corresponding to the transduced resistance marker and grown overnight at 37 °C. For P1 transductions of KEIO gene deletion mutants, plates contained 50 µg/ml kanamycin, and the replacement of genes by the kanamycin resistance cassette was confirmed using PCR.

7. Flip out the Kanamycin resistance cassette using pCP20

To remove the Kanamycin resistance cassette flanked by FRT (FLP recognition target) sites from KEIO gene deletion mutants (Baba et al. 2006; Yamamoto et al. 2009), the pCP20 plasmid encoding a FLP recombinase was used as described before (Datsenko & Wanner 2000). The plasmid pCP20 carrying both ampicillin and chloramphenicol resistance was transformed into the strain of interest using TSS transformation. The cells were grown for 1 h in LB Lennox media while rolling at 30 °C and plated onto agar plates containing 100 µg/ml of ampicillin or 10 µg/ml of chloramphenicol. After overnight growth at 30 °C, the plate was moved to 42 °C for 2-4 hours. Colonies were restreaked on non-selective plates and grown overnight at 37 °C. Using the same tip, multiple colonies were picked and streaked on a kanamycin (50 µg/ml), an ampicillin (100 µg/ml), or chloramphenicol (10 µg/ml) plates and used to inoculate 5 ml of LB Lennox media without selection for overnight growth rolling at 37 °C. A glycerol stock was created from the colonies that were kanamycin and ampicillin/chloramphenicol sensitive. Removal of the kanamycin resistance cassette was confirmed using PCR, and allowed the deletion of a second gene using P1 transduction by kanamycin selection.

8. High-throughput experimental evolution 384-well plates

8.1. Pilot experiments

For the first pilot experiment comparing resistance evolution across different antibiotics, wildtype and *dnaK* KO mutants were streaked out on an LB agar plate, grown overnight at 37 °C and single colonies were used to inoculate different rows of 384-deep well plate (384-Well Deep Well Polypropylene Microplate, Greiner) with 150 µl Mueller-Hinton Broth (MHB) (Merck, cat. no. 70192) per well. A Biomek FXP or i5 liquid handler (Beckman Coulter) was used for all liquid transfers of 96- or 384-well plates. After 24 h of growth shaking with 600 rpm at 37 °C, cultures were transferred using a 1:25 dilution into a new plate containing 0.5x MIC of 18 different antibiotics across different columns. Within the same transfer, cultures were transferred into a shallow 384-well plate (Microplate, 384 well, PS, F-Bottom, Greiner) at $OD_{595\ nm}$ was measured (infinite M1000Pro plate reader, Tecan). After growth in 0.5x MIC, cultures were transferred into 384-deep well plates containing 2x and 3x increases of the used antibiotics with transfer and $OD_{595\ nm}$ measurement every day for several days.

For the pilot experiment to assess different plates and dilution factors, wildtype and 8 to 10 single gene KO mutants were streaked out on an LB agar plate, grown overnight at 37 °C and single colonies were used to inoculate different rows of a 96-deep well plate (Nunc 96 DeepWell plate, Sigma) and a 384-deep well plate. After growth for 24 h, while shaking at 600 rpm at 37 °C, both 96-well plates and 384-well plates were evolved using 2x and 3x antibiotic increases starting at 0.5x MIC of either cefotaxime or ciprofloxacin and 1:25 and 1:100 dilutions into fresh media every 24 h. $OD_{595\ nm}$ was measured after every transfer in a shallow 384-well plate (infinite M1000Pro plate reader, Tecan).

8.2. Main screen

For the main screen, 2 384-well KEIO plates were taken from -80 °C, thawed completely, centrifuged at 400 rpm for 2 minutes, and pinned with long 384-well pins (RePads replicate pins, Singer Instruments) onto LB-agar plates (PlusPlates, Singer Instruments) containing 50 µg/ml kanamycin using a Singer Rotor (Singer Instruments), followed by overnight growth at 37 °C. Colonies were used to inoculate 384-well plates containing 150 µl of MHB with 4-8 replicates per plate. Plates were sealed (AeraSeal, Sigma), centrifuged at 600 rpm for 2 minutes, and grown for 24 h while shaking at 600 rpm at 37 °C. After 24 h of growth, plates were centrifuged again at 600 rpm for 2 minutes, the seal was removed, and cultures were

transferred into fresh media using a 1:25 dilution. After 24 h of growth twice, cultures were transferred using a 3-fold antibiotic increase every day starting at 0.5x MIC of cefotaxime. The $OD_{595\ nm}$ was measured after every transfer using shallow 384-well plates. The first three 384-well plates (1, 3, and 5) were grown only once without cefotaxime before the second day of growth without the drug was added to the protocol for the remaining plates. For plate 1, only 4 replicates were used before two more replicates were added for all following plates. For plate 7, 4 replicates were used from each of two different library stocks and merged to a sum of 8 replicates.

8.3. Data analysis

Fitness, sensitivity, and evolvability were calculated using the background-subtracted yield quantified by $OD_{595\ nm}$. Fitness was calculated from the yield without the drug (day 1) and sensitivity from the yield in the presence of 0.5x MIC of cefotaxime (day 2) relative to the yield without cefotaxime (day 1), both relative to all other mutants of their respective plate. Medians were multiplicatively adjusted in no drug, 0.5x, and 1.5x MIC across plates. Mutants with lower evolvability were identified by comparing $OD_{595\ nm}$ at 1.5x MIC (day 3) with all other mutants of their plate, and mutants with higher evolvability by comparing growth at 1.5x MIC (day 3) and 13.5x MIC (day 5) with all other mutants of their plate. Effect sizes, $\log_2$(fold-change) (L2FC), and significance were calculated from $OD_{595\ nm}$ of all replicates for each mutant relative to its respective plate using a BH-adjusted non-parametric Wilcoxon signed-rank test due to the non-normality of the individual plates' OD distribution. The L2FC was multiplicatively scaled across all plates for day 3 to have the same standard deviation. The replicate correlation per day across all tested KEIO plates was calculated by the Pearson correlation of each replicate with all other replicates per mutant.

To identify evolvability genes with decreased evolvability, genes that displayed fitness or sensitivity lower than 0.75 were filtered out. As additional chemical genetics filtering steps, seven KEIO library mutants that contain potential compensatory mutations based on our lab database were filtered out. The stringency of our sensitivity cut-off was confirmed by testing that none of the evolvability genes after filtering displayed large negative chemical genetics scores (< -2 standard deviations) for cefoxitin and ceftazidime, two compounds from a similar drug class as cefotaxime (Nichols et al. 2011). An effect size cut-off was applied for the evolvability using L2FC lower than -0.5 to prioritize evolvability genes with the highest effect

sizes. To identify genes with increased evolvability, genes with sensitivity higher than 1.25 were filtered out, and an effect size cut-off of L2FC higher than 0.5 was applied.

9. High-throughput experimental evolution 96-well plates

9.1. Validation

Out of 248 genes identified by the screen, literature, gene ontology, protein complex, and functional information were used to select 33 functionally diverse evolvability genes for validation. For the validation experiment, experimental evolution was performed using two independent KEIO library stocks with 8 replicates each in 1 ml volume and 96-deep well plates shaking with 600 rpm at 37 °C for 24 h while keeping the concentrations steps and the 1:25 dilution used in the main screen. Evolvability genes were labeled as validated when both KEIO clones displayed a lower yield than the wildtype (*padj.* < 0.01) determined by BH-adjusted Wilcoxon signed-rank test at 4.5x MIC, based on the highest concentration at which the wildtype still grew to high yield. In addition, cefotaxime MICs were determined for each of these 33 gene KOs. For the MIC test, all mutants were grown in 30 µl MHB media per well using a 384 shallow well plate and 0.01 as a starting $OD_{595\ nm}$ while shaking at 800 rpm and 37 °C for 24 h (infinite M1000Pro plate reader, Tecan). The MIC was determined as the lowest concentration where the background-subtracted yield was below 0.1 after 9 hours of growth. The gene ontology enrichment was calculated using a BH-adjusted Fisher's exact test.

9.2. Delay resistance evolution with drugs

To identify cefotaxime evolution inhibitors, several small molecules were selected using different hypothesis-driven approaches and tested for their ability to delay cefotaxime resistance evolution. To probe perturbed OM function against hydrophobic molecules, vancomycin and the macrolide clarithromycin were selected. Polymyxin B was included since it targets LPS in the inner and outer membranes. Mecillinam, erythromycin, clarithromycin, vancomycin, and polymyxin B were chosen based on the increased resistance in KOs of several *mla* genes in available chemical genetics data (Nichols et al. 2011). The remaining compounds were chosen based on high S-scores with evolvability genes (Nichols et al. 2011), procaine based on *hycG* and *dacA*, cefsulodin and trimethoprim based on *pbpG* and sulfamethizole based on *chaB*. For all drugs, several concentrations were tested with the cefotaxime experimental evolution protocol used for the validation in 96-well plates while adding the extra drug starting at 0.5x MIC cefotaxime.

By comparing sensitivity, *i.e.*, growth in the presence of 0.5x MIC of cefotaxime divided by growth without drug, drug concentrations with similar sensitivity (at least 75%) as only in the presence of 0.5x MIC of cefotaxime without extra drug were chosen. The two runs originated from data acquired by two different plate readers (infinite M1000Pro plate reader, Tecan and BioTek Synergy H1, Agilent), explaining the difference in the wildtype baseline. Drugs delaying resistance evolution were identified by BH-adjusted Wilcoxon signed-rank test relative to the wildtype of their respective run at 4.5x MIC based on $OD_{595\ nm}$, while multiple testing correction was performed, including all tests of both runs.

9.3. Multi-drug resistance evolution of evolvability genes

9 gene KOs with decreased evolvability identified by the screen and confirmed by the validation experiment were selected based on diverse biological processes and functions. These KO mutants were evolved in 8 replicates against 12 antibiotics targeting different processes with an emphasis on different cell wall targeting compounds. Antibiotics resistance was evolved in 1 ml and 96-well plates with 1:25 bottleneck, shaking with 600 rpm at 37 °C for 24 h and the same resistance steps as for cefotaxime (media, media, 0.5x, 1.5x, 4.5x and 13.5x MIC). Evolvability was assessed by BH-adjusted Wilcoxon signed-rank test based on $OD_{595\ nm}$ relative to the wildtype at 1.5x MIC except for cefsulodin and piperacillin at 4.5x MIC, depending on the highest concentration at which the wildtype still grew to high yield.

10. Whole genome sequencing of bacterial mutants

To determine the types of mutations selected under our resistance evolution conditions, 44 individual lineages were selected out of 32 wildtype populations that evolved resistance against cefotaxime in 96-well plates after growth in 4.5x MIC at day 4, taken from the aforementioned validation experiment. The colony-purified lineages after overnight growth rolling at 37 °C were frozen in glycerol stocks. Their MICs were determined on plates containing 0, 1, 2, and 3x MIC of cefotaxime, and genomic DNA was extracted for Illumina sequencing and SNP calling using a genomic DNA extraction kit (Zymo Research), followed by library preparation using the in-house EMBL tagmentation workflow. SNP calling was performed using both (Deatherage & Barrick 2014) and QIAGEN GLC Genomics workbench.

11. Epistatic interaction measurement using CRISPRi

11.1. Plasmid construction

To quantify genetic interactions, an inducible, titratable, and conjugatable CRISPRi plasmid for the targeted knockdown of genes in *E. coli* was constructed by combining components of a system previously used in the lab (Mateus et al. 2020). The chromosomal dCas9 expression cassette using a catalytically inactive version of Cas9 controlled by a TetR repressor driven by a strong *proB* promoter (Qi et al. 2013) was cloned from a published strain (Lawson et al. 2017; Mateus et al. 2020) and combined with the guide RNA scaffold (42 nt Cas9 handle, 20 nt target-specific complementary region and 40 nt transcription terminator from *S. pyogenes*) from the pgRNA plasmid (Qi et al. 2013) on the plasmid backbone pJB37 previously used in the lab (Bobonis et al. 2022) *via* Gibson assembly (Gibson et al. 2009). The system includes a pSC101 origin of replication (~ 5 copies per cell), a spectinomycin resistance cassette, an F-based origin of transfer for conjugation, and a *proB* promoter driving expression of an aTc inducible repressor *tetR-tetO* controlling dCas9 expression (Rogers et al. 2015).

To use BsaI restriction enzyme-mediated Golden Gate cloning (Engler et al. 2008) for integrating new 20 bp guide RNAs (gRNA) conferring CRISPRi specificity into the plasmid, I had to remove two additional BsaI cutting sides from the plasmid by Gibson assembly. Since one of the additional BsaI sides was located inside the *proB* promotor (Davis et al. 2011) driving the expression of tetR (Rogers et al. 2015), I constructed two single point mutations (pSB03_1 and pSB03_2) to remove the BsaI site and tested them for their functional impact on dCas9 repression *via* tetR using different levels of anhydrotetracycline induction.

In order to use *BsaI* restriction enzyme-mediated Golden Gate cloning (Engler et al. 2008) for integrating new 20 bp gRNA conferring CRISPRi specificity into the plasmid, two additional *BsaI* cutting sides were removed from the plasmid by Gibson assembly in two consecutive rounds of cloning. Since the second additional *BsaI* side was located inside the *proB* promotor (Davis et al. 2011) driving the expression of *tetR* (Rogers et al. 2015), two single point mutations (pSB03_1 and pSB03_2) were constructed that removed the *BsaI* site and tested for their functional impact on dCas9 repression *via tetR* using different levels of anhydrotetracycline induction.

11.2. Adding new guide RNAs using Golden Gate

New gRNAs were selected based on existing data containing several guides for every *E. coli* gene (Rousset et al. 2021). To this 20 nt target sequence complementary to the non-template strand of the targeted gene, the Golden Gate site (4 nt), a BsaI site (7 nt), and 10 extra bases for a better hold were added, and the oligo was ordered both in forward and reverse direction. The two single strains were made into a double strand by PCR, the PCR product was purified (PCR Purification Kit, Qiagen) and cloned into the plasmid pSB03_2 at a 7:1 ratio. Golden Gate cloning with T4 DNA ligase (NEB) and BsaI-HF-v2 (NEB) in T4 DNA ligase buffer (NEB) (Engler et al. 2008) was used, thereby replacing 20 bp scrambled target sequence in PSB03_2 including the BsaI sites. The Golden Gate reaction was performed for 2 hours at 37 °C, followed by 5 minutes at 60 °C. 5 µl of the Golden Gate reaction were directly added to the TSS transformation mix containing 200 µl of exponential phase cells and 200 µl of 2x TSS buffer on ice, followed by plating on spectinomycin plates (100 µg/ml) and growth overnight at 37 °C.

11.3. Quantifying gene-gene and gene-gene-drug interactions

To quantify gene-gene and gene-gene-drug interactions between a gene KO and KD in the absence or presence of cefotaxime, the CRISPRi plasmid for targeted KD of the gene of interest was transformed into the KO strains of interest using TSS transformation. The growth of the KO mutants carrying the respective plasmid was measured in the absence or presence of cefotaxime and 0, 150, 300, or 450 ng/ml aTc to induce the CRISPRi system on the plasmid. Growth curves were acquired in 30 µl MHB media using shallow 384-well plates while shaking at 800 rpm and 37 °C and a 1:1000 dilution of an $OD_{595\ nm}$ of 0.01 as a starting OD to ensure depletion of the remaining mRNA and protein.

Gene-gene interactions in the presence and absence of cefotaxime were quantified using the Bliss independence model (Bliss 1939). All growth curves were trimmed at the time point where the untreated wildtype reached the highest $OD_{595\ nm}$, and fitness was determined by the AUC relative to the untreated wildtype AUC without drug and induction. The Bliss interaction score of a mutant carrying a CRISPRi plasmid in the presence of a drug was calculated by the fitness of the respective mutant in the presence of drug and inducer ($f_{mutant_gene(_drug)}$) minus the fitness of the wildtype in the presence of drug and inducer ($f_{wt_gene(_drug)}$) multiplied by the fitness of the untreated mutant in the presence of drug and without inducer ($f_{mutant(_drug)}$).

$$\varepsilon = f_{mutant_gene(_drug)} - f_{wt_gene(_drug)} \, x \, f_{mutant(_drug)}$$

9 interaction scores were calculated between each of the three replicates of mutant and wildtype, respectively. The significance of the CRISPRi-induced epistasis was assessed by comparing these Bliss interaction scores with 450 ng/ml aTc and without inducer for every strain, plasmid, and drug concentration using the BH-adjusted Wilcoxon signed-rank test. Since the wildtype MIC is at 0.032 µl/ml, meaning the wildtype does not grow at this concentration, the interaction term becomes 0, and the Bliss score then only quantified the fitness of the mutant carrying the plasmid in the presence of cefotaxime with and without inducer. Even though Bliss scores are out of the dynamics range if the interaction term becomes 0, it still represented a useful quantification of the decrease in resistance levels upon CRISPRi induction.

11.4. Quantifying gene-gene-gene interactions

The same method was used to measure gene-gene interactions in evolved cefotaxime-resistant mutants and in double KOs of *marR* with 17 other gene deletions to quantify whether the absence of these additional genes affected the gene-gene interaction between *dpaA* KD and *marR* KO. Those double KOs were created by flipping out the kanamycin resistance cassette using pCP20, deleting the additional gene by P1 transduction, and conjugating the CRISPRi plasmid into all double mutants using high-throughput conjugation. This was performed by TSS transformation of the CRISPRi plasmid into the conjugation donor BW25113 pseudoHfr::(trp bla (-)) (Typas et al. 2008), spreading the conjugation donor on a rectangular agar plate, pinning all double mutants on top, and performing conjugation followed by double selection on kanamycin (50 µg/ml) and spectinomycin (100 µg/ml). The process is described in more detail in Chapter VI 14.1.

Bliss scores were calculated as for the *dpaA* KD in the *marR* KO background in the absence of the antibiotic, with the difference being that the Bliss score without inducer was subtracted from the Bliss score with inducer. This calculates the change in Bliss score upon CRISPRi induction and DpaA depletion in every *marR* double KO mutant, which was then compared with the *marR* single KO mutant to answer the question of whether the *marR dpaA* gene-gene interaction was altered in the absence of an extra gene. This analysis should already account for potential interactions between the extra gene deletion and the *marR* KO.

More specifically, I trimmed all growth curves at the time point where the untreated wildtype reached the highest $OD_{595\ nm}$ and determined the fitness by the area under the curve (AUC) relative to the AUC of the wildtype without induction. I calculated the Bliss interaction score of a mutant (single or double KO) carrying a CRISPRi plasmid by the fitness of the respective mutant with inducer ($f_{mutant_drug_gene}$) minus the fitness of the wildtype with inducer ($f_{wt_drug_gene}$) multiplied by the fitness of the mutant without inducer (f_{mutant}).

$$\Delta\varepsilon = (f_{mutant_gene_induced} - f_{wt_gene_induced}\, x\, f_{mutant_uninduced}) - (f_{mutant_gene_uninduced} - f_{wt_gene_uninduced}\, x\, f_{mutant_uninduced})$$

Since I used three replicates for both mutant and wildtype, I calculated nine interaction scores between each replicate of mutant and wildtype, respectively. I subtracted Bliss scores without induction from the Bliss scores with induction to arrive at the change in Bliss score upon CRISPRi induction and DpaA depletion. I assessed the significance by comparing the change in Bliss score between the *marR* single KO and all *marR* double KOs using the BH-adjusted Wilcoxon signed-rank test.

12. High-throughput microscopy using SLIP

12.1. Sample preparation and imaging

The high-throughput imaging protocol SLIP was used (Shi et al. 2017) to acquire live images to identify abnormalities during growth and cell division in the absence and presence of antibiotics. After overnight growth of all strains shaking with 180 rpm at 37 °C, they were diluted to an $OD_{595\ nm}$ of 0.01 and added to a 96-well plate (Nunc 96 well plate, Sigma). These cultures at $OD_{595\ nm}$ of 0.01 were used for live imaging in the exponential phase in the presence or absence of antibiotics. Phase-contrast images were acquired using the SLIP hardware (Ti-E inverted microscope (Nikon Instruments) using a 100X (NA 1.40) oil immersion objective, motorized *xy* stage controller (Applied Scientific Instrumentation) and a Zyla sCMOS camera (Andor Technology)), and software (μManager v.1.4, MATLAB R2014b (MathWorks)) (Shi et al. 2017; Arjes et al. 2022; Edelstein et al. 2010).

For live imaging, the cultures at $OD_{595\ nm}$ of 0.01 were further diluted 1:5, manually pinned on an MHB-agar plate with or without antibiotic poured and solidified on the back of a rectangular

plate (PlusPlates, Singer Instruments) using long-pins (RePads replicate pins, Singer Instruments). After drying the cultures, a rectangular glass cover slip was added on top, and the edges between the coverslip and agar were sealed using VELAB. For live imaging, up to 20 strains were grown on an MHB agar plate in a pre-heated microscope chamber by taking 25 locations per position/well, resulting in 500 images every 5 minutes over the course of 3-4 hours.

13. Mass-spectrometry based proteomics

For the proteomics measurement, single colonies of each mutant were grown in 5 ml MHB until approximately $OD_{595\ nm}$ of 0.5 while rolling at 37 °C and pelleted at 4,000 g for 10 minutes. The supernatant was removed, and the pellet resuspended in PBS. After a second centrifugation at 4,000 g for 10 minutes and removal of the supernatant, the pellets were frozen at -30 °C. Proteomics sample preparation, measurement, and data analysis of protein abundances of *E. coli* KOs relative to the wildtype were performed at the EMBL mass spectrometry core facility as previously described (Banzhaf et al. 2020; Mateus et al. 2020).

14. High-throughput epistatic interaction measurement using CRISPRi

14.1. High-throughput conjugation

To conjugate the CRISPRi plasmid into the KEIO library, the CRISPRi plasmid pSB03_2 carrying the *parC*-targeting gRNA or a scrambled gRNA was transformed into the amp-resistant conjugation donor BW25113 pseudoHfr::(trp bla (-)) (Typas et al. 2008) using TSS transformation and selection in ampicillin (100 µg/ml) and spectinomycin (100 µg/ml). The donor was grown overnight in the presence of amp (100 µg/ml) and spec (100 µg/ml) rolling at 37 °C, $OD_{595\ nm}$ was measured in a spectrophotometer and diluted to an $OD_{595\ nm}$ of 1 using pre-warmed LB Lennox medium to a total volume of 5 ml. Next, glass beads were used to spread 200 µl of the conjugation donor carrying the plasmid carrying the *parC*-targeting or scrambled gRNA across 6 rectangular LB-agar plates each. Plates were incubated for 1 hour at 37 °C in an incubator without humidity to allow growth of the donor and drying of the plates.

Each of the 6 KEIO plates in 1536 format was then pinned onto 3 LB plates, the first with the donor lawn carrying the *parC*-targeting plasmid containing spec (100 µg/ml) and kan (50 µg/ml), the second with the donor lawn carrying the scrambled gRNA plasmid containing spec and kan, and a third without donor used as a growth control later in the workflow containing

only kan. All plates were grown at 37 °C overnight for 12 to 14 h. Each conjugation plate was then replicated onto a new plate containing both spec and kan, followed by overnight growth at 37 °C for 12 to 14h. The selection step was repeated once more. After the second selection, each plate was pinned onto a plate containing spec, kan, and 10 ng/ml of aTc, incubated at 37 °C, and images were taken after 14, 18, and 22 h. The KEIO plates without plasmid were pinned onto LB plates, incubated, and imaged using the same time intervals to identify mutants with decreased fitness in the absence of the plasmid.

14.2. Data processing

The images were processed using IRIS (Kritikos et al. 2017) to extract colony size and opacity. To estimate the quality, noise, and biases of the dataset, the Pearson correlation of opacity was calculated across technical (same strain on different plates) and biological replicates (different strains on the same plate), as well as the correlation of opacity with plate position and chromosomal position of the gene KO. The effect size was calculated using $\log_2$(fold-change) and significance (BH-adjusted non-parametric Mann-Whitney-Wilcoxon test) of colony opacity of a single KO mutant in presence of the *parC*-targeting guide divided by the opacity of that mutant carrying a scrambled guide, relative to the median opacity of all genes of the respective plate carrying a *parC*-targeting guide divided by the opacity carrying a scrambled guide. The gene ontology enrichment was calculated using a BH-adjusted Fisher's exact test.

15. Supplementary data

Supplementary Figure 1: Validation of gene deletions with decreased evolvability in large volumes. *Validation data of two independent KEIO library clones with 8 replicates are shown for all tested evolvability gene KO mutants (subset is shown in Figure 9). Antibiotic increases and bottlenecks otherwise mirrored the setup of the genome-wide screen (Figure 7). $Log_2(OD_{595\ nm})$ at 4.5x MIC is shown, and significance was assessed using the BH-adjusted Wilcoxon signed-rank test.*

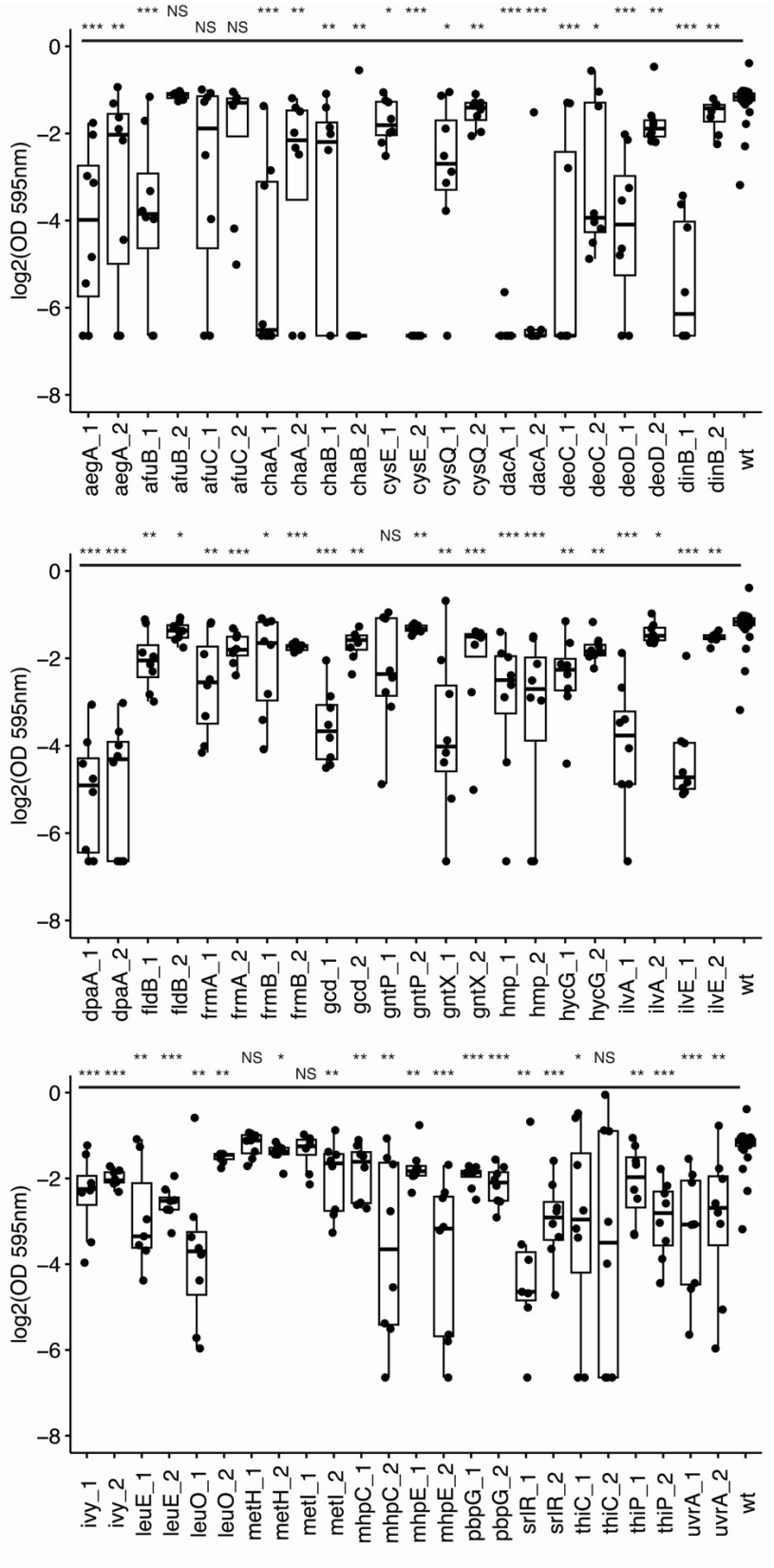

Supplementary Table 1: Top 50 gene KO mutants evolving worse at 1.5x MIC cefotaxime. *Significant hits for worse evolving KO mutants after filtering by relative fitness and relative sensitivity > 0.75 and sorting by log_2(fold-change) at 1.5x MIC. Gene name, relative fitness, sensitivity, relative sensitivity, replicates, KEIO plate, log_2(fold-change) at 1.5x MIC, p-value at 1.5x MIC, padj. at 1.5x MIC, hit calling of decreased or increased evolvability at 1.5x MIC, log_2(fold-change) at 13.5x MIC, p-value at 13.5x MIC, padj. at 13.5x MIC and hit calling of increased evolvability at 13.5x MIC are shown.*

Gene	Relative_Fitness	Sensitivity	Relative_Sensitivity	Replicates	Plate	L2FC_1.5x	pvalue_1.5x	padj_1.5x	Significant_1.5x	L2FC_13.5x	pvalue_13.5x	padj_13.5x	Significant_13.5x
uvrA	0,940	0,768	0,800	6	keio_plate_9	-1,967	6,04E-05	0,00462042	Decreased evolvability	0,000	0,914361681	0,977617912	Not significant
rfaB	1,007	0,907	0,916	6	keio_plate_21	-1,700	0,000277027	0,007122448	Decreased evolvability	0,000	0,376051992	0,755728812	Not significant
yafU	0,988	0,831	0,877	4	keio_plate_7	-1,437	1,17E-05	0,00462042	Decreased evolvability	0,000	0,495994521	0,755728812	Not significant
yjiC	0,973	0,787	0,811	6	keio_plate_9	-1,418	6,66E-05	0,00462042	Decreased evolvability	0,000	0,299629879	0,755728812	Not significant
cyaY	0,969	0,742	0,755	6	keio_plate_9	-1,417	0,000213282	0,006642437	Decreased evolvability	0,000	0,832026023	0,939428449	Not significant
yciA	0,864	0,936	1,105	6	keio_plate_5	-1,410	0,008931321	0,048344948	Decreased evolvability	0,000	0,264367065	0,755728812	Not significant
yihU	1,017	0,804	0,819	6	keio_plate_9	-1,360	5,64E-05	0,00462042	Decreased evolvability	0,000	0,844030083	0,946332581	Not significant
yidL	1,002	0,867	0,847	6	keio_plate_21	-1,356	0,000116031	0,005359588	Decreased evolvability	0,251	0,089508438	0,755728812	Not significant
yhjD	0,978	0,799	0,776	6	keio_plate_9	-1,345	7,07E-05	0,004697992	Decreased evolvability	0,000	0,299629879	0,755728812	Not significant
yfjR	0,900	0,695	0,761	4	keio_plate_7	-1,300	0,001198808	0,015795827	Decreased evolvability	0,000	0,495994521	0,755728812	Not significant
metE	1,086	0,812	0,763	6	keio_plate_11	-1,282	0,000381503	0,008294967	Decreased evolvability	0,000	0,232723133	0,755728812	Not significant
yqcE	0,931	0,808	0,881	6	keio_plate_5	-1,272	0,000158495	0,005681634	Decreased evolvability	0,000	0,552779503	0,755728812	Not significant
dinB	1,021	0,848	0,845	6	keio_plate_13	-1,232	0,005091521	0,035119533	Decreased evolvability	0,000	0,747193546	0,889577951	Not significant
cysQ	0,948	0,975	1,015	6	keio_plate_13	-1,222	7,76E-05	0,004920844	Decreased evolvability	0,000	0,36415569	0,755728812	Not significant
aegA	0,957	0,798	0,845	6	keio_plate_13	-1,222	0,000145879	0,005653755	Decreased evolvability	0,000	0,098617449	0,755728812	Not significant
lysA	1,082	0,808	0,753	6	keio_plate_11	-1,212	0,000702258	0,012079429	Decreased evolvability	0,000	0,232723133	0,755728812	Not significant
yjbB	0,981	0,790	0,794	6	keio_plate_21	-1,203	0,000194141	0,006284356	Decreased evolvability	0,000	0,228734309	0,755728812	Not significant
yafL	0,987	0,898	0,888	4	keio_plate_7	-1,201	4,15E-05	0,00462042	Decreased evolvability	0,000	0,495994521	0,755728812	Not significant
der	0,880	0,699	0,808	6	keio_plate_23	-1,200	0,000910068	0,01375474	Decreased evolvability	0,000	0,857426044	0,953626092	Not significant
ykfB	1,039	0,850	0,814	6	keio_plate_3	-1,192	0,000107634	0,005241946	Decreased evolvability	0,000	0,53325692	0,755728812	Not significant
gspC	1,005	0,799	0,750	6	keio_plate_11	-1,181	0,000341106	0,007770793	Decreased evolvability	0,000	0,948440286	0,990392071	Not significant
fabH	0,775	0,619	0,817	6	keio_plate_13	-1,163	8,41E-05	0,004920844	Decreased evolvability	0,000	0,772987865	0,906893012	Not significant
yhgF	1,013	0,782	0,775	6	keio_plate_15	-1,147	0,000158936	0,005681634	Decreased evolvability	0,000	0,369212922	0,755728812	Not significant
yrdA	1,064	0,807	0,762	6	keio_plate_21	-1,138	0,004149024	0,030899707	Decreased evolvability	0,000	0,944113454	0,989278675	Not significant
yahK	0,982	0,841	0,872	4	keio_plate_7	-1,127	9,77E-05	0,00520662	Decreased evolvability	0,000	0,495994521	0,755728812	Not significant
ivy	1,002	0,982	0,945	4	keio_plate_7	-1,124	3,10E-05	0,00462042	Decreased evolvability	0,000	0,495994521	0,755728812	Not significant
cchB	1,052	0,866	0,841	4	keio_plate_7	-1,116	1,66E-05	0,00462042	Decreased evolvability	0,000	0,495994521	0,755728812	Not significant
ykgD	0,962	1,023	1,037	6	keio_plate_13	-1,113	0,001024771	0,014360884	Decreased evolvability	0,000	0,624084894	0,780533312	Not significant
apt	0,990	0,794	0,816	6	keio_plate_21	-1,097	0,000577652	0,010893252	Decreased evolvability	0,000	0,909533173	0,974811306	Not significant
ompX	1,010	0,943	0,935	6	keio_plate_21	-1,067	0,009449871	0,049997965	Decreased evolvability	0,000	0,228734309	0,755728812	Not significant
yhaM	0,994	0,912	0,942	6	keio_plate_19	-1,064	0,000109638	0,005241946	Decreased evolvability	0,000	0,498780046	0,755728812	Not significant
yjiG	1,107	1,033	0,920	6	keio_plate_9	-1,062	0,000344275	0,007770793	Decreased evolvability	0,000	0,299629879	0,755728812	Not significant
yjgA	1,010	0,804	0,796	6	keio_plate_9	-1,061	0,000190255	0,006207454	Decreased evolvability	0,000	0,299629879	0,755728812	Not significant
nhaA	0,905	0,712	0,820	6	keio_plate_9	-1,058	0,000686136	0,011901714	Decreased evolvability	0,000	0,299629879	0,755728812	Not significant
ycgV	1,172	0,910	0,794	6	keio_plate_5	-1,056	0,000129068	0,005470109	Decreased evolvability	0,000	0,552779503	0,755728812	Not significant
ycjV	0,988	0,858	0,863	6	keio_plate_13	-1,051	0,000567211	0,010795398	Decreased evolvability	0,000	0,36415569	0,755728812	Not significant
yfbH	0,776	0,833	1,065	6	keio_plate_3	-1,050	0,00013755	0,005538206	Decreased evolvability	0,000	0,53325692	0,755728812	Not significant
deoC	1,033	0,821	0,794	6	keio_plate_13	-1,039	0,008547684	0,047167151	Decreased evolvability	0,000	0,757977944	0,896446296	Not significant
mhpC	0,948	0,943	0,996	6	keio_plate_15	-1,035	0,000124509	0,005470109	Decreased evolvability	0,000	0,369212922	0,755728812	Not significant
yceP	0,987	0,829	0,878	6	keio_plate_19	-1,032	0,009186724	0,049047563	Decreased evolvability	0,000	0,498780046	0,755728812	Not significant
afuB	0,977	0,861	0,870	4	keio_plate_7	-1,022	8,65E-05	0,004920844	Decreased evolvability	0,000	0,495994521	0,755728812	Not significant
yfjS	1,043	0,830	0,825	6	keio_plate_21	-1,012	0,002258757	0,021553134	Decreased evolvability	0,000	0,762350603	0,899031362	Not significant
hycG	0,888	0,851	0,908	6	keio_plate_13	-0,999	0,000946611	0,013821373	Decreased evolvability	0,000	0,36415569	0,755728812	Not significant
yaaJ	0,956	0,862	0,917	4	keio_plate_7	-0,998	0,000103854	0,00520662	Decreased evolvability	0,000	0,495994521	0,755728812	Not significant
yafZ	1,030	0,781	0,762	6	keio_plate_3	-0,995	0,002223407	0,021553134	Decreased evolvability	0,000	0,53325692	0,755728812	Not significant
frmB	0,915	0,941	1,020	6	keio_plate_15	-0,990	0,00010301	0,00520662	Decreased evolvability	0,000	0,369212922	0,755728812	Not significant
yaiX	0,981	0,952	0,977	4	keio_plate_7	-0,988	0,000857566	0,013253585	Decreased evolvability	0,000	0,495994521	0,755728812	Not significant
metI	0,989	0,981	0,989	6	keio_plate_19	-0,980	0,000184039	0,006052681	Decreased evolvability	0,000	0,498780046	0,755728812	Not significant
ilvA	0,989	0,808	0,852	6	keio_plate_11	-0,967	0,0002249	0,006848618	Decreased evolvability	0,000	0,971502171	0,998711034	Not significant
yeiQ	0,984	0,959	1,026	4	keio_plate_7	-0,965	0,003115409	0,026145651	Decreased evolvability	0,000	0,495994521	0,755728812	Not significant

Supplementary Table 2: Top 50 gene KO mutants evolving better at 1.5x MIC cefotaxime. *Significant hits for better evolving KO mutants after filtering by relative sensitivity < 1.25 and sorting by log_2(fold-change) at 1.5x MIC. Gene name, relative fitness, sensitivity, relative sensitivity, replicates, KEIO plate, log_2(fold-change) at 1.5x MIC, p-value at 1.5x MIC, padj. at 1.5x MIC, hit calling of decreased or increased evolvability at 1.5x MIC, log_2(fold-change) at 13.5x MIC, p-value at 13.5x MIC, padj. at 13.5x MIC and hit calling of increased evolvability at 13.5x MIC are shown.*

Gene	Relative_Fitness	Sensitivity	Relative_Sensitivity	Replicates	Plate	L2FC_1.5x	pvalue_1.5x	padj_1.5x	Significant_1.5x	L2FC_13.5x	pvalue_13.5x	padj_13.5x	Significant_13.5x
rffD	0,872	0,699	0,802	6	keio_plate_11	2,241	2,65E-05	0,00462042	Increased evolvability	1,034	9,47E-05	0,007483184	Increased evolvability
ybhK	0,871	0,362	0,401	6	keio_plate_5	1,648	2,83E-05	0,00462042	Increased evolvability	0,000	0,264367065	0,755728812	Not significant
ycdB	0,608	0,448	0,743	6	keio_plate_3	1,637	0,000122792	0,005470109	Increased evolvability	0,000	0,003905837	0,129066131	Not significant
yebU	1,074	0,499	0,463	6	keio_plate_19	1,605	0,004035443	0,03027319	Increased evolvability	0,000	0,386629439	0,755728812	Not significant
cbl	0,919	0,485	0,522	4	keio_plate_1	1,580	0,000597012	0,011206915	Increased evolvability	0,208	1,23E-08	3,36E-06	Not significant
yejG	0,757	0,471	0,568	6	keio_plate_3	1,569	0,000963812	0,013853948	Increased evolvability	0,000	0,53325692	0,755728812	Not significant
sapB	0,943	1,099	1,173	6	keio_plate_13	1,556	3,88E-05	0,00462042	Increased evolvability	0,000	0,36415569	0,755728812	Not significant
flgL	0,868	0,888	1,034	6	keio_plate_21	1,553	0,000459029	0,009184884	Increased evolvability	0,000	0,861421718	0,956184033	Not significant
yhjK	1,049	0,656	0,615	6	keio_plate_17	1,545	4,92E-05	0,00462042	Increased evolvability	0,000	0,320458529	0,755728812	Not significant
yjiR	0,934	0,969	1,006	6	keio_plate_9	1,527	4,29E-05	0,00462042	Increased evolvability	0,000	0,163755634	0,755728812	Not significant
yrfA	0,983	0,829	0,857	6	keio_plate_17	1,526	7,20E-05	0,004697992	Increased evolvability	0,000	0,2260386	0,755728812	Not significant
ydcX	0,886	0,678	0,783	6	keio_plate_19	1,505	0,000124642	0,005470109	Increased evolvability	0,000	0,498780046	0,755728812	Not significant
yfjO	0,954	0,846	0,898	6	keio_plate_19	1,502	0,001605072	0,018587185	Increased evolvability	0,000	0,319765584	0,755728812	Not significant
yggS	0,881	0,529	0,624	6	keio_plate_21	1,494	0,001859539	0,019753397	Increased evolvability	0,000	0,849915487	0,948683836	Not significant
malS	1,064	0,901	0,802	6	keio_plate_13	1,491	9,39E-05	0,005148952	Increased evolvability	0,000	0,837240251	0,941421567	Not significant
yggJ	1,098	0,855	0,734	6	keio_plate_15	1,476	3,87E-05	0,00462042	Increased evolvability	0,081	0,00568078	0,158868615	Not significant
rpoN	0,637	0,509	0,873	4	keio_plate_1	1,474	0,000796271	0,012896047	Increased evolvability	0,000	0,102751544	0,755728812	Not significant
yccT	0,576	0,551	0,957	6	keio_plate_5	1,474	4,57E-05	0,00462042	Increased evolvability	0,000	0,552779503	0,755728812	Not significant
yqaC	1,148	0,726	0,643	6	keio_plate_19	1,435	0,000167371	0,005733837	Increased evolvability	0,000	0,391125175	0,755728812	Not significant
yrbE	1,009	1,103	1,062	6	keio_plate_9	1,428	5,27E-05	0,00462042	Increased evolvability	0,000	0,344379673	0,755728812	Not significant
yihS	1,112	0,945	0,859	6	keio_plate_17	1,423	0,004767617	0,033861178	Increased evolvability	0,000	0,156276239	0,755728812	Not significant
ypeC	0,952	0,387	0,388	6	keio_plate_3	1,415	0,00547643	0,036607485	Increased evolvability	0,000	0,53325692	0,755728812	Not significant
yneE	0,999	0,956	0,969	6	keio_plate_19	1,391	0,00023921	0,007025082	Increased evolvability	0,000	0,498780046	0,755728812	Not significant
ycjX	1,030	0,472	0,437	6	keio_plate_5	1,388	0,000150357	0,005670795	Increased evolvability	0,000	0,254639785	0,755728812	Not significant
yrbF	1,078	1,348	1,215	6	keio_plate_15	1,372	4,77E-05	0,00462042	Increased evolvability	0,306	0,00010977	0,008356735	Not significant
manA	1,020	1,174	1,173	6	keio_plate_13	1,352	0,000163174	0,005733407	Increased evolvability	0,629	0,005024343	0,152739587	Not significant
sapC	0,980	0,963	0,914	6	keio_plate_13	1,349	0,000103117	0,00520662	Increased evolvability	0,000	0,36415569	0,755728812	Not significant
narI	1,005	0,800	0,767	6	keio_plate_13	1,347	0,001027025	0,014360884	Increased evolvability	0,000	0,826585115	0,935664621	Not significant
rffM	0,805	0,618	0,740	6	keio_plate_11	1,327	6,74E-05	0,00462042	Increased evolvability	0,000	0,762250899	0,899031362	Not significant
gltP	1,103	0,881	0,805	6	keio_plate_15	1,326	5,19E-05	0,00462042	Increased evolvability	0,000	0,135568466	0,755728812	Not significant
yebV	1,004	0,736	0,772	6	keio_plate_19	1,320	0,000399596	0,008338786	Increased evolvability	0,000	0,498780046	0,755728812	Not significant
galE	1,004	0,916	0,913	6	keio_plate_13	1,319	0,000149194	0,005670795	Increased evolvability	0,000	0,762138493	0,899031362	Not significant
yfgG	0,988	0,842	0,813	6	keio_plate_17	1,305	0,000147154	0,005653755	Increased evolvability	0,000	0,338896597	0,755728812	Not significant
yneI	0,909	1,007	1,072	6	keio_plate_19	1,305	0,000207072	0,006548253	Increased evolvability	0,606	5,15E-05	0,004408925	Increased evolvability
ymfO	1,058	0,380	0,385	6	keio_plate_3	1,295	0,000318464	0,007567662	Increased evolvability	0,000	0,318374356	0,755728812	Not significant
kdsC	0,922	0,847	0,893	6	keio_plate_9	1,291	5,10E-05	0,00462042	Increased evolvability	0,455	0,038685475	0,558021016	Not significant
crr	1,000	1,163	1,239	6	keio_plate_15	1,273	5,95E-05	0,00462042	Increased evolvability	0,000	0,806498478	0,926380342	Not significant
ydhR	0,813	0,335	0,426	6	keio_plate_3	1,273	0,000196073	0,006297313	Increased evolvability	0,000	0,235204359	0,755728812	Not significant
lapB	0,855	0,609	0,741	6	keio_plate_5	1,271	5,95E-05	0,00462042	Increased evolvability	0,846	2,10E-06	0,000331979	Increased evolvability
ygbF	1,019	1,047	1,062	6	keio_plate_19	1,263	0,000393633	0,008302395	Increased evolvability	0,000	0,498780046	0,755728812	Not significant
exo	0,993	0,865	0,874	6	keio_plate_17	1,262	0,003816017	0,029267999	Increased evolvability	0,000	0,186517511	0,755728812	Not significant
ycdK	0,785	0,325	0,427	6	keio_plate_5	1,257	6,62E-05	0,00462042	Increased evolvability	0,000	0,552779503	0,755728812	Not significant
rffA	0,919	0,714	0,842	6	keio_plate_13	1,257	0,00018216	0,006039205	Increased evolvability	0,000	0,36415569	0,755728812	Not significant
ybcK	1,053	0,475	0,464	4	keio_plate_7	1,248	0,00023404	0,007025082	Increased evolvability	0,000	0,40706976	0,755728812	Not significant
ynjA	1,128	0,954	0,843	4	keio_plate_7	1,239	0,000308446	0,007408725	Increased evolvability	0,000	0,020978757	0,3563788	Not significant
intE	1,018	1,057	0,991	6	keio_plate_15	1,234	0,000179002	0,005982745	Increased evolvability	0,000	0,712061664	0,862996904	Not significant
uidC	0,806	0,674	0,864	6	keio_plate_17	1,232	0,000260753	0,007122448	Increased evolvability	0,000	0,3723712	0,755728812	Not significant
ytfK	1,124	1,145	0,996	6	keio_plate_19	1,229	0,00325258	0,02663617	Increased evolvability	0,000	0,498780046	0,755728812	Not significant
ligB	1,019	0,911	0,907	6	keio_plate_17	1,225	0,000128241	0,005470109	Increased evolvability	0,000	0,325948847	0,755728812	Not significant
yjiW	0,930	0,754	0,818	6	keio_plate_21	1,211	0,001976989	0,020420606	Increased evolvability	0,000	0,892484096	0,970378767	Not significant

Supplementary Table 3: Top 50 gene KO mutants evolving better at 13.5x MIC cefotaxime. *Significant hits for better evolving KO mutants after filtering by relative sensitivity < 1.25 and sorting by log_2(fold-change) at 13.5x MIC. Gene name, relative fitness, sensitivity, relative sensitivity, replicates, KEIO plate, log_2(fold-change) at 1.5x MIC, p-value at 1.5x MIC, padj. at 1.5x MIC, hit calling of decreased or increased evolvability at 1.5x MIC, log_2(fold-change) at 13.5x MIC, p-value at 13.5x MIC, padj. at 13.5x MIC and hit calling of increased evolvability at 13.5x MIC are shown.*

Gene	Relative_Fitness	Sensitivity	Relative_Sensitivity	Replicates	Plate	L2FC_1.5x	pvalue_1.5x	padj_1.5x	Significant_1.5x	L2FC_13.5x	pvalue_13.5x	padj_13.5x	Significant_13.5x
yedK	1,113	1,312	1,186	6	keio_plate_5	0,190	0,149626756	0,306943908	Not significant	4,763	9,00E-25	3,70E-21	Increased evolvability
mutH	0,949	0,789	0,816	6	keio_plate_19	-0,160	0,741768964	0,847058948	Not significant	3,806	2,77E-09	1,14E-06	Increased evolvability
yfeY	1,330	1,285	0,963	6	keio_plate_3	0,189	0,276537464	0,455491765	Not significant	3,701	2,78E-06	0,000394163	Increased evolvability
yeaG	1,120	1,079	0,929	4	keio_plate_7	0,278	0,81691447	0,90002618	Not significant	3,285	4,99E-09	1,58E-06	Increased evolvability
nrfE	1,070	1,136	1,071	6	keio_plate_15	-0,196	0,494104896	0,657146255	Not significant	3,215	4,07E-06	0,000539768	Increased evolvability
atpI	1,000	0,782	0,788	6	keio_plate_17	0,986	0,009973115	0,051898071	Not significant	2,784	0,000372663	0,024709953	Increased evolvability
yfaD	1,125	1,273	1,159	6	keio_plate_3	0,525	0,012445811	0,059355836	Not significant	2,497	6,22E-06	0,000775138	Increased evolvability
ribD	1,013	1,115	1,106	6	keio_plate_23	0,805	0,000967738	0,013861917	Increased evolvability	2,252	4,19E-10	2,16E-07	Increased evolvability
uvrD	1,073	0,701	0,652	4	keio_plate_7	0,517	0,098976643	0,233981011	Not significant	2,219	7,19E-09	2,11E-06	Increased evolvability
ybgJ	0,948	0,604	0,615	4	keio_plate_7	1,022	0,000802379	0,012896047	Increased evolvability	2,211	3,60E-13	2,96E-10	Increased evolvability
yfaT	1,211	1,180	1,036	6	keio_plate_3	-0,172	0,209457887	0,383213784	Not significant	2,123	9,96E-15	1,02E-11	Increased evolvability
mutS	0,975	0,987	1,041	6	keio_plate_19	0,055	0,851868958	0,919680032	Not significant	2,101	7,78E-13	5,33E-10	Increased evolvability
aroK	0,775	0,609	0,786	6	keio_plate_23	0,794	0,011472785	0,056893388	Not significant	2,052	3,47E-09	1,30E-06	Increased evolvability
yjcC	0,977	1,010	1,034	6	keio_plate_9	0,775	0,001500321	0,018247984	Increased evolvability	2,023	7,96E-05	0,00641304	Increased evolvability
ycjD	1,100	1,145	1,004	6	keio_plate_19	0,085	0,550581648	0,699024445	Not significant	1,860	2,28E-05	0,002407281	Increased evolvability
ynaE	1,051	0,598	0,592	4	keio_plate_7	-0,067	0,330181231	0,505728405	Not significant	1,832	3,57E-05	0,003414253	Increased evolvability
mutT	0,983	0,966	0,988	6	keio_plate_21	-0,692	0,054234893	0,157346256	Not significant	1,828	3,80E-05	0,003548316	Increased evolvability
rfaI	0,949	1,084	1,149	6	keio_plate_11	-0,161	0,599809044	0,74178251	Not significant	1,816	0,000574122	0,032780762	Increased evolvability
yhjE	0,945	1,037	1,114	6	keio_plate_9	0,450	0,035641494	0,118641443	Not significant	1,797	2,57E-06	0,000386203	Increased evolvability
fes	0,901	1,053	1,143	6	keio_plate_11	0,601	0,008650643	0,047543839	Increased evolvability	1,788	1,50E-05	0,001671304	Increased evolvability
yjhF	0,885	0,982	1,083	6	keio_plate_9	-0,797	0,000923725	0,013821373	Decreased evolvability	1,763	0,000129564	0,009684357	Increased evolvability
yggH	0,887	0,793	0,887	6	keio_plate_9	-0,217	0,261308526	0,439541469	Not significant	1,720	4,72E-09	1,58E-06	Increased evolvability
nlpI	0,687	0,782	1,127	6	keio_plate_9	0,743	0,002017201	0,020525225	Increased evolvability	1,704	2,10E-06	0,000331979	Increased evolvability
ycdG	0,959	1,121	1,123	6	keio_plate_19	1,102	0,001874842	0,019813562	Increased evolvability	1,662	1,65E-08	4,24E-06	Increased evolvability
yfjP	1,021	1,105	1,110	6	keio_plate_19	0,364	0,119941896	0,264670496	Not significant	1,638	2,57E-05	0,002642678	Increased evolvability
ompC	0,809	0,418	0,518	4	keio_plate_1	0,028	0,99418228	0,997032221	Not significant	1,568	7,76E-05	0,00638222	Increased evolvability
yqgA	0,893	1,006	1,167	6	keio_plate_9	0,211	0,055490131	0,160237811	Not significant	1,555	4,68E-06	0,00060145	Increased evolvability
eco	0,973	1,140	1,146	6	keio_plate_15	-0,554	0,00723033	0,042706736	Decreased evolvability	1,515	8,86E-08	2,14E-05	Increased evolvability
mpl	0,946	0,921	0,982	6	keio_plate_11	0,163	0,869101557	0,932865927	Not significant	1,506	1,43E-05	0,001635064	Increased evolvability
cheR	1,004	1,034	1,030	6	keio_plate_11	-0,154	0,361102877	0,537054942	Not significant	1,328	5,04E-05	0,004408925	Increased evolvability
ribE	1,068	1,090	1,036	6	keio_plate_23	0,893	0,060318753	0,169032306	Not significant	1,299	0,000450274	0,027628019	Increased evolvability
yggM	0,878	1,020	1,169	6	keio_plate_9	-0,100	0,677836327	0,804441437	Not significant	1,295	0,000504409	0,029623238	Increased evolvability
prfA	0,925	1,109	1,092	6	keio_plate_23	1,106	0,001036652	0,014405981	Increased evolvability	1,294	0,000429643	0,026761545	Increased evolvability
hypE	0,937	1,163	1,243	6	keio_plate_21	0,589	0,021274469	0,085160021	Not significant	1,289	0,000149526	0,010784207	Increased evolvability
yagU	1,096	0,531	0,470	6	keio_plate_3	0,563	0,288709701	0,467830343	Not significant	1,287	6,65E-06	0,000803887	Increased evolvability
yqeG	1,018	1,061	1,058	6	keio_plate_15	-0,199	0,22813831	0,404431476	Not significant	1,266	2,74E-05	0,002746456	Increased evolvability
gloA	0,976	1,045	1,031	6	keio_plate_11	0,062	0,536781585	0,688735673	Not significant	1,217	5,03E-05	0,004408925	Increased evolvability
yhbV	1,103	0,986	0,938	6	keio_plate_23	0,522	0,017289903	0,075215651	Not significant	1,208	0,000559033	0,032368795	Increased evolvability
prsA	0,568	0,617	1,057	6	keio_plate_23	0,297	0,265522739	0,444810098	Not significant	1,193	9,18E-06	0,00107785	Increased evolvability
rsgA	1,109	0,840	0,731	6	keio_plate_15	0,221	0,141243685	0,295949434	Not significant	1,184	3,25E-05	0,003181583	Increased evolvability
ycgL	1,041	0,943	0,857	6	keio_plate_5	0,794	0,000274033	0,007122448	Increased evolvability	1,183	5,15E-11	3,02E-08	Increased evolvability
ydjH	0,992	0,877	0,846	6	keio_plate_19	0,390	0,040064253	0,127975249	Not significant	1,175	1,93E-05	0,00208604	Increased evolvability
gshA	0,930	1,033	1,092	6	keio_plate_11	0,762	0,00276316	0,02480208	Increased evolvability	1,172	1,33E-06	0,000249374	Increased evolvability
yhcF	0,945	1,033	1,093	6	keio_plate_9	0,036	0,577106857	0,721559091	Not significant	1,112	0,000385574	0,025160223	Increased evolvability
pgk	0,934	0,962	1,082	6	keio_plate_23	0,855	0,014325409	0,065672043	Not significant	1,096	0,000403262	0,025903256	Increased evolvability
rffD	0,872	0,699	0,802	6	keio_plate_11	2,241	2,65E-05	0,00462042	Increased evolvability	1,034	9,47E-05	0,007483184	Increased evolvability
yiiT	1,065	0,779	0,713	6	keio_plate_15	-0,617	0,017565098	0,076010649	Not significant	1,002	4,57E-07	9,39E-05	Increased evolvability
ydaS	0,921	0,528	0,577	4	keio_plate_7	0,751	0,110490033	0,251787432	Not significant	0,983	5,74E-05	0,004819668	Increased evolvability
ymfG	1,085	1,072	0,999	6	keio_plate_15	-0,158	0,62474258	0,764379984	Not significant	0,972	2,48E-07	5,36E-05	Increased evolvability
yrfB	1,045	1,073	1,042	6	keio_plate_9	0,420	0,010640472	0,054406694	Not significant	0,940	0,000490599	0,02922975	Increased evolvability

Supplementary Table 4: Whole-genome sequencing of resistant mutants. *Strain identified, SNP called by CLC Genomics workbench, structural variant called by CLC Genomics workbench, position called by Snippy, Gene called by Snippy, Biological process called by Ecocyc, Type called by Snippy, Impact called by Snippy, Duplication identified by CLC Genomics workbench and MIC of cefotaxime determined by streaking out on MHB agar plates.*

Well	Strain	SNP	Structural variant	Position (Snippy)	Gene (Snippy)	Ecocyc biological process	Type (Snippy)	Impact (Snippy)	Duplication	MIC Cefo Resistance
G9	Evo 17a	**marR missense mutation**	lon IS insertion upstream	1613609	marR	DNA-binding transcriptional repressor	missense_variant	MODERATE		2x
H9	Evo 17b	**marR missense mutation**	lon IS insertion upstream	1613609	marR	DNA-binding transcriptional repressor	missense_variant	MODERATE		2x
D9	Pool 30	**marR missense mutation**	rnlA IS insertion	1613627	marR	DNA-binding transcriptional repressor	missense_variant	MODERATE		2x
H10	Evo 32a	**marR missense mutation**	-	1613627	marR	DNA-binding transcriptional repressor	missense_variant	MODERATE		2x
C10	Evo 24	**marR missense mutation**	-	1613725	marR	DNA-binding transcriptional repressor	stop_gained	HIGH		2x
A10	Evo 20a	**marR frameshift**	lon IS insertion upstream	1613570	marR	DNA-binding transcriptional repressor	frameshift_variant	HIGH		2x
D10	Evo 25a	**marR frameshift**	acrR IS insertion + pykF IS insertion upstream	1613747	marR	DNA-binding transcriptional repressor	frameshift_variant	HIGH		2x
B9	Pool 28	**marR frameshift**	-	1613753	marR	DNA-binding transcriptional repressor	frameshift_variant	HIGH		2x
A11	Evo 32b	-	**marR 5bp deletion**	1613509	marR	DNA-binding transcriptional repressor	frameshift_variant	HIGH		2x
E10	Evo 25b	-	**marR 19bp duplication + waaQ IS insertion**	1613596	marR	DNA-binding transcriptional repressor	frameshift_variant&stop_gained	HIGH		2x
A8	Pool 19	**ompR missense mutation**	-	3529613	ompR	omp regulator	missense_variant	MODERATE		2x
D8	Pool 22	**ompR missense mutation**	-	3529820	ompR	omp regulator	missense_variant	MODERATE		2x
F9	Pool 32	**ompR missense mutation**	yraJ IS insertion upstream	3529915	ompR	omp regulator	missense_variant	MODERATE		2x
G5	Pool 1	**ompR missense mutation**	-	3529805	ompR	omp regulator	stop_gained	HIGH		2x
D6	Pool 6	**ompR missense mutation**	-	3529805	ompR	omp regulator	stop_gained	HIGH		2x
F8	Pool 24	**ompR missense mutation**	-	3529352	ompR	omp regulator	stop_gained	HIGH		2x
B10	Evo 20b	-	**ompR 4bp duplication**	3529372	ompR	omp regulator	frameshift_variant	HIGH	Yes	2x
E9	Pool 31	-	ompR IS insertion							2x
E6	Pool 7	**ompF missense mutation**	-	982040	ompF	outer membrane porin F	stop_gained	HIGH		2x
F6	Pool 8	**ompF missense mutation**	-	982177	ompF	outer membrane porin F	stop_gained	HIGH		2x
E8	Pool 23	**ompF missense mutation**		981731	ompF	outer membrane porin F	stop_gained	HIGH		2x
B8	Pool 20	ompF upstream	-	982618	aspC	aspartate aminotransferase	upstream_gene_variant	MODIFIER		2x
G8	Pool 25	ompF mutation downstream	-	981315	aspC	aspartate aminotransferase	upstream_gene_variant	MODIFIER		2x
A6	Pool 3	-	ompF IS insertion							2x
B6	Pool 4	-	ompF IS insertion							2x
C6	Pool 5	-	ompF IS insertion							2x
H7	Pool 18	-	ompF IS insertion							2x
C8	Pool 21	**astE missense mutation**	ompF IS insertion upstream	1820283	astE	succinylglutamate desuccinylase	missense_variant	MODERATE	Yes	2x
C9	Pool 29	-	ompF IS insertion upstream							2x
B7	Pool 12	-	ompF 78bp deletion						Yes	2x
H5	Pool 2	-	lon IS insertion upstream							1x
A7	Pool 11	-	lon IS insertion upstream							1x
C7	Pool 13	**yfcF missense mutation**	lon IS insertion upstream	2413891	yfcF	glutathione S-transferase	missense_variant	MODERATE		1x
F7	Pool 16	-	lon IS insertion upstream							1x
G7	Pool 17	-	lon IS insertion upstream							2x
H8	Pool 26	**wbbJ frameshift**	lon IS insertion upstream	2098354	wbbJ	putative lipopolysaccharide biosynthesis O-acetyl transferase	frameshift_variant	HIGH		2x
F10	Evo 27a	**hycI missense mutation**	-	2836392	hycI	hydrogenase 3 maturation protease	missense_variant	MODERATE		2x
F10	Evo 27a	**frdD missense mutation -> upstream of ampC**	-	4368852	frdD	fumarate reductase membrane protein	missense_variant	MODERATE		2x
G10	Evo 27b	**frdD missense mutation -> upstream of ampC**	IS insertion between ynfA and ynfB	4368852	frdD	fumarate reductase membrane protein	missense_variant	MODERATE		2x
A9	Pool 27	**frdD missense mutation -> upstream of ampC**	-	4368852	frdD	fumarate reductase membrane protein	missense_variant	MODERATE		2x
H6	Pool 10	**gabD missense mutation**	-	2785270	gabD	succinate-semialdehyde dehydrogenase (NADP+)	synonymous_variant	LOW		1x
E7	Pool 15	soxR mutation upstream	-	4267367	uvrA	UvrABC excision nuclease subunit A	upstream_gene_variant	MODIFIER		1x
E8	Pool 23	**srlQ frameshift**	yjhI IS insertion	2823383	srlQ	D-arabinose 5-phosphate isomerase	frameshift_variant	HIGH		2x
G6	Pool 9	-	-						Yes	1x
D7	Pool 14	-	-							1x

Bibliography

Abouhamad WN & Manson MD (1994) The dipeptide permease of *Escherichia coli* closely resembles other bacterial transport systems and shows growth-phase-dependent expression. *Mol Microbiol* 14, 1077–1092.

Aguilar-Rodríguez J, Sabater-Muñoz B, Montagud-Martínez R, Berlanga V, Alvarez-Ponce D, Wagner A & Fares MA (2016) The molecular chaperone DnaK is a source of mutational robustness. *Genome Biol Evol* 8, 2979–2991.

Ahmad SI & Pritchard RH (1969) A map of four genes specifying enzymes involved in catabolism of nucleosides and deoxynucleosides in *Escherichia coli*. *Mol Gen Genet* 104, 351–359.

Alekshun MN & Levy SB (2007) Molecular mechanisms of antibacterial multidrug resistance. *Cell* 128, 1037–1050.

Alekshun MN & Levy SB (1999) The *mar* regulon: multiple resistance to antibiotics and other toxic chemicals. *Trends Microbiol* 7, 410–413.

Alt S, Mitchenall LA, Maxwell A & Heide L (2011) Inhibition of DNA gyrase and DNA topoisomerase IV of *Staphylococcus aureus* and *Escherichia coli* by aminocoumarin antibiotics. *Journal of Antimicrobial Chemotherapy* 66, 2061–2069.

Andersson DI & Hughes D (2014) Microbiological effects of sublethal levels of antibiotics. *Nat Rev Microbiol* 12, 465.

Arjes HA, Sun J, Liu H, Nguyen TH, Culver RN, Celis AI, Walton SJ, Vasquez KS, Yu FB, Xue KS, Newton D, Zermeno R, Weglarz M, Deutschbauer A, Huang KC & Shiver AL (2022) Construction and characterization of a genome-scale ordered mutant collection of *Bacteroides thetaiotaomicron*. *BMC Biol* 20, 285.

Ascensao JA, Wetmore KM, Good BH, Arkin AP & Hallatschek O (2023) Quantifying the local adaptive landscape of a nascent bacterial community. *Nat Commun* 14, 248.

Asmar AT, Ferreira JL, Cohen EJ, Cho S-H, Beeby M, Hughes KT & Collet J-F (2017) Communication across the bacterial cell envelope depends on the size of the periplasm. *PLoS Biol* 15, e2004303.

Baba T, Ara T, Hasegawa M, Takai Y, Okumura Y, Baba M, Datsenko KA, Tomita M, Wanner BL & Mori H (2006) Construction of *Escherichia coli* K-12 in-frame, single-gene knockout mutants: the Keio collection. *Mol Syst Biol* 2, 2006.0008. Available at: https://doi.org/10.1038/msb4100050.

Babu M, Arnold R, Bundalovic-Torma C, Gagarinova A, Wong KS, Kumar A, Stewart G, Samanfar B, Aoki H, Wagih O, Vlasblom J, Phanse S, Lad K, Yeou Hsiung Yu A, Graham C, Jin K, Brown E, Golshani A, Kim P, Moreno-Hagelsieb G, Greenblatt J, Houry WA, Parkinson J & Emili A (2014) Quantitative genome-wide genetic interaction screens reveal global epistatic relationships of protein complexes in *Escherichia coli*. *PLoS Genet* 10, e1004120-.

Babu M, Díaz-Mejía JJ, Vlasblom J, Gagarinova A, Phanse S, Graham C, Yousif F, Ding H, Xiong X, Nazarians-Armavil A, Alamgir M, Ali M, Pogoutse O, Pe'er A, Arnold R, Michaut M, Parkinson J, Golshani A, Whitfield C, Wodak SJ, Moreno-Hagelsieb G, Greenblatt JF & Emili A (2011) Genetic interaction maps in *Escherichia coli* reveal functional crosstalk among cell envelope biogenesis pathways. *PLoS Genet* 7, e1002377-.

Bahadur R, Chodisetti PK & Reddy M (2021) Cleavage of Braun's lipoprotein Lpp from the bacterial peptidoglycan by a paralog of L,D-transpeptidases, LdtF. *Proceedings of the National Academy of Sciences* 118. Available at: https://www.pnas.org/content/118/19/e2101989118.

Banzhaf M, van den Berg van Saparoea B, Terrak M, Fraipont C, Egan A, Philippe J, Zapun A, Breukink E, Nguyen-Distèche M, den Blaauwen T & Vollmer W (2012)

Cooperativity of peptidoglycan synthases active in bacterial cell elongation. *Mol Microbiol* 85, 179–194.

Banzhaf M, Yau HCL, Verheul J, Lodge A, Kritikos G, Mateus A, Cordier B, Hov AK, Stein F, Wartel M, Pazos M, Solovyova AS, Breukink E, van Teeffelen S, Savitski MM, den Blaauwen T, Typas A & Vollmer W (2020) Outer membrane lipoprotein NlpI scaffolds peptidoglycan hydrolases within multi-enzyme complexes in *Escherichia coli*. *EMBO J* 39, e102246.

Baquero F & Levin BR (2021) Proximate and ultimate causes of the bactericidal action of antibiotics. *Nat Rev Microbiol* 19, 123–132.

Barb AW, Jiang L, Raetz CRH & Zhou P (2007) Structure of the deacetylase LpxC bound to the antibiotic CHIR-090: time-dependent inhibition and specificity in ligand binding. *Proceedings of the National Academy of Sciences* 104, 18433–18438.

Barb AW, McClerren AL, Snehelatha K, Reynolds CM, Zhou P & Raetz CRH (2007) Inhibition of lipid A biosynthesis as the primary mechanism of CHIR-090 antibiotic activity in *Escherichia coli*. *Biochemistry* 46, 3793–3802.

Barna JCJ & Williams DH (1984) The structure and mode of action of glycopeptide antibiotics of the vancomycin group. *Annu Rev Microbiol* 38, 339–357.

Barreteau H, Kovač A, Boniface A, Sova M, Gobec S & Blanot D (2008) Cytoplasmic steps of peptidoglycan biosynthesis. *FEMS Microbiol Rev* 32, 168–207.

Benn G, Mikheyeva I V, Inns PG, Forster JC, Ojkic N, Bortolini C, Ryadnov MG, Kleanthous C, Silhavy TJ & Hoogenboom BW (2021) Phase separation in the outer membrane of *Escherichia coli*. *Proceedings of the National Academy of Sciences* 118, e2112237118.

Bertsche U, Kast T, Wolf B, Fraipont C, Aarsman MEG, Kannenberg K, Von Rechenberg M, Nguyen-Distèche M, Den Blaauwen T, Höltje J-V & Vollmer W (2006) Interaction between two murein (peptidoglycan) synthases, PBP3 and PBP1B, in *Escherichia coli*. *Mol Microbiol* 61, 675–690.

Bhujbalrao R & Anand R (2019) Deciphering determinants in ribosomal methyltransferases that confer antimicrobial resistance. *J Am Chem Soc* 141, 1425–1429.

Bishop RE (2008) Structural biology of membrane-intrinsic β-barrel enzymes: sentinels of the bacterial outer membrane. *Biochimica et Biophysica Acta (BBA) - Biomembranes* 1778, 1881–1896.

Den Blaauwen T, de Pedro MA, Nguyen-Distèche M & Ayala JA (2008) Morphogenesis of rod-shaped sacculi. *FEMS Microbiol Rev* 32, 321–344.

Bliss CI (1939) The toxicity of poisons applied jointly. *Annals of Applied Biology* 26, 585–615.

Bobonis J, Mitosch K, Mateus A, Karcher N, Kritikos G, Selkrig J, Zietek M, Monzon V, Pfalz B, Garcia-Santamarina S, Galardini M, Sueki A, Kobayashi C, Stein F, Bateman A, Zeller G, Savitski MM, Elfenbein JR, Andrews-Polymenis HL & Typas A (2022) Bacterial retrons encode phage-defending tripartite toxin–antitoxin systems. *Nature* 609, 144–150.

Boneca IG & Chiosis G (2003) Vancomycin resistance: occurrence, mechanisms and strategies to combat it. *Expert Opin Ther Targets* 7, 311–328.

Boos W & Shuman H (1998) Maltose/maltodextrin system of *Escherichia coli*: transport, metabolism, and regulation. *Microbiology and Molecular Biology Reviews* 62, 204–229.

Bos MP & Tommassen J (2004) Biogenesis of the Gram-negative bacterial outer membrane. *Curr Opin Microbiol* 7, 610–616.

Braun V & Rehn K (1969) Chemical characterization, spatial distribution and function of a lipoprotein (murein-lipoprotein) of the *E. coli* cell wall. *Eur J Biochem* 10, 426–438.

Braun V & Wolff H (1970) The murein-lipoprotein linkage in the cell wall of *Escherichia coli*. *Eur J Biochem* 14, 387–391.

Brochado AR, Telzerow A, Bobonis J, Banzhaf M, Mateus A, Selkrig J, Huth E, Bassler S, Zamarreño Beas J, Zietek M, Ng N, Foerster S, Ezraty B, Py B, Barras F, Savitski MM, Bork P, Göttig S & Typas A (2018) Species-specific activity of antibacterial drug combinations. *Nature* 559, 259–263.

Burlingame R & Chapman PJ (1983) Catabolism of phenylpropionic acid and its 3-hydroxy derivative by *Escherichia coli*. *J Bacteriol* 155, 113–121.

Bush NG, Diez-Santos I, Abbott LR & Maxwell A (2020) Quinolones: mechanism, lethality and their contributions to antibiotic resistance. *Molecules* 25.

Cacace E, Kritikos G & Typas A (2017) Chemical genetics in drug discovery. *Curr Opin Syst Biol* 4, 35–42.

Calloni G, Chen T, Schermann SM, Chang H, Genevaux P, Agostini F, Tartaglia GG, Hayer-Hartl M & Hartl FU (2012) DnaK functions as a central hub in the *E. coli* chaperone network. *Cell Rep* 1, 251–264.

Campbell EA, Korzheva N, Mustaev A, Murakami K, Nair S, Goldfarb A & Darst SA (2001) Structural mechanism for rifampicin inhibition of bacterial RNA polymerase. *Cell* 104, 901–912.

Campos AI & Zampieri M (2019) Metabolomics-driven exploration of the chemical drug space to predict combination antimicrobial therapies. *Mol Cell* 74, 1291-1303.e6.

Carmine AA, Brogden RN, Heel RC, Speight TM & Avery GS (1983) Cefotaxime: a review of its antibacterial activity, pharmacological properties and therapeutic use. *Drugs* 25, 223–289.

Castañeda-García A, Blázquez J & Rodríguez-Rojas A (2013) Molecular mechanisms and clinical impact of acquired and intrinsic fosfomycin resistance. *Antibiotics* 2, 217–236.

Caveney NA, Caballero G, Voedts H, Niciforovic A, Worrall LJ, Vuckovic M, Fonvielle M, Hugonnet J-E, Arthur M & Strynadka NCJ (2019) Structural insight into YcbB-mediated beta-lactam resistance in *Escherichia coli*. *Nat Commun* 10, 1849.

Chen C-C, Chou M-Y, Huang C-H, Majumder A & Wu H-Y (2005) A cis-spreading nucleoprotein filament Is responsible for the gene silencing activity found in the promoter relay mechanism*. *Journal of Biological Chemistry* 280, 5101–5112.

Chen C-C, Fang M, Majumder A & Wu H-Y (2001) A 72-base pair AT-rich DNA sequence element functions as a bacterial gene silencer *. *Journal of Biological Chemistry* 276, 9478–9485.

Chodisetti PK & Reddy M (2019) Peptidoglycan hydrolase of an unusual cross-link cleavage specificity contributes to bacterial cell wall synthesis. *Proceedings of the National Academy of Sciences* 116, 7825–7830.

Chong Z-S, Woo W-F & Chng S-S (2015) Osmoporin OmpC forms a complex with MlaA to maintain outer membrane lipid asymmetry in *Escherichia coli*. *Mol Microbiol* 98, 1133–1146.

Chopra I & Roberts M (2001) Tetracycline antibiotics: mode of action, applications, molecular biology, and epidemiology of bacterial resistance. *Microbiology and Molecular Biology Reviews* 65, 232–260.

Clarke CA, Scheurwater EM & Clarke AJ (2010) The vertebrate lysozyme inhibitor Ivy functions to inhibit the activity of lytic transglycosylase*. *Journal of Biological Chemistry* 285, 14843–14847. Available at: https://www.sciencedirect.com/science/article/pii/S0021925819585027.

Cohen EJ, Ferreira JL, Ladinsky MS, Beeby M & Hughes KT (2017) Nanoscale-length control of the flagellar driveshaft requires hitting the tethered outer membrane. *Science (1979)* 356, 197–200.

Consuegra J, Gaffé J, Lenski RE, Hindré T, Barrick JE, Tenaillon O & Schneider D (2021) Insertion-sequence-mediated mutations both promote and constrain evolvability during a long-term experiment with bacteria. *Nat Commun* 12, 980.

Costanzo M, VanderSluis B, Koch EN, Baryshnikova A, Pons C, Tan G, Wang W, Usaj M, Hanchard J, Lee SD, Pelechano V, Styles EB, Billmann M, van Leeuwen J, van Dyk N, Lin Z-Y, Kuzmin E, Nelson J, Piotrowski JS, Srikumar T, Bahr S, Chen Y, Deshpande R, Kurat CF, Li SC, Li Z, Usaj MM, Okada H, Pascoe N, San Luis B-J, Sharifpoor S, Shuteriqi E, Simpkins SW, Snider J, Suresh HG, Tan Y, Zhu H, Malod-Dognin N, Janjic V, Przulj N, Troyanskaya OG, Stagljar I, Xia T, Ohya Y, Gingras A-C, Raught B, Boutros M, Steinmetz LM, Moore CL, Rosebrock AP, Caudy AA, Myers CL, Andrews B & Boone C (2016) A global genetic interaction network maps a wiring diagram of cellular function. *Science (1979)* 353, 1420.

Cox EC (1976) Bacterial mutator genes and the control of spontaneous mutation. *Annu Rev Genet* 10, 135–156. Available at: https://www.annualreviews.org/doi/abs/10.1146/annurev.ge.10.120176.001031.

Dalebroux ZD, Matamouros S, Whittington D, Bishop RE & Miller SI (2014) PhoPQ regulates acidic glycerophospholipid content of the *Salmonella Typhimurium* outer membrane. *Proceedings of the National Academy of Sciences* 111, 1963–1968.

Dam S, Pagès J-M & Masi M (2017) Dual regulation of the small RNA MicC and the quiescent porin OmpN in response to antibiotic stress in *Escherichia coli*. *Antibiotics* 6.

Darby EM, Trampari E, Siasat P, Gaya MS, Alav I, Webber MA & Blair JMA (2023) Molecular mechanisms of antibiotic resistance revisited. *Nat Rev Microbiol* 21, 280–295.

Darphorn TS, Bel K, Koenders-van Sint Anneland BB, Brul S & Ter Kuile BH (2021) Antibiotic resistance plasmid composition and architecture in *Escherichia coli* isolates from meat. *Sci Rep* 11, 2136.

Darwin C (1859) *On the origin of species by means of natural selection, or preservation of favoured races in the struggle for life*, John Murray.

Datsenko KA & Wanner BL (2000) One-step inactivation of chromosomal genes in *Escherichia coli* K-12 using PCR products. *Proceedings of the National Academy of Sciences* 97, 6640–6645.

Davis JH, Rubin AJ & Sauer RT (2011) Design, construction and characterization of a set of insulated bacterial promoters. *Nucleic Acids Res* 39, 1131–1141.

Deatherage DE & Barrick JE (2021) High-throughput characterization of mutations in genes that drive clonal evolution using multiplex adaptome capture sequencing. *Cell Syst* 12, 1187-1200.e4.

Deatherage DE & Barrick JE (2014) Identification of mutations in laboratory-evolved microbes from next-generation sequencing data using *breseq*. In L. Sun & W. Shou, eds. *Engineering and Analyzing Multicellular Systems*. New York, NY: Springer New York, pp.165–188.

Dekker N (2000) Outer-membrane phospholipase A: known structure, unknown biological function. *Mol Microbiol* 35, 711–717.

Deter HS, Hossain T & Butzin NC (2021) Antibiotic tolerance is associated with a broad and complex transcriptional response in E. coli. *Sci Rep* 11, 6112. Available at: https://doi.org/10.1038/s41598-021-85509-7.

Dijkstra AJ & Keck W (1996) Identification of new members of the lytic transglycosylase family in *Haemophilus influenzae* and *Escherichia coli*. *Microbial Drug Resistance* 2, 141–145.

Dippel R & Boos W (2005) The maltodextrin system of *Escherichia coli*: metabolism and transport. *J Bacteriol* 187, 8322–8331.

Dobzhansky T (1946) Genetics of natural populations; recombination and variability in populations of *Drosophila pseudoobscura*. *Genetics* 31, 269–290.
Doi Y, Wachino J & Arakawa Y (2016) Aminoglycoside resistance: the emergence of acquired 16S ribosomal RNA methyltransferases. *Infect Dis Clin North Am* 30, 523–537.
Dong T, Yu R & Schellhorn H (2011) Antagonistic regulation of motility and transcriptome expression by RpoN and RpoS in *Escherichia coli*. *Mol Microbiol* 79, 375–386.
Dukan S, Farewell A, Ballesteros M, Taddei F, Radman M & Nyström T (2000) Protein oxidation in response to increased transcriptional or translational errors. *Proceedings of the National Academy of Sciences* 97, 5746–5749.
Edelstein A, Amodaj N, Hoover K, Vale R & Stuurman N (2010) Computer control of microscopes using μManager. *Curr Protoc Mol Biol* 92, 14.20.1-14.20.17.
Egan AJF, Errington J & Vollmer W (2020) Regulation of peptidoglycan synthesis and remodelling. *Nat Rev Microbiol* 18, 446–460.
Eggeling L & Sahm H (2003) New ubiquitous translocators: amino acid export by *Corynebacterium glutamicum* and *Escherichia coli*. *Arch Microbiol* 180, 155–160.
Ekiert DC, Bhabha G, Isom GL, Greenan G, Ovchinnikov S, Henderson IR, Cox JS & Vale RD (2017) Architectures of lipid transport systems for the bacterial outer membrane. *Cell* 169, 273-285.e17.
Emiola A, Andrews SS, Heller C & George J (2016) Crosstalk between the lipopolysaccharide and phospholipid pathways during outer membrane biogenesis in *Escherichia coli*. *Proceedings of the National Academy of Sciences* 113, 3108–3113.
Emiola A, Falcarin P, Tocher J & George J (2013) A model for the proteolytic regulation of LpxC in the lipopolysaccharide pathway of *Escherichia coli*. *Comput Biol Chem* 47, 1–7.
Emiola A, George J & Andrews SS (2015) A complete pathway model for lipid A biosynthesis in *Escherichia coli*. *PLoS One* 10, e0121216.
Engler C, Kandzia R & Marillonnet S (2008) A one pot, one step, precision cloning method with high throughput capability. *PLoS One* 3, e3647.
Eric C, Alain B, Marthe G, Jean-Claude L & Roland L (2002) Pal lipoprotein of *Escherichia coli* plays a major role in outer membrane integrity. *J Bacteriol* 184, 754–759.
Fourmy D, Recht MI, Blanchard SC & Puglisi JD (1996) Structure of the A site of *Escherichia coli* 16S ribosomal RNA complexed with an aminoglycoside antibiotic. *Science (1979)* 274, 1367–1371.
Fuhrer T, Zampieri M, Sévin DC, Sauer U & Zamboni N (2017) Genomewide landscape of gene–metabolome associations in *Escherichia coli*. *Mol Syst Biol* 13, 907.
Gagarinova A, Stewart G, Samanfar B, Phanse S, White CA, Aoki H, Deineko V, Beloglazova N, Yakunin AF, Golshani A, Brown ED, Babu M & Emili A (2016) Systematic genetic screens reveal the dynamic global functional organization of the bacterial translation machinery. *Cell Rep* 17, 904–916.
García del Portillo F & de Pedro MA (1990) Differential effect of mutational impairment of penicillin-binding proteins 1A and 1B on *Escherichia coli* strains harboring thermosensitive mutations in the cell division genes ftsA, ftsQ, ftsZ, and pbpB. *J Bacteriol* 172, 5863–5870.
Germain E, Guiraud P, Byrne D, Douzi B, Djendli M & Maisonneuve E (2019) YtfK activates the stringent response by triggering the alarmone synthetase SpoT in *Escherichia coli*. *Nat Commun* 10, 5763.
Ghachi M El, Bouhss A, Blanot D & Mengin-Lecreulx D (2004) The *bacA* gene of *Escherichia coli* encodes an undecaprenyl pyrophosphate phosphatase activity*. *Journal of Biological Chemistry* 279, 30106–30113.

Gibson DG, Young L, Chuang R-Y, Venter JC, Hutchison CA & Smith HO (2009) Enzymatic assembly of DNA molecules up to several hundred kilobases. *Nat Methods* 6, 343–345.

Gifford DR, Berríos-Caro E, Joerres C, Suñé M, Forsyth JH, Bhattacharyya A, Galla T & Knight CG (2023) Mutators can drive the evolution of multi-resistance to antibiotics. *PLoS Genet* 19, e1010791. Available at: https://doi.org/10.1371/journal.pgen.1010791.

Good BH & Desai MM (2015) The impact of macroscopic epistasis on long-term evolutionary dynamics. *Genetics* 199, 177–190.

Good BH, McDonald MJ, Barrick JE, Lenski RE & Desai MM (2017) The dynamics of molecular evolution over 60,000 generations. *Nature* 551, 45–50.

Gray AN, Egan AJF, van't Veer IL, Verheul J, Colavin A, Koumoutsi A, Biboy J, Altelaar AFM, Damen MJ, Huang KC, Simorre J-P, Breukink E, den Blaauwen T, Typas A, Gross CA & Vollmer W (2015) Coordination of peptidoglycan synthesis and outer membrane constriction during *Escherichia coli* cell division G. Storz, ed. *Elife* 4.

Guest RL, Guerra DS, Wissler M, Grimm J & Silhavy TJ (2020) YejM modulates activity of the YciM/FtsH protease complex to prevent lethal accumulation of lipopolysaccharide. *mBio* 11, 10.1128/mbio.00598-20.

Guest RL, Rutherford ST & Silhavy TJ (2021) Border control: regulating LPS biogenesis. *Trends Microbiol* 29, 334–345.

Gurnani Serrano CK, Winkle M, Martorana AM, Biboy J, Morè N, Moynihan P, Banzhaf M, Vollmer W & Polissi A (2021) ActS activates peptidoglycan amidases during outer membrane stress in *Escherichia coli*. *Mol Microbiol* 116, 329–342.

Gutheil WG, Kasimoglu E & Nicholson PC (1997) Induction of glutathione-dependent formaldehyde dehydrogenase activity in *Escherichia coli* and *Hemophilus influenza*. *Biochem Biophys Res Commun* 238, 693–696.

Gutierrez A, Laureti L, Crussard S, Abida H, Rodríguez-Rojas A, Blázquez J, Baharoglu Z, Mazel D, Darfeuille F, Vogel J & Matic I (2013) β-lactam antibiotics promote bacterial mutagenesis via an RpoS-mediated reduction in replication fidelity. *Nat Commun* 4, 1610. Available at: https://doi.org/10.1038/ncomms2607.

Hao Z, Lou H, Zhu R, Zhu J, Zhang D, Zhao BS, Zeng S, Chen X, Chan J, He C & Chen PR (2014) The multiple antibiotic resistance regulator MarR is a copper sensor in *Escherichia coli*. *Nat Chem Biol* 10, 21–28. Available at: https://doi.org/10.1038/nchembio.1380.

Hawkins JS, Silvis MR, Koo B-M, Peters JM, Osadnik H, Jost M, Hearne CC, Weissman JS, Todor H & Gross CA (2020) Mismatch-CRISPRi reveals the co-varying expression-fitness relationships of essential genes in *Escherichia coli* and *Bacillus subtilis*. *Cell Syst* 11, 523-535.e9.

Heidrich C, Ursinus A, Berger J, Schwarz H & Höltje J-V (2002) Effects of multiple deletions of murein hydrolases on viability, septum cleavage, and sensitivity to large toxic molecules in *Escherichia coli*. *J Bacteriol* 184, 6093–6099.

Hiniker A, Collet J-F & Bardwell JCA (2005) Copper stress causes an *in vivo* requirement for the *Escherichia coli* disulfide isomerase DsbC*. *Journal of Biological Chemistry* 280, 33785–33791. Available at: https://www.sciencedirect.com/science/article/pii/S0021925820789611.

Hiroshi N (2003) Molecular basis of bacterial outer membrane permeability revisited. *Microbiology and Molecular Biology Reviews* 67, 593–656.

Hooper DC (2000) Mechanisms of action and resistance of older and newer fluoroquinolones. *Clinical Infectious Diseases* 31, S24–S28.

Hualan L, N. PM, Jordan WR, Jayashree R, K. CH, S. LJ, Romy C, P. AA, M. DA & Nassos T (2018) Magic pools: parallel assessment of transposon delivery vectors in bacteria. *mSystems* 3.

Hughes GW, Hall SCL, Laxton CS, Sridhar P, Mahadi AH, Hatton C, Piggot TJ, Wotherspoon PJ, Leney AC, Ward DG, Jamshad M, Spana V, Cadby IT, Harding C, Isom GL, Bryant JA, Parr RJ, Yakub Y, Jeeves M, Huber D, Henderson IR, Clifton LA, Lovering AL & Knowles TJ (2019) Evidence for phospholipid export from the bacterial inner membrane by the Mla ABC transport system. *Nat Microbiol* 4, 1692–1705.

Hugonnet J-E, Mengin-Lecreulx D, Monton A, den Blaauwen T, Carbonnelle E, Veckerlé C, Brun V. Y, van Nieuwenhze M, Bouchier C, Tu K, Rice LB & Arthur M (2016) Factors essential for L,D-transpeptidase-mediated peptidoglycan cross-linking and β-lactam resistance in *Escherichia coli* M. S. Gilmore, ed. *Elife* 5, e19469.

Imai Y, Meyer KJ, Iinishi A, Favre-Godal Q, Green R, Manuse S, Caboni M, Mori M, Niles S, Ghiglieri M, Honrao C, Ma X, Guo JJ, Makriyannis A, Linares-Otoya L, Böhringer N, Wuisan ZG, Kaur H, Wu R, Mateus A, Typas A, Savitski MM, Espinoza JL, O'Rourke A, Nelson KE, Hiller S, Noinaj N, Schäberle TF, D'Onofrio A & Lewis K (2019) A new antibiotic selectively kills Gram-negative pathogens. *Nature* 576, 459–464.

Jana B, Liu X, Dénéréaz J, Park H, Leshchiner D, Liu B, Gallay C, Veening J-W & Opijnen T van (2023) CRISPRi-TnSeq: A genome-wide high-throughput tool for bacterial essential-nonessential genetic interaction mapping. *bioRxiv*, 2023.05.31.543074.

Jiang X, Tan WB, Shrivastava R, Seow DCS, Chen SL, Guan XL & Chng S-S (2020) Mutations in enterobacterial common antigen biosynthesis restore outer membrane barrier function in *Escherichia coli tol-pal* mutants. *Mol Microbiol* 114, 991–1005.

Jin DJ & Gross CA (1988) Mapping and sequencing of mutations in the *Escherichia coli rpoB* gene that lead to rifampicin resistance. *J Mol Biol* 202, 45–58.

Johnson AP, Uttley AH, Woodford N & George RC (1990) Resistance to vancomycin and teicoplanin: an emerging clinical problem. *Clin Microbiol Rev* 3, 280–291.

Johnson JL, Indermaur LW & Rajagopalan K V (1991) Molybdenum cofactor biosynthesis in *Escherichia coli*. Requirement of the chlB gene product for the formation of molybdopterin guanine dinucleotide. *Journal of Biological Chemistry* 266, 12140–12145.

Kaur H, Jakob RP, Marzinek JK, Green R, Imai Y, Bolla JR, Agustoni E, Robinson C V, Bond PJ, Lewis K, Maier T & Hiller S (2021) The antibiotic darobactin mimics a β-strand to inhibit outer membrane insertase. *Nature* 593, 125–129.

Kim JH, Bothe JR, Frederick RO, Holder JC & Markley JL (2014) Role of IscX in iron–sulfur cluster biogenesis in *Escherichia coli*. *J Am Chem Soc* 136, 7933–7942.

Kinsler G, Geiler-Samerotte K & Petrov DA (2020) Fitness variation across subtle environmental perturbations reveals local modularity and global pleiotropy of adaptation V. S. Cooper, N. Barkai, V. S. Cooper, & D. Gresham, eds. *Elife* 9, e61271.

Kjeldsen TSB, Sommer MOA & Olsen JE (2015) Extended spectrum β-lactamase-producing *Escherichia coli* forms filaments as an initial response to cefotaxime treatment. *BMC Microbiol* 15, 63.

Klein G, Kobylak N, Lindner B, Stupak A & Raina S (2014) Assembly of lipopolysaccharide in *Escherichia coli* requires the essential LapB heat shock protein*. *Journal of Biological Chemistry* 289, 14829–14853.

Kneidinger B, Marolda C, Graninger M, Zamyatina A, McArthur F, Kosma P, Valvano MA & Messner P (2002) Biosynthesis pathway of ADP-l-glycero-β-d-manno-heptose in *Escherichia coli*. *J Bacteriol* 184, 363–369.

Knopp M & Andersson DI (2018) Predictable phenotypes of antibiotic resistance mutations G. D. L. Wright Bruce Martinez, Jose, ed. *mBio* 9.

Kritikos G, Banzhaf M, Herrera-Dominguez L, Koumoutsi A, Wartel M, Zietek M & Typas A (2017) A tool named Iris for versatile high-throughput phenotyping in microorganisms. *Nat Microbiol* 2, 17014.

Kumar A, Beloglazova N, Bundalovic-Torma C, Phanse S, Deineko V, Gagarinova A, Musso G, Vlasblom J, Lemak S, Hooshyar M, Minic Z, Wagih O, Mosca R, Aloy P, Golshani A, Parkinson J, Emili A, Yakunin AF & Babu M (2016) Conditional epistatic interaction maps reveal global functional rewiring of genome integrity pathways in *Escherichia coli*. *Cell Rep* 14, 648–661.

Kusser W & Ishiguro EE (1986) Lysis of nongrowing *Escherichia coli* by combinations of beta-lactam antibiotics and inhibitors of ribosome function. *Antimicrob Agents Chemother* 29, 451–455.

Kutukova EA, Livshits VA, Altman IP, Ptitsyn LR, Zyiatdinov MH, Tokmakova IL & Zakataeva NP (2005) The yeaS (leuE) gene of *Escherichia coli* encodes an exporter of leucine, and the Lrp protein regulates its expression. *FEBS Lett* 579, 4629–4634.

Kwon JH & Powderly WG (2021) The post-antibiotic era is here. *Science (1979)* 373, 471.

Labia R, Kazmierczak A, Guionie M & Masson JM (1980) Some bacterial proteins with affinity for cefotaxime. *Journal of Antimicrobial Chemotherapy* 6, 19–23.

Larsson DGJ & Flach C-F (2022) Antibiotic resistance in the environment. *Nat Rev Microbiol* 20, 257–269.

Lawson MJ, Camsund D, Larsson J, Baltekin Ö, Fange D & Elf J (2017) In situ genotyping of a pooled strain library after characterizing complex phenotypes. *Mol Syst Biol* 13, 947.

Lee M, Hesek D, Llarrull LI, Lastochkin E, Pi H, Boggess B & Mobashery S (2013) Reactions of all *Escherichia coli* lytic transglycosylases with bacterial cell wall. *J Am Chem Soc* 135, 3311–3314.

Lennon CW, Thamsen M, Friman ET, Cacciaglia A, Sachsenhauser V, Sorgenfrei FA, Wasik MA & Bardwell JCA (2015) Folding optimization in vivo uncovers new chaperones. *J Mol Biol* 427, 2983–2994.

Lenski RE & Travisano M (1994) Dynamics of adaptation and diversification: a 10,000-generation experiment with bacterial populations. *Proceedings of the National Academy of Sciences* 91, 6808–6814.

Levin-Reisman I, Ronin I, Gefen O, Braniss I, Shoresh N & Balaban NQ (2017) Antibiotic tolerance facilitates the evolution of resistance. *Science (1979)* 355, 826 LP – 830.

Levy SF, Blundell JR, Venkataram S, Petrov DA, Fisher DS & Sherlock G (2015) Quantitative evolutionary dynamics using high-resolution lineage tracking. *Nature* 519, 181–186.

Lewinson O, Padan E & Bibi E (2004) Alkalitolerance: a biological function for a multidrug transporter in pH homeostasis. *Proc Natl Acad Sci U S A* 101, 14073–14078.

Li G-W, Burkhardt D, Gross C & Weissman JS (2014) Quantifying absolute protein synthesis rates reveals principles underlying allocation of cellular resources. *Cell* 157, 624–635.

Lima LM, Silva BNM da, Barbosa G & Barreiro EJ (2020) β-lactam antibiotics: an overview from a medicinal chemistry perspective. *Eur J Med Chem* 208, 112829.

Lin H, Fischbach MA, Liu DR & Walsh CT (2005) *In vitro* characterization of salmochelin and enterobactin trilactone hydrolases IroD, IroE, and Fes. *J Am Chem Soc* 127, 11075–11084.

Liu G, Yong MYJ, Yurieva M, Srinivasan KG, Liu J, Lim JSY, Poidinger M, Wright GD, Zolezzi F, Choi H, Pavelka N & Rancati G (2015) Gene essentiality Is a quantitative property linked to cellular evolvability. *Cell* 163, 1388–1399.

Liu J, Tassinari M, Souza DP, Naskar S, Noel JK, Bohuszewicz O, Buck M, Williams TA, Baum B & Low HH (2021) Bacterial Vipp1 and PspA are members of the ancient ESCRT-III membrane-remodeling superfamily. *Cell* 184, 3660-3673.e18.

Liu X, Bakker V de, Heggenhougen MV, Mårli MT, Frøynes AH, Salehian Z, Porcellato D, Angeles DM, Veening J-W & Kjos M (2023) Genome-wide CRISPRi screens reveal the essentialome and determinants for susceptibility to dalbavancin in *Staphylococcus aureus*. *bioRxiv*, 2023.08.30.555613.

Long H, Miller SF, Strauss C, Zhao C, Cheng L, Ye Z, Griffin K, Te R, Lee H, Chen C-C & Lynch M (2016) Antibiotic treatment enhances the genome-wide mutation rate of target cells. *Proceedings of the National Academy of Sciences* 113.

Lucinda N-M, Thea K & Thomas F (2002) *rpoS* mutations and loss of general stress resistance in *Escherichia coli* populations as a consequence of conflict between competing stress responses. *J Bacteriol* 184, 806–811.

Lukačišinová M, Fernando B & Bollenbach T (2020) Highly parallel lab evolution reveals that epistasis can curb the evolution of antibiotic resistance. *Nat Commun* 11, 3105. Available at: https://doi.org/10.1038/s41467-020-16932-z.

Lynch M (2010) Evolution of the mutation rate. *Trends Genet* 26, 345–352.

Macnab RM (1992) Genetics and biogenesis of bacterial flagella. *Annu Rev Genet* 26, 131–158.

Magalhães MLB, Argyrou A, Cahill SM & Blanchard JS (2008) Kinetic and mechanistic analysis of the *Escherichia coli* ribD-encoded bifunctional deaminase-reductase involved in riboflavin biosynthesis. *Biochemistry* 47, 6499–6507.

Magnet S, Bellais S, Dubost L, Fourgeaud M, Mainardi J-L, Petit-Frère S, Marie A, Mengin-Lecreulx D, Arthur M & Gutmann L (2007) Identification of the L,D-transpeptidases responsible for attachment of the Braun lipoprotein to *Escherichia coli* peptidoglycan. *J Bacteriol* 189, 3927–3931.

Mahalakshmi S, Sunayana MR, SaiSree L & Reddy M (2014) *yciM* is an essential gene required for regulation of lipopolysaccharide synthesis in *Escherichia coli*. *Mol Microbiol* 91, 145–157.

Majumder A, Fang M, Tsai K-J, Ueguchi C, Mizuno T & Wu H-Y (2001) LeuO expression in response to starvation for branched-chain amino acids*. *Journal of Biological Chemistry* 276, 19046–19051.

Malinverni JC & Silhavy TJ (2009) An ABC transport system that maintains lipid asymmetry in the Gram-negative outer membrane. *Proceedings of the National Academy of Sciences* 106, 8009–8014.

Malojčić G, Andres D, Grabowicz M, George AH, Ruiz N, Silhavy TJ & Kahne D (2014) LptE binds to and alters the physical state of LPS to catalyze its assembly at the cell surface. *Proceedings of the National Academy of Sciences* 111, 9467–9472.

Manat G, El Ghachi M, Auger R, Baouche K, Olatunji S, Kerff F, Touzé T, Mengin-Lecreulx D & Bouhss A (2015) Membrane topology and biochemical characterization of the *Escherichia coli* BacA undecaprenyl-pyrophosphate phosphatase. *PLoS One* 10, e0142870.

Maniyeri A, Wieczorek A, Ayyolath A, Sugalska W, Klein G & Raina S (2023) Suppressors of *lapC* mutation identify new regulators of LpxC, which mediates the first committed step in lipopolysaccharide biosynthesis. *Int J Mol Sci* 24.

Markley JL & Wencewicz TA (2018) Tetracycline-inactivating enzymes. *Front Microbiol* 9.

Masi M, Vergalli J, Ghai I, Barba-Bon A, Schembri T, Nau WM, Lafitte D, Winterhalter M & Pagès J-M (2022) Cephalosporin translocation across enterobacterial OmpF and OmpC channels, a filter across the outer membrane. *Commun Biol* 5, 1059.

Mateus A, Hevler J, Bobonis J, Kurzawa N, Shah M, Mitosch K, Goemans C V, Helm D, Stein F, Typas A & Savitski MM (2020) The functional proteome landscape of *Escherichia coli*. *Nature* 588, 473–478. Available at: https://doi.org/10.1038/s41586-020-3002-5.

Mathelié-Guinlet M, Asmar AT, Collet J-F & Dufrêne YF (2020) Lipoprotein Lpp regulates the mechanical properties of the *E. coli* cell envelope. *Nat Commun* 11, 1789.

Matsuhashi M, Maruyama IN, Takagaki Y, Tamaki S, Nishimura Y & Hirota Y (1978) Isolation of a mutant of *Escherichia coli* lacking penicillin-sensitive D-alanine carboxypeptidase IA. *Proceedings of the National Academy of Sciences* 75, 2631–2635.

Matsuhashi M, Takagaki Y, Maruyama IN, Tamaki S, Nishimura Y, Suzuki H, Ogino U & Hirota Y (1977) Mutants of *Escherichia coli* lacking in highly penicillin-sensitive D-alanine carboxypeptidase activity. *Proceedings of the National Academy of Sciences* 74, 2976–2979.

Matsuhashi M, Tamaki S, Curtis SJ & Strominger JL (1979) Mutational evidence for identity of penicillin-binding protein 5 in *Escherichia coli* with the major D-alanine carboxypeptidase IA activity. *J Bacteriol* 137, 644–647.

Matsuyama S, Tajima T & Tokuda H (1995) A novel periplasmic carrier protein involved in the sorting and transport of *Escherichia coli* lipoproteins destined for the outer membrane. *EMBO J* 14, 3365–3372.

Matsuyama S, Yokota N & Tokuda H (1997) A novel outer membrane lipoprotein, LolB (HemM), involved in the LolA (p20)-dependent localization of lipoproteins to the outer membrane of *Escherichia coli*. *EMBO J* 16, 6947–6955. Available at: https://doi.org/10.1093/emboj/16.23.6947.

Matthias W, M. H-RV, Karthik P, A. GEC, M. MA, Joe G, R. HI, Alessandra P & Waldemar V (2021) DpaA detaches Braun's lipoprotein from peptidoglycan. *mBio* 12. Available at: https://doi.org/10.1128/mBio.00836-21.

McCarty NS, Graham AE, Studená L & Ledesma-Amaro R (2020) Multiplexed CRISPR technologies for gene editing and transcriptional regulation. *Nat Commun* 11, 1281.

Mehner D, Osadnik H, Lünsdorf H & Brüser T (2012) The Tat system for membrane translocation of folded proteins recruits the membrane-stabilizing Psp machinery in *Escherichia coli**. *Journal of Biological Chemistry* 287, 27834–27842.

Mehta P, Jovanovic G, Lenn T, Bruckbauer A, Engl C, Ying L & Buck M (2013) Dynamics and stoichiometry of a regulated enhancer-binding protein in live *Escherichia coli* cells. *Nat Commun* 4, 1997.

Meier-Dieter U, Barr K, Starman R, Hatch L & Rick PD (1992) Nucleotide sequence of the *Escherichia coli rfe* gene involved in the synthesis of enterobacterial common antigen. Molecular cloning of the rfe-rff gene cluster. *Journal of Biological Chemistry* 267, 746–753.

Meier-Dieter U, Starman R, Barr K, Mayer H & Rick PD (1990) Biosynthesis of enterobacterial common antigen in *Escherichia coli*. Biochemical characterization of Tn10 insertion mutants defective in enterobacterial common antigen synthesis. *Journal of Biological Chemistry* 265, 13490–13497.

Mengin-Lecreulx D, J van H & Park JT (1996) Identification of the *mpl* gene encoding UDP-N-acetylmuramate: L-alanyl-gamma-D-glutamyl-meso-diaminopimelate ligase in *Escherichia coli* and its role in recycling of cell wall peptidoglycan. *J Bacteriol* 178, 5347–5352.

Million-Weaver S, Samadpour AN, Moreno-Habel DA, Nugent P, Brittnacher MJ, Weiss E, Hayden HS, Miller SI, Liachko I & Merrikh H (2015) An underlying mechanism for the increased mutagenesis of lagging-strand genes in *Bacillus subtilis*. *Proceedings of the National Academy of Sciences* 112, E1096–E1105.

Minh PN Le, Devroede N, Massant J, Maes D & Charlier D (2009) Insights into the architecture and stoichiometry of *Escherichia coli* PepA•DNA complexes involved in transcriptional control and site-specific DNA recombination by atomic force microscopy. *Nucleic Acids Res* 37, 1463–1476.

Mohammadi T, van Dam V, Sijbrandi R, Vernet T, Zapun A, Bouhss A, Diepeveen-de Bruin M, Nguyen-Distèche M, de Kruijff B & Breukink E (2011) Identification of FtsW as a transporter of lipid-linked cell wall precursors across the membrane. *EMBO J* 30, 1425–1432.

Mohapatra SS, Dwibedy SK & Padhy I (2021) Polymyxins, the last-resort antibiotics: mode of action, resistance emergence, and potential solutions. *J Biosci* 46, 85.

Monchois V, Abergel C, Sturgis J, Jeudy S & Claverie J-M (2001) *Escherichia coli* ykfE ORFan eene encodes a potent inhibitor of C-type lysozyme*. *Journal of Biological Chemistry* 276, 18437–18441. Available at: https://www.sciencedirect.com/science/article/pii/S0021925819317922.

Morè N, Martorana AM, Biboy J, Otten C, Winkle M, Serrano CKG, Silva AM, Atkinson L, Yau H, Breukink E, den Blaauwen T, Vollmer W & Polissi A (2019) Peptidoglycan remodeling enables Escherichia coli to survive severe outer membrane assembly defect. *mBio* 10.

Mörtl S, Fischer M, Richter G, Tack J, Weinkauf S & Bacher A (1996) Biosynthesis of riboflavin: lumazine synthase of *Escherichia coli**. *Journal of Biological Chemistry* 271, 33201–33207.

Moya-Torres A, Mulvey MR, Kumar A, Oresnik IJ & Brassinga AK (2014) The lack of OmpF, but not OmpC, contributes to increased antibiotic resistance in Serratia marcescens. *Microbiology (N Y)* 160, 1882–1892.

Mueller EA, Iken AG, Ali Öztürk M, Winkle M, Schmitz M, Vollmer W, Di Ventura B & Levin PA (2021) The active repertoire of *Escherichia coli* peptidoglycan amidases varies with physiochemical environment. *Mol Microbiol* 116, 311–328.

Mühlberg E, Umstätter F, Kleist C, Domhan C, Mier W & Uhl P (2019) Renaissance of vancomycin: approaches for breaking antibiotic resistance in multidrug-resistant bacteria. *Can J Microbiol* 66, 11–16.

Murray BE (1997) Vancomycin-resistant enterococci. *Am J Med* 102, 284–293.

Murray CJL, Ikuta KS, Sharara F, Swetschinski L, Robles Aguilar G, Gray A, Han C, Bisignano C, Rao P, Wool E, Johnson SC, Browne AJ, Chipeta MG, Fell F, Hackett S, Haines-Woodhouse G, Kashef Hamadani BH, Kumaran EAP, McManigal B, Agarwal R, Akech S, Albertson S, Amuasi J, Andrews J, Aravkin A, Ashley E, Bailey F, Baker S, Basnyat B, Bekker A, Bender R, Bethou A, Bielicki J, Boonkasidecha S, Bukosia J, Carvalheiro C, Castañeda-Orjuela C, Chansamouth V, Chaurasia S, Chiurchiù S, Chowdhury F, Cook AJ, Cooper B, Cressey TR, Criollo-Mora E, Cunningham M, Darboe S, Day NPJ, De Luca M, Dokova K, Dramowski A, Dunachie SJ, Eckmanns T, Eibach D, Emami A, Feasey N, Fisher-Pearson N, Forrest K, Garrett D, Gastmeier P, Giref AZ, Greer RC, Gupta V, Haller S, Haselbeck A, Hay SI, Holm M, Hopkins S, Iregbu KC, Jacobs J, Jarovsky D, Javanmardi F, Khorana M, Kissoon N, Kobeissi E, Kostyanev T, Krapp F, Krumkamp R, Kumar A, Kyu HH, Lim C, Limmathurotsakul D, Loftus MJ, Lunn M, Ma J, Mturi N, Munera-Huertas T, Musicha P, Mussi-Pinhata MM, Nakamura T, Nanavati R, Nangia S, Newton P, Ngoun C, Novotney A, Nwakanma D, Obiero CW, Olivas-Martinez A, Olliaro P, Ooko E, Ortiz-Brizuela E, Peleg AY, Perrone C, Plakkal N, Ponce-de-Leon A, Raad M, Ramdin T, Riddell A, Roberts T, Robotham JV, Roca A, Rudd KE, Russell N, Schnall J, Scott JAG, Shivamallappa M, Sifuentes-Osornio J, Steenkeste N, Stewardson AJ, Stoeva T, Tasak N, Thaiprakong A, Thwaites G, Turner C, Turner P, van Doorn HR, Velaphi S, Vongpradith A, Vu H, Walsh T, Waner

S, Wangrangsimakul T, Wozniak T, Zheng P, Sartorius B, Lopez AD, Stergachis A, Moore C, Dolecek C & Naghavi M (2022) Global burden of bacterial antimicrobial resistance in 2019: a systematic analysis. *The Lancet* 399, 629–655.

Nguyen Ba AN, Cvijović I, Rojas Echenique JI, Lawrence KR, Rego-Costa A, Liu X, Levy SF & Desai MM (2019) High-resolution lineage tracking reveals travelling wave of adaptation in laboratory yeast. *Nature* 575, 494–499.

Nguyen D, Kelly K, Qiu N & Misra R (2020) YejM controls LpxC levels by regulating protease activity of the FtsH/YciM complex of *Escherichia coli*. *J Bacteriol* 202.

Nichols RJ, Sen S, Choo YJ, Beltrao P, Zietek M, Chaba R, Lee S, Kazmierczak KM, Lee KJ, Wong A, Shales M, Lovett S, Winkler ME, Krogan NJ, Typas A & Gross CA (2011) Phenotypic landscape of a bacterial cell. *Cell* 144, 143–156.

Nicoloff H & Andersson DI (2013) Lon protease inactivation, or translocation of the lon gene, potentiate bacterial evolution to antibiotic resistance. *Mol Microbiol* 90, 1233–1248.

Nikaido H (2005) Restoring permeability barrier function to outer membrane. *Chem Biol* 12, 507–509.

Norioka S, Ramakrishnan G, Ikenaka K & Inouye M (1986) Interaction of a transcriptional activator, OmpR, with reciprocally osmoregulated genes, *ompF* and *ompC*, of *Escherichia coli*. *J Biol Chem* 261, 17113–17119.

Nowak MA (2006) What evolution is. In *Evolutionary Dynamics*. Exploring the Equations of Life. Harvard University Press, pp.9–26.

Okuda S, Freinkman E & Kahne D (2012) Cytoplasmic ATP hydrolysis powers transport of lipopolysaccharide across the periplasm in *E. coli*. *Science (1979)* 338, 1214–1217.

Ortmayr K, de la Cruz Moreno R & Zampieri M (2022) Expanding the search for small-molecule antibacterials by multidimensional profiling. *Nat Chem Biol* 18, 584–595.

Owens TW, Taylor RJ, Pahil KS, Bertani BR, Ruiz N, Kruse AC & Kahne D (2019) Structural basis of unidirectional export of lipopolysaccharide to the cell surface. *Nature* 567, 550–553.

Ozden K & Carlson EE (2015) Profiling of β-lactam selectivity for penicillin-binding proteins in *Escherichia coli* strain DC2. *Antimicrob Agents Chemother* 59, 2785–2790.

Padan E, Bibi E, Ito M & Krulwich TA (2005) Alkaline pH homeostasis in bacteria: new insights. *Biochimica et Biophysica Acta (BBA) - Biomembranes* 1717, 67–88.

Paradis-Bleau C, Markovski M, Uehara T, Lupoli TJ, Walker S, Kahne DE & Bernhardt TG (2010) Lipoprotein cofactors located in the outer membrane activate bacterial cell wall polymerases. *Cell* 143, 1110–1120.

Parker CT, Kloser AW, Schnaitman CA, Stein MA, Gottesman S & Gibson BW (1992) Role of the *rfaG* and *rfaP* genes in determining the lipopolysaccharide core structure and cell surface properties of *Escherichia coli* K-12. *J Bacteriol* 174, 2525–2538.

Paternoga H, Crowe-McAuliffe C, Bock L V, Koller TO, Morici M, Beckert B, Myasnikov AG, Grubmüller H, Nováček J & Wilson DN (2023) Structural conservation of antibiotic interaction with ribosomes. *Nat Struct Mol Biol* 30, 1380–1392.

Periasamy H, Joshi P, Palwe S, Shrivastava R, Bhagwat S & Patel M (2020) High prevalence of *Escherichia coli* clinical isolates in India harbouring four amino acid inserts in PBP3 adversely impacting activity of aztreonam/avibactam. *Journal of Antimicrobial Chemotherapy* 75, 1650–1651.

Peters JM, Colavin A, Shi H, Czarny TL, Larson MH, Wong S, Hawkins JS, Lu CHS, Koo B-M, Marta E, Shiver AL, Whitehead EH, Weissman JS, Brown ED, Qi LS, Huang KC & Gross CA (2016) A comprehensive, CRISPR-based functional analysis of essential genes in bacteria. *Cell* 165, 1493–1506.

Peters JM, Silvis MR, Zhao D, Hawkins JS, Gross CA & Qi LS (2015) Bacterial CRISPR: accomplishments and prospects. *Curr Opin Microbiol* 27, 121–126.

Peters K, Pazos M, Edoo Z, Hugonnet J-E, Martorana AM, Polissi A, VanNieuwenhze MS, Arthur M & Vollmer W (2018) Copper inhibits peptidoglycan LD-transpeptidases suppressing β-lactam resistance due to bypass of penicillin-binding proteins. *Proceedings of the National Academy of Sciences* 115, 10786–10791.

Pisabarro AG, De Pedro MA & Ishiguro EE (1990) Dissociation of the ampicillin-induced lysis of amino acid-deprived *Escherichia coli* into two stages. *J Bacteriol* 172, 2187–2190.

Plamann MD, Rapp WD & Stauffer G V (1983) *Escherichia coli* K12 mutants defective in the glycine cleavage enzyme system. *Mol Gen Genet* 192, 15–20.

Pomposiello PJ, Bennik MHJ & Demple B (2001) Genome-wide transcriptional profiling of the *Escherichia coli* responses to superoxide stress and sodium salicylate. *J Bacteriol* 183, 3890–3902.

Pongs O, Bald R & Erdmann VA (1973) Identification of chloramphenicol-binding protein in *Escherichia coli* ribosomes by affinity labeling*. *Proceedings of the National Academy of Sciences* 70, 2229–2233.

Poolman B, Knol J, Van Der Does C, Henderson PJF, Liang W-J, Leblanc G, Pourcher T & Mus-Veteau I (1996) Cation and sugar selectivity determinants in a novel family of transport proteins. *Mol Microbiol* 19, 911–922.

Pootoolal J, Neu J & Wright GD (2002) Glycopeptide antibiotic resistance. *Annu Rev Pharmacol Toxicol* 42, 381–408.

Pratt RF (2008) Substrate specificity of bacterial DD-peptidases (penicillin-binding proteins). *Cellular and Molecular Life Sciences* 65, 2138–2155.

Pribis JP, García-Villada L, Zhai Y, Lewin-Epstein O, Wang AZ, Liu J, Xia J, Mei Q, Fitzgerald DM, Bos J, Austin RH, Herman C, Bates D, Hadany L, Hastings PJ & Rosenberg SM (2019) Gamblers: an antibiotic-induced evolvable cell subpopulation differentiated by reactive-oxygen-induced general stress response. *Mol Cell* 74, 785–800.

Qi LS, Larson MH, Gilbert LA, Doudna JA, Weissman JS, Arkin AP & Lim WA (2013) Repurposing CRISPR as an RNA-guided platform for sequence-specific control of gene expression. *Cell* 152, 1173–1183.

Qian J, Garrett TA & Raetz CRH (2014) In vitro assembly of the outer core of the lipopolysaccharide from *Escherichia coli* K-12 and *Salmonella typhimurium*. *Biochemistry* 53, 1250–1262.

Qin J, Hong Y, Morona R & Totsika M (2023) O antigen biogenesis sensitises *Escherichia coli* K-12 to bile salts, providing a plausible explanation for its evolutionary loss. *PLoS Genet* 19, e1010996.

Rachwalski K, Tu MM, Madden SJ, French S, Hansen DM & Brown ED (2024) A mobile CRISPRi collection enables genetic interaction studies for the essential genes of *Escherichia coli*. *Cell Reports Methods* 4, 100693.

Raetz CRH & Whitfield C (2002) Lipopolysaccharide endotoxins. *Annu Rev Biochem* 71, 635–700.

Ragheb MN, Thomason MK, Hsu C, Nugent P, Gage J, Samadpour AN, Kariisa A, Merrikh CN, Miller SI, Sherman DR & Merrikh H (2019) Inhibiting the evolution of antibiotic resistance. *Mol Cell* 73, 157–165. Available at: http://www.sciencedirect.com/science/article/pii/S1097276518308475.

Ramani N, Hedeshian M & Freundlich M (1994) micF antisense RNA has a major role in osmoregulation of OmpF in *Escherichia coli*. *J Bacteriol* 176, 5005–5010.

Ramirez MS & Tolmasky ME (2010) Aminoglycoside modifying enzymes. *Drug Resistance Updates* 13, 151–171.

Ramos JL, Martínez-Bueno M, Molina-Henares AJ, Terán W, Watanabe K, Zhang X, Gallegos MT, Brennan R & Tobes R (2005) The TetR family of transcriptional repressors. *Microbiology and Molecular Biology Reviews* 69, 326–356.

Rancati G, Moffat J, Typas A & Pavelka N (2018) Emerging and evolving concepts in gene essentiality. *Nat Rev Genet* 19, 34–49.

Richter G, Fischer M, Krieger C, Eberhardt S, Lüttgen H, Gerstenschläger I & Bacher A (1997) Biosynthesis of riboflavin: characterization of the bifunctional deaminase-reductase of *Escherichia coli* and *Bacillus subtilis*. *J Bacteriol* 179, 2022–2028.

Rick PD, Hubbard GL & Barr K (1994) Role of the *rfe* gene in the synthesis of the O8 antigen in *Escherichia coli* K-12. *J Bacteriol* 176, 2877–2884.

Rodionov DG & Ishiguro EE (1995) Direct correlation between overproduction of guanosine 3',5'-bispyrophosphate (ppGpp) and penicillin tolerance in *Escherichia coli*. *J Bacteriol* 177, 4224–4229.

Rogers JK, Guzman CD, Taylor ND, Raman S, Anderson K & Church GM (2015) Synthetic biosensors for precise gene control and real-time monitoring of metabolites. *Nucleic Acids Res* 43, 7648–7660.

Rojas ER, Billings G, Odermatt PD, Auer GK, Zhu L, Miguel A, Chang F, Weibel DB, Theriot JA & Huang KC (2018) The outer membrane is an essential load-bearing element in Gram-negative bacteria. *Nature* 559, 617–621.

Romeis T & Höltje J-V (1994) Penicillin-binding protein 7/8 of *Escherichia coli* is a dd-endopeptidase. *Eur J Biochem* 224, 597–604.

Roopal M & Scott CW (2002) 30S ribosomal subunit assembly is a target for inhibition by aminoglycosides in *Escherichia coli*. *Antimicrob Agents Chemother* 46, 1546–1549.

Roth Barbara, Falco EA, Hitchings GH & Bushby SRM (1962) 5-Benzyl-2,4-diaminopyrimidines as antibacterial agents. I. Synthesis and antibacterial activity *in vitro*. *J Med Pharm Chem* 5, 1103–1123.

Rousset F, Cabezas-Caballero J, Piastra-Facon F, Fernández-Rodríguez J, Clermont O, Denamur E, Rocha EPC & Bikard D (2021) The impact of genetic diversity on gene essentiality within the *Escherichia coli* species. *Nat Microbiol* 6, 301–312.

Ruiz N, Wu T, Kahne D & Silhavy TJ (2006) Probing the barrier function of the outer membrane with chemical conditionality. *ACS Chem Biol* 1, 385–395.

Russ D & Kishony R (2018) Additivity of inhibitory effects in multidrug combinations. *Nat Microbiol* 3, 1339–1345.

Russo M, Crisafulli G, Sogari A, Reilly NM, Arena S, Lamba S, Bartolini A, Amodio V, Magrì A, Novara L, Sarotto I, Nagel ZD, Piett CG, Amatu A, Sartore-Bianchi A, Siena S, Bertotti A, Trusolino L, Corigliano M, Gherardi M, Lagomarsino MC, Di Nicolantonio F & Bardelli A (2019) Adaptive mutability of colorectal cancers in response to targeted therapies. *Science (1979)* 366, 1473–1480.

Sabnis A, Hagart KLH, Klöckner A, Becce M, Evans LE, Furniss RCD, Mavridou DAI, Murphy R, Stevens MM, Davies JC, Larrouy-Maumus GJ, Clarke TB & Edwards AM (2021) Colistin kills bacteria by targeting lipopolysaccharide in the cytoplasmic membrane P. A. Cole, L. Gao, & W. van Schaik, eds. *Elife* 10.

Samsudin F, Ortiz-Suarez ML, Piggot TJ, Bond PJ & Khalid S (2016) OmpA: a flexible clamp for bacterial cell wall attachment. *Structure* 24, 2227–2235.

Sandegren L & Andersson DI (2009) Bacterial gene amplification: implications for the evolution of antibiotic resistance. *Nat Rev Microbiol* 7, 578–588.

Sauvage E, Kerff F, Terrak M, Ayala JA & Charlier P (2008) The penicillin-binding proteins: structure and role in peptidoglycan biosynthesis. *FEMS Microbiol Rev* 32, 234–258.

Schenk MF, Zwart MP, Hwang S, Ruelens P, Severing E, Krug J & de Visser JAGM (2022) Population size mediates the contribution of high-rate and large-benefit mutations to parallel evolution. *Nat Ecol Evol* 6, 439–447.

van Schie BJ, Hellingwerf KJ, van Dijken JP, Elferink MG, van Dijl JM, Kuenen JG & Konings WN (1985) Energy transduction by electron transfer via a pyrrolo-quinoline quinone-dependent glucose dehydrogenase in *Escherichia coli*, *Pseudomonas aeruginosa*, and *Acinetobacter calcoaceticus* (var. lwoffi). *J Bacteriol* 163, 493–499.

Schofield MJ & Hsieh P (2003) DNA mismatch repair: molecular mechanisms and biological function. *Annu Rev Microbiol* 57, 579–608.

Schroeder U, Henrich B, Fink J & Plapp R (1994) Peptidase D of *Escherichia coli* K-12, a metallopeptidase of low substrate specificity. *FEMS Microbiol Lett* 123, 153–159.

Sébastien B-G, Jean-Pierre B & Jean-Marie L (2017) Osmoregulated periplasmic glucans. *EcoSal Plus* 7, 10.1128/ecosalplus.ESP-0001–2017.

Sharma P, Haycocks JRJ, Middlemiss AD, Kettles RA, Sellars LE, Ricci V, Piddock LJ V & Grainger DC (2017) The multiple antibiotic resistance operon of enteric bacteria controls DNA repair and outer membrane integrity. *Nat Commun* 8, 1444.

Sherman DJ, Lazarus MB, Murphy L, Liu C, Walker S, Ruiz N & Kahne D (2014) Decoupling catalytic activity from biological function of the ATPase that powers lipopolysaccharide transport. *Proceedings of the National Academy of Sciences* 111, 4982–4987.

Shi H, Colavin A, Lee TK & Huang KC (2017) Strain library imaging protocol for high-throughput, automated single-cell microscopy of large bacterial collections arrayed on multiwell plates. *Nat Protoc* 12, 429–438.

Shu S & Mi W (2022) Regulatory mechanisms of lipopolysaccharide synthesis in *Escherichia coli*. *Nat Commun* 13, 4576.

Silhavy TJ, Kahne D & Walker S (2010) The bacterial cell envelope. *Cold Spring Harb Perspect Biol* 2.

Silver LL (2017) Fosfomycin: mechanism and resistance. *Cold Spring Harb Perspect Med* 7.

Singh SK, SaiSree L, Amrutha RN & Reddy M (2012) Three redundant murein endopeptidases catalyse an essential cleavage step in peptidoglycan synthesis of *Escherichia coli* K12. *Mol Microbiol* 86, 1036–1051.

Sit B, Crowley SM, Bhullar K, Lai CC-L, Tang C, Hooda Y, Calmettes C, Khambati H, Ma C, Brumell JH, Schryvers AB, Vallance BA & Moraes TF (2015) Active transport of phosphorylated carbohydrates promotes intestinal colonization and transmission of a bacterial pathogen. *PLoS Pathog* 11, e1005107.

Sommer MOA, Munck C, Toft-Kehler R V & Andersson DI (2017) Prediction of antibiotic resistance: time for a new preclinical paradigm? *Nat Rev Microbiol* 15, 689–696.

Sophie M, Lionel D, Arul M, Michel A & Laurent G (2008) Identification of the L,D-transpeptidases for peptidoglycan cross-linking in *Escherichia coli*. *J Bacteriol* 190, 4782–4785.

Sperandeo P, Pozzi C, Dehò G & Polissi A (2006) Non-essential KDO biosynthesis and new essential cell envelope biogenesis genes in the *Escherichia coli* yrbG–yhbG locus. *Res Microbiol* 157, 547–558.

Sperandeo P, Villa R, Martorana AM, Šamalikova M, Grandori R, Dehò G & Polissi A (2011) New insights into the Lpt machinery for lipopolysaccharide transport to the cell surface: LptA-LptC interaction and LptA stability as sensors of a properly assembled transenvelope complex. *J Bacteriol* 193, 1042–1053.

Spratt BG (1975) Distinct penicillin binding proteins involved in the division, elongation, and shape of *Escherichia coli* K12. *Proceedings of the National Academy of Sciences* 72, 2999–3003.

Spratt BG & Strominger JL (1976) Identification of the major penicillin-binding proteins of *Escherichia coli* as d-alanine carboxypeptidase IA. *J Bacteriol* 127, 660–663.
Stapleton PD & Taylor PW (2002) Methicillin resistance in *Staphylococcus aureus*: mechanisms and modulation. *Sci Prog* 85, 57–72.
Sugiyama Y, Nakamura A, Matsumoto M, Kanbe A, Sakanaka M, Higashi K, Igarashi K, Katayama T, Suzuki H & Kurihara S (2016) A novel putrescine exporter SapBCDF of *Escherichia coli**. *Journal of Biological Chemistry* 291, 26343–26351.
Sulavik MC, Gambino LF & Miller PF (1995) The MarR repressor of the multiple antibiotic resistance (*mar*) operon in *Escherichia coli*: prototypic member of a family of bacterial regulatory proteins Involved in sensing phenolic compounds. *Molecular Medicine* 1, 436–446.
Sutterlin HA, Shi H, May KL, Miguel A, Khare S, Huang KC & Silhavy TJ (2016) Disruption of lipid homeostasis in the Gram-negative cell envelope activates a novel cell death pathway. *Proceedings of the National Academy of Sciences* 113, 1565–1574.
Tekin E, White C, Kang TM, Singh N, Cruz-Loya M, Damoiseaux R, Savage VM & Yeh PJ (2018) Prevalence and patterns of higher-order drug interactions in *Escherichia coli*. *NPJ Syst Biol Appl* 4, 31.
Thong S, Ercan B, Torta F, Fong ZY, Wong HYA, Wenk MR & Chng S-S (2016) Defining key roles for auxiliary proteins in an ABC transporter that maintains bacterial outer membrane lipid asymmetry G. Storz, ed. *Elife* 5, e19042.
Tomohiro S, Kaneyoshi Y & Akira I (2009) Involvement of the leucine response transcription factor LeuO in regulation of the genes for sulfa drug efflux. *J Bacteriol* 191, 4562–4571.
Tooke CL, Hinchliffe P, Bragginton EC, Colenso CK, Hirvonen VHA, Takebayashi Y & Spencer J (2019) β-lactamases and β-lactamase inhibitors in the 21st century. *J Mol Biol* 431, 3472–3500.
Toprak E, Veres A, Michel J-B, Chait R, Hartl DL & Kishony R (2012) Evolutionary paths to antibiotic resistance under dynamically sustained drug selection. *Nat Genet* 44, 101–105.
Toprak E, Veres A, Yildiz S, Pedraza JM, Chait R, Paulsson J & Kishony R (2013) Building a morbidostat: an automated continuous-culture device for studying bacterial drug resistance under dynamically sustained drug inhibition. *Nat Protoc* 8, 555–567.
Törk L, Moffatt CB, Bernhardt TG, Garner EC & Kahne D (2023) Single-molecule dynamics show a transient lipopolysaccharide transport bridge. *Nature*.
Touzé T, Tran AX, Hankins J V, Mengin-Lecreulx D & Trent MS (2008) Periplasmic phosphorylation of lipid A is linked to the synthesis of undecaprenyl phosphate. *Mol Microbiol* 67, 264–277.
Trimble MJ, Mlynárčik P, Kolář M & Hancock REW (2016) Polymyxin: alternative mechanisms of action and resistance. *Cold Spring Harb Perspect Med* 6.
Trindade S, Sousa A, Xavier KB, Dionisio F, Ferreira MG & Gordo I (2009) Positive epistasis drives the acquisition of multidrug resistance. *PLoS Genet* 5, e1000578.
Truong TT, Vettiger A & Bernhardt TG (2020) Cell division is antagonized by the activity of peptidoglycan endopeptidases that promote cell elongation. *Mol Microbiol* 114, 966–978.
Typas A, Banzhaf M, van den Berg van Saparoea B, Verheul J, Biboy J, Nichols RJ, Zietek M, Beilharz K, Kannenberg K, von Rechenberg M, Breukink E, den Blaauwen T, Gross CA & Vollmer W (2010) Regulation of peptidoglycan synthesis by outer-membrane proteins. *Cell* 143, 1097–1109.
Typas A, Banzhaf M, Gross CA & Vollmer W (2012) From the regulation of peptidoglycan synthesis to bacterial growth and morphology. *Nat Rev Microbiol* 10, 123–136.

Typas A, Nichols RJ, Siegele DA, Shales M, Collins SR, Lim B, Braberg H, Yamamoto N, Takeuchi R, Wanner BL, Mori H, Weissman JS, Krogan NJ & Gross CA (2008) High-throughput, quantitative analyses of genetic interactions in *E. coli*. *Nat Methods* 5, 781–787.

Valentin-Hansen P, Boëtius F, Hammer-Jespersen K & Svendsen L (1982) The primary structure of *Escherichia coli* K12 2-deoxyribose 5-phosphate aldolase. *Eur J Biochem* 125, 561–566.

Vázquez-Laslop N & Mankin AS (2018) How macrolide antibiotics work. *Trends Biochem Sci* 43, 668–684.

Venkataram S, Dunn B, Li Y, Agarwala A, Chang J, Ebel ER, Geiler-Samerotte K, Hérissant L, Blundell JR, Levy SF, Fisher DS, Sherlock G & Petrov DA (2016) Development of a comprehensive genotype-to-fitness map of adaptation-driving mutations in yeast. *Cell* 166, 1585–1596.

Vinella D, Albrecht C, Cashel M & D'Ari R (2005) Iron limitation induces SpoT-dependent accumulation of ppGpp in *Escherichia coli*. *Mol Microbiol* 56, 958–970.

Voedts H, Dorchêne D, Lodge A, Vollmer W, Arthur M & Hugonnet J (2021) Role of endopeptidases in peptidoglycan synthesis mediated by alternative cross-linking enzymes in *Escherichia coli*. *EMBO J* 40, e108126.

Vollmer W, Blanot D & De Pedro MA (2008) Peptidoglycan structure and architecture. *FEMS Microbiol Rev* 32, 149–167.

Vollmer W, Joris B, Charlier P & Foster S (2008) Bacterial peptidoglycan (murein) hydrolases. *FEMS Microbiol Rev* 32, 259–286.

Wagner K, Moolenaar G, van Noort J & Goosen N (2009) Single-molecule analysis reveals two separate DNA-binding domains in the *Escherichia coli* UvrA dimer. *Nucleic Acids Res* 37, 1962–1972.

Wang B, Grant RA & Laub MT (2020) ppGpp coordinates nucleotide and amino-acid synthesis in *E. coli* during starvation. *Mol Cell* 80, 29–42.

Webb E, Claas K & Downs D (1998) *thiBPQ* encodes an ABC transporter required for transport of thiamine and thiamine pyrophosphate in *Salmonella typhimurium**. *Journal of Biological Chemistry* 273, 8946–8950.

Weber H, Polen T, Heuveling J, Wendisch VF & Hengge R (2005) Genome-wide analysis of the general stress response network in *Escherichia coli*: σS-dependent genes, promoters, and sigma factor selectivity. *J Bacteriol* 187, 1591–1603.

Weiner L, Brissette JL & Model P (1991) Stress-induced expression of the *Escherichia coli* phage shock protein operon is dependent on sigma 54 and modulated by positive and negative feedback mechanisms. *Genes Dev* 5, 1912–1923.

Weiner L & Model P (1994) Role of an *Escherichia coli* stress-response operon in stationary-phase survival. *Proceedings of the National Academy of Sciences* 91, 2191–2195.

Weinreich DM, Delaney NF, DePristo MA & Hartl DL (2006) Darwinian evolution can follow only very few mutational paths to fitter proteins. *Science (1979)* 312, 111–114.

Weinreich DM, Watson RA & Chao L (2005) Perspective: sign epistasis and genetic constraint on evolutionary trajectories. *Evolution (N Y)* 59, 1165–1174.

Wetmore KM, Price MN, Waters RJ, Lamson JS, He J, Hoover CA, Blow MJ, Bristow J, Butland G, Arkin AP & Deutschbauer A (2015) Rapid quantification of mutant fitness in diverse bacteria by sequencing randomly barcoded transposons. *mBio* 6.

WHO (2016) Antimicrobial resistances: global report on surveillance. *World Health Organization*.

Wilmaerts D, Focant C, Matthay P & Michiels J (2022) Transcription-coupled DNA repair underlies variation in persister awakening and the emergence of resistance. *Cell Rep* 38.

Wise EM & Abou Donia MM (1975) Sulfonamide resistance mechanism in *Escherichia coli*: R plasmids can determine sulfonamide-resistant dihydropteroate synthases. *Proceedings of the National Academy of Sciences* 72, 2621–2625.

Wiser MJ, Ribeck N & Lenski RE (2013) Long-term dynamics of adaptation in asexual populations. *Science (1979)* 342, 1364–1367.

Yamada M & Saier MH (1987) Physical and genetic characterization of the glucitol operon in *Escherichia coli*. *J Bacteriol* 169, 2990–2994.

Yamada M & Saier MH (1988) Positive and negative regulators for glucitol (gut) operon expression in *Escherichia coli*. *J Mol Biol* 203, 569–583.

Yamamoto N, Nakahigashi K, Nakamichi T, Yoshino M, Takai Y, Touda Y, Furubayashi A, Kinjyo S, Dose H, Hasegawa M, Datsenko KA, Nakayashiki T, Tomita M, Wanner BL & Mori H (2009) Update on the Keio collection of *Escherichia coli* single-gene deletion mutants. *Mol Syst Biol* 5, 335. Available at: https://doi.org/10.1038/msb.2009.92.

Yeow J, Tan KW, Holdbrook DA, Chong Z-S, Marzinek JK, Bond PJ & Chng S-S (2018) The architecture of the OmpC–MlaA complex sheds light on the maintenance of outer membrane lipid asymmetry in *Escherichia coli*. *Journal of Biological Chemistry* 293, 11325–11340.

Yethon JA, Heinrichs DE, Monteiro MA, Perry MB & Whitfield C (1998) Involvement of *waaY*, *waaQ*, and *waaP* in the modification of *Escherichia coli* lipopolysaccharide and their role in the formation of a stable outer membrane*. *Journal of Biological Chemistry* 273, 26310–26316.

Yoshida T, Qin L, Egger LA & Inouye M (2006) Transcription regulation of OmpF and OmpC by a single transcription factor, OmpR*. *Journal of Biological Chemistry* 281, 17114–17123.

Zakataeva NP, Aleshin V V, Tokmakova IL, Troshin P V & Livshits VA (1999) The novel transmembrane *Escherichia coli* proteins involved in the amino acid efflux. *FEBS Lett* 452, 228–232.

Zhang N & Buck M (2015) A perspective on the enhancer dependent bacterial RNA polymerase. *Biomolecules* 5, 1012–1019.

Zhao J, Cochrane CS, Najeeb J, Gooden D, Sciandra C, Fan P, Lemaitre N, Newns K, Nicholas RA, Guan Z, Thaden JT, Fowler VG, Spasojevic I, Sebbane F, Toone EJ, Duncan C, Gammans R & Zhou P (2023) Preclinical safety and efficacy characterization of an LpxC inhibitor against Gram-negative pathogens. *Sci Transl Med* 15, 5668.